TECHNISCHE UNIVERSITÄT WIEN

ESEA
Institut für Energiesysteme und Elektrische Antriebe

Master Thesis

Impact of locally controlled distributed generation on the total behaviour of LV and MV Link_Grids

Author

Stefan Petrusic, BSc

supervised by

Univ.-Prof. Dr. ing. W. Gawlik
Ass.-Prof. Dr. techn. A. Ilo

of the

Technische Universität Wien
Faculty of Electrical Engineering and Information Technology
Institute of Energy Systems and Electrical Drives

Vienna, June 2019

Acknowledgement

I would like to express my deep gratitude to my supervisor Ass.Prof. Dipl.-Ing. Dr.techn. Albana Ilo for her incredible patience, encouragement and guidance. Her understanding and expertise have been very important for completing this master thesis. Furthermore, I am very thankful to Univ.-Prof. Dr.-Ing. Wolfgang Gawlik for giving me the opportunity to finish my master thesis at the Institute of Energy Systems and Electrical Drives. Very special thanks go to Dipl.-Ing. Daniel-Leon Schultis, who gave a significant contribution to the development of this thesis as well.

None of this would have been possible without the incredible sacrifice of my family. My greatest thanks therefore go to my parents, Nevena and Zoran, and to my brother Andrija, for believing in me all this time and giving me their enormous love and support.

Abstract

The EU regulations strive the development of the electric power sector aiming to overcome issues related to security of supply, environmental impacts and energy efficiency. Distributed generation (DG) plays the important role in resolving many of the aforementioned issues. Currently, the electric power system is undergoing a transformation caused by increased penetration level of DG based on renewable energy sources (RES). The stochastic nature of RES, such as wind and sun, makes the integration of this type of DG in distribution grids quite demanding. Especially, times when the grid experiences high DG production and low load demand, could cause some operational challenges, such as voltage rise and increased power flow losses along the grid. These challenges call for a prompt attention of distributed system operators (DSOs), who need to find some proper solutions so that a secure and reliable electric power supply can be guaranteed to the end-users at all time.

Exactly those challenges and other impacts that are caused by increased penetration level of DGs are the focal points of this thesis. For that purpose several MV and LV test grids are modelled and implemented as MV and LV Link_Grids, which are based on the new developed approach called *LINK*-Solution. For simulating their effects on the MV Link_Grids, LV Link_Grids were modelled in two different ways. Representation of DGs in MV and LV Link_Grids is realized with PV systems, which inverters, in correspondence to the customer class and grid type, are either equipped with appropriate reactive power voltage control *Q(U)* or without any control (*cos* φ = 1). Behaviour of the grids under different load/production scenarios is analysed by evaluating grid losses, exchanged reactive power between LV/MV and MV/HV Link_Grids and voltage profiles deriving from extensive power flow simulations.

Results of the analysis have shown that the grids' behaviour changes substantially when two different load/production scenarios are compared. In case of high PV production and relatively low load power demand the related grid losses, exchanged reactive power and voltage levels across the grid are much higher than in case of no PV production and high load power demand. Additionally, by taking into consideration the "used" and the "proposed" model of LV Link_Grids in theoretical MV Link_Grids, differences between the corresponding models are much more evident in case of the overhead-line feeder as the feeder length increases. Lastly, power flow simulations for the first load/production scenario in Real MV Link_Grids reveal that the number of upper voltage limit violations, reactive power exchange with the overlaid HV Link_Grid and the corresponding grid losses are much higher in case of the "proposed" model. Therefore, in order to properly assess the performance of MV distribution grids more realistically, lumped load models of LV distribution grids should be represented without unnecessary simplifications of their load behaviour.

Keywords: low and medium voltage distribution grids, distributed generation, photovoltaic systems, renewable energy sources, *LINK*-Solution, Customer Plant, power flow calculations, voltage fluctuation, voltage profiles, reverse power flow, voltage control, *Q(U)*-control, lumped load characteristic

Kurzfassung

Die EU Regularien streben nach einer Weiterentwicklung des elektrischen Energieversorgungssektors um die zukünftigen Herausforderungen von Versorgungssicherheit, Umwelteinfluss und Effizienz zu bewerkstelligen. Dezentrale Erzeugung spielt eine wichtige Rolle in der Umsetzung dieser erwähnten Anstrengungen. Derzeit durchläuft das elektrische Energiesystem eine Transformation, hervorgerufen durch die steigende dezentrale Energieerzeugung aus der erneuerbaren Energiequellen. Die stochastische Charakteristik dieser Quellen, wie Wind und Sonnenlicht, erschweren die Integration dieser Art von dezentraler Energieerzeugung in das bestehende System. Besonders die Zeiten in denen die dezentrale Erzeugung im Verteilnetz sehr hoch und gleichzeitig die allgemeine Last niedrig ist, können im Betrieb Unregelmäßigkeiten wie Anstieg der Netzspannung und Netzverluste Schwierigkeiten bereiten. Diese Probleme verlangen die Aufmerksamkeit der Energienetzbetreiber, um eine Lösung zu finden, damit eine sichere und verlässliche Versorgung der Endkunden garantiert werden kann.

Genau mit diesen Herausforderungen und anderen Einflüssen, hervorgerufen durch die steigende dezentrale Energieerzeugung, beschäftigt sich diese Arbeit. Dafür wurden mehrere Testnetze in Mittelspannung (MS) und Niederspannung (NS) modelliert und als MS Link_Grids und NS Link_Grids implementiert, basierend auf einem neu entwickelten Konzept namens *LINK*-Solution. Um deren Effekt auf das MS Link_Grid zu simulieren, wurden NS Link_Grids in zwei verschiedenen Arten modelliert. Die dezentrale Erzeugung wurde mit PV Systemen realisiert, deren Wechselrichter, abhängig von Kunden- und Netztyp, entweder mit Blindleistungsregelung *Q(U)* oder ohne Regelung (*cos* φ = 1) ausgestattet sind. Durch die Evaluierung von Netzverlusten, Blindleistungsaustausch zwischen NS/MS und MS/HS Ling_Grids und Spannungsprofilen, abgeleitet aus ausgiebigen Lastflusssimulationen, wird das Netzverhalten für verschiedene Last/Erzeugungsszenarien analysiert.

Die Ergebnisse der Analyse haben gezeigt, dass sich das Netzverhalten drastisch ändert wenn die zwei untersuchten Last/Erzeugungsszenarien verglichen werden. Im Fall einer hohen PV Erzeugung bei kleiner Nachfrage sind die Netzverluste, der Blindleistungsaustausch und die Spannungsniveaus im Netz merkbar höher als bei keiner PV Erzeugung und hoher Nachfrage. Vergleicht man die zwei verwendeten Modelle von NS Link_Grids, „used“ und „proposed“, zeigt sich in theoretischen MS Link_Grids, dass die Unterschiede bei der Verwendung von Freileitungen für hohere Leitungslängen viel erkennbarer sind. Letztlich sieht man anhand der Lastflusssimulationen für das erste Last/Erzeugungsszenario in realen MV Link_Grids, dass die Anzahl an Überschreitungen der oberen Spannungsgrenze, Blindleistungsaustausch mit dem darüberliegenden HS Link_Grid und die zugehörigen Netzverluste im Falle des „proposed“ Modells größer sind. Daraus schließt sich, dass das Verhalten von MS Verteilnetzen realistischer nachgebildet werden kann wenn die sogenannten konzentrierten Lastcharakteristiken der NS Verteilnetze ohne unnötige Vereinfachhungen ihres Lastverhaltens dargestellt werden.

Schlüsselwörter: Nieder- und Mittelspannungsverteilnezte, dezentrale Energieerzeugung, Photovoltaikanlagen, erneuerbare Energiequellen, *LINK*-Solution, Customer Plant, Lastflussberechnugen, Spannungsfluktuationen, Leistungsflussumkehr, Spannungsprofile, Spannungsregelung, *Q(U)*-Regelung, konzentrierte Lastcharakteristik

Contents

1 Introduction

The introductory chapter is intended to familiarize the reader with the concept of distributed generation (DG) and its effects on the low voltage (LV) and especially medium voltage (MV) distribution grids. Furthermore, it presents the importance of proper modelling of distribution grids, focusing on grids' behaviour in extreme load/production scenarios. At the end, information about how this thesis is organized is provided in this chapter as well.

1.1 Background

Historically, electric power systems were originally developed as the vertically integrated centralized system, following the "top-down" approach, where large quantities of electricity with unidirectional power flows were delivered to end-consumers.

In recent years governments started paying more attention to the effects that electric power system has on the environment. Consequently, various EU energy policies have been defined in last 30 years, most recent being "2030 Climate and Energy Framework" adopted by the European Council in October 2014 [1]. The main goals of EU energy policies are to reduce the greenhouse gas emission, increase the energy efficiency and enlarge the portion of energy production with renewable energy sources (RES). Due to its decentralised nature and environmental impact, DG based on RES can significantly contribute to fulfilment of all aforementioned objectives.

DG offers concrete benefits to the electric power system concerning the security of supply and the system efficiency. It decreases the fossil fuel consumption and power system losses. Although DG brings a lot of advantages to an entire electric power system, many years need to pass before produced electric energy from DG surpasses the amount of electric energy originating from centralized generation.

By increasing the presence of DGs that are primarily based on RES, numerous technical issues within the entire electric power system can emerge, e.g. quality of power supply, system stability and protection issues as well. One possible solution in mitigating or fully eliminating those issues is the integration of DGs with ability to offer reactive power support, voltage control or any other ancillary service to the Distribution System Operator (DSO).

1.2 Motivation

The large-scale integration of DG provokes in many cases a reverse power flow, which can cause the violation of the upper voltage limit. Therefore, DSOs are obliged to take countermeasures to avoid this kind of violation. DG inverters, mostly PV inverters, can be used as a voltage control strategy in the medium and low voltage radial distribution grids. $Q(U)$ is one of the most popular local control strategies used almost exclusively in low voltage level. It aggravates an uncontrolled reactive power flow on the superordinate medium voltage grid. During the power flow calculations in medium voltage grid, this exchanged reactive power is not considered in the lumped model of the low voltage grid. This can lead to the significant inaccuracy of the model, especially in case of the high PV penetration level in low voltage grid.

1.3 Scope

The analysis and the power flow simulations in this work are performed on medium and low voltage distribution grids.

1.4 Objectives

One of the possible approaches to assess the impacts of the increased penetration level of DGs to distribution grid's performance is to compare specific situation when the grid is stressed out the most. Targeting the moments when a high level of DG integration with a low load power demand on one side, and no DG production with a high load power demand on the other side is expected, this thesis focuses on the following objectives:

- To define and compare different lumped load models of LV distribution grids, which are vital for the proper modelling of MV distribution grids
- To examine the behaviour of the LV and especially MV distribution grids in regard to its voltage profile, grid losses and reactive power exchange with the overlaid grid.

1.5 Thesis Structure

Chapter 2 lays out the historical development of the European electric power grid in terms of various technical, structural and operational changes. Furthermore, it introduces a relatively new concept of distributed generation and possible solutions in mitigating its effects on distribution grids. Chapter 3 describes the LV and MV Link_Grids that have been used in the course of this master thesis. The exact modelling of the most important grids' components is shown in Chapter 4. Chapter 5 highlights different load and production scenarios of the corresponding LV and MV Link_Grids. Chapter 6 explains the required power flow simulations and calculation procedures. The gathered results, which are needed for better comprehension of distribution grids' behaviour, are analysed in Chapter 7. Finally, Chapter 8 ties up various findings and conclusions that were drawn upon the entire thesis.

2 Theoretical Background

Section 2.1 describes the basic structure of the European and especially the Austrian electric power system. This section should give an answer how and why the concept of electric power system has evolved in last 150 years. Further, it introduces the *LINK*-Solution, a possible answer to challenges that come with extensive integration of Renewable energy distributed generation into today's infrastructure. Section 2.2 gives a closer look on distributed generation, namely its definition and classification. Lastly, Section 2.3 describes behaviour of distribution grids in terms of voltage dropping and voltage control.

2.1 Electric Power Systems in Europe

Electric power systems have been operating for the last 100 years using the same fundamental principles. So far, technology has allowed an improvement of their performance, but it has not revolutionized the basic principles. Perhaps the most important, and unique, feature of an electric power system is that electric energy cannot be easily and conveniently stored in large quantities [6]. Although some energy is naturally stored in the inertia of large generators, this is only enough to compensate small unbalances, which continuously occur and cause small variations of frequency and voltage, while still remaining within rather restrictive limits [7]. This means that at any time the energy demand has to be met by corresponding generation.

2.1.1 Structure of Electric Power Systems

Despite the constant evolution of an electric power system that will be discussed later on, electric power system In Europe can be divided into three main groups [7]: generation, transmission and distribution of electric energy. Structure of European electric power system is illustrated in Figure 2.1. According to some sources, sub transmission of electric energy can be viewed as a fourth group. In reality, it can be considered as a subset of transmission, since voltage levels are overlapping and the way they are operated and protected is quite similar [8].

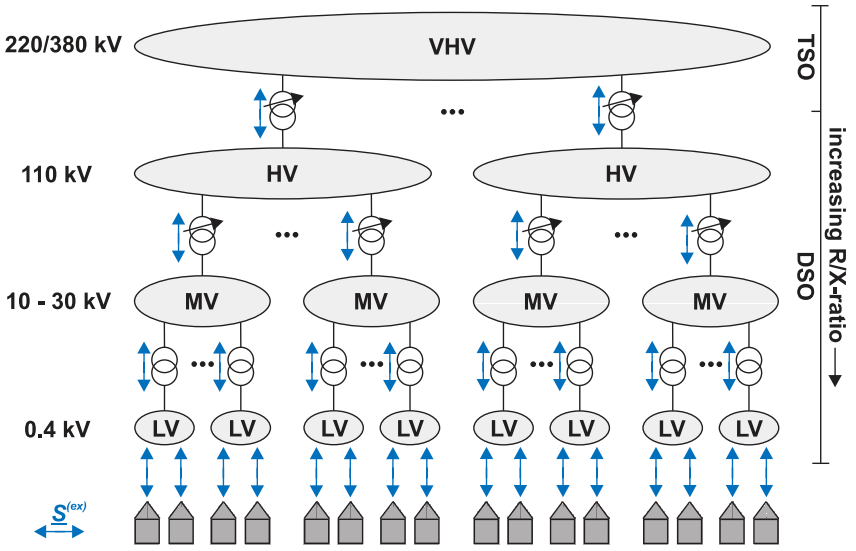

Figure 2.1 - Structure of European electric power system [9]

A. Generation

Generation of electric energy represents the backbone of our electric power system. Energy produced by burning coal, oil and gas, by falling water, by nuclear reaction, or by any other primary resource, is converted through various methods into electric energy, which is illustrated in Figure 2.2. Electric generators in thermal plants are driven by steam or gas turbines, or by water turbines in the case of hydropower plants. There are also some other methods, that are already or may become a big part of energy production. These alternative methods include solar cells, geothermal systems, wind-powered systems, magneto hydrodynamic (MHD) systems, nuclear fusion systems, and fuel cells [10]. Voltage levels at conventional power plants are typically 10-20 kV. By using generator step-up transformers, these voltage levels can be transformed to the appropriate transmission voltage levels.

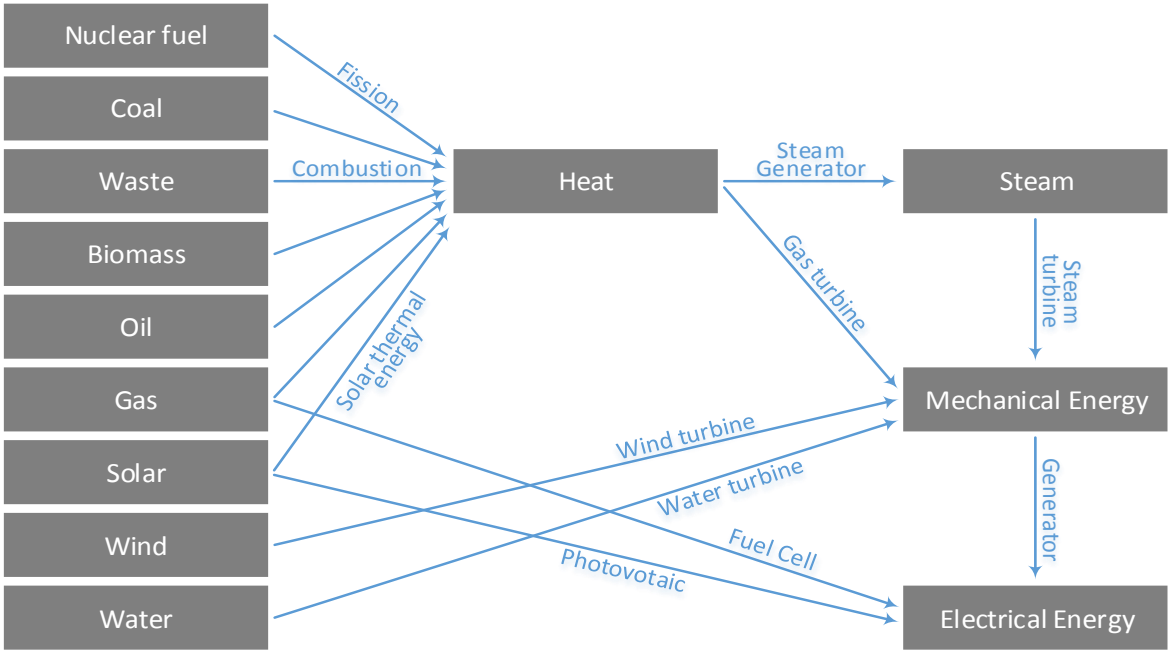

Figure 2.2 - Different technologies for conversion into electrical energy [11]

B. Transmission

Transmission of electric power is the bulk transport of electric power through interconnected systems, more known as transmission grids, from generation cites to distribution grids. Transmission grids, which consist of transmission lines, operate at different voltage levels: high voltage HV 110 kV (subtransmission) and extra-high voltage EHV 220 kV, 380 kV and 750 kV. Transmission transformers connect different parts of the transmission and subtransmission grids operating at different voltage levels, supply distribution grids and connect large industrial consumers directly to the transmission grids [6]. Generally, the EHV/HV transformers have on-load tap changers for regulating the transformation ratio. Transmission lines need to operate at these higher voltage levels, in order to minimize the power losses, which are proportional to I^2. If a lower operating voltage level for the same amount of transported power had been chosen, the current through the lines would have been bigger. Thus, the power losses would have also been bigger. Normally, transmission lines are overhead lines, due to their higher transmission capacity and lower costs when compared to underground cables. They are used in populated areas, underwater, or anywhere where overhead lines can't be used. Usually, the transmission grid has a robust, meshed structure in order to provide many possible routes for electric power flow, thereby improving the flexibility and reliability of the system [6]. The basic design

of the transmission grid is determined by the total amount of electric power and the distance over which electric power has to be transported.

Figure 2.3 shows that the nominal system voltage gets higher, as the distance and the transported electric power get higher.

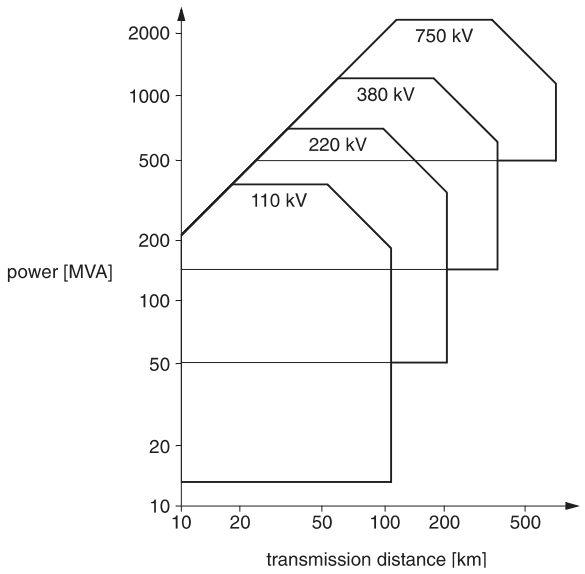

Figure 2.3 - Power and voltage dependence from transmission distance [12]

C. Distribution

Distribution of electric energy is the final stage in the delivery of electric energy to end-users. Design of the distribution systems is influenced by several factors, such as the need to supply costumers adequately and efficiently, the need to create a system that can be operated safely and the need to select the most economical choice. Distribution of electric energy starts in substations, where the electric power is transferred from the (sub)transmission grids to medium voltage MV distribution grids. The substations are equipped with HV/MV step-down transformers, which decrease the operating voltage of 110 kV to 30 kV, 20kV or 10kV. Further, protection equipment is also installed together with the circuit breakers and disconnectors that perform the switching operations. The MV distribution grids are mostly radial structure. The advantages of this simple topology, such as low capital investment cost, simple operation and protection equipment have to be compared with the disadvantage that, in case of failure of lines, the faulted lines cannot be used for electric power supply until they are repaired or replaced. Although the purpose of MV distribution grids is to forward electric power to low voltage LV distribution grids, MV distribution grids can directly supply some larger industrial and commercial customers. LV distribution grids deliver electric power to the different residential, industrial or commercial customers from MV/LV distribution transformers, which lower the operating voltage level to 400 V. They can be located in substations, along overhead lines or under/on the ground in case of (under)ground cables. As in case of MV distribution grid, LV distribution grids typically have a radial structure as well.

2.1.2 Development of Electric Power Systems

In last 150 years, the European electric power systems have experienced various technical, structural and operational changes. Those changes influenced the establishment of different eras, which are illustrated in Figure 2.4.

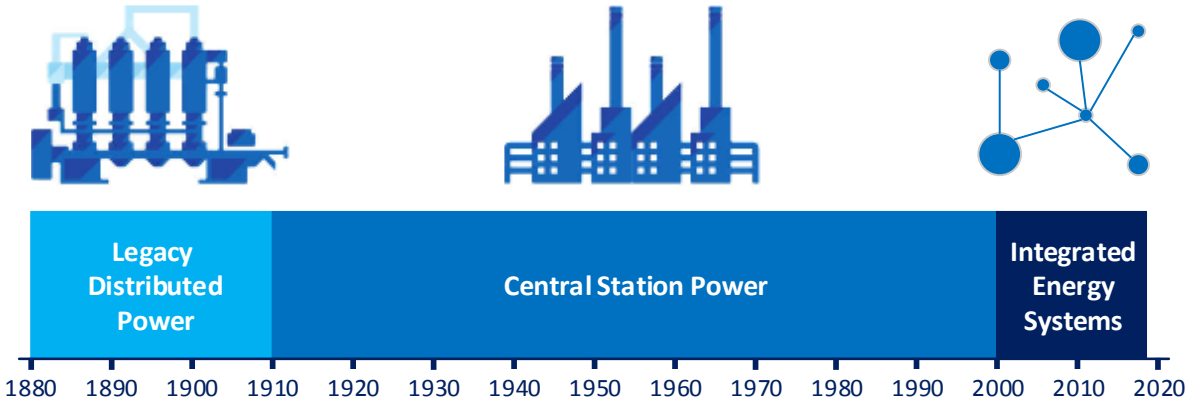

Figure 2.4 - Development of electric power systems [13]

The following text describes three different eras: Legacy Distributed Power, Central Station Power and Integrated Energy Systems. As it can be seen from the figure above, we are currently in the era of the Integrated Energy Systems. The following text describes the most relevant facts and characteristics about each era, with emphasis on the main differences regarding generation, transmission, distribution and finally utilization of electric energy between Central Station Power and Integrated Energy Systems era. It also includes the undergoing transformation of the Integrated Energy Systems era.

A. Legacy Distributed Power Era

Legacy Distributed Power era didn't last long, it began in 1880 and ended in 1910. Distributed Generation (DG), described in detail later on in Section 2.2, has emerged as a new type of generation of electric energy. First coal-fired power stations, Pearl Street Station in Manhattan and Holborn Viaduct Station in London, both constructed in 1882 by Thomas Edison's company, can be viewed as the beginning points of this era. This era was dominated by small-distributed power plants that provided electricity to local customers through DC power lines. In 1910, distributed power plants were accounted for 100% of global electric capacity additions. The biggest disadvantage with the Edison direct current system was that it ran at 110 volts from generation to its final destination giving it a relatively short useful transmission range, due to higher transmission losses. With the development of transformers in Europe and by Westinghouse Electric in the US in 1885–1886, it became possible to transmit AC long distances over thinner and cheaper wires with less power losses, and to step down the voltage at the destination for distribution to users [14]. At the end of the 19th century, the AC electricity supply system, created by Nikola Tesla, won the "War of the currents" over the Edison's DC electricity supply system. The first transmission of three-phase AC using high voltage took place in 1891 during the International electricity exhibition in Frankfurt. A 25-kV transmission line, approximately 175 km long, connected Lauffen am Neckar and Frankfurt [15]. Additionally, steam turbines experienced a high degree of innovation [13]. At the turn of the 20th century, these technology innovations cemented the movement to a new era of electric power systems, more known as the Central Station Power era.

B. Central Station Power Era

Central station power era lasted from 1910 until 2000. By correctly selecting system frequency, lightning, motor and other loads could be properly served. Rotary converters and mercury-arc valves, invented by Peter Cooper Hewitt at the beginning of the 20th century, provided DC power where it was needed. Remote and low-cost sources of energy, such as hydroelectric power or coal, could be exploited to lower energy production cost. By using this kind of generating plants for every type of load, lower overall capital investments and important economies of scale were achieved and load factor on each plant was increased, allowing for higher efficiency and a lower cost for the costumer, resulting in increased electric power consumption. Reliability was improved by the fact that the standby generating capacity could be shared over many more customers and a wider geographic area. Operating at voltage levels higher than 70 kV, 55 transmission grids were in service by the begin of 1914, with the highest one being the 150 kV. The rapid industrialization in the 20th century made electrical transmission lines and grids a critical part of the infrastructure in most industrialized nations. Interconnection of local generation plants and small distribution networks was greatly spurred by the requirements of WWI and WWII, where large generating plants were built by governments to provide power to munitions factories [15]. After WWII, electrification was brought to the other parts of Europe that at that point were without it. Distributed power technologies accounted for less than 10% of global electric capacity additions. Distributed power was used as backup generators and in transportation applications [13].

Until the liberalization process of electric energy sector that began in the last decade of the 20th century, electric power systems in Europe were dominated by large utilities that can be viewed as a "vertically integrated systems". These utilities had exclusive rights within a certain geographical area to handle all operations in regard to generation, transmission and in some cases distribution of electric energy as well. Normally, each country had only one such utility. The operation and coordination of such a system was very simple. Generation stayed centralized, i.e. it occurred in large-scale power stations, near to the available primary resources and far away from the energy consumption. Conventional thermal plants and hydropower plants were some of the most common power stations. Additionally, nuclear power plants emerged as a cheap way of generating electric power. More transmission grids with higher voltage levels of 220 kV, 380 kV and even in some cases 750 kV were constructed in order to cut power losses. To maximize supply reliability, i.e. minimize power outages, interconnection between national transmission grids continued. Distribution grids were designed under the "fit and forget" approach. In this approach, distribution grids were dimensioned based on historical demand patterns, after which they are not regularly monitored to determine whether they are either under- or over-designed [16]. They can be viewed as the "passive" grids, due to the fact that their main purpose is to forward electric energy down to the customers. Customers can be recognized exclusively as consumers without any automated or "smart" consumption of electric energy. The overview of electric power system in this era is illustrated in Figure 2.5.

The power flow is unidirectional, what means that electric energy, generated in power stations, is delivered through transmission and distribution grids to the costumers. This implicates further that the electric power system is operated "vertically". The bidirectional information flow exists only between generation and transmission.

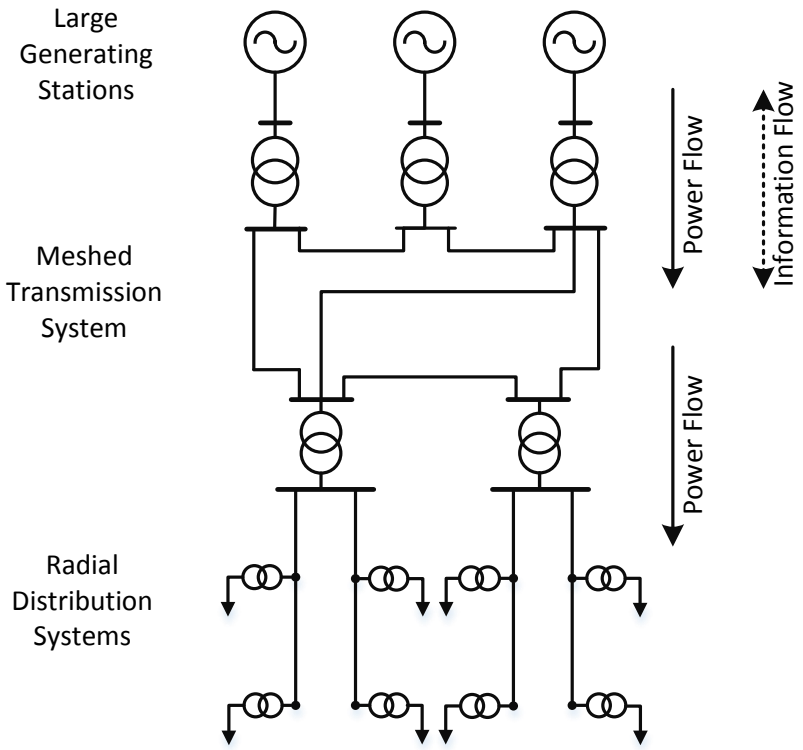

Figure 2.5 - Electric power system in the Central Station Power era [17]

This concept raises many challenges. The most essential are environment pollution induced by producing the electric energy in not environment-friendly power plants and high investment costs of the infrastructure (new power plants, new transmission lines, etc.). In addition, centralized generation cannot answer to fast changes in energy demand, due to the large inertia of installed generators and the slow dynamics of non-electrical actuators (e.g. fuel injection). Because of all of these reasons, switch to a new era was needed.

C. Integrated Energy Systems Era

Contrary to both first eras, which were characterized only by a gradual and progressive technical evolution [18], the era of Integrated Energy Systems is additionally characterized by a turbulent restructuring of the electricity sector. This era began in 2000 and its transition can be unfolded in two phases.

The first transition phase started under the influence of the electricity market liberalization. The aim of liberalization, which can be described as a revolutionary process, was to create a competitive electricity market in order to increase economic efficiency and reduce the role of the state. With technological advances in electric power generation and transmission, the reform of the electricity sector became possible and unavoidable. Although the first draft of the Electricity Directive was issued in 1992 with clearly stated principles of free electricity trade between member states and third-party network access, it was not until 1996 when the first Electricity Directive 96/92/EC2 was passed. It created the necessary preconditions for the fully liberalization of the electricity sector within the EU and the abandoning of the idea of national sovereignty over electrical energy. The Directive 96/92/EC also required the unbundling of previously vertically integrated monopolistic companies and the creation of new market participants, namely Transmission System Operators (TSOs) and Distribution System Operators (DSOs). The Electricity Directive 2009/72/EC introduced three possible solutions for the TSO's unbundling: full ownership unbundling, independent system operator (ISO) and independent

transmission operator (ITO) [19]. The other relevant EU Directives and Regulations that guided the liberalization of electricity market can be found in Appendix C. On 19th December 2008, the European Network of Transmission System Operators (ENTSO-E) was established to promote the implementation of EU energy policies and to support achieving Europe's energy & climate policy objectives and goals. It represents 43 TSOs from 36 countries across Europe, thus including countries beyond EU borders [20]. Distribution system operator must be legally and organizationally independent from other activities within the vertically integrated company, while ownership separation has not yet been conditioned. The competition in generation activities was brought in either through the creation of power pools, provision for direct bilateral transactions or bidding in the spot markets. In terms of retail competition, the electricity consumers got the opportunity to choose or change their suppliers.

The second phase of the Integrated Energy Systems era, which is currently active, was stimulated by the recurring rise of the small-scale distributed power systems. In this modern concept, distributed generation that mostly uses renewable energy sources (RES), such as sun, wind, water etc. for end-conversion into electric energy, is trying to overshadow the large-scale central generation of electric energy. Although DG has a lot of advantages, centralized generation Is still dominating in amount of produced electric energy. The implementation of DG transforms the "passive" distribution grids into an "active" one. By generating electric energy themselves, customers are not anymore only consumers, rather they can be viewed as "Prosumers". If their local production surpasses their demand on electric energy, customers can inject electric energy into the distribution grids, what further leads to reversed power flows. In this way, "vertically" operated electric power system is transforming into "horizontally" operated, which means that electric power can be transferred from one MV or LV distribution grid to another and from distributed generators directly to loads within the same MV or LV distribution grid. Therefore, MV and LV distribution grids can no longer be considered as grids with unidirectional power flow, which was a base for traditional design of distribution grids. A brief overview of current electric power system can be seen in Figure 2.6. Unlike the situation in the previous era, where the information flow existed also between transmission and generation, information data are interchanged between transmission and distribution grids as well. The MV distribution grids have marginal number of real-time measurements and are equipped in small degree with intelligent software. On the other hand, the LV distribution grids have no real-time measurements and no intelligent software.

The bidirectional power flow raises many challenges in grid operations, such as frequency and voltage stability, power flow optimization, etc. In the future, the grid operators will need to change their way of thinking. They'll have to adjust or totally change their control and protection strategies. The number of the real-time measurements in MV grids should increase. By using the intelligent software, a full monitoring of the MV and LV grids will be enabled. Smart meters should substitute the traditional meters entirely. Different storage technologies (e.g. batteries, flywheel or compressed air energy storage) that are currently in development process should increase the balancing capacity of electric power system [18].

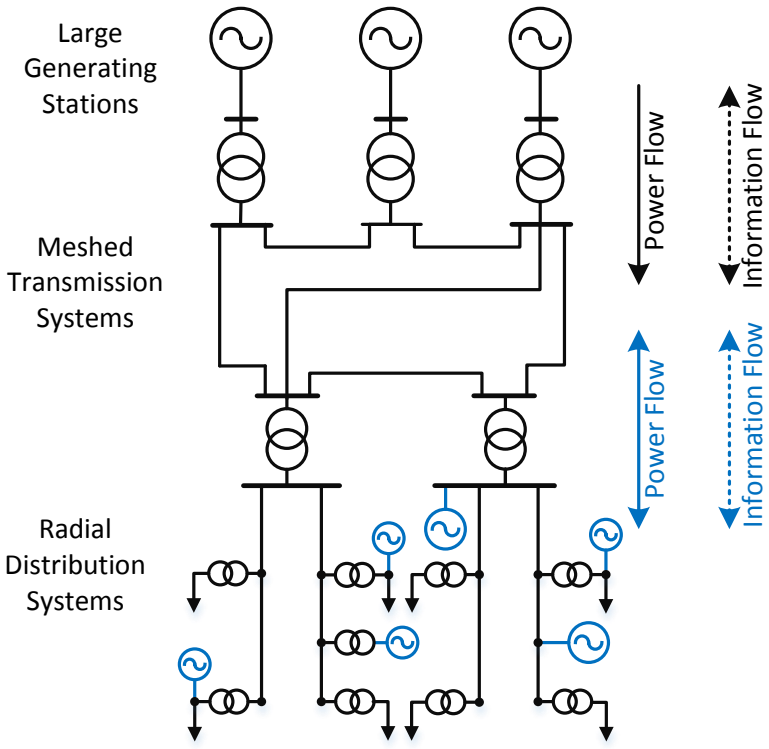

Figure 2.6 - Electric power system in the Integrated Energy Systems era [17]

2.1.3 The Austrian Experience

Following up the previous subsection, the Austrian experience shows the current structure and the historical development of the Austrian electric power system. It explains especially how the tree main groups of an electric power system, namely generation, transmission and distribution, have changed during the electric market liberalization period. Finally, it describes the growth of an electric energy consumption in the last 30 years.

A. Structure

Today, the main legal document for Austrian electricity sector is the Federal Electricity Management and Organisation Act 2010 (Elektrizitätswirtschafts- und organisationsgesetz EIWOG 2010), that regulates rights and duties of the market participants and especially their obligations to the consumers. Other relevant acts providing regulations on electricity on a federal level can be found in Appendix B. The main objectives [21] of the EIWOG 2010 are given down below:

- Provision of low-priced high-quality electricity to the Austrian population and economy;
- Establishment of a market organisation in accordance with European law;
- Use of the potential of power-heat coupling to save energy and provide sustainable security of supply;
- Implementation of a legal framework assuring sustainable security of network operation and supply;
- Further development of electricity generation from renewable resources;
- Safeguarding of network accessibility for electricity generation from renewable resources; and
- Imposition of public service obligations on electricity undertakings.

The Austrian power system, like any other, is designed to meet reliability requirements at all voltage levels taking into consideration circumstances related to its geographical position and the limitation that it imposes in their interconnection capability. This is reflected in the established grid structures at the different voltage levels, which are listed down below [11], and provides a solid basis for integration of DG.

- Level 1: EHV Transmission Grid, 380 kV or 220 kV
- Level 2: EHV/HV Substations
- Level 3: HV Distribution Grid, 110 kV
- Level 4: HV/MV Substations
- Level 5: MV Distribution Grid, 10-30 kV
- Level 6: MV/LV Substations
- Level 7: LV Distribution Grid, 400 V or 230 V

Table 2.1 shows the length of the public grid and its overhead lines and cables at different voltage levels, as well as their total length combined at the end of 2017.

Table 2.1 - Length of the public grid at year-end 2017

Voltage Level	***Overhead lines***		***Cables***		***Total***	
	[km]	[%]	[km]	[%]	[km]	[%]
380 kV	1 383	0,5	53	0,0	1 436	0,5
220 kV	1 880	0,8	6	0,0	1 886	0,8
110 kV	6 085	2,6	605	0,3	6 690	2,9
1 kV *to* 110 kV	24 840	10,5	40 035	16,9	64 876	27,4
Up to 1 kV	31 386	13,2	130 912	55,2	162 298	68,4
Total	**65 574**	**27,6**	**171 612**	**72,4**	**237 186**	**100**

Number of transformers and their total capacity in EHV/HV. HV/MV and MV/LV substations are represented in Table 2.2.

Table 2.2 - Number of transformers and their total capacity at different voltage levels

Voltage Level	***Number of transformers***	***Total capacity*** [MVA]
EHV/HV	88	30 675
HV/MV	1 028	43 138
MV/LV	78 953	31 694
Total	**79 645**	**104 054**

B. Generation

The Austrian electricity generation has historically grown as a composite system of hydro and thermal power plants. From the 1950s an intensive expansion of hydropower plants took place, accompanied by the construction of calorific power plants, in which above all coal and natural gas were used for generation of electricity. Based on a Ministerial Council decision in 1969, the first nuclear power plant was built in Zwentendorf (Lower Austria), but was not put into operation after a referendum in 1978. The Austria's refusal to use nuclear power ultimately resulted in the Federal act on the prohibition of the use of nuclear fission for the energy supply in Austria 1978. The Federal Constitutional Act for a Nuclear-Free Austria 1999 was motivated subsequently by the nuclear catastrophe of Chernobyl in

1986. Since the nuclear catastrophe of Fukushima in 2011 far more political and social agreement on the rejection of nuclear power has been prevailing. The power supply was based until the 1990s almost exclusively on the combination of hydro and thermal power. The graph in Figure 2.7 illustrates how the production of electric energy, including its domestic consumption, has been developing from 1990 until now.

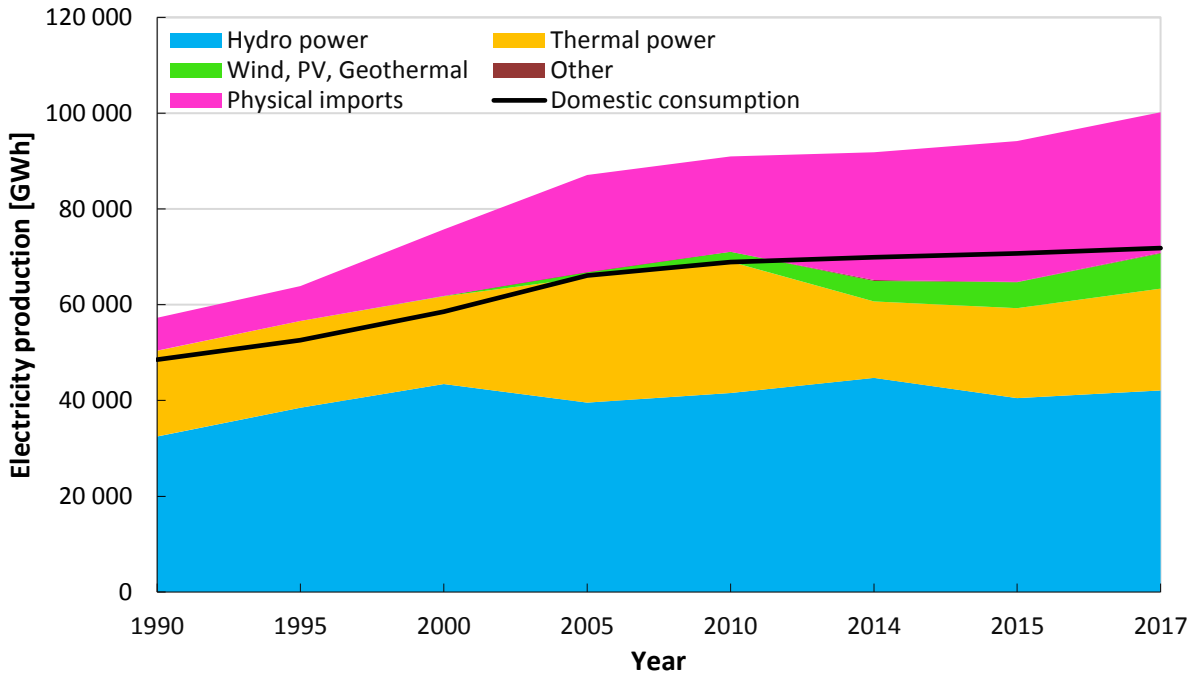

Figure 2.7 - Production and domestic consumption of electricity in Austria from 1990 to 2017 [22]

Until the liberalisation of the Austrian electricity market in October 2001, which was based on the European Union (EU) electricity directives and regulations, the electricity sector followed up post-war policy: public utilities participated on the Austrian electricity market and prices were regulated by the state [21]. From 2001 onwards, Austria began trading electricity with other European countries as well. The balancing of electricity supply and demand across the national borders subsequently led to reduction of domestic electricity production from thermal power plants in favour of electricity import. Austria switched from net electricity exporter to net electricity importer, which stands today as well. Further, from the year 2000, there was an expending electricity generation from the "new renewables", i.e. wind power, photovoltaic and geothermal power.

With the Green Electricity Act 2003 started the first significant upswing of the photovoltaic market. In 2013, a record increase in installing new PV capacities was triggered by the dramatic support of the state. In the following years, annual expansion rate was between 150 and 160 MWp, which can be seen in Figure 2.8. In 2017 it was recorded a total output of 172,479 MWp, which corresponds to an increase of 11% compared to 2016. At the end of 2017, this led to a cumulative total output of all PV systems of around 1269 MWp.

The gross production of electric energy in Austria during 2017 is represented in Appendix C, in Table C.1. It shows the values for different subcategories of thermal, hydro and renewable power plants. A value of generation where the origin cannot be linked to any of the typical power plants is also given. Almost 60% of whole production came from hydropower plants. The second biggest share with 30% makes electricity production in thermal power plants. The share of renewables, i.e. wind, PV and geothermal is approximately 10%, which as the years go by should only be increasing.

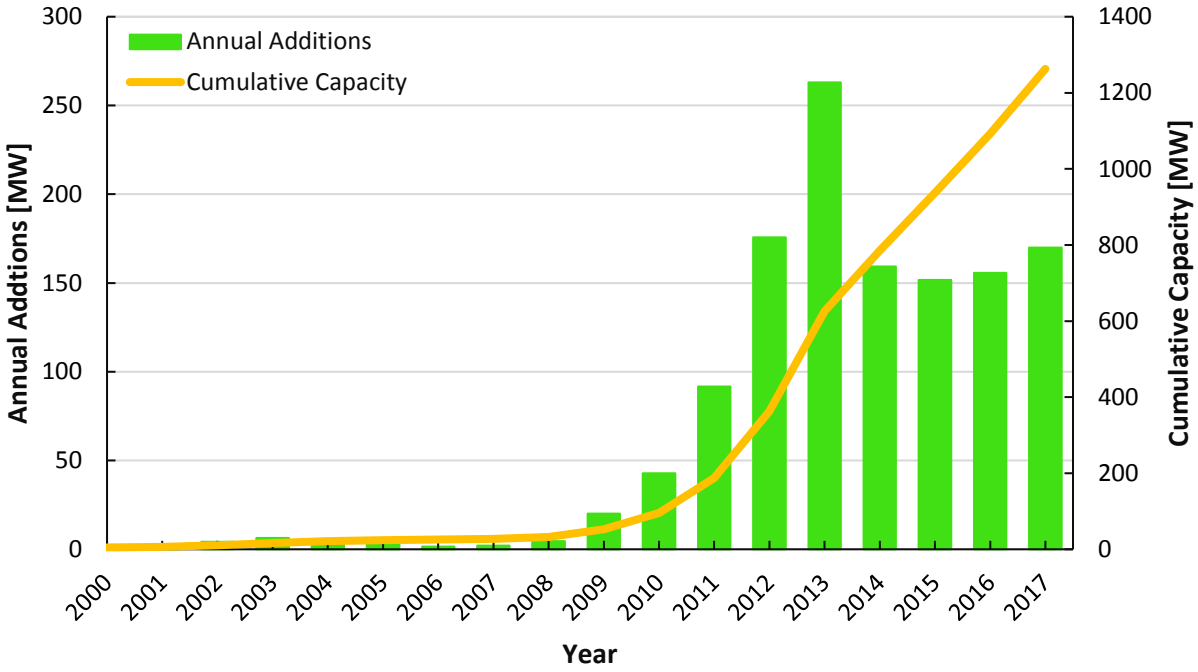

Figure 2.8 - Development of photovoltaic capacity in Austria until 2017

C. Transmission

The Austrian transmission grid is generally separated into three different control areas: East, Tyrol and Vorarlberg. Austrian Power Grid (APG), a certified Independent Transmission Operator (ITO) and the main Control Area Manager (CAM), operates and controls East region. Since 2011 APG has operated the transmission grid in Tyrol, but the grid itself is still in property of Tiroler Wasserkraft AG - TIWAG [23]. Up until 31.12.2011, the transmission grid in Vorarlberg, owned by Vorarlberger Übertragungsnetz GmbH (VUEN), was part of the German control block. As of 01.01.2012, APG and VUEN have negotiated a cooperation regarding the operation of control area. Vorarlberg control area was integrated into the control block Austria, under the management of APG [24]. From that point forward APG have remained a sole CAM in whole Austria.

Approved by E-Control Austria, APG's Network Development Plan (NDP) 2017 [25] is based on the long-term strategic planning in APG's Masterplan 2030 and NDP 2016, as well as the Ten Year NDP from ENTSO-E. It presents the plans for the transmission system in Austria for the next ten years. The extensive grid reinforcement and expansion projects in NDP 2017 will have to be implemented by 2027. They include following projects:

- New transmission line projects extending over approximately 220 km
- Conversion of 100 km of transmission lines to a higher voltage level
- Reinforcement and reconstruction of 400 km of existing transmission lines
- Construction and expansion of numerous substations with approximately 140 switch bays at voltage levels of 380/220/110 kV
- Construction of approximately 30 transformers with a total capacity of approx. 10,500 MVA
- Extensive line coordination and optimisation measures are being implemented within the framework of major projects, e.g. the 380-kV Salzburg line (construction of new lines over approximately 128 km), leading to the removal of ca. 400 km old, low-capacity lines
- Furthermore, extensive reinforcement measures of substations and lines are planned

Figure 2.9 illustrates various parts of Austria, where these projects are already or will be taking place.

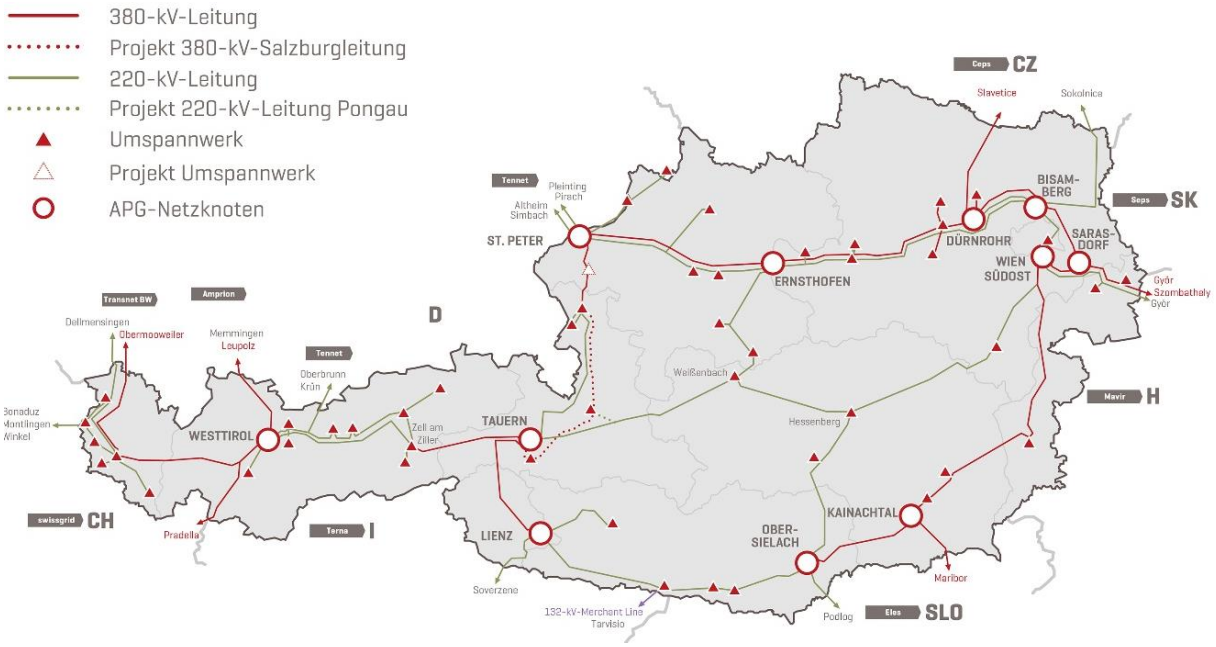

Figure 2.9 - Projects according to APG's Network Development Plan 2017 [25]

D. Distribution

The Austrian distribution grids at HV, MV and LV levels are overseen by more than 140 distribution system operators. Some of the main distribution system operators in Austria are Wien Energie GmbH, Energieversorgung Niederösterreich (EVN) AG, Linz Strom GmbH, Salzburg Netz GmbH and Kärntner Elektrizitäts-Aktiengesellschaft (KELAG). In order to operate a distribution grid, DSO requires a concession, which has to be granted under conditions set out in the respective electricity acts of the nine federal states (Burgenland, Carinthia, Lower Austria, Salzburg, Styria, Tyrol, Upper Austria, Vienna and Vorarlberg) [26]. Consumers may not switch their DSOs, as the place of residence determines the competent DSO. Throughout history, DSOs have shown very good and close cooperation with TSO in processes like grid restoration, grid planning, setting the tap positions in transformers, etc. According to the study from the International Council on Large Electric Systems (CIGRE)[1] [27] about electric power system in Austria more data and know-how should be exchanged between DSOs and TSO, so that this cooperation could be brought on more proficient level. Some of the future challenges for DSOs, as well as for TSO, in Austria are:

- Renewable integration
- Congestion management
- Neutral market facilitator

E. Consumption

The Austrian electricity consumption has increased about with a growth rate of 1,2% per year in the last twenty-five years. The strongest increases are recorded in manufacturing and households' sectors. There was a slight decline in the services sector, while the agricultural sector remained to have a stable consumption [28]. In the period from 2010 to 2016, the increase in domestic consumption has been

[1] French: *Conseil International des Grands Réseaux Électriques*, *CIGRÉ*

significantly lower, as it can be seen in Figure 2.10. This is particularly due to measures at national and European level to maximize energy efficiency, which is the key of securing the future energy supply. Total consumption of electricity in 2017 compared to the previous years, had a significant leap, because Austria exported more energy than usually.

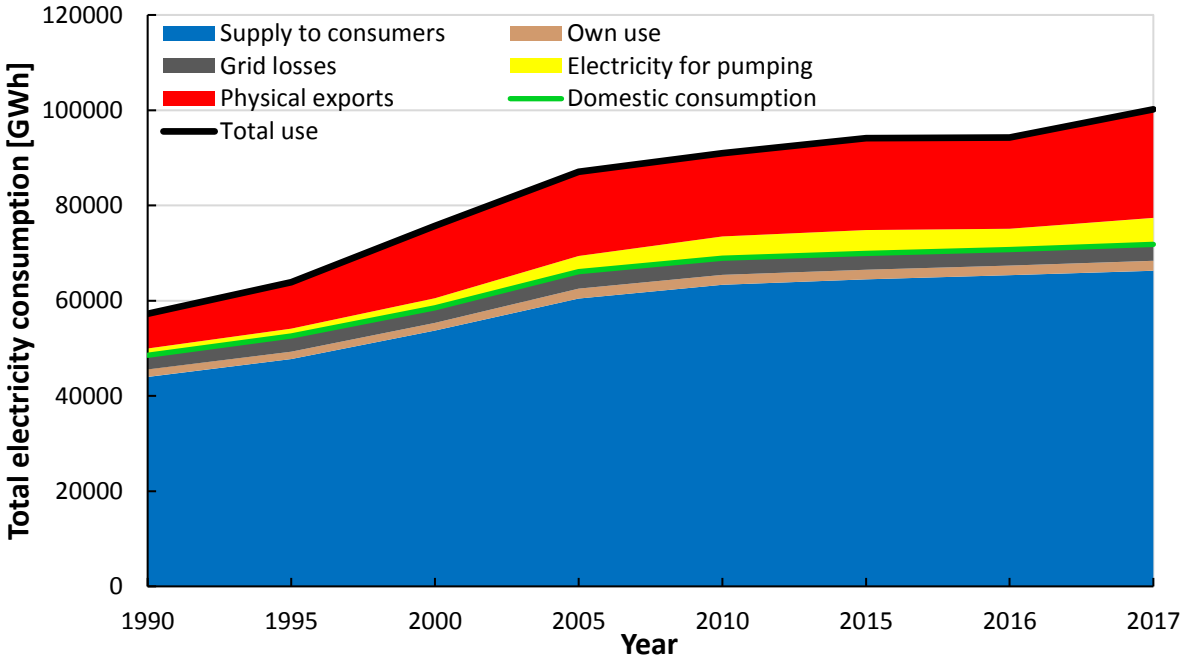

Figure 2.10 - Total consumption of electricity in Austria from 1990 to 2017 [22]

In 2017, different sectors in Austria consumed more than 66 000 GWh. The biggest share of consumed energy had fallen on the transportation sector, while the private households consumed almost 25%. Agricultural and service sector consumed about 2% and 10%, respectively. An average Austrian household consumes about 4,415 kWh of electrical energy per year. The heating (20,5%), large household appliances (17,4%), hot water (17,1%) and refrigeration (12,3%) account for the largest share of electricity consumption in one household. Lighting (8,6%) and office and entertainment equipment (7,0%) make up a significant portion of electricity consumption as well. The standby operations of household appliances use more than 4% of the total electrical energy per year [28].

2.1.4 The *LINK*-Solution

The design of the future power system architecture is still a work in progress, but it's generally characterized by large growth of sensors, communication, computation and control. Technical University of Vienna has been developing the *LINK,* a unique approach, that offers a complete solution to the more demanding and complex smart grids challenges and processes. *LINK*-Solution is developed based on the *LINK*-Paradigm and the unified *LINK*-based architecture. Some of the main benefits of the *LINK*-Solution are [29]:

- Guaranties secure and reliable power supply
- Vastly reduces the cyber-attacks danger from outside
- Keeps data privacy for end consumers and the grid
- Allows the decarbonisation of the power industry through the large-scale integration of decentralized energy resources
- Fully utilisation of existing infrastructures, thus postponing the capital expenditures

The *LINK*-Paradigm is based on the "Energy Supply Chain Net" model, which is defined as follows: 'An "Energy Supply Chain Net" is a set of automated power grids, intended for "Chain Links" or "Links", which fit into one another to establish a flexible and reliable electrical connection. Each individual "Link" or a "Link"-bundle operates independently and have contractual arrangements with other relevant boundary "Links", "Link"-bundles, and suppliers which inject directly to their own grid. Each "Link" or "Link"-bundle can communicate with the other relevant "Links" or "Link"-bundle's via the usual communication instruments' [30]. An overview of the power grid according to the "Energy Supply Chain Net" is represented in Figure 2.11 down below.

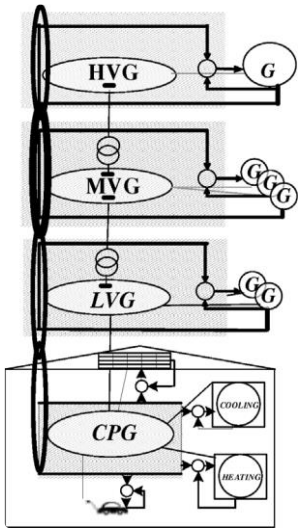

Figure 2.11 - An overview of the power grid according to "The Energy Supply Chain Net" [30]

As it can be seen from the figure above, two different axes can be identified. In the horizontal axis are set interconnected High Voltage Grids (HVGs), which are operated from the related TSO. On the other side, in the vertical axis are set Medium Voltage Grid (MVGs) and Low Voltage Grids (LVGs), which are operated from the corresponding DSOs [31].

The *LINK*-Paradigm is defined as a composition of an electrical appliance (be a grid part, producer or storage), the corresponding controlling schema and the Link interface [30]. Figure 2.12 gives an overview of the "Link"-Paradigm. Three different architecture components can be derived from the "Link"-paradigm: "Grid-Link", "Producer-Link" and "Storage-Link".

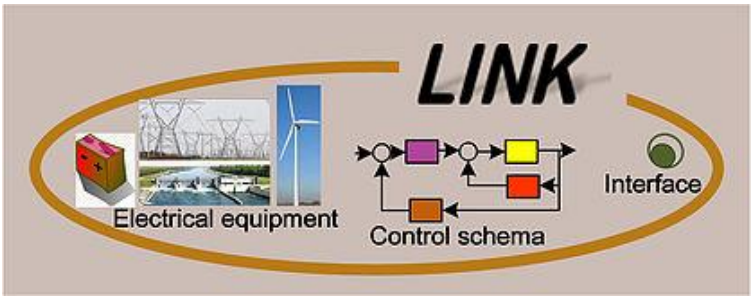

Figure 2.12 - An overview of the "Link"-paradigm [29]

Two different controlling methods can be used: primary or secondary control. Primary control refers to control actions that are done locally (power plant, device level) based on predefined setpoints. The actual measured values are compared to these setpoints. For example. any resulted deviation will influence a primary-controlled power plant or transformer. Respectively, the excitation current or

transformers steps have to be adjusted properly in such a way that the desired power or voltage is reached. Thus, the priority task is to bring back the frequency and the voltage back to the acceptable values. Secondary control is also done locally and refers to control actions that are calculated based on a control area and fulfil a predefined objective function. Additionally, the undesired effects derived from the unavoidable control errors of primary control has also to be compensated by secondary control. Only disturbances within its own control area are "seen" from the secondary controller.

The information, such as different frequency and voltage measurements, predefined P- and Q setpoints and dynamic load characteristics being exchanged trough interfaces between different "Grid-Links". This should provide a secure and reliable operation by means of load generation balance, static and dynamic security, and optimization processes for each "Grid-Link", "Producer-Link" and "Storage-Link".

A. Grid-Link

The "Grid-Link" or simplified just the "link" is defined as a composition of a grid part, called Link_Grid, with the corresponding secondary control and the Link_Interfaces. It operates as a single autonomous system and provides the required flexibility through the secondary control. The size of the Link_Grid is normally characterized by the area, where the Secondary-Control is embedded. The size of the area can differ in such a way, that the "link" can represent a Microgrid, Nanogrid or even some large high voltage grids (HVGs). The Link_Grid refers to electrical equipment like lines/cables, transformers and reactive power devices, which are connected directly to each other by forming an electrical unity. Each Link_Grid has a specific number of boundary nodes, which are used for connection with other neighbour Links directly connected Producer- and Storage-Links and loads that are supplied from the Link_Grid. These nodes are called Boundary Link Node (BLiN), Boundary Producer Node (BPN), Boundary Storage Node (BSN) and Boundary Load Node (BLoN), respectively. As per definition, the Link_Grid is upgraded with secondary control for both major entities of power systems frequency and voltage. Its algorithm needs to fulfil technical issues and calculate the set points by respecting the dynamic constraints which are necessary to enable a stable operation. Actually, Link_Grid own facilities, transformers and the reactive power devices are almost upgraded with primary/local control. Thus, the secondary control will send set points to own facilities and to all entities connected at the boundary nodes [30]. The Figure 2.13 illustrates three different types of the "link": medium voltage link (MVL), low voltage link (LVL) and customer plant link (CPL). They are based on size of the corresponding Link_Grids, namely MV, LV and CP Link_Grids, which have been used during this thesis.

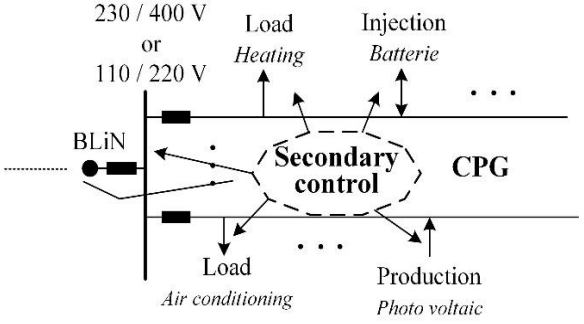

a) Customer Plant "Grid-Link" (CPL)

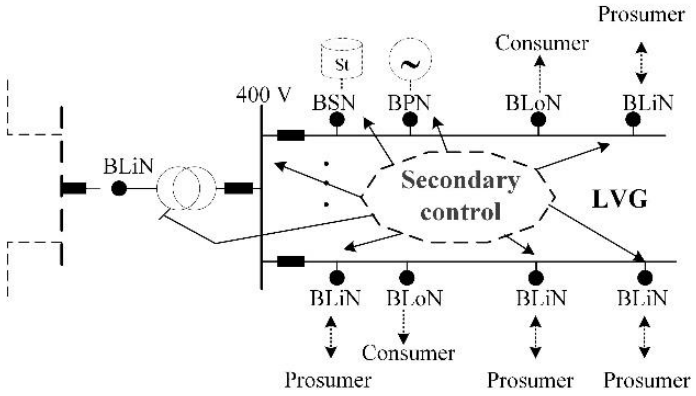

b) Low Voltage "Grid-Link" (LVL)

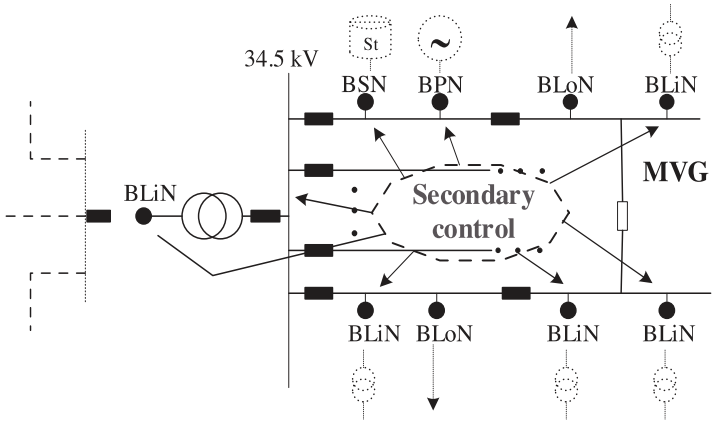

c) Medium Voltage "Grid-Link" (MVL)

Figure 2.13 - Three different types of the "Grid-Link": a) Customer Plant "Grid-Link" (CPL), b) Low Voltage "Grid-Link" (LVL) and c) Medium Voltage "Grid-Link" (MVL) [30]

B. Producer-Link

The "Producer-Link" is defined a composition of an electricity production facility, generator, photovoltaic, etc., its Primary-Control and the Producer_Interface. Each "Producer-Link" has a connection point with the Link_Grid through a BPN, where the electricity is being injected. Figure 2.14a illustrates the "Producer-Link".

C. Storage-Link

The "Storage-Link" is defined as a composition of a storage facility, generator of a pump power plant, batteries, etc., its Primary-Control and the Storage_Interface. Each "Storage-Link" has one boundary node BSN through which it is connected to the Link_Grid. Figure 2.14b illustrates the "Storage-Link".

a) b)

Figure 2.14 - a) The "Producer-Link" and b) The "Storage-Link" [30]

2.2 Distributed Generation

Due to technological innovations and change in economic and regulatory conditions in the last twenty-five years, attention for a small-scaled generation, commonly called distributed generation (DG), has risen. The following subsections focus on distributed generation, or more precisely how DG is defined and classified.

2.2.1 Definition of DG

The US Environmental Protection Agency (EPA) defines DG as following: 'a variety of technologies that generate electricity at or near where it will be used, such as solar panels and combined heat and power. Distributed generation may serve a single structure, such as a home or business, or it may be part of a microgrid (a smaller grid that is also tied into the larger electricity delivery system), such as at a major industrial facility, a military base, or a large college campus. When connected to the electric utility's lower voltage distribution lines, distributed generation can help support delivery of clean, reliable power to additional customers and reduce electricity losses along transmission and distribution lines' [32].

On the other hand, according to International Energy Agency (IEA), DG is 'generating plant serving a customer on-site or providing support to a distribution network, connected to the grid at distribution-level voltages. The technologies generally include engines, small (and micro) turbines, fuel cells, and photovoltaic systems. It generally excludes wind power, since that is mostly produced on wind farms rather than for on-site power requirements' [33].

2.2.2 Classification of DG

There have been a lot of uncertainties in trying to classify distributed generation systems. In the following, some of the possible criteria for dividing DG into different groups are going to be considered.

A. Output Power

The first and the most elementary classification is the type of generated power, which can be AC or DC. In terms of output power size, DG systems can be grouped into four different systems [34]:

- Micro (1W-5kW)
- Small (5kW-5MW)
- Medium (5MW-50MW)
- Large (50MW-300MW)

B. DG Technology

Regarding the types of technologies that can be used for the electric energy production in DG systems, a distinction can be made between Fuel-based, Renewable energy-based and Energy storage-based technologies [35]. Fuel-based DG systems normally use some kind of fossil fuel as an energy source, before all coal, gas or oil. Additionally, electrochemical energy can be used as fuel. Alternatively, renewable energy sources such as wind, solar, hydropower, geothermal etc. have found their use in Renewable energy-based DG systems. Various batteries have a broad appliance in Energy storage-based DG systems. The most important technologies, that are used in above mentioned DG systems, can be found down below.

Fuel-based DG

- Combustion engines
- Microturbines
- Diesel generators
- Biomass
- Fuel cells

Renewable energy-based DG

- Wind turbines
- Hydroelectric plants
- PV cell
- Geothermal Systems

Energy storage-based DG

- Magnetic Superconductors
- Large Capacitor Banks
- Compressed Air Storage
- Hydraulic Pump Storage

C. Grid Connection

In terms of how DG systems are connected to the grid, we have direct grid-connected and indirect grid-connected DG [17], [35].

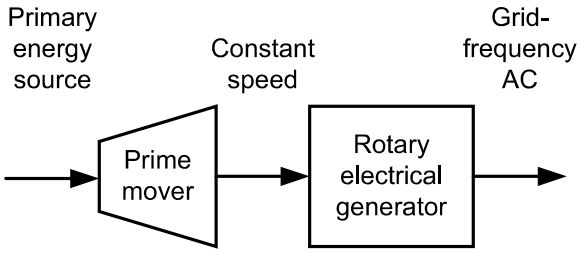

Figure 2.15 - Direct grid-connected DG [17]

Direct connection to the grid can be done by means of either a synchronous or an induction generator. By controlling the prime mover, so that it operates at a constant speed, synchronous generator can produce electric power at the 50 Hz grid-frequency[2], which further means, that direct coupling with the grid is possible (Figure 2.15). A synchronous generator is usually applied in steam turbines, gas turbines, big hydro-power plant and internal combustion engines. The only difference is in the energy source that drives the prime mover. Synchronisation with the grid and controlling the generator's excitation system are some of the biggest challenges.

An induction generator can be put to use in smaller hydropower plants or in smaller wind turbines of older design. Here the generator speed may vary with the turning force applied to it. Normally, a gearbox is used to connect the low-speed driving shaft to the high-speed generator shaft (Figure 2.16). One of the disadvantages of this type of generator include the possibility of working in motor mode. When the rotor speed is less than synchronous speed, current will be drawn from the grid.

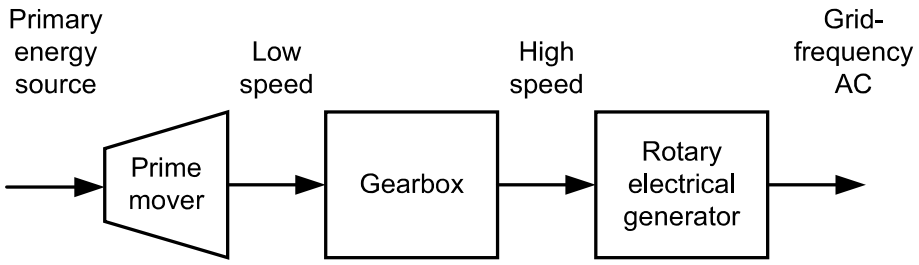

Figure 2.16 - Direct grid-connected DG with gearbox [17]

In cases where DG systems are indirectly connected to the grid, a sort of power electronic converter needs to be in between, so that the 50 Hz grid-frequency could be achieved.

[2] Electric Power System in Europe works with 50 Hz-frequency; in United States of America with 60 Hz

DGs with DC output (e.g. photovoltaic panels and fuel cells) are characterized by static electric generation, i.e. no rotating part are involved. Before converted to AC at the grid-frequency, DC output goes through a capacitor, which filters out the fluctuations. Figure 2.17 shows a typical layout of such a system.

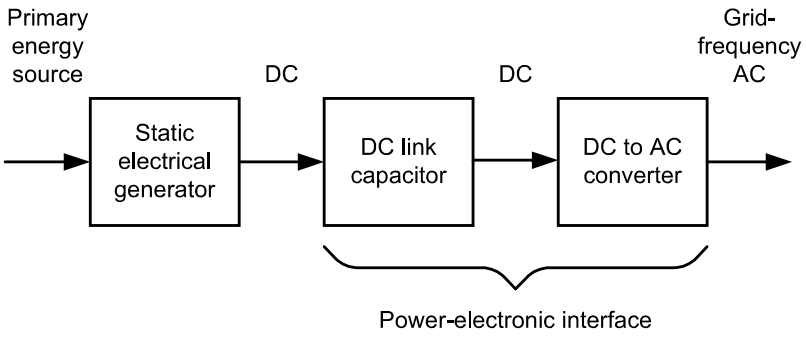

Figure 2.17 - Indirect grid-connected DG with DC output [17]

On the other hand, DGs with high-frequency AC electricity (e.g. microturbines) and variable-frequency AC electricity (e.g. some types of wind turbines) are equipped with an AC-AC converter, which consists of an AC-DC converter, a DC link capacitor and a DC-AC converter. Firstly, AC-DC converter rectifies the high-frequency AC signal or AC signal with variable frequency. A DC link capacitor is used for creating a smoother DC signal, before it is finally converted with a help of a DC-AC converter into grid-frequency AC signal. A layout of such a system is illustrated in Figure 2.18.

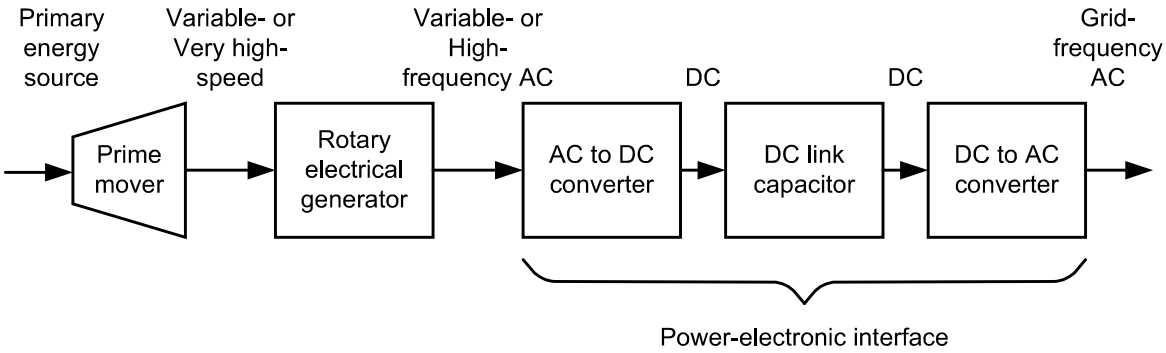

Figure 2.18 - Indirect grid-connected DG with AC output [17]

A special case of indirect connection to the grid represents an induction generator with variable speed which stator windings are directly connected to the grid, while its rotor windings are connected to bi-directional power electronic AC-AC converter. Independently of the mechanical rotor speed, the stator and rotor electrical frequency can be matched. A layout of such a system is represented in Figure 2.19.

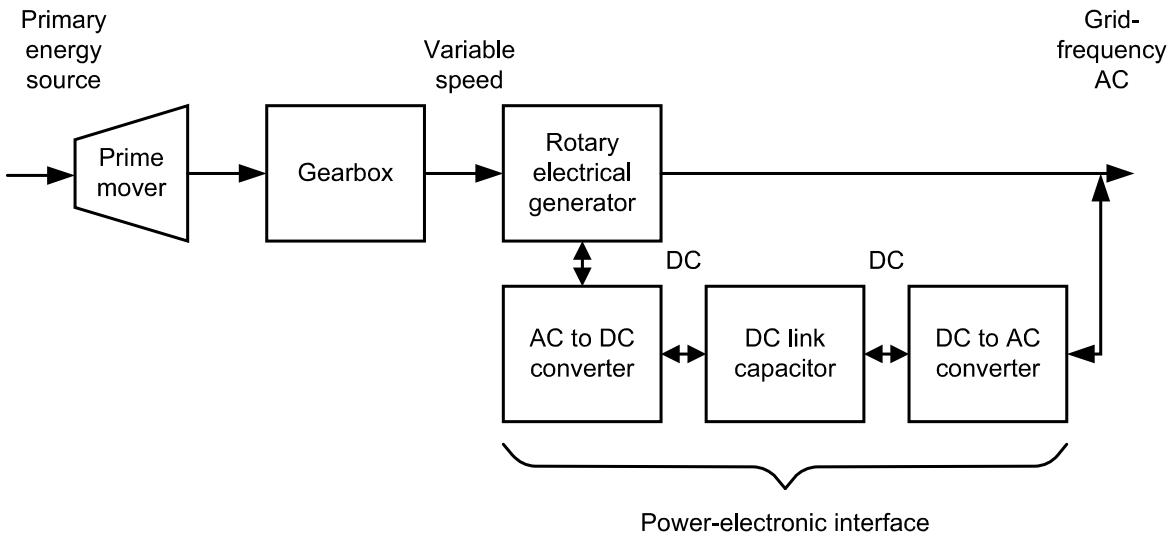

Figure 2.19 - Induction generator with AC-AC converter in the rotor [17]

D. Controllability

In reference to the controlling ability, DG systems can be classified into controllable and non-controllable systems [36].

Under controllable DG systems is meant, that the primary energy source of the respective technology can be regulated. Consequently, the output power is dispatchable and can be predetermined. Among others, conventional fossil fuel-based generators, microturbines, fuel cells, geothermal power plants and biomass driven power plants belong to this group of systems.

On the other hand, non-controllable DG technologies are characterised by the fact that the DG operator cannot dispatch DG system. Reason for that is the output power dependence from availability of the primary energy source. Normally, DG technologies that use RES, such as small hydropower plants, wind turbines or PV, are the non-controllable one.

2.3 Behaviour of Distribution Grids in Presence of DG

High penetration level of DG in the radial operated MV and LV distribution grids brings many technical and operational challenges. Two of the most important technical issues are the voltage rise and the increased power flow across the grids. The following text introduces two cases that show how DG can influence this increase in voltage and power flow. Special importance is given to the effects of the reactive power injection on the same and higher grid level.

A. LVG with a single load and a single DG

In order to see in which way a single DG in LVG impacts voltage rise, a traditional LVG needs to be examined first. It is supposed to be a “passive” system, where no DG is included. Figure 2.20 shows the single-line diagram and the corresponding phasor diagram of a traditional LVG with a single load. This load can represent a maximal consumption of one typical house during the day, where all electrical household appliances are taken into account.

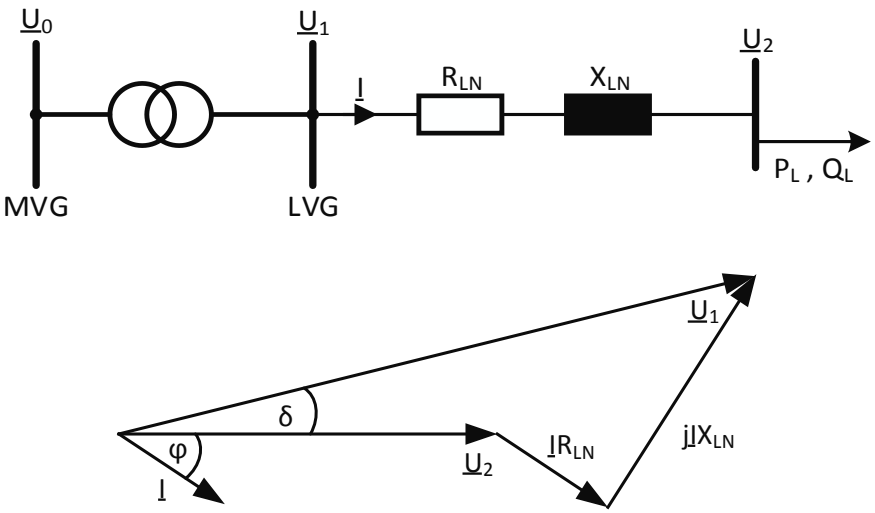

Figure 2.20 - Single-line diagram of a traditional LV distribution grid and the corresponding phasor diagram for an illustration of the voltage drop along the feeder [17]

The current $\underline{I}$ is given by a function of the load complex apparent power $\underline{S_L}$ and the load voltage $\underline{U_2}$,

$$\underline{I} = \frac{\underline{S_L^*}}{\underline{U_2^*}} = \frac{P_L - jQ_L}{\underline{U_2^*}} \tag{2–1}$$

where P_L and Q_L are the active and reactive power of the load, respectively. The voltage drop of the feeder is given by following equations:

$$\Delta U = \left|\underline{U_1} - \underline{U_2}\right| = \left|\underline{I} \cdot (R_{LN} + jX_{LN})\right| \tag{2–2}$$

$$\Delta U = \left|\frac{(R_{LN} \cdot P_L + X_{LN} \cdot Q_L) - j(X_{LN} \cdot P_L - R_{LN} \cdot Q_L)}{\underline{U_2}}\right| \tag{2–3}$$

where R_{LN} and X_{LN} are the resistance and reactance of the feeding line, respectively. For a small power flow, the angle δ between $\underline{U_1}$ and $\underline{U_2}$ is small and the imaginary part in equation (2–3) can be overlooked. Consequently, the voltage drop can be approximated by the following equation:

$$\Delta U \cong \frac{R_{LN} \cdot P_L + X_{LN} \cdot Q_L}{U_2} = \frac{\frac{R_{LN}}{X_{LN}} \cdot P_L + Q_L}{U_2} \tag{2–4}$$

With methods from subsection 2.2.2(C), a DG system can be connected to the LV distribution grid, for example a photovoltaic system is installed on the rooftop of the same house from the traditional grid. Generally, DG can either generate or absorb reactive power. Third mode, where DG doesn't exchange reactive power with the grid at all means that the power factor $cos\varphi = 1$. DGs with synchronous generators or power electronic interfaces can operate in all three modes as well, while DGs with induction generators always absorb reactive power from the grid. In the grid with DG and load, as shown in Figure 2.21, and under assumption that DG only generates active power ($P_{DG} \geq 0$), voltage change across the feeder can be approximated with the following equation:

$$\Delta U \cong \frac{R_{LN} \cdot (P_L - P_{DG}) + X_{LN} \cdot (Q_L \pm Q_{DG})}{U_2} \tag{2–5}$$

where P_{DG} and Q_{DG} are DG active and reactive power, respectively. Equation (2–5) indicates that the voltage drop along the feeder decreases in case when DG generates reactive power. Furthermore, case when P_{DG} is greater than P_L will cause a voltage rise and a change in power flow direction, i.e. from DG connection point towards the secondary side of the MV/LV transformer. If DG absorbs reactive power from the grid, voltage drop can should be increased.

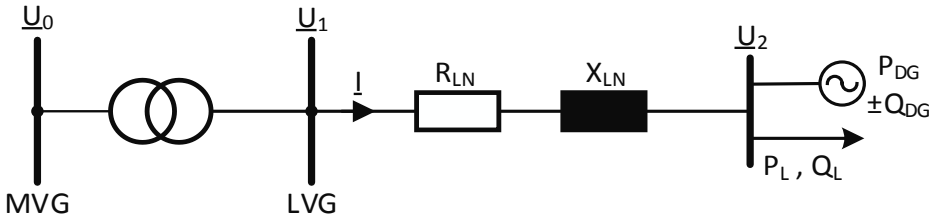

Figure 2.21 - Single-line diagram of a LV distribution system with an addition of DG [17]

When the parameters R_{LN} and X_{LN} are further examined, more qualitative conclusions about the voltage change along the feeder can be drawn. In Table 2.3 the values of specific resistance R'_{LN}, specific reactance X'_{LN}, their ratio and typical rated current values I_{rated} for LV as well as for other voltage levels are given.

Table 2.3 - Line parameters and typical current value in HV, MV and LV grids

$\boldsymbol{Voltage\ Level}$	$\boldsymbol{R'_{LN}}$ $[\Omega/\boldsymbol{km}]$	$\boldsymbol{X'_{LN}}$ $[\Omega/\boldsymbol{km}]$	$\boldsymbol{I_{rated}}$ $[\boldsymbol{A}]$	$\boldsymbol{\frac{R'_{LN}}{X'_{LN}}}$
HV	0,033	0,252	645	0,13
MV	0,161	0,190	396	0,85
LV	0,642	0,083	142	7,74

Since in LV distribution grids resistive part of the line dominates over the reactive one ($R'_{LN}/X'_{LN} \gg 1$), term $X_{LN} \cdot (Q_L \pm Q_{DG})$ can be neglected. Hence, the voltage change is mainly affected by the active power term $R_{LN} \cdot (P_L - P_{DG})$. When compared to the traditional LV grid, that would always implicate a voltage rise at the connection point due to the active power injection of the installed DG. From table above it can be seen that the voltage change in HV case is mainly caused by a reactive power and in MV case both active and reactive power are sources of voltage change along the feeder.

B. MVG with distributed loads and a lumped DG

Simulation study done in [37] shows which effects a reactive power injection of a single DG has on the two MVGs of different voltage levels. A 33 kV supplying feeder supplies through a 20 MVA transformer with fixed tap position two different feeders, Feeder 1 and Feeder 2, which are connected to a 11 kV bus bar. Figure 2.22 shows a single-line diagram of this test grid. Evenly distributed loads, which are

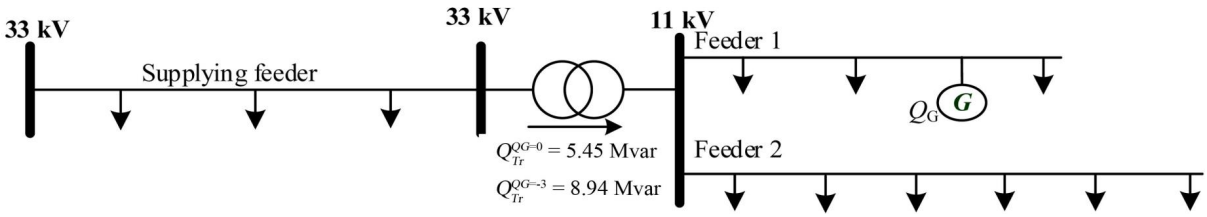

Figure 2.22 - A single-line diagram of the test grid [37]

modelled with polynomial equations of the second degree, are connected across the feeders. Additionally, an 8 MW lumped generator is connected to Feeder 1. It represents all DG that were connected along this feeder. Two cases were observed:

- Case A: generator injects only active power, no reactive power exchange with the grid
  $(P_G = 8\,MW, Q_G = 0\,MW)$
- Case B: generator injects active power and absorbs reactive power
  $(P_G = 8\,MW, Q_{G,IND} = 3\,MW)$

Evaluation of the simulation results exposed two different effects of additional reactive power injections, namely "local" and "global" effect. The "local" effect refers to the effect that is found directly at the point of DG injection and that vanishes along the related feeder. Contrary to the "local" effect, the "global" effect is observed at the other parts of the grid, i.e. on other feeders with the same or even different voltage level. Figure 2.23 shows how the voltage value of the corresponding feeder changes with its length. This dependency is more known under the name of voltage profile. Dashed lines represent the voltage profiles in case A, while the solid lines correlate to the voltage profiles in case B. Circled red solid lines give the information where the above-mentioned effects are to be found.

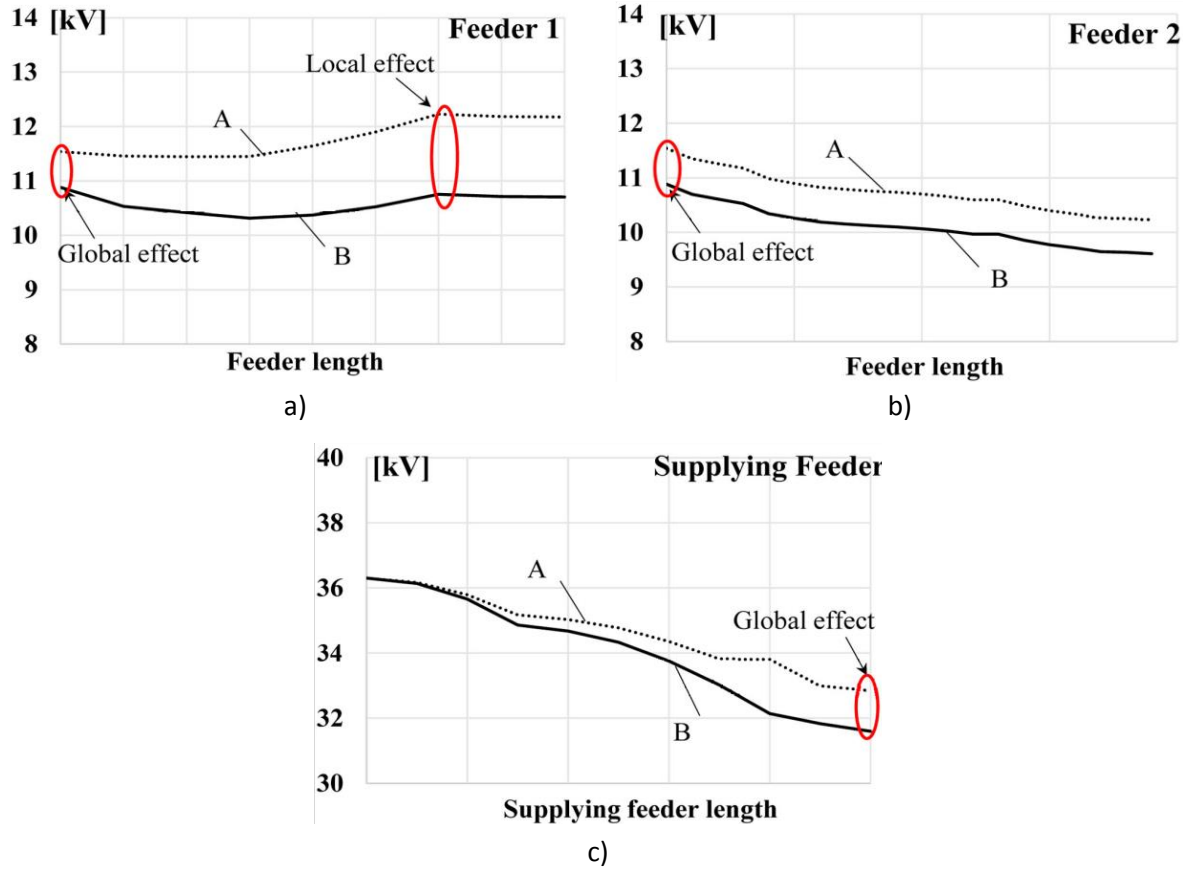

Figure 2.23 - Voltage profiles of different feeders in the test grid [37]:
a) Feeder 1, b) Feeder 2 and c) Supplying feeder

As it can be seen from Figure 2.23a, in Feeder 1 both effects are present, at the 11 kV bus bar and at the connection point. At both places the voltage was decreased. Although Feeder 2 has no connected DGs, it displays the "global" effect in case B. The decrease in voltage can be seen at the 11 kV bus bar. When compared to case B, it seems that the voltage profile is displaced evenly along the feeder length. The voltage profile of the supplying feeder reveals that the "global" effect is also present. This can be

explained due to increase in power flow values through the transformer, which can be found in Figure 2.22. The "global" effect is less apparent as we move from the high side of transformer. At the left 33 kV bus bar, the "global" effect vanishes totally. In order to prevent these voltage fluctuations across the distribution grids, some voltage control strategies can be applied.

2.4 Voltage Control in Distribution Grids

To ensure the proper functioning of the grid components and its connected devices, the supply voltage must be contained within certain limits. The supply voltage and other main voltage parameters are defined in the "EN 50160" standard [5]. Further, EN 50160 also gives their permissible deviation ranges at the customer's point of common coupling (PCC) in public LV and MV distribution grids under normal operating conditions. In regard to the limits of the supply voltage, 95% of the 10 min mean RMS values of the supply voltage during each period of one week shall be within the range of $\pm 10\%\ U_n$. Here, U_n stands for the nominal voltage and has the same value as the declared supply voltage U_c, which is also defined in the standard. Some countries can additionally have some extra requirements. In Germany, for example, voltage change at every PCC in LV distribution grid that was caused by all generating plants connected to this LV distribution grid, must not exceed the value of 3% compared to the voltage when these generating plants were not connected.

As one of the main focuses of this thesis is to see in which way some available solutions contain supply voltage within these limits and mitigate the DG effects on distribution grids, the following text will explain a couple of solutions. Some of them are already performed by the responsible DSOs, so that at every time a reliable power supply to the end-users is guaranteed, while the others could become a vital part of voltage control strategies in the near future. During the modelling of the grid and its components, as it will be shown later on, a few strategies that are described here are taken into consideration.

2.4.1 Transformers with tap changers

Equipping the transformers at HV/MV or MV/LV substations with tap changers is one of the possibilities to keep the voltage values at LV and MV levels within the statutory permissible voltage range for LV and MV distribution grids, respectively. Using a tap changer can change the ratio of a transformer in discrete steps by adding turns to or subtracting turns from either the primary or the secondary transformer's winding. Thus, a tap changer can be located at the primary or the secondary side of the transformer. The π-equivalent circuit diagram of a tap-changing transformer is illustrated in Figure 2.24. Notations $\underline{U}, \underline{I}$ and $\underline{Y}$ represent voltage, current and admittance of the transformer.

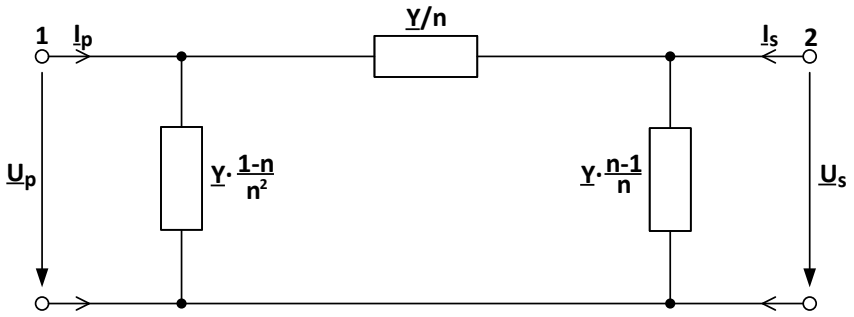

Figure 2.24 - The π-equivalent diagram of a tap-changing transformer [17]

Subscripts p and s indicate transformer's primary and secondary side. Transformer's turns ratio n gives a relation between the number of turns in the primary winding N_p and the number of turns in the secondary winding N_s.

For a tap changer's position, a transformer's higher-voltage winding is normally chosen, due to higher value of a lower-voltage winding's current. Another reason is that more turns are available on the higher-voltage side, thus making voltage regulation more precise. Additionally, in a core-type transformer the inner winding is normally the one with the lower voltage, which makes taking out the access points or taps from the lower-voltage winding even more difficult. In this way, by adjusting the tap position, voltage at the lower-voltage side can be regulated more or less to desired value.
Primarily, there are two types of tap changers:

- On-load tap changer (OLTC): expensive; space and extra maintenance are required; tap changing is performed automatically; the corresponding transformer supplies the connected loads without any interruption of the power flow
- No-load tap changer (NLTC): cheap and robust; tap changing is performed manually; the corresponding transformer needs to be disconnected from the grid, which can lead to interruption of the power supply (e.g. when another supplying transformer doesn't operate in parallel)

In the traditional distribution grids voltage control is almost exclusively performed at HV/MV substations by transformers with OLTC. Simple and very common OLTC control strategy is to keep the voltage at the transformers' MV side on a constant level. As a result, the voltage value at the beginning of the feeder will not change in case where load changes. Contrarily, the voltage at the end of the feeder will decrease as the load increases. As the other very common, but more complex strategy, a line drop compensation (LDC) can be used. Based on the loading of the corresponding transformer, the voltage value at MV side can be controlled. In case of increased load, the voltage at the beginning of the feeder increases, while the voltage at the end of the feeder decreases. If the same feeder is considered, case without LDC or with fixed voltage at MV side would display a bigger voltage drop at the end of the feeder [38]. Both strategies reduce the voltage fluctuation due to load variations.

As long as the voltage in MV distribution grids is within certain limits, voltage values in LV distribution grids don't have to be controlled through MV/LV transformers. Therefore, most of the MV/LV transformers are provided with a NLTC. A fixed tap position is chosen when the related transformer is put into service. In case where structural changes in load occur, a tap changer needs to be manually adjusted. In some rare occasions, OLTC can be used for MV/LV transformers as well.

A high penetration level of distributed generation at LV and MV levels could disrupt this type of control. The local production of DGs reduces the power demand that the voltage regulating HV/MV transformers notice. Due to a misinterpretation of this power demand, this could result in a lower set point for the voltage control, which could ultimately lead to unintended tap changes. If this and any other conventional control strategies cannot tame the effect of higher DG penetration, some other possibilities should be explored. According to [39], an advanced LDC control that includes the influence of DG production has already been introduced.

2.4.2 Controllable DG

Voltage control in distribution grids is realized mainly by OLTCs, which implicates that the secondary side of the OLTC transformer in HV/MV substation is the last measured point [40]. As the number of DG-units connected to the MV and LV distribution grids increases, voltage rise at the point of common coupling cannot be identified. Thus, classical voltage control strategies don't allow a large penetration of DG-units into the system. For that reason, DG-units in distribution grids can also participate in keeping the voltage within statutory limits, either by controlling the reactive power exchange with the grid or by the active power curtailment method, which is discussed in the following text.

A. Reactive power control (RPC)

In Austria, for example, DG-units that are connected to distribution grids need to comply with the Austrian technical and organisational rules (TOR) for parallel operation of generating stations in MV and LV distribution grids [41]. Reactive power requirements for DGs with an inverter's capability larger than 3,68 kVA in LV and MV distribution grids are illustrated in Figure 2.25.

When connected to LVG, a DG-unit is obligated to be able to provide reactive power Q up to at least ±43,6% of its inverter's rated apparent power S_{RATED}. The inverter's output is freely adjustable if its active power output P exceeds 90% of S_{RATED} (green area). If P lies between 20% and 90% of S_{RATED}, the inverter needs to be able to inject (for $cos\varphi = 0{,}9$ overexcited) and absorb (for $cos\varphi = 0{,}9$ underexcited) at least 43,6% of S_{RATED} (red framed area). The exact compliance is not required if P is less than 20% of S_{RATED} (grey area).

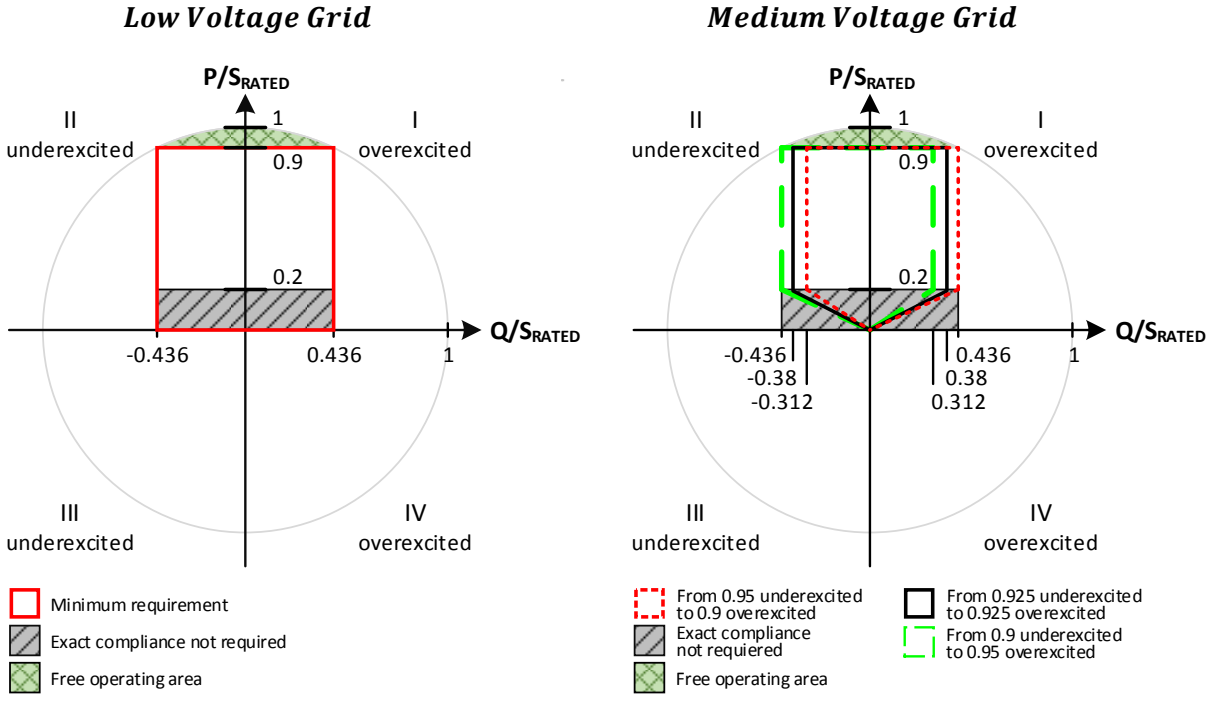

Figure 2.25 - Reactive power requirements for a DG with an inverter > 3,68 kV in low and medium voltage distribution grids [41]

As it can be seen from the figure above, DG-units connected to MVG have similar reactive power requirements. The only difference is that normally, when P lies between 20% and 90% of S_{RATED}, the inverter needs to be able to inject (for $cos\varphi = 0{,}925$ overexcited) and absorb (for $cos\varphi = 0{,}925$ underexcited) at least 38% of S_{RATED} (black framed area). When needed, the responsible DSO can

need some additional operating range from a DG inverter. In first case, the inverter has to be able to inject 31,2% of S_{RATED} (for $cos\varphi = 0{,}95$ overexcited) and absorb 43,6% of S_{RATED} (for $cos\varphi = 0{,}9$ underexcited), which is represented through green dashed line. In second case, the inverter has to be able to inject 43,6% of S_{RATED} (for $cos\varphi = 0{,}9$ overexcited) and absorb 31,2% of S_{RATED} (for $cos\varphi = 0{,}95$ underexcited), which is represented through red dotted line. For P-values that are bigger than 90% of S_{RATED} or smaller than 20% of S_{RATED}, the same reactive power requirements are needed as for DGs in LVGs.

Focusing on guidelines from [41], three different concepts of reactive power control (RPC) are described: constant power factor ($\cos\varphi = const$), active power dependent power factor ($\cos\varphi\,(P)$) and voltage dependent reactive power ($Q(U)$). The power factor $\cos\varphi$ is always measured at PCC between the DG-unit and the grid. It is assumed that every DG-unit is connected to the grid over an inverter.

(1) Constant power factor, $\cos\varphi = const$

When an inverter of a DG-unit operates underexcited with a fixed power factor smaller than 1 ($\cos\varphi = \varphi_0$, where $\varphi_0 < 1$), a DG-unit absorbs reactive power from the grid. This concept is a straightforward method of consuming reactive power. If every generating unit is equipped with this type of control, voltage rise could be very easily be prevented. Because of the independency between the injected reactive power and the voltage, it could happen that even in case of no relevant voltage rise due to implementation of DGs, a huge amount of reactive power will be absorbed from the grid. As this amount is getting higher, grid losses are getting higher as well. These unnecessary losses are representing one of the biggest disadvantages of this concept. By using this constant power factor control, as shown in Figure 2.26, it is apparent that the reactive power is proportional to the active power generation of a DG-unit. In case of a low irradiance, the reactive power will be as small as the active power generation. If the maximal active power generation P_{max} of a DG-unit is reached, the inverter will be absorbing ($cos\varphi = 0{,}9\ ind.$) injecting ($cos\varphi = 0{,}9\ cap.$) maximal reactive power Q_{max} as well.

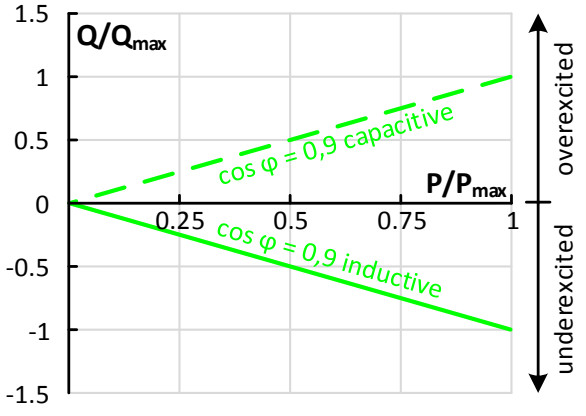

Figure 2.26 - Constant power factor characteristic of a DG inverter

(2) Active power dependent power factor, $\cos\varphi\,(P)$

Another method that prevents the voltage rise is to set an inverter of a DG-unit to operate with a variable power factor $\cos\varphi$. Depending on the active power generation of a DG-unit, $\cos\varphi$ changes its value. Figure 2.27 represent a typical $\cos\varphi\,(P)$-control of a DG inverter, which was proposed by the current Austrian guidelines. As is it can be seen from the figure, $\cos\varphi$ is equal to 1 as long as the

half of the maximal active power generation is not reached, which means that there is no any reactive power exchange $Q = 0$ between a DG-unit and the grid. This can be explained through the fact that in case of a lower irradiance, a DG-unit doesn't cause a significant voltage rise at a connection point, which further means that there is still no need for voltage correction. When the value of $P_{max}/2$ is passed, a DG inverter begins to operate in underexcited mode. In this operating area $\cos\varphi$ lowers its value linearly. A DG inverter starts absorbing more and more reactive power from the grid. At the P_{max}-point, power factor reaches its limit value and a DG inverter absorbs the maximal reactive power Q_{max} from the grid. One characteristic of this type of control is that all DG inverters will absorb reactive power regardless of the location of the corresponding DG-unit along the feeder. Although an overall better voltage control is assumed, it may still be the case that the reactive power injection into the grid can occur in times when that may not be required. These insignificant overvoltage situations may lead to undesired additional grid losses.

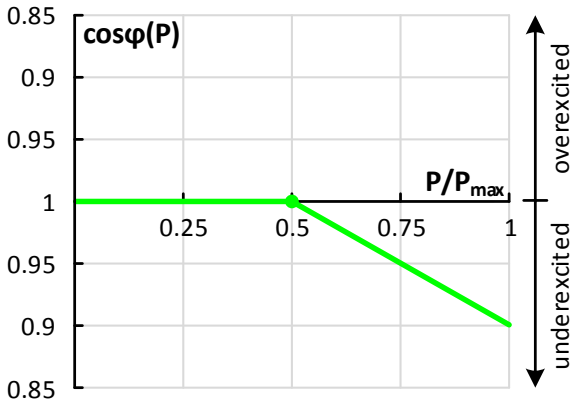

Figure 2.27 - Active power dependent power factor control of a DG inverter

(3) Voltage dependent reactive power, $Q(U)$

Contrary to the first two controlling mechanisms that are using measurements of the local active power generation of a DG-unit as an input, the voltage dependent reactive power control $Q(U)$ of a DG inverter uses local voltage information. A case where high irradiation values coincide with the high-power demand values may lead to an insignificant voltage rise at the connection point. In this case, by using any of the above-mentioned methods, the undesired grid losses may be created. Due to the fact that $Q(U)$-control uses a voltage value as an input, those additional grid losses can be avoided. Figure 2.28 shows a typical form of $Q(U)$-control of a DG inverter.

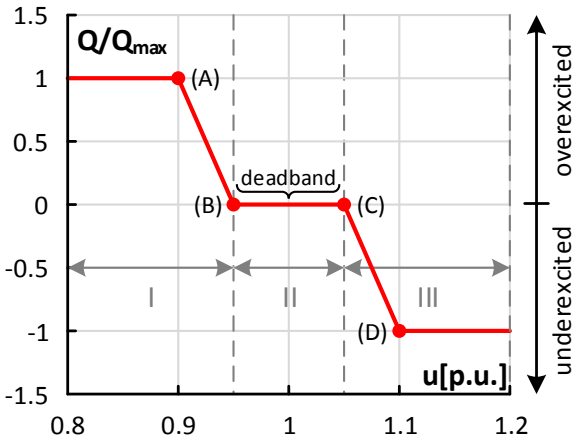

Figure 2.28 - *Q(U)*-control of a DG inverter

The operational intervals that can be seen in the figure above are described in Table 2.4. The deadband interval allows a delay of reactive power exchange between the grid and a DG inverter $(Q = 0)$ in favour of generating the maximal available active power. This area should restrict any unwanted reactive power flow when the small variations around the nominal voltage value at the connection point occur. In situation where each DG-unit along the feeders has a $Q(U)$-controlled inverter, a too wide deadband interval could have some negative effects. Namely, DG-units closer to the supplying transformer would not participate at regulating the voltage level, while the ones at the end of the feeders would have to absorb their maximal reactive power from the grid.

Table 2.4 - Operational intervals of *Q(U)*-control

Interval	***Description***
I	*DG inverter operates overexcited and injects reactive power; main goal is to increase the voltage at PCC;*
II	*Deadband interval, in which DG inverter doesn't absorb or inject any reactive power*
III	*DG inverter operates underexcited and absorbs reactive power; main goal is to increase the voltage at PCC;*

The four different breakpoints of $Q(U)$-control are explained in Table 2.6. The breakpoints B and C define the width of the deadband interval. The breakpoints A and D are usually chosen depending on the lower and higher voltage limits of a DG inverter.

Table 2.6 - Different breakpoints of *Q(U)*-control

Breakpoint	***Description***
A	*Voltage threshold bellow which DG inverter should inject the maximal reactive power* Q_{max}
B	*Voltage minimum of deadband interval; for lower values DG inverter operates overexcited, while for higher values* $Q = 0$
C	*Voltage maximum of deadband interval; for higher values DG inverter operates underexcited, while for lower values* $Q = 0$
D	*Voltage threshold above which DG inverter should absorb the maximal reactive power* Q_{max}

B. Active power curtailment (APC)

Exceeding the overvoltage limits can be prevented not only by controlling the reactive power Q of a DG-unit, but also by controlling its active power output P. This type of control is more known as the active power curtailment (APC). Opposite to RPC, APC doesn't provoke any undesired grid losses and doesn't require the over-dimensioned DG inverters, because they should operate with unity power factor $(\cos\varphi = 1)$ at all times. As already seen in Table 2.3, the LV feeders have much higher R'_{LN}/X'_{LN} then the MV feeders. This means that the voltage drops or rises in LVGs are far more sensitive to changes in active power flow then in MVGs. Because of that, APC should normally be implemented in LVGs. In [42] it can be seen that PV systems reach their peak production per year only for a short time, when compared to the peak production from wind power or hydropower plants. Therefore, an eventual APC of peak production should not have such a big impact on PV systems. From DGO's standpoint, APC could be seen as a very appealing solution, as long as an increase in DG hosting capacity would be possible without any major grid reinforcements. On the other hand, owners of DGs would experience a loss of production, which would lead to a loss of their revenue. One of the biggest APC disadvantages is the unfair treatment of DG-units that are located at the end of feeders. They would be the first in line to be affected by the reduction of their active power output, while those

closer to the supplying transformer may not even be affected at all. In this way, those “first in line” owners would experience an additional loss of revenue. Some of the possible implementation methods of APC, which are proposed in [42], are described in the following text.

(1) Disconnection of the generation units in case of overvoltage

This type of active power curtailment is a very simple controlling mechanism. The daily active power and voltage profiles for this type of APC is represented in Figure 2.29.

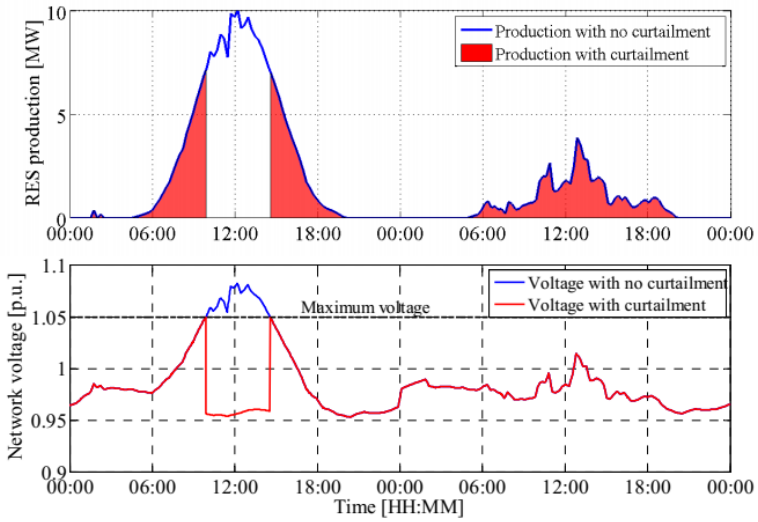

Figure 2.29 - Disconnection of the generation unit in case of overvoltage [42]

As soon as the voltage at PCC reaches the maximum allowed value, a DG-unit is getting automatically disconnected from the grid by its overvoltage protection. In addition, by equipping a DG-unit with a remote controller, the grid operator would be able to optimize the curtailment in order to mitigate grid congestions located in different areas [42].

(2) Fixed power curtailment

Fixed power curtailment is another type of active power curtailment, in which the maximum power injection of a DG-unit is being constantly held under a certain limit value. The daily active power and voltage profiles for the fixed power curtailment scenario is represented in Figure 2.30.

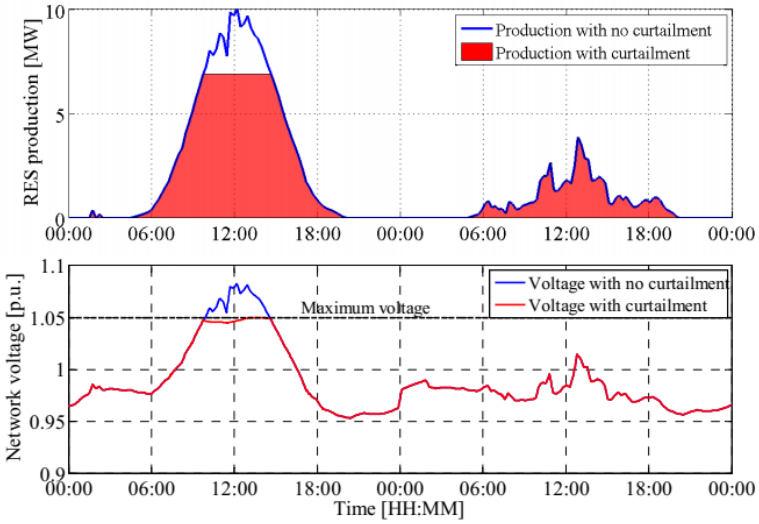

Figure 2.30 - Fixed power curtailment [42]

The working principle of this method is quite simple: a power limiter is automatically activated as soon as a predefined active power threshold is reached [42]. In this way any possible overvoltage situations could be very easily be avoided. When compared to the figure above, fixed power curtailment brings on less energy losses. The further simulations that have been performed in [42] show an overall better performance of this method.

(3) Volt/watt droop control, $P(U)$

The third method for implementing APC is the so-called Volt/watt droop control or voltage dependent active power control *P(U)*, in which a DG inverter adjusts the active power output depending on the voltage value at PCC. The *P(U)*-characteristic of a DG inverter is illustrated in Figure 2.31 [41].

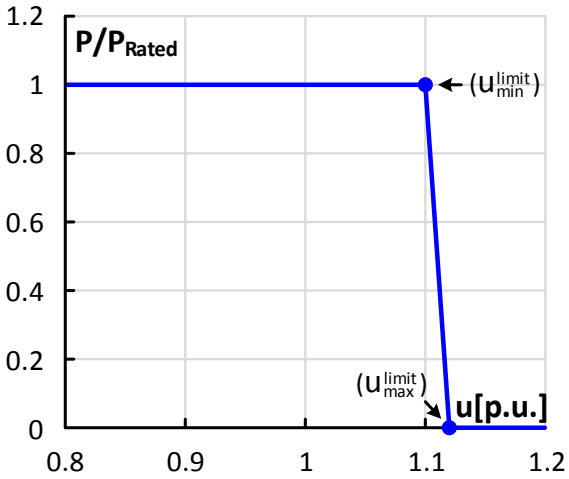

Figure 2.31 - *P(U)*-control of a DG inverter

To a certain degree, *P(U)*-control can be viewed as a combination of the first two controlling methods. From the figure above, it is obvious that *P(U)*-control has three different operating areas, which are more or less specified by two different breakpoints (u_{min}^{limit} and u_{max}^{limit}). According to [41], their values should be 1,1 and 1,12, respectively. The working principle of this method is explained in Table 2.5.

Table 2.5 - Operational intervals of *P(U)*-control

Interval	***Description***
$u < u_{min}^{limit}$	*no active power curtailment at this point;* *DG inverter injects maximal available P* $(ideally\ P = P_{Rated})$
$u_{min}^{limit} < u < u_{max}^{limit}$	*DG inverter injects active power that is being linearly reduced*
$u > u_{min}^{limit}$	*active power curtailment at its maximum;* *DG inverter doesn't inject any active power* $(P = 0)$

The daily active power and voltage profiles in case of the volt/watt droop control are shown in Figure 2.32 [42]. Further simulations in [42] have shown that the *P(U)*-control displays the highest potential among other controls in terms of increasing the DG hosting capacity without curtailing too much energy.

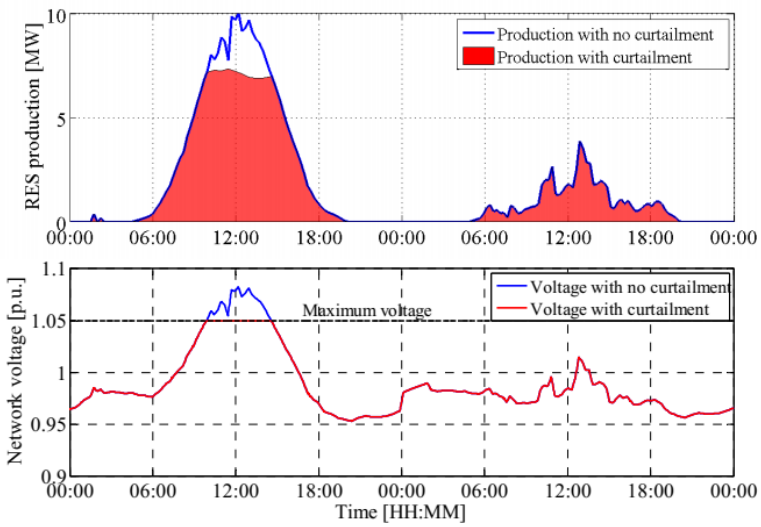

Figure 2.32 - Volt/watt droop control [42]

(4) Generation of a fixed portion of the available production

The fourth type of the APC is the generation of a fixed portion of the available production P_{av}, which doesn't take into account the voltage value at the point of connection between the grid and a corresponding DG-unit. By choosing the right setpoints, a DG inverter always injects percentage-wise the same amount of P_{av} (e.g. $P = 70\%\ P_{av}$), which prevents the PCC voltage to exceed the predefined overvoltage limit. shows how the daily profiles of the injected active power and voltage at PCC look for this type of APC. With respect to the first three types from above, this control implicates the largest amount of curtailed energy. Therefore, if DG owners applied this control, they would experience the biggest loss of revenue. The daily active power and voltage profiles in case of generation with a fixed portion of the available production are shown in Figure 2.33 [42].

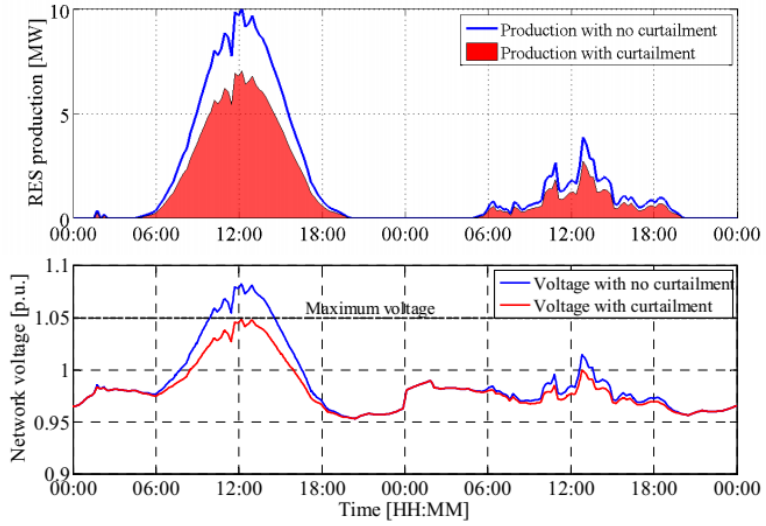

Figure 2.33 - Generation of a fixed portion of the available production [42]

3 Description of Test Link_Grids

This chapter describes medium voltage and low voltage Link_Grids that have been used during various power flow simulations. Section 3.1 introduces LV Real Link_Grids, which are based on the existing Austrian low voltage distribution grids. Section 3.2 gives an overview of the used MV Link_Grids. There are two types of MV Link_Grids: real and theoretical. MV Real Link_Grids are based on the existing Austrian medium voltage distribution grids. On the other hand, MV Theoretical Link_Grids were created with much simpler structure than MV Real Link_Grids.

3.1 LV Link_Grids

The four different LV Real Link_Grids were created: Large Urban, Small Urban, Rural and Industrial. Each LV Link_Grid has a radial structure and consists of one MV/LV distribution transformer and several feeders that differentiate in size. Further, each feeder has at least one main-branch that consists of numerous main-branch nodes. One or more sub-branches starts from every main-branch node. At the end of every sub-branch lies a sub-branch node that represents a connection point for a Customer Plant CP. A schematic overview of a typical LV Link_Grid is represented in Figure 3.1. Every CP that is connected to a LV Link_Grid is characterized by its native load and a linked Producer-Link, which consists of an inverter-controlled PV system. Depending on the customers' load composition that changed drastically in the last couple of years, CPs that are connected to LV Link_Grid are divided into three separate classes: residential, small commercial and industrial.

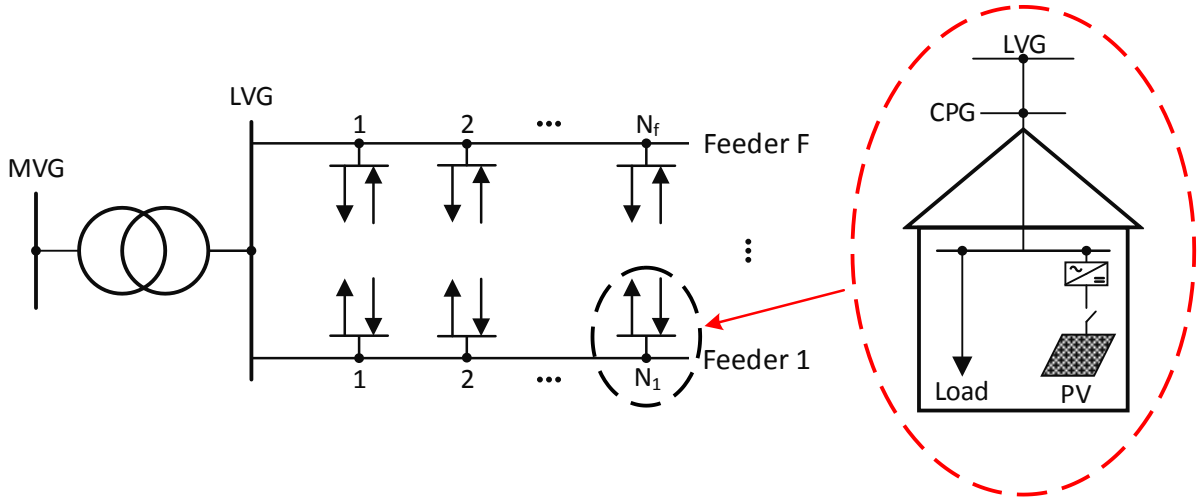

Figure 3.1 - Schematic overview of a typical LV Link_Grid

The "Institute of Energy Systems and Electrical Drives" of the "Vienna University of Technology" provided the data regarding LV Link_Grids. With exception of electrical data of the overhead lines, all other data used in the models were directly gathered from the responsible distribution system operator. The provided data include grid topology, different line parameters and transformer electrical data. The production value of the actual PV systems, as well as the class and contracted active power value of each customer are also included. Some of the most important data regarding the LV Link_Grids' structure, such as number of feeders F, number of connected CPs for each class $N_{RES}^{CP\_LV}$, $N_{SC}^{CP\_LV}$ and $N_{IND}^{CP\_LV}$, total feeder length l_{TOT} and cable share c_{SHARE} are presented in Table 3.1. Total number of connected customers corresponds to the number of sub-branch nodes.

Table 3.1 - Parameters regarding the structure of LV Link_Grids

LV Link-Grid	***F***	$N_{RES}^{CP\_LV}$	$N_{SC}^{CP\_LV}$	$N_{IND}^{CP\_LV}$	l_{TOT} [km]	c_{SHARE} [%]
Large Urban	9	175	0	0	12,815	96,14
Small Urban	6	91	0	0	4,975	81,11
Rural	4	61	0	0	6,335	58,64
Industrial	3	7	4	10	2,091	100

Additionally, total annual consumption E_{SEC}^{2016} and peak active power at the secondary side of the distribution transformer $P_{2016\_MAX}^{DTR\_SCD}$ for each LV Link_Grid are also provided for this thesis. Their values, as well as the values for total basic power production of every LV Link_Grid, are shown in Table 3.2 below.

Table 3.2 - Production and consumption of LV Link_Grids

LV Link-Grid	$P_{PV\_BASIC}^{TOTAL}$ [kW]	E_{SEC}^{2016} [kWh]	$P_{2016\_MAX}^{DTR\_SCD}$ kW
Large Urban	168	1 127 040	349
Small Urban	101	990 755	242
Rural	20	320 165	85
Industrial	30	1 022 510	455

A. Rural LV Link_Grid

As it can be observed from previous tables, Rural LV Link_Grid is a small-sized distribution grid with the total feeder length of 6,335 km, of which almost 60% consists of cables. Four different feeders supply only residential customers in a rural area. In comparison with other Link_Grids, Rural LV Link_Grid has the smallest total annual consumption, total production of all PV systems and the peak active power in 2016. A MV/LV distribution transformer in this grid operates with a fixed tap position A schematic overview is given in Figure 3.2, whereby only the main-branches and their related nodes are represented. Figure A.1 in Appendix A shows the more detailed version of Rural LV Link_Grid.

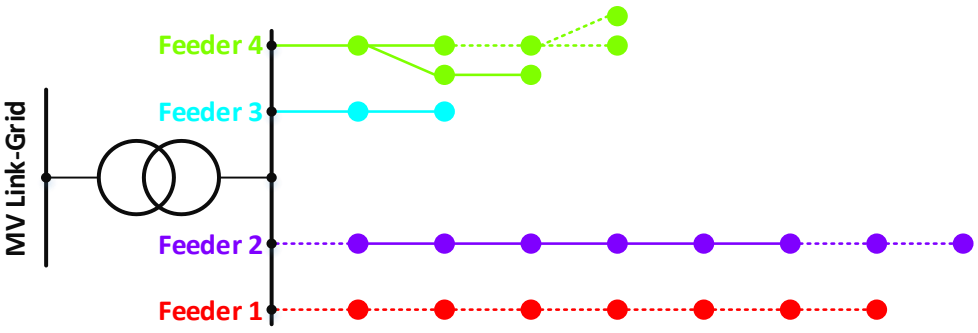

Figure 3.2 - Simplified overview of Rural LV Link_Grid

B. Small Urban LV Link_Grid

Placed in an urban area, Small Urban LV Link_Grid is as well a small-sized distribution grid. Although it has smaller total length of overhead lines and cables than Rural LV Link_Grid, due to higher population density, it supplies larger number of residential customers. It has cable share of approximately 80% and 6 different feeders. A MV/LV distribution transformer with larger rated apparent power than one in Rural LV Link_Grid operates as well with a fixed tap position. A schematic overview of the grid with

only main-branches is shown Figure 3.3, while the more detailed one can be seen in Figure A.2, in Appendix A.

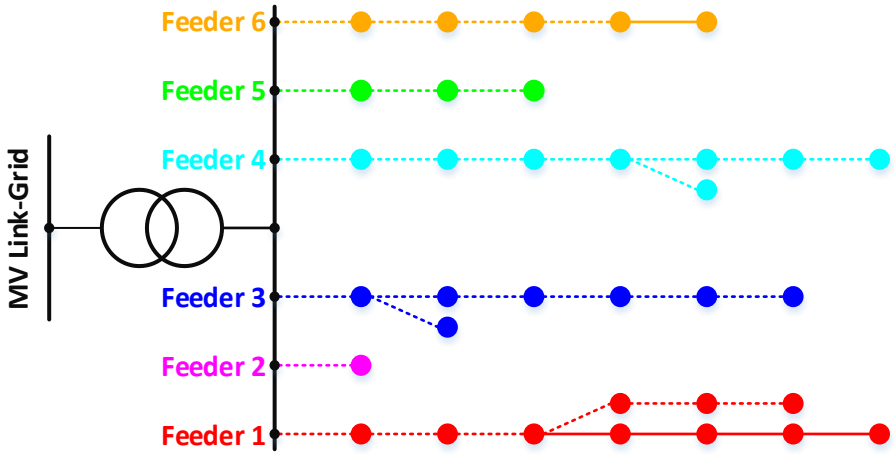

Figure 3.3 - Simplified overview of Small Urban LV Link_Grid

C. Large Urban LV Link_Grid

Large Urban LV Link_Grid is a big-sized distribution grid that supplies 175 residential customers through nine different feeders. It has a leading spot in almost all parameters that are listed in tables above.

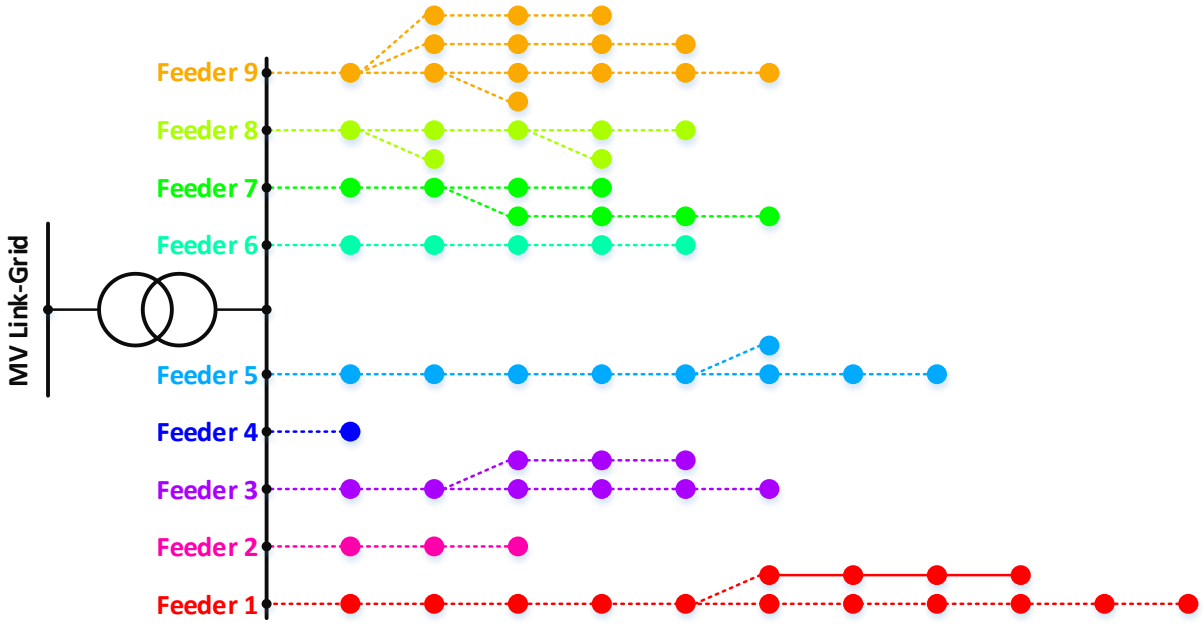

Figure 3.4 - Simplified overview of Large Urban LV Link_Grid

Its total feeder length, of which approximately 96% consist of cables, has a value that is twice as big as the total feeder length of Rural LV Link_Grid. As in every other grid, a MV/LV distribution transformer has a fixed tap position. A brief overview of the grid is shown in Figure 3.4, while the one with more details can be found in Appendix A, in Figure A.3.

D. Industrial LV Link_Grid

Placed outside of the urban area, Industrial LV Link_Grid with cable share of 100% has three different feeders that supply all three types of individual customers. The biggest one among all industrial

customers is connected on the Feeder 3, which main-branch due to this large load consists of two parallel cables. On the other hand, main-branch of Feeder 2 does not have two parallel cables, because it provides electric energy for different small commercial and residential customers that normally have a smaller consumption. Feeder 1 supplies almost only industrial customers and is the longest one. In comparison with other LV Link_Grids, Industrial LV Link_Grid has recorded the biggest peak of active power $P_{2016\_MAX}^{DTR\_SCD}$ at the secondary side of the distribution transformer, which also has a fixed tap position. Figure A.4 in Appendix A represents the more detailed version of the Industrial LV Link_Grid's structure, while the simplified one is represented here in Figure 3.5.

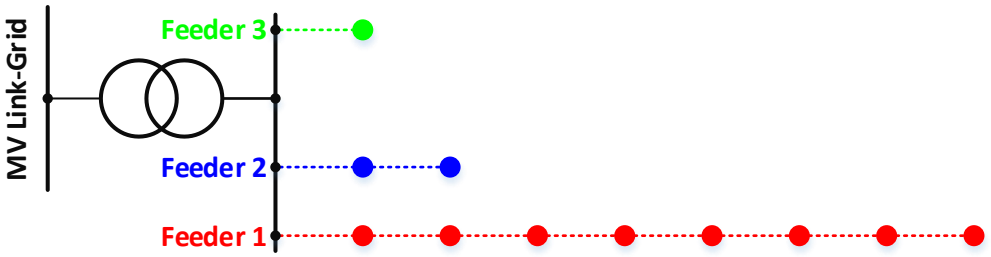

Figure 3.5 - Simplified overview of Industrial LV Link_Grid

3.2 MV Link_Grids

Two different MV Real Link_Grids were created: Real I and Real II. Both grids can be interconnected by a single cable (type: C-AL-240; length: 2,5 km). Location of the cable's start- and end-node can be seen in Appendix A, in Figure A.5 and Figure A.6, which give a detailed overview of Real I and Real II MV Link_Grid's structure, respectively. The electric energy supply for both MV Link_Grids goes over two HV/MV power transformer that are located in HV/MV substations. Each MV Link_Grid is a distribution grid with radial structure that consists of different number of feeders. To enhance system reliability, some feeders have switches that are open during the normal operating state of the grid. When some kind of failure occurs, switches close and a corresponding MV Link_Grid starts to operate as a ring grid. These so-called "tie-switches" can reconfigure the supply paths of the loads in the grid, so that the time of the load restoration can be significantly reduced [43]. Their locations can also be viewed in Figure A.5 and Figure A.6, respectively. As in case of the LV Real Link_Grids, MV Real Link_Grids have the same structure as LV Link_Grids concerning the topology of main- and sub-branches, as well as of main- and sub-branch nodes. One of the differences is that the main-branch nodes can also be a connection point for a CP or a LV Link_Grids. A schematic overview of a typical MV Link_Grid is portrayed in Figure 3.6, where it is apparent that a node can represent a connection point either for a CP (green dashed line) or for a LV Link_Grid (blue dashed line), on which a large number of CPs are connected. Customer plants that are connected to a MV Link_Grid are separated into two different classes: industrial and large commercial. The four different LV Link_Grids from Subsection 3.1 have been used: Rural, Small Urban, Large Urban and Industrial. To know exactly what type of LVGs or CPs is connected to MVGs, an assigning process is needed, which is described later on in Appendix B.

For both grids, the "Institute of Energy Systems and Electrical Drives" of the "Vienna University of Technology" provided the data again. The gathered data include single-line models, grid topology, various parameters of lines and transformers, values of active power production of installed photovoltaic systems that correspond to their installed peak power and values of active power consumption of individual customers and whole LVGs, which correspond to their estimated peak demands.

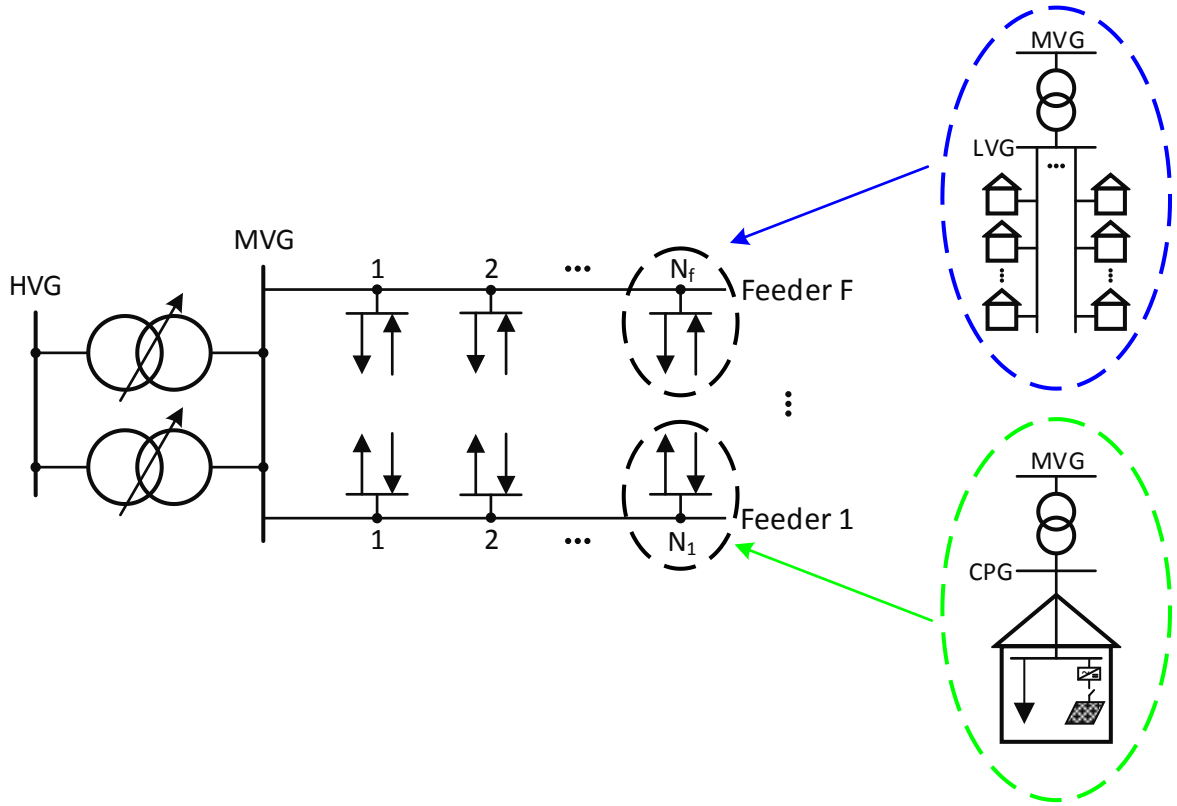

Figure 3.6 - Schematic overview of a typical MV Link_Grid

Additionally, two MV Theoretical Link_Grids were also created. Their purpose is the better understanding of MV Link_Grid behaviour when different approaches in modelling of the LV Link_Grids are carried out.

Table 3.3 - Different parameters regarding the physical aspect of the Real MV Link_Grid

MV Link_Grid	***F***	l_{TOT} [km]	c_{SHARE} [%]
Theoretical I	1	1/12,5/25	0/100
Theoretical II	1	25	0/100
Real I	6	245,15	73,2
Real II	4	156,96	43,132

Some of the most important data regarding the MV Link_Grids' physical apsect, such as number of feeders F, total feeder length l_{TOT} and cable share c_{SHARE}[3] are presented in Table 3.3.

Number of feeders F and total number of different CPs and LV Link_Grids are shown in Table 3.4. The parameters $N_{LC}^{CP\_MV}$ and $N_{IND}^{CP\_MV}$ correspond to the number of large commercial and industrial MV CPs, while N_{RUR}^{LVG}, N_{SU}^{LVG}, N_{LU}^{LVG} and N_{IND}^{LVG} correspond to the number of Rural, Small Urban, Large Urban and Industrial LV Link_Grids, respectively.

[3] total feeder length and cable share have been calculated without taking into consideration the above mentioned interconnecting lines

Table 3.4 - Total number of different CPs and LVGs in Real MV Link_Grids

MV Link_Grid	$N_{LC}^{CP\_MV}$	$N_{IND}^{CP\_MV}$	N_{RUR}^{LVG}	N_{SU}^{LVG}	N_{LU}^{LVG}	N_{IND}^{LVG}
Theoretical I	0	0	0	0	1	0
Theoretical II	0	0	0	0	3	0
Real I	69	4	75	45	7	1
Real II	30	0	60	49	3	1

A. Real I MV Link_Grid

Real I MV Link_Grid is a relatively large distribution grid with total feeder length of approximately 245 km, from which roughly 80 % consist of cables, as it can be seen from Table 3.3. Figure 3.7 illustrates a schematic overview of Real I MV Link_Grid, whereby only main-branches and main-branch nodes are represented. Its more detailed overview is represented in Appendix A (Figure A.6).

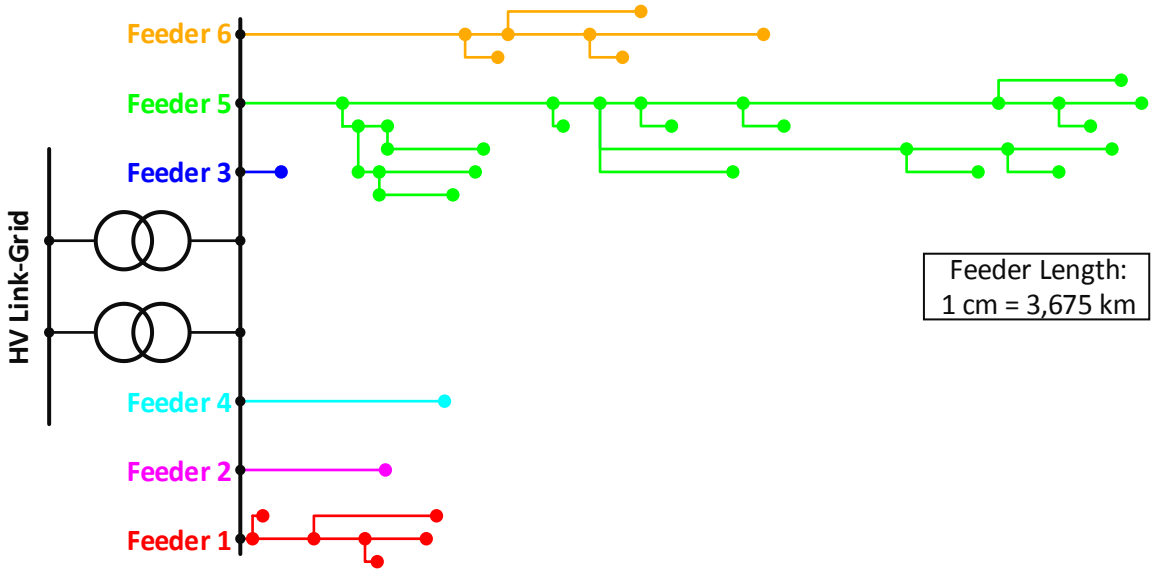

Figure 3.7 - Simplified overview of Real I MV Link_Grid

A much bigger use of cables than in Real II MV Link_Grid can be interpreted as an effort to make electric power supply even more reliable. Real I MV Link_Grid is bigger in size and in number of feeders than Real II MV Link_Grid. Through parallel operating mode of two power transformers, which are connecting HV with MV, a much reliable electric energy supply is guaranteed. Both of them are equipped with an On Load Tap Changer.

B. Real II MV Link_Grid

Real II MV Link_Grid is a smaller distribution grid with total feeder length of approximately 157 km and cable share of almost 50%, as it is shown in Table 3.3. This larger share of overhead lines than in Real I MV Link_Grid can be explained with the fact that overhead lines are less expansive and easier to maintain than cables. Real II MV Link_Grid receives electric power as well through two HV/MV power transformers. If one of them has some kind of failure, the other one can freely supply the four different feeders. Just as in case of Real I, they also possess an OLTC. A brief overview of the structure of Real II MV Link_Grid is shown in Figure 3.8, while more detailed version can be found in Appendix A (Figure A.5).

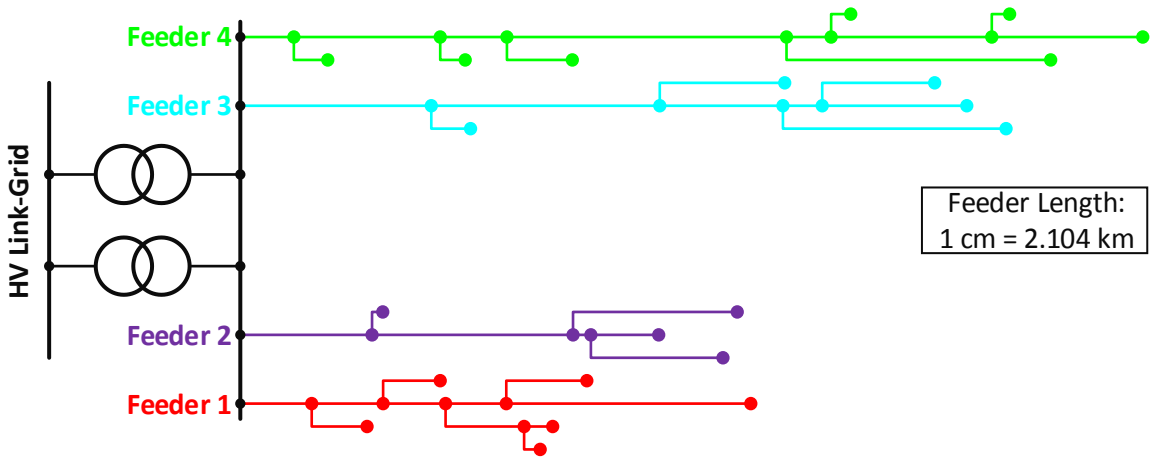

Figure 3.8 - Simplified overview of Real II MV Link_Grid

C. *Theoretical I MV Link_Grid*

Theoretical I MV Link_Grid is a distribution grid that has only one feeder and a HV/MV transformer with OLTC. During simulations in this grid, the feeder had different values of length: 1 km, 12,5 km and 25 km, respectively. Additionally, two different types of feeder have been used, which are the most dominant among other feeder types in Real I MV Link_Grid. Their most important parameters are listed in Table 3.5.

Table 3.5 - Parameters of feeder types used in Theoretical I MV Link_Grid

Feeder Type	R' $[\Omega/km]$	X' $[\Omega/km]$	C' $[\mu F/km]$	I_{th} $[A]$
OL-35/6	0,835	0,376	0,009	170
C-AL-150	0,206	0,122	0,254	320

A schematic overview of this grid is shown in Figure 3.9, where the feeder length is 25 km. A single Large Urban LV Link_Grid is connected at the end of the feeder, which is represented with a red doted circle.

Figure 3.9 - Schematic overview of Theoretical I MV Link_Grid

D. *Theoretical II MV Link_Grid*

Another grid created during this thesis is Theoretical II MV Link_Grid, which has only one feeder with total length size of 25 km. As in case of Theoretical I, same types of feeder have been used. Three same-sized Large Urban LV Link_Grids are connected at the beginning, middle and end of the feeders. The same HV/MV transformer from Theoretical I has been used in this grid as well. A schematic overview of this grid is represented in Figure 3.10, while the more detailed version is shown in Figure A.5.

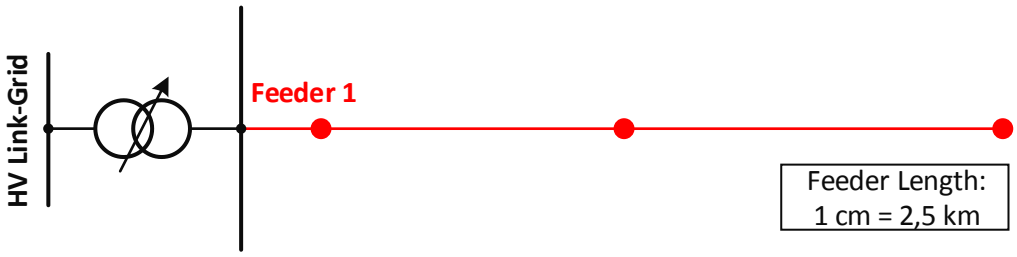

Figure 3.10 - Schematic overview of Theoretical II MV Link_Grid

4 System Modelling

The differences in time scales or frequency bands in which the various phenomena in electric power systems occur is one of the biggest challenges in finding the appropriate model for various system components. In this thesis, a steady state of system is assumed, which means that we are restricted to small and gradual changes in the system operating conditions. Therefore, transient stability phenomena are of no interest. Thus, only static models, which are time-invariant, have been chosen for different system components. Section 4.1 shows the modelling of the transformers that are present in both LV and MV Link_Grids. It also includes the representation of their most important parameters. Section 4.2 provides the most important electrical data information of line model, as well as its equivalent circuit diagram. Section 4.3 describes how the modelling of the Customer Plants (CPs) in LV Link_Grids is performed. Furthermore, Section 4.4 points out how the modelling of CPs that are connected to the Real MV Link_Grids is achieved. Lastly, Section 4.5 gives two different approaches of LV Link_Grids' modelling, which are connected to the Theoretical as well as to the Real MV Link_Grids.

4.1 Transformer Modelling

Each MV Link_Grid is equipped with two HV/MV power transformer and each LV Link_Grid with one MV/LV distribution transformer. All transformers used in these simulations are modelled according to the following circuit diagram, which is shown in Figure 4.1.

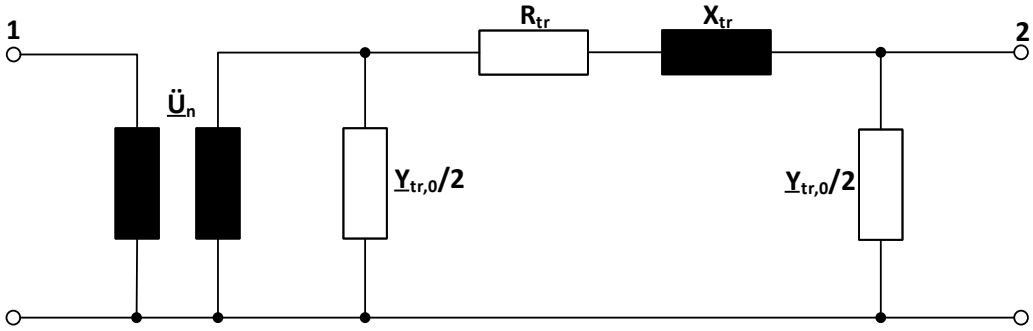

Figure 4.1 - Model of transformer in MV and LV Link_Grids

The rated transformation ratio $\ddot{U}_n$ can be calculated with the equation (4–1), where $U_{tr,pr}$ the primary rated voltage and $U_{tr,sec}$ the secondary rated voltage of transformer is.

$$\ddot{U}_n = \frac{U_{tr,pr}}{U_{tr,sec}} \tag{4–1}$$

Short circuit impedance $\underline{Z}_{tr}[\Omega]$ and no-load admittance $\underline{Y}_0[S]$ can be determined with equations (4–2) and (4–3), where $S_{tr}[kVA]$ rated apparent power, $u_r[\%]$ relative short circuit voltage, $u_k[\%]$ ohmic part of the u_r, $i_0[\%]$ no-load current and $V_{FE}[kW]$ iron losses in transformer represents.

$$\underline{Z}_{tr} = R_{tr} + jX_{tr} = \frac{U_{tr,sec}^2 \cdot \left(u_r + j\sqrt{u_k^2 - u_r^2}\right) \cdot 10^{-2}}{S_{tr}} \tag{4–2}$$

$$\underline{Y}_0 = \frac{V_{FE} \cdot 10^{-3} - j\sqrt{(i_0 \cdot 10^{-2} \cdot S_{tr})^2 - (V_{FE} \cdot 10^{-3})^2}}{U_{tr,sec}^2} \tag{4–3}$$

If the iron losses and the no-load current are neglected, as for this thesis has been done, then the no-load admittance $\underline{Y}_0$ is equal to zero. All the parameters in equations (4–1) to (4–3), as well as the vector group and tap range of transformers in LV and MV Link_Grids are listed in Table 4.1 and Table 4.2, respectively.

Table 4.1 - MV/LV transformer parameters in each LV Link_Grid

LV Link-Grid	S_{tr} [kVA]	$U_{tr,pr}$ [kV]	$U_{tr,sec}$ [kV]	u_k [%]	u_r [%]	*Vector group*	*Tap range*
Large Urban	630	20	0,4	4	1	$Dyn5$	$1-3$
Small Urban	400	20	0,4	3,7	1	$Dyn5$	$1-3$
Rural	160	21	0,42	3,7	1	$Dyn5$	$1-3$
Industrial	160	20	0,4	4,04	1	$Yzn5$	$1-3$

Table 4.2 - HV/MV transformer parameters in each MV Link_Grid

MV Link-Grid	S_{tr} [kVA]	$U_{tr,pr}$ [kV]	$U_{tr,sec}$ [kV]	u_k [%]	u_r [%]	*Vector group*	i_0 [%]	V_{FE} [kW]	*Tap range*
Real I	40 000	110	20	10,84	0,309	$YNyn6$	0,08	18,9	$1-25$
Real II	40 000	110	20	10,84	0,309	$YNyn6$	0,08	18,9	$1-25$
Theoretical I	40 000	110	20	10,84	0,309	$YNyn6$	0,08	18,9	$1-25$
Theoretical II	40 000	110	20	10,84	0,309	$YNyn6$	0,08	18,9	$1-25$

4.2 Line Modelling

In MV and LV Link_Grids two types of feeder are used: overhead lines and cables. The π-equivalent circuit diagram from Figure 4.2 illustrates the modelling of both types.

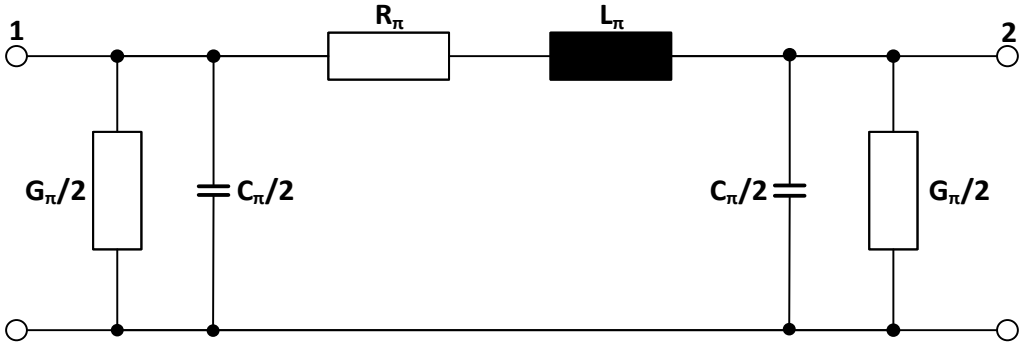

Figure 4.2 - Model of a line in LV and MV Link_Grids

Equations (4–4) and (4–5), as well as the data from Table A.1 and

Table A.2 are used to calculate electrical impedance $\underline{Z}_\pi$ and electrical admittance $\underline{Y}_\pi$ of the LV-lines and the MV-lines, where $R'_\pi\left[\frac{\Omega}{km}\right]$ specific resistance, $X'_\pi\left[\frac{\Omega}{km}\right]$ specific inductive reactance, $C'_\pi\left[\frac{nF}{km}\right]$ specific capacitance, $G'_\pi\left[\frac{\Omega}{km}\right]$ specific conductance, $\omega\left[\frac{rad}{s}\right]$ angular frequency and $l[km]$ length of the line is.

$$\underline{Z}_\pi = (R'_\pi + jX'_\pi) \cdot l = R_\pi + jX_\pi \tag{4–4}$$

$$\underline{Y}_\pi = (G'_\pi + j\omega C'_\pi) \cdot l = G_\pi + j\omega C_\pi \tag{4–5}$$

4.3 Modelling of Customer Plants in LV Link_Grids

As already explained in Chapter 3, a large number of CPs with the corresponding Producer-Link are connected to LV Link_Grids. In every CP a certain amount of active and reactive power is consumed by its native load. This active and reactive power consumption, which depends on the load scenario, is represented with the load model parameters $P_{LOAD}^{CP\_LV(f,n_f)}$ and $Q_{LOAD}^{CP\_LV(f,n_f)}$. Additionally, each CP, or more precisely its corresponding PV system can produce active power $P_{PV}^{CP\_LV(f,n_f)}$, which depends on the production scenario. The reactive power value $Q_{PV}^{CP\_LV(f,n_f)}$ depends on the control of the corresponding PV inverter. Both CPs' load and production scenarios are defined afterwards in Chapter 5. Indices f and n represent the exact connection position of CP in the grid, where f has a value of the corresponding feeder and n_f a value of the corresponding node. This means that a linear combination of an appropriate load and generator model gives the overall value of CP's active $P^{CP\_LV(f,n_f)}$ and reactive power $Q^{CP\_LV(f,n_f)}$. which is illustrated in Figure 4.3.

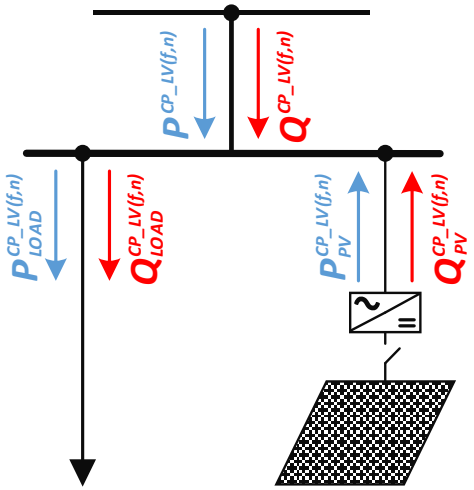

Figure 4.3 - Model of a Customer Plant in LV Link_Grids

If the directions of P- and Q-flows are set according to the figure above, values of $P^{CP\_LV(f,n_f)}$ and $Q^{CP\_LV(f,n_f)}$ can be determined with the following equations.

$$P^{CP\_LV(f,n_f)} = P_{LOAD}^{CP\_LV(f,n_f)} - P_{PV}^{CP\_LV(f,n_f)} \tag{4–6}$$

$$Q^{CP\_LV(f,n_f)} = Q_{LOAD}^{CP\_LV(f,n_f)} - Q_{PV}^{CP\_LV(f,n_f)} \tag{4–7}$$

In case where CP produces more active power than it consumes, $P^{CP\_LV(f,n_f)}$ value will have a negative sign, which further means, that CP will inject active power into the grid. In case of $Q^{CP\_LV(f,n_f)}$, the situation is not so clear, as this value, next to the sheer amount of $Q_{LOAD}^{CP\_LV(f,n_f)}$ and $Q_{PV}^{CP\_LV(f,n_f)}$, depends on the load behaviour and inverter's operating mode. It is assumed that the native load of each CP class in LV Link_Grids can be regarded as the inductive load. This means that each CP load absorbs reactive power ($Q_{LOAD}^{CP\_LV(f,n_f)} > 0$). From Figure 2.25 it is obvious that a PV inverter is capable of operating in overexcited (capacitive) and underexcited (inductive) mode as well. In correspondence with Figure 4.3 and Equation (4–7), a PV inverter in overexcited mode injects reactive power ($Q_{PV}^{CP\_LV(f,n_f)} > 0$) into the grid, while in underexcited mode it absorbs reactive power ($Q_{PV}^{CP\_LV(f,n_f)} <$

0) from the grid. The following text describes how the load and generator modelling has been carried out.

A. Load Model

Load composition of customers plays a vital role in choosing the appropriate load model. Load composition is based on the customer class and is dependent on many factors such as the type, size behaviour and equipment technology of the customer. As already stated, there are three major customer classes: residential, small commercial and industrial. In each class, the aggregate or equivalent load consists of the sum of different load components. A load component is defined as the aggregate equivalent of all devices with similar behaviour, i.e. lightning equipment (fluorescent, halogen...), household appliances (refrigerators, freezers, microwaves…) and power-electronics devices (TVs, laptops, chargers…). With the change in weather conditions, economic situation and culture, load composition of each class changes its behaviour [44].

As during this thesis, only steady states of grids were relevant, a static load model was used, which per definition is a time-independent load model that provides information on relevant load characteristics as a function of known or specified system parameters [45]. Every load is characterised by its active and reactive power consumption that are normally depended on the value of their supplying voltage. A list of well-known static load models is shown in Figure 4.4, whereby the ZIP model (blue coloured) is the chosen model.

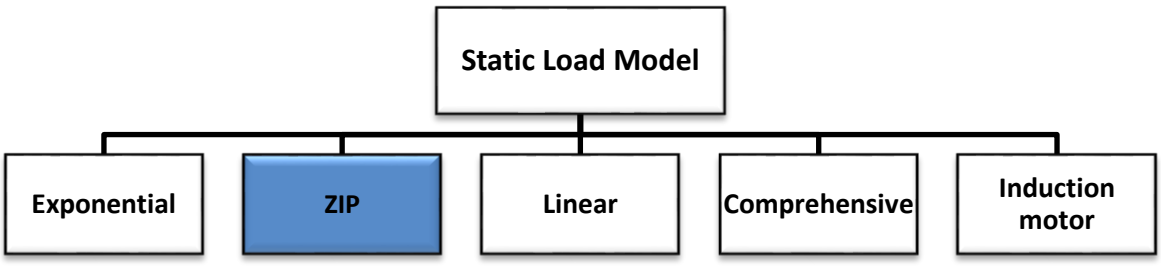

Figure 4.4 - Overview of most common static load models

The ZIP model views load of CP as a composition of three different components, where (Z) constant impedance, (I) constant current and (P) constant power load component is [46]. With the help of the following equations, it is possible to determine active power consumption $P_{LOAD}^{CP\_LV(f,n_f)}$ and reactive power consumption $Q_{LOAD}^{CP\_LV(f,n_f)}$ at operating voltage $U^{CP\_LV(f,n_f)}$ for each CP load, whereby $P_{IN,LOAD}^{CP\_LV(f,n_f)}$ and $Q_{IN,LOAD}^{CP\_LV(f,n_f)}$ are the initial active and reactive power at the nominal voltage $U_{NOM}^{CP\_LV(f,n_f)}$; Z_P, I_P and P_P are the ZIP coefficients for active power; and Z_Q, I_Q and P_Q are the ZIP coefficients for reactive power.

$$\frac{P_{LOAD}^{CP\_LV(f,n_f)}}{P_{IN.LOAD}^{CP\_LV(f,n_f)}} = Z_P \cdot \left(\frac{U^{CP\_LV(f,n_f)}}{U_{NOM}^{CP\_LV(f,n_f)}}\right)^2 + I_P \cdot \left(\frac{U^{CP\_LV(f,n_f)}}{U_{NOM}^{CP_{LV(f,n_f)}}}\right) + P_P \qquad (4\text{–}8)$$

$$\frac{Q_{LOAD}^{CP\_LV(f,n_f)}}{Q_{IN.LOAD}^{CP\_LV(f,n_f)}} = Z_Q \cdot \left(\frac{U^{CP\_LV(f,n_f)}}{U_{NOM}^{CP\_LV(f,n_f)}}\right)^2 + I_Q \cdot \left(\frac{U^{CP\_LV(f,n_f)}}{U_{NOM}^{CP\_LV(f,n_f)}}\right) + P_Q \qquad (4\text{–}9)$$

In order to calculate accurately $P_{LOAD}^{CP\_LV(f,n_f)}$ and $Q_{LOAD}^{CP\_LV(f,n_f)}$ of each CP load, some requirements have to be met. These requirements are mathematically formulated with Equation (4–10) and (4–11), respectively.

$$Z_P + I_P + P_P = 1 \tag{4–10}$$

$$Z_Q + I_Q + P_Q = 1 \tag{4–11}$$

The value of $P_{IN.LOAD}^{CP\_LV(f,n_f)}$ is specified by the scenario, while the value of initial reactive power consumption $Q_{IN.LOAD}^{CP\_LV(f,n_f)}$ can be calculated from $P_{IN.LOAD}^{CP\_LV(f,n_f)}$ and the corresponding $\cos\varphi$, which is shown later on in Section 5.1. Depending on the class of the l customers, a specific value of the power factor is assigned to each class, which is shown in Table 4.3.

Table 4.3 - Power factor of different customer classes in LV Link_Grids

	Residential	***Small commercial***	***Industrial***
$\boldsymbol{\cos\varphi}$	0,95	0,90	0,90

In regard to the ZIP coefficients, they also differ from one customer class to another. The ZIP coefficients, which have been used for residential, small commercial and industrial customer class in this thesis, are listed in Table 4.4.

Table 4.4 - ZIP coefficients for different customer classes in LV Link_Grids [46]

Customer class	***Sub class***	$\boldsymbol{Z_P}$	$\boldsymbol{I_P}$	$\boldsymbol{P_P}$	$\boldsymbol{Z_Q}$	$\boldsymbol{I_Q}$	$\boldsymbol{P_Q}$
Residential	*Type A*	1,31	−1,94	1,63	9,2	−15,27	7,07
	Type B	0,96	−1,17	1,21	6,28	−10,16	4,88
	Type C	1,18	−1,64	1,47	8,29	−13,67	6,38
Small Commercial	*Drug store*	0,27	−0,33	1,06	5,48	−9,7	5,22
	Restaurant	0,69	0,04	0,27	1,82	−2,24	1,43
	Laundromat	0,77	−0,84	1,07	8,09	−13,65	6,56
	Optics	0,55	0,24	0,21	0,55	−0,09	0,54
Industrial	/	1,21	−1,61	1,41	4,35	−7,08	3,72

As in [46] is stated, annual energy consumption is different for each subclass of residential customers In Table 4.5 is shown how the subclasses and therefore their corresponding ZIP coefficients for residential customers in each LV Link_Grids have been chosen.

Table 4.5 - Subclass assignment to residential customers in every LV Link_Grid

LV Link- Grid	***Sub class***
Large Urban	*Type B*
Small Urban	*Type C*
Rural	*Type B*
Industrial	*Type A*

As it can be seen from Table 4.4, small commercial customers have also their own subclasses. Since Industrial LV Link_Grid has four small commercial customers, each of them has a different subclass and

therefore different ZIP coefficients. The assignment of subclasses is adopted from [9] and listed in Table 4.6. The numbering of these four nodes is overtaken from Figure A.4 (see Appendix A).

Table 4.6 - Sub class assignment for small commercial customers in Industrial LV Link_Grid

Node	***Sub class***
(1,9)	*drug store*
(2,3)	*restaurant*
(2,4)	*laundromat*
(3,1)	*optics*

B. Generation Model

A power generation of CPs or precisely the connected Producer-Links is represented through a photovoltaic system, better known as PV system. It consists of an arrangement of several components, including PV-array to absorb and convert sunlight into electricity, an overvoltage protection, an inverter that works as DC-AC converter, as well as mounting, cabling and other electrical accessories that enable PV system to work properly. Every PV system is characterized by its active power value $P_{PV}^{CP\_LV(f,n_f)}$ and reactive power value $Q_{PV}^{CP\_LV(f,n_f)}$, which are generated by an inverter. Depending on the case in the corresponding LV Link_Grid, those values are characterized in the following chapter. As shown in Chapter 2, different active and reactive power controls of an inverter can influence $P_{PV}^{CP\_LV(f,n_f)}$ and $Q_{PV}^{CP\_LV(f,n_f)}$ values. It is assumed that the inverters work without losses, i.e. they have efficiency $\eta_{PV\_INV} = 100\%$. When connected to the grid, a PV system generates constantly its rated active power, which is also its maximum output. The rated apparent power $S_{RAT.PV\_INV}^{CP\_LV(f,n_f)}$ of the inverter doesn't have the same value as the rated active power output of the related PV system. If those values were the same and the PV system operated at a power factor $\cos\varphi \neq 1$, this would lead to active power curtailment during periods of high active power output. Instead, the inverters have been oversized in order to provide the rated active power at the power factor $\cos\varphi = 0{,}9$ and under nominal voltage at a connection point. The following equations show how the inverter's rated apparent power is dimensioned and how maximum reactive power capability of a PV system $Q_{MAX.PV}^{CP\_LV(f,n_f)}$ can be calculated.

$$S_{RAT.PV\_INV}^{CP\_LV(f,n_f)} = VA_{BASE} \tag{4–12}$$

$$S_{RAT.PV\_INV}^{CP\_LV(f,n_f)} = \frac{P_{RAT.PV}^{CP\_LV(f,n_f)}}{0{,}9} = 1\ p.u. \tag{4–13}$$

$$Q_{MAX.PV}^{CP\_LV(f,n_f)} = \pm\sqrt{S_{RAT.PV\_INV}^{CP\_LV(f,n_f)^2} - P_{RAT.PV}^{CP\_LV(f,n_f)^2}} = \pm 0{,}436\ p.u. \tag{4–14}$$

The reasoning behind is that all generating plants need to operate in accordance with the Austrian grid code for generating plants connected to the low voltage distribution grids. This further means that the operating power factor is limited to the following range, respectively:

$$0{,}9\ (cap.) \leq \cos\varphi \leq 1 \tag{4–15}$$

$$0{,}9\ (ind.) \leq \cos\varphi \leq 1 \tag{4–16}$$

A DC surge protector against overvoltage, which is installed between PV-array and PV-inverter, can have an impact on $P_{PV}^{CP\_LV(f,n_f)}$ values. In case where the predefined voltage limit of the connection point is surpassed, a PV-array is getting automatically disconnected. Figure 4.5 illustrates how the overvoltage protection works in case of this generation model under assumption that a PV system always generates the rated active power.

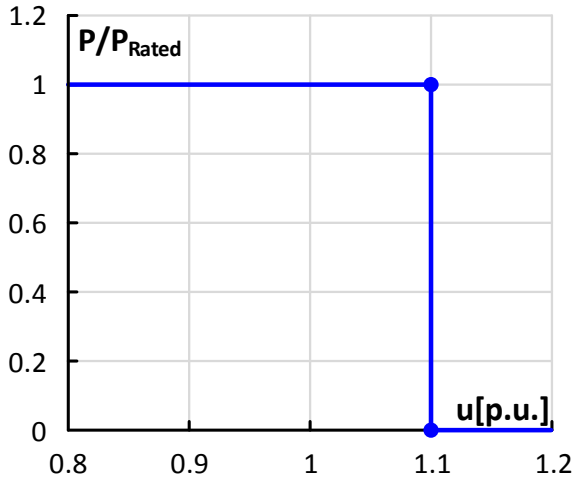

Figure 4.5 - *P(U)*-characteristic of a PV-array in case of overvoltage

During simulations in this thesis, the PV-systems were either modelled with uncontrolled or $Q(U)$-controlled inverters. All CP connected to Small Urban and Industrial LV Link_Grids have PV systems that have been modelled only with uncontrolled inverters, because during the power flow calculations the predefined voltage limits were not exceeded. The uncontrolled inverters ($\cos\varphi = 1$) generate active power without generating or absorbing any reactive power.

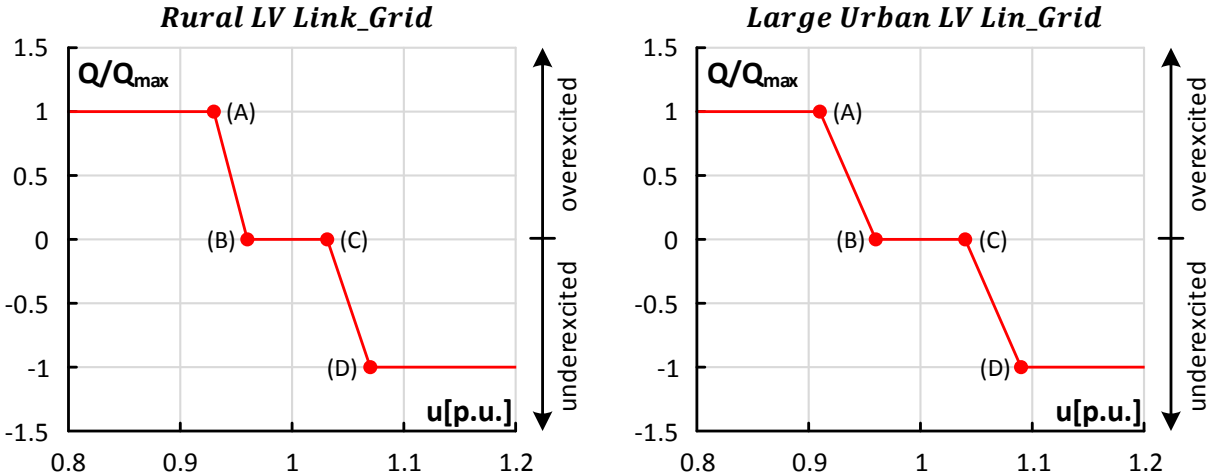

Figure 4.6 - *Q(U)*-characteristic of the PV inverters in Rural and Large Urban LV Link_Grid

On the other hand, the $Q(U)$-controlled inverters, which are used in Large Urban and Rural LV Link_Grids, inject active and inject or absorb reactive power as well. It is assumed that the $P_{PV}^{CP\_LV(f,n_f)}$ values are not affected by the $Q(U)$-control. Reactive power injection/absorption is a function of the voltage at the connection point to the LV Link_Grids. Figure 4.6 shows the $Q(U)$-characteristic of the PV inverters in Large Urban and Rural LV Link_Grid.

Four characteristic breakpoints of $Q(U)$-control for each PV inverter in Rural and Large Urban LV Link_Grid are represented in Table 4.7.

Table 4.7 - Different breakpoints of *Q(U)*-control

LV Link_Grid	*A*	*B*	*C*	*D*
Rural	0,93	0,96	1,03	1,07
Large Urban	0,91	0,96	1,04	1,09

4.4 Modelling of Customer Plants in MV Link_Grids

As in case of CPs in LV Link_Grids, CPs connected to MV Link_Grids produce electric power through their corresponding PV system. Figure 4.7 gives a schematic overview of a typical CP's model in MV Link_Grids, whereby the overall active $P^{CP\_MV(f,n_f)}$ and reactive power values $Q^{CP\_MV(f,n_f)}$ of CPs in MV link_Grids are gathered in the same way as it has been done for $P^{CP\_MV(f,n_f)}$ and $Q^{CP\_MV(f,n_f)}$ values of CPs in LV Link_Grids.

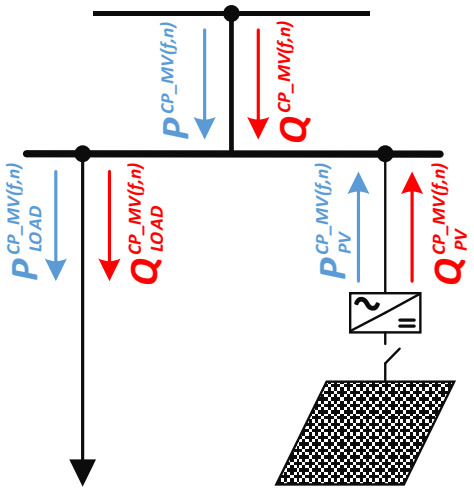

Figure 4.7 - Model of a Customer Plant in LV Link_Grids

Based on the CPs' load composition, there are two types of CPs that are connected to MV Link_Grids: large commercial and industrial. In reality, those CP aren't connected directly to a MV Link_Grid, rather they usually own a distribution transformer which steps down MV to LV level (in this case 20 kV to 400 V). As a simplification, it is assumed that these distribution transformers don't have any active and reactive power losses. As it is already known, one of transformers' key features is the power invariance. With respect to this feature and previously mentioned simplification, CPs in MV Link_Grids can be modelled in the same fashion as CPs in LV Link_Grids.

A. Load Model

Load model is represented with the ZIP model. The differences are the used ZIP coefficients and values for initial active $P_{IN.LOAD}^{CP\_MV(f,n_f)}$ and reactive $Q_{IN.LOAD}^{CP\_MV(f,n_f)}$ power consumption, as well as the nominal and actual voltage level. To determine actual active $P_{LOAD}^{CP\_MV(f,n_f)}$ and reactive $Q_{LOAD}^{CP\_MV(f,n_f)}$ power consumption of each CP load, the already familiar equations (4–17) and (4–18) have been used.

$$\frac{P_{LOAD}^{CP\_MV(f,n_f)}}{P_{IN.LOAD}^{CP\_MV(f,n_f)}} = Z_P \cdot \left(\frac{U^{CP\_MV(f,n_f)}}{U_{NOM}^{CP\_MV(f,n_f)}}\right)^2 + I_P \cdot \left(\frac{U^{CP\_MV(f,n_f)}}{U_{NOM}^{CP\_MV(f,n_f)}}\right) + P_P \quad (4\text{–}17)$$

$$\frac{Q_{LOAD}^{CP\_MV(f,n_f)}}{Q_{IN.LOAD}^{CP\_MV(f,n_f)}} = Z_Q \cdot \left(\frac{U^{CP\_MV(f,n_f)}}{U_{NOM}^{CP\_MV(f,n_f)}}\right)^2 + I_Q \cdot \left(\frac{U^{CP\_MV(f,n_f)}}{U_{NOM}^{CP\_MV(f,n_f)}}\right) + P_Q \quad (4\text{–}18)$$

Values of $P_{IN.LOAD}^{CP\_MV(f,n_f)}$ and $Q_{IN.LOAD}^{CP\_MV(f,n_f)}$ for each CP's class have been characterized in Chapter 5. Once again, the same requirements for ZIP coefficients have to be fulfilled, which is expressed with the following equations.

$$Z_P + I_P + P_P = 1 \quad (4\text{–}19)$$

$$Z_Q + I_Q + P_Q = 1 \quad (4\text{–}20)$$

Based on the customer class, different ZIP coefficients, which are listed in Table 4.8, have been used. Although industrial customers in MV Link_Grids consume a lot more electric power than those in LV Link_Grids, it is assumed that regardless their size, all industrial customers show similar characteristic in regard to their individual load composition. Therefore, class of large industrial customers doesn't exist, which means that the same ZIP coefficients can be used for every industrial customer.

Table 4.8 - ZIP coefficients for large commercial and industrial customers [46]

Customer class	***Subclass***	Z_P	I_P	P_P	Z_Q	I_Q	P_Q
Large Commercial	*School*	0,4	−0,41	1,01	4,43	−7,98	4,56
	Hotel	0,76	−0,52	0,76	6,92	−11,75	5,83
Industrial	/	1,21	−1,61	1,41	4,35	−7,08	3,72

From Table 4.8 it is apparent that the large commercial class can be divided into two different subclasses. During the simulations in MV Link_Grids, ZIP coefficients of subclass "School" have been used for all connected large commercial CPs.

B. Generation Model

Power production of CPs in MV Link_Grids, or more precisely, their corresponding PV system have been modelled in pretty much the same manner as it has been done for PV systems of CPs in LV Link_Grids. Output values of each PV system $P_{PV}^{CP\_MV(f,n_f)}$ and $Q_{PV}^{CP\_MV(f,n_f)}$ are characterized in the following chapter. Once again, it is assumed that PV inverters operate without and reactive power losses ($\eta_{PV\_INV} = 100\%$). At every time, in accordance with requirements from [41], each PV inverter has to be in position to inject or absorb its maximum reactive power value, which reaches 38% of the inverter's rated apparent power $S_{RAT.PV\_INV}^{CP\_MV(f,n_f)}$. This is mathematically expressed in the following equations.

$$S_{RAT.PV\_INV}^{CP\_MV(f,n_f)} = \frac{P_{RAT.PV}^{CP\_MV(f,n_f)}}{0{,}925} = 1\ p.u. \quad (4\text{–}21)$$

$$Q_{MAX.PV}^{CP\_MV(f,n_f)} = \pm\sqrt{S_{RAT.PV\_INV}^{CP\_MV(f,n_f)^2} - P_{RAT.PV}^{CP\_MV(f,n_f)^2}} = \pm 0{,}38\ p.u. \quad (4\text{–}22)$$

During simulations in MV Link_Grids, the PV systems of Industrial CPs were equipped with uncontrolled inverters ($\cos\varphi = 1$), while the ones of Large Commercial CPs had *Q(U)*-controlled inverters. Figure 4.6 shows the *Q(U)*-characteristic of PV inverters for Large Commercial CPs in MV Link_Grids.

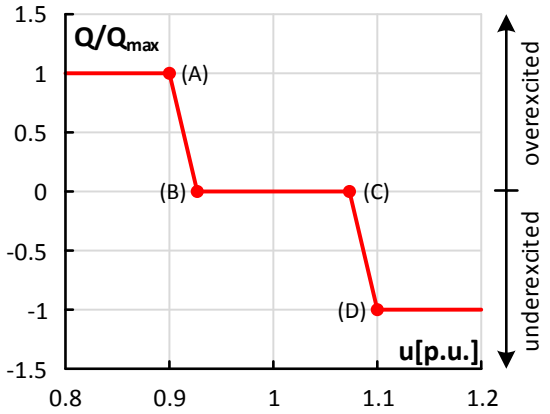

Figure 4.8 - *Q(U)*-characteristic for PV inverters of Large Commercial CPs

Four distinctive breakpoints of this *Q(U)*-control are shown in Table 4.9.

Table 4.9 - Different breakpoints of *Q(U)*-control for Large Commercial CPs

CP type	***A***	***B***	***C***	***D***
Large Commercial	0,90	0,93	1,07	1,10

4.5 Modelling of LV Link_Grids in MV Link_Grids

As already known, not only Large Commercial and Industrial CPs are connected to MV Link_Grids, but the whole LV Link_Grids as well. They need to be properly modelled so that the behaviour of MV Link_Gris can be further investigated when the high penetration level of DGs is present. During this thesis LV Link_Grids were modelled in two different ways, which are shown in the text that follows.

4.5.1 "Used" Model

The first lumped model of a LV Link_Grid is the so called "used" model, which is nowadays applied when the modelling of MV Link_Grids is performed. This model is almost entirely based on the model parameters of CPs that are connected to LV Link_Grids. Figure 4.9 illustrates the present lumped model of a typical LV Link_Grid, whereby P^{Lmpd_LVG} and Q^{Lmpd_LVG} are overall active and reactive power values of the related grid. According to the figure bellow, P^{Lmpd_LVG} and Q^{Lmpd_LVG} can be represented through superposition of load and generation model, which is shown in the following equations.

$$P^{Lmpd\_LVG} = P_{PV}^{Lmpd\_LVG} - P_{LOAD}^{Lmpd\_LVG} \tag{4–23}$$

$$Q^{Lmpd\_LVG} = Q_{PV}^{Lmpd\_LVG} - Q_{LOAD}^{Lmpd\_LVG} \tag{4–24}$$

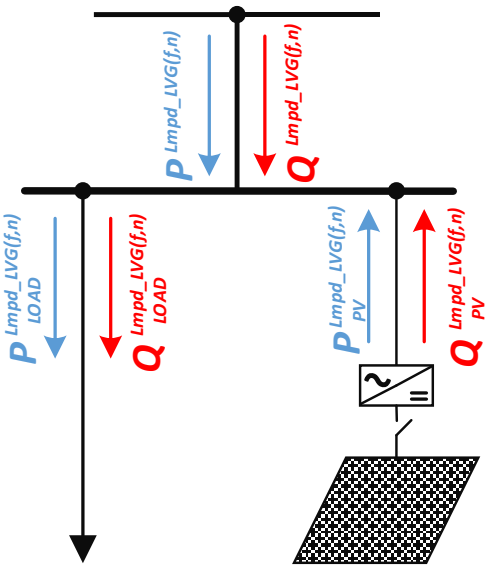

Figure 4.9 - Used model of a typical LV Link_Grid

A. *Load Model*

Active $P_{LOAD}^{Lmpd\_LVG}$ and reactive power consumption $Q_{LOAD}^{Lmpd\_LVG}$ can be determined with the help of already familiar ZIP model equations, which are given down below.

$$\frac{P_{LOAD}^{Lmpd\_LVG}}{P_{IN.LOAD}^{Lmpd\_LVG}} = Z_P \cdot \left(\frac{U^{Lmpd\_LVG}}{U_{NOM}^{Lmpd\_LVG}}\right)^2 + I_P \cdot \left(\frac{U^{Lmpd\_LVG}}{U_{NOM}^{Lmpd\_LVG}}\right) + P_P \qquad (4\text{–}25)$$

$$\frac{Q_{LOAD}^{Lmpd\_LVG}}{Q_{IN.LOAD}^{Lmpd\_LVG}} = Z_Q \cdot \left(\frac{U^{Lmpd\_LVG}}{U_{NOM}^{Lmpd\_LVG}}\right)^2 + I_Q \cdot \left(\frac{U^{Lmpd\_LVG}}{U_{NOM}^{Lmpd\_LVG}}\right) + P_Q \qquad (4\text{–}26)$$

Values of used ZIP coefficients for each grid are adopted from the ZIP coefficients for those CP types, which are the most common in the related grid.

Table 4.10 - ZIP coefficients of present lumped model for each LV Link_Grid

LV Link- Grid	***Customer Class***	Z_P	I_P	P_P	Z_Q	I_Q	P_Q
Large Urban	*Residential*	0,96	−1,17	1,21	6,28	−10,16	4,88
Small Urban	*Residential*	1,18	−1,64	1,47	8,29	−13,67	6,38
Rural	*Residential*	0,96	−1,17	1,21	6,28	−10,16	4,88
Industrial	*Industrial*	1,21	−1,61	1,41	4,35	−7,08	3,72

Criteria on which load model parameters $P_{IN.LOAD}^{Lmpd\_LVG}$ and $Q_{IN.LOAD}^{Lmpd\_LVG}$ have been chosen are fully described in Chapter 6, while exact values for each grid are represented in Chapter 7.

B. *Generation Model*

Total power generation of every LV Link_Grid is represented with a model of inverter-controlled PV system, where its active and reactive power output are $P_{PV}^{Lmpd\_LVG}$ and $Q_{PV}^{Lmpd\_LVG}$, respectively. $Q_{PV}^{Lmpd\_LVG}$ value depends on the actual inverter control, which is characterized with its maximum reactive power capability $Q_{MAX.PV\_INV}^{Lmpd\_LVG}$. In which way have the values for $P_{PV}^{Lmpd\_LVG}$ and $Q_{PV}^{Lmpd\_LVG}$

been defined is explained in Chapter 6, while their exact values for each grid are represented in Chapter 7.

4.5.2 "Proposed" Model

Another lumped model of a LV Link_Grid is the "proposed" model, which was created from the simulation results in the related LV Link_Grid. For this modelling an overall active and reactive power consumption or injection of used LV Link_Grid is required, which depend on the load and production scenario of connected CPs. From the load flow simulations, the voltage-dependent active P^{DTR_PRM} and reactive power value Q^{DTR_PRM} at the primary side of the related distribution transformer were gathered. An exact simulation and calculation procedure are explained in Chapter 6, while the related results are represented in Chapter 7.

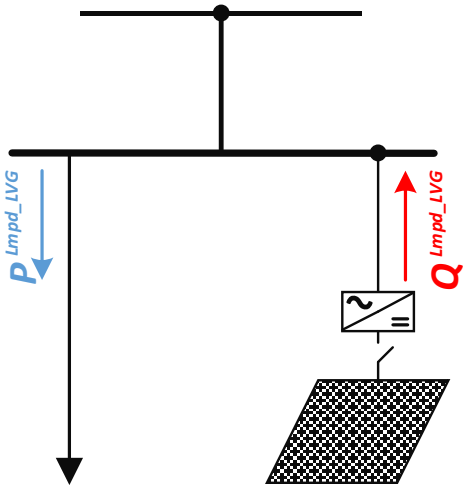

Figure 4.10 - Proposed model of a typical LV Link_Grid

The proposed model of a typical LV Link_Grid is illustrated schematically in Figure 4.10, whereby P^{Lmpd_LVG} and Q^{Lmpd_LVG} are the overall active and reactive power values of the related grid. These values should match the corresponding values of P^{DTR_PRM} and Q^{DTR_PRM}, respectively. As in case of "used" model, this model was built through a superposition of load and generation model.

A. Load Model

Contrarily to load models of Customer Plants, proposed load model of LV Link_Grid has only a P-component. The already mentioned ZIP model has been used in this case as well, which is formulated with the following equations.

$$\frac{P^{Lmpd\_LVG}}{P_{INIT}^{Lmpd\_LVG}} = Z_P \cdot \left(\frac{U^{Lmpd\_LVG}}{U_{NOM}^{Lmpd\_LVG}}\right)^2 + I_P \cdot \left(\frac{U^{Lmpd\_LVG}}{U_{NOM}^{Lmpd\_LVG}}\right) + P_P \qquad (4\text{–}27)$$

$$Z_P + I_P + P_P = 1 \qquad (4\text{–}28)$$

In order to calculate P^{Lmpd_LVG} value, it is necessary to determine other parameters from Equation (4–27). Characterization of $P_{INIT}^{Lmpd\_LVG}$ and ZIP coefficients for active power for all LV Link_Grids, which depend on the load and production scenarios of related grid, will be shown in Chapter 7. With so

acquired ZIP coefficients and $P_{INIT}^{Lmpd\_LVG}$, it is possible to estimate the value of P^{Lmpd_LVG} at any given voltage level.

B. Generation Model

Proposed generation model of a LV Link_Grid needs to have only a Q-component Q^{Lmpd_LVG}, which should represent total reactive power exchange between the corresponding LV and MV Link_Grid. This can be achieved with a model of the inverter-controlled PV system. The inverter's reactive power output Q^{Lmpd_LVG} relies upon the load and production situation in the corresponding LV Link_Grid. Chapter 6 shows in what way has Q^{Lmpd_LVG} been defined, while its true value for each grid is outlined in Chapter 7.

5 Scenarios Definition

In this chapter different scenarios are defined that are crucial for assessment of DG impact on the total behaviour of LV and MV Link_Grids. Section 5.1 points out in which way the initial load model values define the load scenarios of CPs in LV and MV Link_Grids. Section 5.2 shows how the rated power of PV systems characterize the production scenarios of CPs in LV and MV Link_Grids. The combinations of different CP's load and production scenarios reveal the most relevant cases for LV and MV Link_Grids, which are represented in Section 5.3.

5.1 Consideration of different Initial Load Model Values

The most essential criteria for defining load scenarios is the value of the initial consumption. Two cases are going to be observed. First case represents the load scenario where the *P*- and *Q*-demand of each CP is observed at 20h, because at that particular time the related PV systems don't generate any active power. In second case, midday (12h) has been chosen as the reference point, where a high-level production of corresponding PVs is expected.

A. Customer Plants in LV Link_Grids

Characterization of initial active power consumption of each CP in LV Link_Grids has been carried out with the help of CPs' daily load and production profiles, which is illustrated in Figure 5.1. While each customer class shows different load characteristic, there is no difference in their production profile.

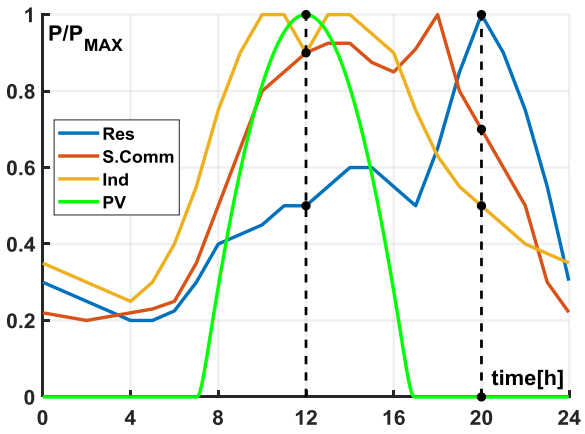

Figure 5.1 - Daily load and production profile of CPs in LV Link_Grids

As already seen, Large Urban, Small Urban and Rural LV Link_Grid have only residential CPs, which according to the figure above reach their maximum exactly at 20h. Under assumption that they consume the same amount of power, initial active power consumption at 20h $P_{IN.LOAD\_20h}^{CP\_LV(f,n_f)}$ of each residential CP in Large Urban, Small Urban and Rural LV Link_Grid can be calculated from the number of residential customers $N_{RES}^{CP\_LV}$ in each of these three LV Link_Grids and the maximum active power $P_{2016\_MAX}^{DTR\_SCD}$ measured at the secondary side of the corresponding MV/LV distribution transformer in 2016. The final value of $P_{IN.LOAD\_20h}^{CP\_LV(f,n_f)}$, as shown in Equation (5–1), has to be a little bit smaller than the calculated value, because the line and transformer losses have to be taken in consideration as well. With Equation (5–2) the initial reactive power consumption at 20h $Q_{IN.LOAD\_20h}^{CP\_LV(f,n_f)}$ of each CP in Large

Urban, Small Urban and Rural LV Link_Grid can be determined from $P_{IN.LOAD\_20h}^{CP\_LV(f,n_f)}$ and corresponding value of $\cos\varphi^{(f,n_f)}$.

$$P_{IN.LOAD\_20h}^{CP\_LV(f,n_f)} \cong \frac{P_{2016\_MAX}^{DTR\_SCD}}{N_{RES}} \tag{5–1}$$

$$Q_{IN.LOAD\_20h}^{CP\_LV(f,n_f)} = P_{IN.LOAD\_20h}^{CP\_LV(f,n_f)} \cdot \tan\varphi^{(f,n_f)} = P_{IN.LOAD\_20h}^{CP\_LV(f,n_f)} \cdot \frac{\sqrt{1-cos^2\varphi^{(f,n_f)}}}{\cos\varphi^{(f,n_f)}} \tag{5–2}$$

Table 5.1 shows the number of CPs, *P*- and *Q*-demand of each CP and accumulated *P*- and *Q*-demand in Large Urban, Small Urban and Rural LV Link_Grid. These values characterize the "20h" load scenario.

Table 5.1 - "20h" load scenario of CPs in Large Urban, Small Urban and Rural LV Link_Grid

LV Link-Grid	$N_{RES}^{CP\_LV}$	$P_{IN.LOAD\_20h}^{CP\_LV(f,n_f)}$ $[kW]$	$P_{IN.LOAD\_20h}^{CP\_LV(f,n_f)}$ $[kVAr]$	$P_{IN.LOAD\_20h}^{TOT.CP\_LV}$ $[kW]$	$Q_{IN.LOAD\_20h}^{TOT.CP}$ $[kVAr]$
Large Urban	175	1,956	0,6429	342,3	112,509
Small Urban	91	2,62	0,8612	238,42	78,365
Rural	61	1,368	0,4496	83,448	27,428

In case of Industrial LV Link_Grid, where all three types of CPs are connected, another approach needs to be taken. Based on the contracted power of each CP in Industrial LV Link_Grid, the gathered value of $P_{2016\_MAX}^{DTR\_SCD}$ and Figure 5.1, the active power consumption at 14h $P_{IN.LOAD\_14h}^{CP\_LV(f,n_f)}$ is calculated for each CP. Regarding the customer class, initial active power consumption at 20h $P_{IN.LOAD\_14h}^{CP\_LV(f,n_f)}$ of each CP are determined in the following way.

Residential: $$P_{IN.LOAD\_20h}^{CP\_LV(f,n_f)} = P_{IN.LOAD\_14h}^{CP\_LV(f,n_f)} \cdot 1,\overline{666} \tag{5–3}$$

Small commercial: $$P_{IN.LOAD\_20h}^{CP\_LV(f,n_f)} = P_{IN.LOAD\_14h}^{CP\_LV(f,n_f)} \cdot 0,\overline{756} \tag{5–4}$$

Industrial: $$P_{IN.LOAD\_20h}^{CP\_LV(f,n_f)} = P_{IN.LOAD\_14h}^{CP\_LV(f,n_f)} \cdot 0,5 \tag{5–5}$$

The classification of CPs that are connected to Industrial LV Link_Grid, as well as their individual $P_{IN.LOAD\_20h}^{CP\_LV(f,n_f)}$ and $Q_{IN.LOAD\_20h}^{CP\_LV(f,n_f)}$ values are represented in Table 5.2.

The initial active power consumption of each CPs at 12h $P_{IN.LOAD\_12h}^{CP\_LV(f,n_f)}$ is acquired with the help of the daily load profiles of different customer classes in LV Link_Grids and the corresponding $P_{IN.LOAD\_20h}^{CP\_LV(f,n_f)}$ value, which is represented in the following equations.

Residential: $$P_{IN.LOAD\_12h}^{CP\_LV(f,n_f)} = P_{IN.LOAD\_20h}^{CP\_LV(f,n_f)} \cdot 0,5 \tag{5–6}$$

Small commercial: $$P_{IN.LOAD\_12h}^{CP\_LV(f,n_f)} = P_{IN.LOAD\_20h}^{CP\_LV(f,n_f)} \cdot 1,28571 \tag{5–7}$$

Industrial: $$P_{IN.LOAD\_12h}^{CP\_LV(f,n_f)} = P_{IN.LOAD\_20h}^{CP\_LV(f,n_f)} \cdot 1,8 \tag{5–8}$$

Table 5.2 - "20h" load scenario of CPs in Industrial LV Link_Grid

Node	**Customer Class**	$P_{IN.LOAD\_20h}^{CP\_LV(f,n_f)}$ [**kW**]	$Q_{IN.LOAD\_20h}^{CP\_LV(f,n_f)}$ [**kVAr**]	**Node**	**Customer Class**	$P_{IN.LOAD\_20h}^{CP\_LV(f,n_f)}$ [**kW**]	$Q_{IN.LOAD\_20h}^{CP\_LV(f,n_f)}$ [**kVAr**]
(1,1)	*residential*	8,944	2,9398	(1,9)	*small comm.*	4,472	2,1659
(1,2)	*industrial*	7,826	3,7903	(1,10)	*industrial*	5,59	2,7074
(1,3)	*industrial*	4,472	2,1659	(1,11)	*industrial*	44,72	21,6589
(1,4)	*industrial*	4,472	2,1659	(2,1)	*residential*	22,36	7,3494
(1,5)	*industrial*	41,366	20,0345	(2,2)	*small comm.*	22,36	10,8294
(1,6)	*industrial*	4,472	2,1659	(2,3)	*small comm.*	27,95	13,5368
(1,7)	*industrial*	1,118	0,5415	(2,4)	*small comm.*	13,416	6,4977
(1,8)	*industrial*	11,18	5,4147	(3,1)	*industrial*	223,6	108,2944

$Q_{IN.LOAD\_12h}^{CP\_LV(f,n_f)}$ values are derived from $P_{IN.LOAD\_12h}^{CP\_LV(f,n_f)}$ values in the same way as it has been done previously for $Q_{IN.LOAD\_20h}^{CP\_LV(f,n_f)}$ values. The most important data about the midday load scenario of CPs in Large Urban, Small Urban and Rural LV Link_Grid are represented in Table 5.3.

Table 5.3 - "12h" load scenario of CPs in Rural, Small Urban and Large Urban LV Link_Grid

LV Link-Grid	N_{RES}	$P_{IN.LOAD\_12h}^{CP\_LV(f,n_f)}$ [**kW**]	$Q_{IN.LOAD\_12h}^{CP\_LV(f,n_f)}$ [**kVAr**]	$P_{IN.LOAD\_12h}^{TOT.CP\_LV}$ [**kW**]	$Q_{IN.LOAD\_12h}^{TOT.CP\_LV}$ [**kVAr**]
Large Urban	175	0,978	0,3043	171,15	56,254
Small Urban	91	1,31	0,4306	119,21	39,182
Rural	61	0,684	0,2248	41,724	13,714

Regarding the midday load scenario of CPs in Industrial LV Link_Grid, Table 5.4 gives the class of each CP and its exact position in the grid, as well as their individual *P*- and *Q*-consumption.

Table 5.4 - "12h" load scenario of CPs in Industrial LV Link_Grid

Node	**Customer Class**	$P_{IN.LOAD\_12h}^{CP\_LV(f,n_f)}$ [**kW**]	$Q_{IN.LOAD\_12h}^{CP\_LV(f,n_f)}$ [**kVAr**]	**Node**	**Customer Class**	$P_{IN.LOAD\_12h}^{CP\_LV(f,n_f)}$ [**kW**]	$Q_{IN.LOAD\_12h}^{CP\_LV(f,n_f)}$ [**kVAr**]
(1,1)	*residential*	4,48	1,473	(1,9)	*small comm.*	4,032	1,953
(1,2)	*industrial*	7,056	3,417	(1,10)	*industrial*	5,04	2,441
(1,3)	*industrial*	4,032	1,953	(1,11)	*industrial*	40,32	19,528
(1,4)	*industrial*	4,032	1,953	(2,1)	*residential*	11,2	3,681
(1,5)	*industrial*	37,296	18,063	(2,2)	*small comm.*	20,16	9,764
(1,6)	*industrial*	4,032	1,953	(2,3)	*small comm.*	25,2	12,205
(1,7)	*industrial*	1,008	0,488	(2,4)	*small comm.*	12,096	5,858
(1,8)	*industrial*	10,08	4,882	(3,1)	*industrial*	201,6	97,639

B. Customer Plants in MV Link_Grids

As it is already known , there are 30 large commercial customers in Real I MV Link Grid, while Real II MV Link_Grid has 69 large commercial and 4 industrial customers. Each connected CP reaches its maximum of consumed active power at 8h ($P_{IN.LOAD\_8h}^{CP\_MV(f,n_f)}$) and 10h ($P_{IN.LOAD\_10h}^{CP\_MV(f,n_f)}$), which can be viewed in Figure 5.2. For those maximal values the estimated peak power values from 2016 have been used, which were gathered from the "Institute of Energy Systems and Electrical Drives".

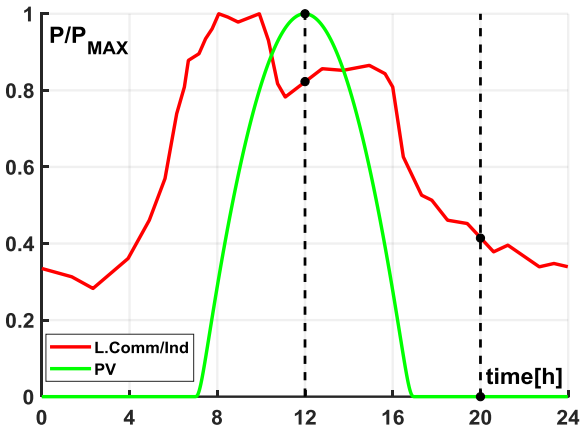

Figure 5.2 - Daily load and production profile of CPs in MV Link_Grids

In regard to the daily load profiles of industrial and large commercial CP, the initial active power value at 20h $P_{IN.LOAD\_20h}^{CP\_MV(f,n_f)}$ for each CP in MV Link_Grids can be calculated in the following way.

Large commercial: $$P_{IN.LOAD\_20h}^{CP\_MV(f,n_f)} = P_{IN.LOAD\_10h}^{CP\_MV(f,n_f)} \cdot 0{,}41624 \quad (5\text{–}9)$$

Industrial: $$P_{IN.LOAD\_20h}^{CP\_MV(f,n_f)} = P_{IN.LOAD\_10h}^{CP\_MV(f,n_f)} \cdot 0{,}41624 \quad (5\text{–}10)$$

The initial reactive power value at 20h $Q_{IN.LOAD\_20h}^{CP\_MV(f,n_f)}$ for each CP is determined with the help of the already familiar Equation (5–16) equation. For all connected large commercial and industrial CPs, $cos\varphi^{(f,n_f)} = 0{,}9$ has been chosen.

$$Q_{IN.LOAD\_20h}^{CP\_MV(f,n_f)} = P_{IN.LOAD\_20h}^{CP\_MV(f,n_f)} \cdot \frac{\sqrt{1 - cos^2\varphi^{(f,n_f)}}}{cos\varphi^{(f,n_f)}} = P_{IN.LOAD\_20h}^{CP\_MV(f,n_f)} \cdot 0{,}48432 \quad (5\text{–}11)$$

Equation (5–12) and (5–13) show how the accumulated initial active and reactive power demand for "20h" load scenario of all connected CPs to single MV Link_Grid can be estimated.

$$P_{IN,LOAD\_20h}^{TOT.CP\_MV} = \sum_{f=1}^{F} \sum_{n_f=1}^{N} P_{IN.LOAD\_20h}^{CP\_MV(f,n_f)} \quad (5\text{–}12)$$

$$Q_{IN,LOAD\_20h}^{TOT.CP\_MV} = \sum_{f=1}^{F} \sum_{n_f=1}^{N} Q_{IN.LOAD\_20h}^{CP\_MV(f,n_f)} = 0{,}48432 \cdot P_{IN,LOAD\_20h}^{TOT.CP\_MV} \quad (5\text{–}13)$$

The most important parameters regarding the "20h" load scenario of CPs in Real I and Real II MV Link Grid are listed in Table 5.5. For the reason that the value of $Q_{IN,LOAD\_20h}^{TOT.CP\_MV}$ differs from the value of $P_{IN,LOAD\_20h}^{TOT.CP\_MV}$ just in a multiplying factor, share of large commercial on the $P_{IN,LOAD\_20h}^{TOT.CP\_MV}$ is the same as its share on the $Q_{IN,LOAD\_20h}^{TOT.CP\_MV}$ value. Therefore, the parameter LC_{PQ_Share} is adopted. In the same manner this can be applied to the industrial customers' share IND_{PQ_Share}.

Table 5.5 - "20h" load scenario of CPs in Real I and Real II MV Link_Grid

$MV\ Link\text{-}Grid$	$N_{LC}^{CP\_MV}$	$N_{IND}^{CP\_MV}$	$P_{IN.LOAD\_20h}^{TOT.CP\_MV}$ [kW]	$Q_{IN.LOAD\_20h}^{TOT.CP\_MV}$ [$kVAr$]	LC_{PQ_Share} [%]	IND_{PQ_Share} [%]
Real I	69	4	19 430,753	9 410,378	3,5	96,5
Real II	30	0	505,201	244,583	100	/

In the second scenario, where the CPs' load behaviour is observed at 12h, the initial active and reactive power load values are calculated in the following way.

Large commercial:

$$P_{IN.LOAD\_12h}^{CP\_MV(f,n_f)} = P_{IN.LOAD\_10h}^{CP\_MV(f,n_f)} \cdot 0{,}82139 \quad (5\text{–}14)$$

$$Q_{IN.LOAD\_12h}^{CP\_MV(f,n_f)} = P_{IN.LOAD\_12h}^{CP\_MV(f,n_f)} \cdot 0{,}48432 \quad (5\text{–}15)$$

Industrial:

$$P_{IN.LOAD\_12h}^{CP\_MV(f,n_f)} = P_{IN.LOAD\_10h}^{CP\_MV(f,n_f)} \cdot 0{,}82139 \quad (5\text{–}16)$$

$$Q_{IN.LOAD\_12h}^{CP\_MV(f,n_f)} = P_{IN.LOAD\_12h}^{CP\_MV(f,n_f)} \cdot 0{,}48432 \quad (5\text{–}17)$$

The most important parameters regarding the "20h" load scenario of CPs in Real I and Real II MV Link Grid are listed in Table 5.6.

Table 5.6 - "12h" load scenario of CPs in Real I and Real II MV Link_Grid

$MV\ Link\text{-}Grid$	$N_{LC}^{CP\_MV}$	$N_{IND}^{CP\_MV}$	$P_{IN.LOAD\_12h}^{TOT.CP\_MV}$ [kW]	$Q_{IN.LOAD\_12h}^{TOT.CP\_MV}$ [$kVAr$]	LC_{PQ_Share} [%]	IND_{PQ_Share} [%]
Real I	69	4	38 342,349	18 569,953	3,5	96,5
Real II	69	3	997,938	483,321	/	100

5.2 Consideration of different Photovoltaic Penetration Levels

Definition of production scenarios of CPs in LV and MV Link_Grids relies almost entirely on characterization of their outputs of the corresponding PV system. As in case of load scenarios, two different production scenarios are observed as well. The first one is labelled as the no production scenario and the second one is labelled as the maximum production scenario. According to Figure 5.1, where the daily production profile of typical CP in LV Link_Grids is represented, time points 20h and 12h define exactly when the no and maximum production scenario occur. The same time points characterize both production scenarios of CPs in MV Link_Grids, which complies with the outlook of the daily production profile in Figure 5.2.

A. Customer Plants in LV Link_Grids

As already stated, only residential customers with the same amount of initial active power consumption are present in Rural, Small Urban and Large Urban LV Link_Grid. Therefore, for those CPs an identical PV system with the rated active power of 5 kW has been chosen. In case of maximum production, those PV systems always generate 5 kW at their output $P_{PV}^{CP\_LV(f,n_f)}$. For no production scenario, the same PV systems are disconnected from the CP grid. Thus, they don't generate any power

($P_{PV}^{CP\_LV(f,n_f)} = 0$). If the number of presented PV systems $N_{PV}^{CP\_LV}$ is known, total production $P_{PV}^{TOT.CP\_LV}$ for any of these three LV Link_Grids can be calculated with Equation (5–18).

$$P_{PV}^{TOT.CP\_LV} = P_{PV}^{CP\_LV(f,n_f)} \cdot N_{PV}^{CP\_LV} \tag{5–18}$$

Table 5.7 recaps the above-mentioned parameters for each of those three LV Link_Grids and specific production scenario.

Table 5.7 - Important parameters regarding the production scenarios for CPs in Rural, Small Urban and Large Urban Link_Grid

LV Link-Grid	***Production Scenario***	$N_{PV}^{CP\_LV}$	$P_{PV}^{CP\_LV(f,n_f)}$ [kW]	$P_{PV}^{TOT.CP\_LV}$ [kW]
Large Urban	*no*	175	0	0
	max	175	5	875
Small Urban	*no*	91	0	0
	max	91	5	455
Rural	*no*	61	0	0
	max	61	5	305

For the characterization of the important parameters regarding the production scenarios of CPs in Industrial LV Link_Grid, which are divided in several customer classes (residential, small commercial and industrial) that have different initial active power values, some other approach needs to be taken. Maximum production of each connected CP should cover double the amount of its maximum initial active power consumption $P_{IN.LOAD\_14h}^{CP\_LV(f,n_f)}$, which is expressed with the following approximation.

$$P_{PV}^{CP\_LV(f,n_f)} \approx P_{IN.LOAD\_14h}^{CP\_LV(f,n_f)} \cdot 2 \tag{5–19}$$

On the other hand, a same strategy as before is kept when the no production scenario needs to be considered. This means that every CP in Industrial LV Link_Grid doesn't provide any active power on its output. Once again, $P_{PV}^{CP\_LV(f,n_f)} = 0$ is assumed. Furthermore, Equation (5–20) shows how the total production $P_{PV}^{TOT.CP\_LV}$ of Industrial LV Link_Grid can be estimated.

$$P_{PV}^{TOT.CP\_LV} = \sum_{f=1}^{F} \sum_{n=1}^{N} P_{PV}^{CP\_LV(f,n_f)} \tag{5–20}$$

By taking into consideration all CPs in Industrial LV Link_Grid and their respective active power output, which is represented in Table 5.8, no production scenario gives a total production $P_{PV}^{TOT.CP\_LV}$ of 0 kW, while maximum production provides 897 kW.

Table 5.8 - Active power value of CPs in Industrial LV Link_Grid for both production scenarios

Node	**Production Scenario**	$P_{PV}^{CP\_LV(f,n_f)}$ [**kW**]	**Node**	**Production Scenario**	$P_{PV}^{CP\_LV(f,n_f)}$ [**kW**]
(1,1)	*max/no*	0/18	(1,9)	*max/no*	0/9
(1,2)	*max/no*	0/16	(1,10)	*max/no*	0/11
(1,3)	*max/no*	0/9	(1,11)	*max/no*	0/89
(1,4)	*max/no*	0/9	(2,1)	*max/no*	0/45
(1,5)	*max/no*	0/83	(2,2)	*max/no*	0/45
(1,6)	*max/no*	0/9	(2,3)	*max/no*	0/56
(1,7)	*max/no*	0/2	(2,4)	*max/no*	0/12
(1,8)	*max/no*	0/22	(3,1)	*max/no*	0/447

B. Customer Plants in MV Link_Grids

Like in case of CPs in LV Link_Grids, CPs that are connected to MV Link_Grids provide as their output $P_{PV}^{CP\_MV(f,n_f)}$ either their maximal active power or no active power at all. Those values define maximum production case and no production case, respectively. For maximum production scenario, the output value of each CP in MV Link_Grids can be calculated by using the already familiar Equation (5–21).

$$P_{PV}^{CP\_MV(f,n_f)} \approx P_{IN.LOAD\_10h}^{CP\_MV(f,n_f)} \cdot 2 \tag{5–21}$$

As already explained, $P_{IN.LOAD\_10h}^{CP\_MV(f,n_f)}$-value of each CP complies with its estimated peak demand from 2016, which was gathered from the "Institute of Energy Systems and Electrical Drives" of the "Vienna University of Technology". For no production scenario, it is expected that the output of every CP $P_{PV}^{CP\_MV(f,n_f)}$ is equal to 0 kW. Due to a large number of connected customer plants in MV Link_Grids, the individual calculated values from Equation (5–21) are left out of this thesis. Nevertheless, they've been used in Equation (5–22) for the estimation of the total production of both Real MV Link_Grids.

$$P_{PV}^{TOT.CP\_MV} = \sum_{f=1}^{F} \sum_{n_f=1}^{N} P_{PV}^{CP\_MV(f,n_f)} \tag{5–22}$$

The calculated values for both production scenarios within Real I and Real II MV Link Grid can be seen in Table 5.9. In addition, Table 5.9 includes the number of large commercial $N_{LC}^{CP\_MV}$ and industrial customers $N_{IND}^{CP\_MV}$, as well as their share on the total CPs' production of the related MV Link_Grid, LC_{PV_Share} and IND_{PV_Share}, respectively. As it can be observed, four industrial customers produce roughly 96,5 %. Other 3,5 % can be attributed to 69 large commercial customers. Total production of CPs in Real II MV Link_Grid can be attributed entirely to 30 large commercial customers.

Table 5.9 - max and no production scenario of CPs in Real MV Link_Grids

MV Link-Grid	***Production Scenario***	$P_{PV}^{TOT.CP\_MV}$ [**kW**]	$N_{LC}^{CP\_MV}$	$N_{IND}^{CP\_MV}$	LC_{PV_Share} [%]	IND_{PV_Share} [%]
Real I	*no*	0	/	/	/	/
	max	19 430	69	4	3,5	96,5
Real II	*no*	0	/	/	/	/
	max	11 045	30	/	100	/

5.3 Overview of LVG and MVG Scenarios

Table 5.10 gives an overview of scenarios in LV Link_Grids in correspondence to the loading and production situation of connected CPs. For easier distinction during result evaluation, to each scenario a name is given, that clearly indicates which load and production situation is viewed.

Table 5.10 - Different scenarios for each LV Link_Grid

LV Link-Grid	***CP_LV Load***	***CP_LV Production***	***Scenario Name***
Large Urban	$12h$	max	$\boldsymbol{L_{12h}^{LV} - G_{MAX}^{LV}}$
	$20h$	no	$\boldsymbol{L_{20h}^{LV} - G_{NO}^{LV}}$
Small Urban	$12h$	max	$\boldsymbol{L_{12h}^{LV} - G_{MAX}^{LV}}$
	$20h$	no	$\boldsymbol{L_{20h}^{LV} - G_{NO}^{LV}}$
Rural	$12h$	max	$\boldsymbol{L_{12h}^{LV} - G_{MAX}^{LV}}$
	$20h$	no	$\boldsymbol{L_{20h}^{LV} - G_{NO}^{LV}}$
Industrial	$12h$	max	$\boldsymbol{L_{12h}^{LV} - G_{MAX}^{LV}}$
	$20h$	no	$\boldsymbol{L_{20h}^{LV} - G_{NO}^{LV}}$

Additionally to situation of CPs in LV Link_Grid, scenarios in MV Link_Grids are influenced by the load demand and production of Industrial and Large Urban CPs, which is outlined in Table 5.11. Contrarily to Real, Theoretical MV Link_Grids are exclusively affected by the load and production situation of CPs in LV Link_Grids.

Table 5.11 - Different scenarios for each MV Link_Grid

MV Link-Grid	***CP_MV Load***	***CP_MV Production***	***CP_LV Load***	***CP_LV Production***	***Scenario Name***
Theoretical I	/	/	$12h$	max	$\boldsymbol{L_{12h}^{MV} - G_{MAX}^{MV}}$
	/	/	$20h$	no	$\boldsymbol{L_{20h}^{MV} - G_{NO}^{MV}}$
Theoretical II	/	/	$12h$	max	$\boldsymbol{L_{12h}^{MV} - G_{MAX}^{MV}}$
	/	/	$20h$	no	$\boldsymbol{L_{20h}^{MV} - G_{NO}^{MV}}$
Real I	$12h$	max	$12h$	max	$\boldsymbol{L_{12h}^{MV} - G_{MAX}^{MV}}$
	$20h$	no	$20h$	no	$\boldsymbol{L_{20h}^{MV} - G_{NO}^{MV}}$
Real II	$12h$	max	$12h$	max	$\boldsymbol{L_{12h}^{MV} - G_{MAX}^{MV}}$
	$20h$	no	$20h$	no	$\boldsymbol{L_{20h}^{MV} - G_{NO}^{MV}}$

6 Simulation and Calculation Procedure

Section 6.1 describes an exact procedure of load flow simulations within LV and MV Link_Grids, which were carried out in the course of this master thesis. In order to evaluate behaviour of simulated grids, some calculations are needed, which are explained in Section 6.2.

6.1 Simulation Procedure

All load flow simulations were performed in Siemens PSS®SINCAL[4] by using the Newton Raphson algorithm. Due to the unequal number of unknown variables and independent equations, unique numerical solutions cannot be found in power flow calculation without reference voltage magnitude and reference angle (normally 0°). A slack bus overtakes this task, which injects or absorbs as much active and reactive power as needed for balancing the power flow while keeping the voltage constant at desired value. Location of the slack bus during the simulations in LV Link_Grids was always at the primary side of MV/LV transformers. Therefore, voltage value at the slack bus and is at the same time the voltage value at the primary side of the related transformer. On the other hand, during simulations in MV Link_Grids, slack was placed directly on the main MV bus bar, so that the grid performance could be observed without any influence of the tap changer in HV/MV transformers. By increasing the slack voltage from 0,8 p.u. to 1,2 p.u.[5] in small steps (0,001 p.u. for U^{LVG_Slack} and 0,002 p.u. for U^{MVG_Slack}) and depending on the grid type, for each of these voltage values the following parameters have been gathered directly from the extensive simulations.

- $U^{(f,n_f)}$ - voltage value at each node in LV and MV Link_Grids, excluding the voltage value at the primary and secondary side of the MV/LV distribution transformers
- U^{DTR_PRM}, U^{DTR_SCD} - voltage value at the primary and secondary side of the MV/LV distribution transformers
- P^{DTR_PRM}, Q^{DTR_PRM} - active and reactive power value at the primary side of the MV/LV distribution transformers
- $P^{DTR}_{LOSSES}, Q^{DTR}_{LOSSES}$ - active and reactive power losses of the MV/LV distribution transformers
- $P^{LV\_LINE(f,n_f)}, Q^{LV\_LINE(f,n_f)}$ - active and reactive power flow through each line segment in LV Link_Grids
- $P^{LV\_LINE(f,n_f)}_{LOSSES}, Q^{LV\_LINE(f,n_f)}_{LOSSES}$ - active and reactive power losses of each line segment in LV Link_Grids
- $P^{MV\_LINE(f,n_f)}, Q^{MV\_LINE(f,n_f)}$ - active and reactive power flow through each line segment in MV Link_Grids
- $P^{MV\_LINE(f,n_f)}_{LOSSES}, Q^{MV\_LINE(f,n_f)}_{LOSSES}$ - active and reactive power losses of each line segment in MV Link_Grids
- $P^{CP\_LV(f,n_f)}_{LOAD}, Q^{CP\_LV(f,n_f)}_{LOAD}$ - active and reactive power consumption of each CP in LV Link_Grids
- $P^{CP\_LV(f,n_f)}_{PV}, Q^{CP\_LV(f,n_f)}_{PV}$ - active and reactive power production of each CP in LV Link_Grids

[4] Simulation software for the analysis and planning of all grid types

[5] Normalized to the nominal voltage of the transformers primary side ($20\ kV$ and $110\ kV$)

- $P_{LOAD}^{CP\_MV(f,n_f)}, Q_{LOAD}^{CP\_MV(f,n_f)}$ - active and reactive power consumption of each CP in MV Link_Grids
- $P_{PV}^{CP\_MV(f,n_f)}, Q_{PV}^{CP\_MV(f,n_f)}$ - active and reactive power production of each CP in MV Link_Grids
- $P^{Lmpd\_LVG}, Q^{Lmpd\_LVG}$ - overall active and reactive power consumption/injection of each connected LV Link_Grid in MV Link_Grids[6]

6.2 Calculation Procedure

All calculations performed during this thesis were based on the values of the above-mentioned parameters, which were gathered from the simulation processes.

A. Power Losses in LV Link_Grids

All grid losses depend on the load and production scenario of the related grid. Total active P_{LOSSES}^{LVG} and reactive power losses Q_{LOSSES}^{LVG} in simulated LV Link_Grids are calculated with Equations (6–1) and (6–2). As it can be seen, power losses of each line segment in LV Link_Grids have to be taken into consideration. Power losses of the corresponding MV/LV distribution transformer contribute to a small degree as well, but not merely as total line losses.

$$P_{LOSSES}^{LVG} = \sum_{f=1}^{F} \sum_{n_f=1}^{N_f} (P_{LOSSES}^{LV\_LINE(f,n_f)}) + P_{LOSSES}^{DTR} \quad (6–1)$$

$$Q_{LOSSES}^{LVG} = \sum_{f=1}^{F} \sum_{n_f=1}^{N_f} (Q_{LOSSES}^{LV\_LINE(f,n_f)}) + Q_{LOSSES}^{DTR} \quad (6–2)$$

B. Slack values in LV Link_Grids

Active P^{LVG_Slack} and reactive power values Q^{LVG_Slack} of the slack bus are a direct output of the power flow simulations in LV Link_Grids, as those values match the values of P^{DTR_PRM} and Q^{DTR_PRM}, respectively. If needed, they can be also calculated by considering total power generation, load consumption and grid losses, which is mathematically expressed with the equations down below.

$$P^{LVG\_Slack} = \sum_{f=1}^{F} \sum_{n_f=1}^{N_f} (P_{PV}^{CP\_LV(f,n_f)} - P_{LOAD}^{CP\_LV(f,n_f)}) - P_{LOSSES}^{LVG} \quad (6–3)$$

$$Q^{LVG\_Slack} = \sum_{f=1}^{F} \sum_{n_f=1}^{N_f} (Q_{PV}^{CP\_LV(f,n_f)} - Q_{LOAD}^{CP\_LV(f,n_f)}) - Q_{LOSSES}^{LVG} \quad (6–4)$$

C. Parameters of the "proposed" model of LV Link_Grids

From these voltage-dependent P^{LVG_Slack} and Q^{LVG_Slack} values, a proper lumped *P,Q*-model for each LV Link_Grid in MV Link_Grids needs to be acquired. As accurate as possible, P^{Lmpd_LVG} and Q^{Lmpd_LVG} values should be equal to calculated P^{LVG_Slack} and Q^{LVG_Slack} values of the related LV Link_Grid.

ZIP coefficients that indicate the voltage dependency of P^{Lmpd_LVG} are determined in the following fashion. Firstly, for the chosen LV Link_Grid and its specific load and production scenario, P^{LVG_Slack}

[6] Depending on its production and load scenario, LVG can consume or inject both active and reactive power

value is gathered at three separate voltage values. As first two voltage points U^{LVG_Slack}, the upper and the lower voltage limit (±10% of $U_{NOM}^{LVG\_Slack}$) have been chosen. The third and final value is exactly the value of $U_{NOM}^{LVG\_Slack}$. Value of P^{LVG_Slack} acquired for $U^{LVG\_Slack} = U_{NOM}^{LVG\_Slack}$ has been chosen as the value of initial active power P_0. For better clarity, the following identities describe the above mentioned assignment process.

$$P_0 = P^{LVG\_Slack}(U_{NOM}^{LVG\_Slack})$$
$$P_1 = P^{LVG\_Slack}(0{,}9\ U_{NOM}^{LVG\_Slack})$$
$$P_2 = P^{LVG\_Slack}(1{,}1\ U_{NOM}^{LVG\_Slack})$$
$$P_3 = P^{LVG\_Slack}(U_{NOM}^{LVG\_Slack})$$

By solving a linear system of three equations for already known ZIP model, which are represented down below, three unknown coefficients Z_P, I_P and P_P can be determined for the given load and production scenario of the related LV Link_Grid.

$$\frac{P_1}{P_0} = Z_P \cdot \left(\frac{0{,}9\ U_{NOM}^{LVG\_Slack}}{U_{NOM}^{LVG\_Slack}}\right)^2 + I_P \cdot \left(\frac{0{,}9\ U_{NOM}^{LVG\_Slack}}{U_{NOM}^{LVG\_Slack}}\right) + P_P \quad (6\text{–}5)$$

$$\frac{P_2}{P_0} = Z_P \cdot \left(\frac{1{,}1\ U_{NOM}^{LVG\_Slack}}{U_{NOM}^{LVG\_Slack}}\right)^2 + I_P \cdot \left(\frac{1{,}1\ U_{NOM}^{LVG\_Slack}}{U_{NOM}^{LVG\_Slack}}\right) + P_P \quad (6\text{–}6)$$

$$\frac{P_3}{P_0} = 1 = Z_P \cdot \left(\frac{U_{NOM}^{LVG\_Slack}}{U_{NOM}^{LVG\_Slack}}\right)^2 + I_P \cdot \left(\frac{U_{NOM}^{LVG\_Slack}}{U_{NOM}^{LVG\_Slack}}\right) + P_P \quad (6\text{–}7)$$

The exact calculated values of ZIP coefficients for each LV Link_Grid and its load and production scenario can be found in Chapter 7.

In regard to the corresponding generation model, inverter's maximum reactive power capability $Q_{MAX.PV\_INV}^{Lmpd\_LVG}$ is determined with the following equation.

$$Q_{MAX.PV\_INV}^{Lmpd\_LVG} = \max(Q^{LVG\_Slack})_{|U^{LVG\_Slack}=0{,}8\text{ p.u. to }1{,}2\text{ p.u.}} \quad (6\text{–}8)$$

As it can be seen, maximal reactive power value that the inverter can inject into or absorb from a MV Link_Grid is purely conditioned by the maximal reactive power at the slack bus, which was estimated during power flow simulations in the related grid.

Values of initial active $P_{INIT}^{Lmpd\_LVG}$ and reactive power $Q_{INIT}^{Lmpd\_LVG}$ for the proposed model of LV Link_Grids are determined with the following equations.

$$P_{INIT}^{Lmpd\_LVG} = P^{LVG\_Slack}{}_{|U^{LVG\_Slack}=1\text{ p.u.}} \quad (6\text{–}9)$$

$$Q_{INIT}^{Lmpd\_LVG} = Q^{LVG\_Slack}{}_{|U^{LVG\_Slack}=1\text{ p.u.}} \quad (6\text{–}10)$$

D. Parameters of the "used" model of LV Link_Grids

As mentioned in Subsection 4.5.1, parameters for this model are calculated based on the load and production scenario of the corresponding LV Link_Grid. Their characterization is represented with the equations down below. The values of average active power losses $P_{AV.LOSSES}^{LVG}$ depend on the grid's actual loading and production situation. Their values are shown in the following chapter. For Rural, Small Urban and Large Urban LV Link_Grid $cos\varphi = 0{,}95$ is assumed, as there only residential CPs are

present. On the other hand, as Industrial and Small Commercial are the most common CPs in Industrial LV Link, $cos\varphi = 0{,}90$ is assumed.

$$P_{IN.LOAD}^{Lmpd\_LVG} = P_{AV.LOSSES}^{LVG} + \sum_{f=1}^{F} \sum_{n_f=1}^{N_f} P_{IN.LOAD}^{CP\_LV(f,n_f)} \quad (6\text{–}11)$$

$$Q_{IN.LOAD}^{Lmpd\_LVG} = P_{IN.LOAD}^{Lmpd\_LVG} \cdot \frac{\sqrt{1 - cos^2\varphi}}{cos\varphi} \quad (6\text{–}12)$$

Values of $P_{PV}^{Lmpd\_LVG}$ and $Q_{MAX.PV\_INV}^{Lmpd\_LVG}$ are defined with the following equations. These generation model parameters take into consideration all connected PV systems in the corresponding LV Link_Grid.

$$P_{PV}^{Lmpd\_LVG} = \sum_{f=1}^{F} \sum_{n=1}^{N_f} P_{PV}^{CP\_LV(f,n_f)} \quad (6\text{–}13)$$

$$Q_{MAX.PV\_INV}^{Lmpd\_LVG} = \sum_{f=1}^{F} \sum_{n=1}^{N_f} \pm S_{RAT.PV\_INV}^{CP\_LV(f,n_f)} \quad (6\text{–}14)$$

The actual reactive power output $Q_{PV}^{Lmpd\_LVG}$ depends on the control of a PV inverter. A *Q(U)*-controlled PV inverter has been used in case of Rural and Large Urban LV Link_Grid, while an uncontrolled one in case of Small Urban and Industrial LV Link_Grid. Based on the equations (4–23) and (4–24), parameters $P_{IN.LOAD}^{Lmpd\_LVG}$, $Q_{IN.LOAD}^{Lmpd\_LVG}$, $P_{PV}^{Lmpd\_LVG}$ and $Q_{PV}^{Lmpd\_LVG}$, values of initial active $P_{INIT}^{Lmpd\_LVG}$ and reactive power $Q_{INIT}^{Lmpd\_LVG}$ of the LV Link_Grids' currently used model are determined with the following equations.

$$P_{INIT}^{Lmpd\_LVG} = P_{AV.LOSSES}^{LVG} + \sum_{f=1}^{F} \sum_{n_f=1}^{N_f} (P_{IN.LOAD}^{CP\_LV(f,n_f)} - P_{PV}^{CP\_LV(f,n_f)}) \quad (6\text{–}15)$$

$$Q_{INIT}^{Lmpd\_LVG} = Q_{IN.LOAD}^{Lmpd\_LVG} - Q_{PV}^{Lmpd\_LVG} \quad (6\text{–}16)$$

E. Power losses in MV Link_Grids

Compared to the situation in simulated LV Link_Grids, power losses of MV Link_Grids are caused only by the related overall line losses, as the HV/MV transformers were disconnected during simulations. The following equations show how the total active and reactive power losses can exactly be estimated.

$$P_{LOSSES}^{MVG} = \sum_{f=1}^{F} \sum_{n_f=1}^{N_f} (P_{LOSSES}^{MV\_LINE(f,n_f)}) \quad (6\text{–}17)$$

$$Q_{LOSSES}^{MVG} = \sum_{f=1}^{F} \sum_{n_f=1}^{N_f} (Q_{LOSSES}^{MV\_LINE(f,n_f)}) \quad (6\text{–}18)$$

7 Impact of DGs on the Behaviour of LV and MV Link_Grids

The main focus of this chapter is to represent the most important power flow simulation results of LV and MV Link_Grids and to assess the of impacts of DGs on the grids' behaviour. Section 7.1 deals with the behaviour of the four tested LV Link_Grids. Furthermore, Section 0 shows how the required parameters of the "used" and the "proposed" model for the related LV Link_Grids have been determined. Lastly, Section 7.3 describes the behaviour of Theoretical and Real MV Link_Grids for both load/production scenarios.

7.1 Behaviour of LV Link_Grids

This section portrays the behaviour of four LV Link_Grids during simulation processes, i.e. first and foremost how the load demand and production of CPs, grid losses and total exchanged power between LV and MV Link_Grid change their values in relation to the increased voltage at the transformer's primary side. Two different grid scenarios which are listed in Table 5.10 are going to be examined for every simulated grid.

7.1.1 Rural LV Link_Grid

Figure 7.1 shows voltage-dependent active P^{LVG_Slack} and reactive power Q^{LVG_Slack} value at the primary side of the corresponding transformer, active P_{LOSSES}^{LVG} and reactive grid losses Q_{LOSSES}^{LVG}, as well as overall load demand $P_{LOAD}^{TOT.CP\_LV}$ and production $P_{PV}^{TOT.CP\_LV}$ of CPs which are connected to Rural LV Link Grid in case of $L_{20h}^{LV} - G_{NO}^{LV}$ scenario. It is obvious that the related PV systems don't generate any power. Furthermore, slack's *P*- and *Q*-characteristic have the same form as the load characteristic of CPs. Difference of the values comes from the active grid losses, which are almost constant during the slack voltage increase.

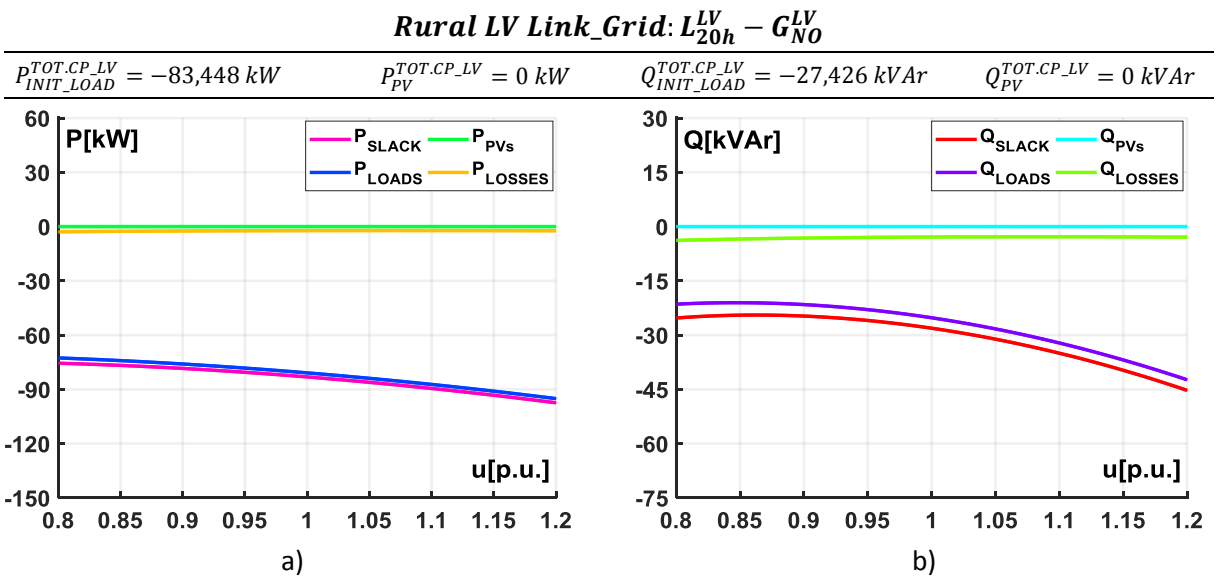

Figure 7.1 - Lumped load characteristic of the Rural LV Link_Grid for $L_{20h}^{LV} - G_{NO}^{LV}$ scenario: a) active power and b) reactive power

In regard to simulation results for $L_{12h}^{LV} - G_{MAX}^{LV}$ scenario, which are represented in Figure 7.2, total active production of CPs or more precisely their PV systems $P_{PV}^{TOT.CP\_LV}$ is 305 kW. Positive P^{LVG_Slack} values indicate that $P_{PV}^{TOT.CP\_LV}$ transcend CPs' total load demand of active power $P_{LOAD}^{TOT.CP\_LV}$ together with the corresponding value of P_{LOSSES}^{LVG}. As far as *Q(U)*-characteristic of all PV systems is concerned, its form resembles the *Q(U)*-control of a single PV inverter, which was represented in Figure 4.6. The discrepancy could be attributed to the small deadband of the used *Q(U)*-control. Due to this small window and different voltage at their PCC, it is highly unlikely that all PV systems don't exchange reactive power with the grid at the same time. Clearly, some of the PV systems operate underexcited or overexcited. Also, PV systems that are connected far enough from the distribution transformer don't need to operate in full overexcited mode, as they never reach the required voltage value. This is probably due to effects of active power injection of all PV systems that are connected before them.

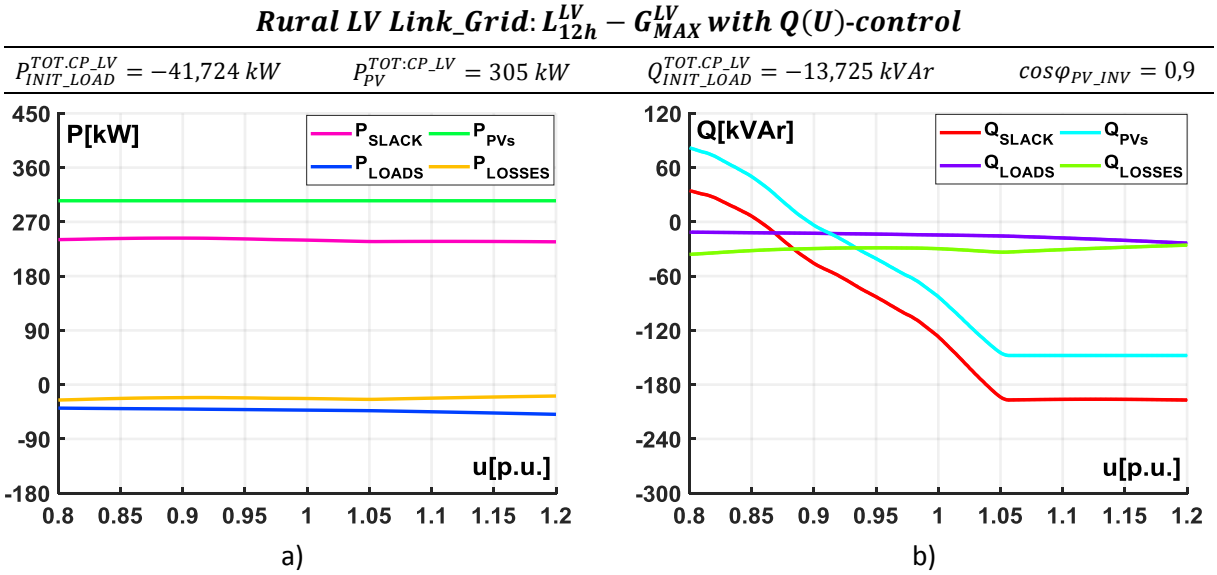

Figure 7.2 - Lumped load characteristic of the Rural LV Link_Grid for $L_{12h}^{LV} - G_{MAX}^{LV}$ scenario: a) active power and b) reactive power

Average active and reactive power losses for both scenarios are listed in Table 7.1. As seen down below, bigger grid losses are present in case of $L_{12h}^{LV} - G_{MAX}^{LV}$ scenario, which is expected, as the loading of all lines and transformer increases due to much bigger active and reactive power flow across the grid, caused by connected PV systems.

Table 7.1 - Average grid losses in the Rural LV Link_Grid for both load/production scenarios

Scenario	$P_{AV.LOSSES}^{LVG}$ $[kW]$	$Q_{AV.LOSSES}^{LVG}$ $[kVAr]$
$L_{20h}^{LV} - G_{NO}^{LV}$	2,393	3,218
$L_{12h}^{LV} - G_{MAX}^{LV}$	22,299	30,338

7.1.2 Small Urban LV Link_Grid

Results of power flow simulations in Small Urban LV Link_Grid for $L_{20h}^{LV} - G_{NO}^{LV}$ scenario are portrayed in Figure 7.3. As expected, P^{LVG_Slack} and Q^{LVG_Slack} values don't differ much from $P_{LOAD}^{TOT.CP\_LV}$ and $Q_{LOAD}^{TOT.CP\_LV}$ values, as PV systems don't produce any electric power. Like in case of Rural LV Link_Grid, total grid losses don't change drastically even if the slack voltage is increased.

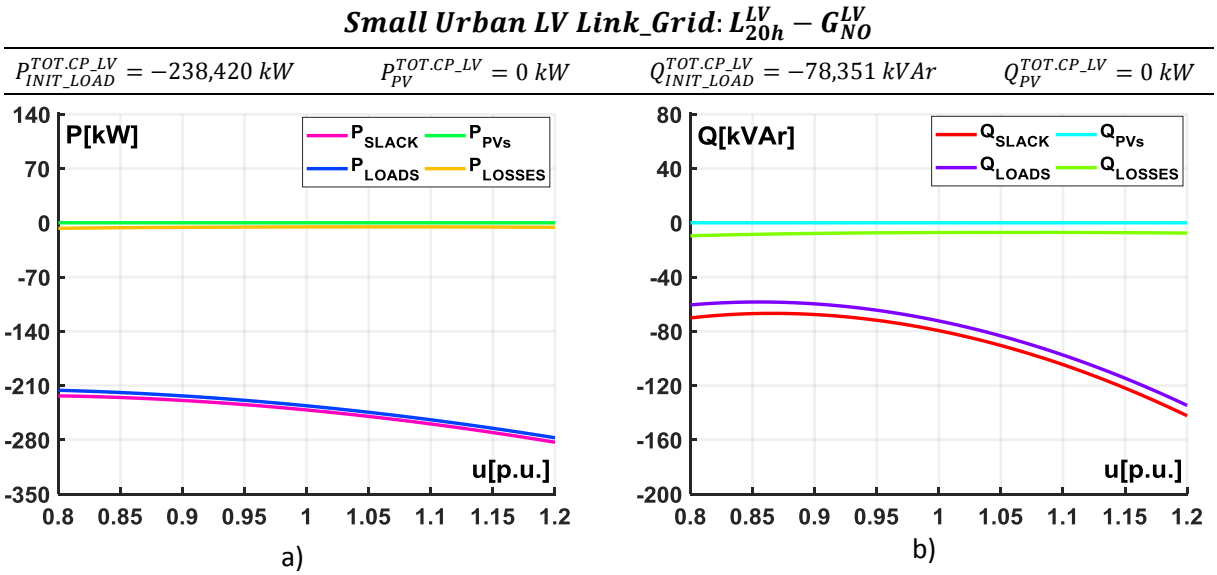

Figure 7.3 - Lumped load characteristic of the Small Urban LV Link_Grid for $L_{20h}^{LV} - G_{NO}^{LV}$ scenario: a) active power and b) reactive power

Changes of active and reactive power flows in Small Urban LV Link_Grid for $L_{12h}^{LV} - G_{MAX}^{LV}$ scenario when the slack voltage is varied, are shown in Figure 7.4. Because each PV system is equipped with

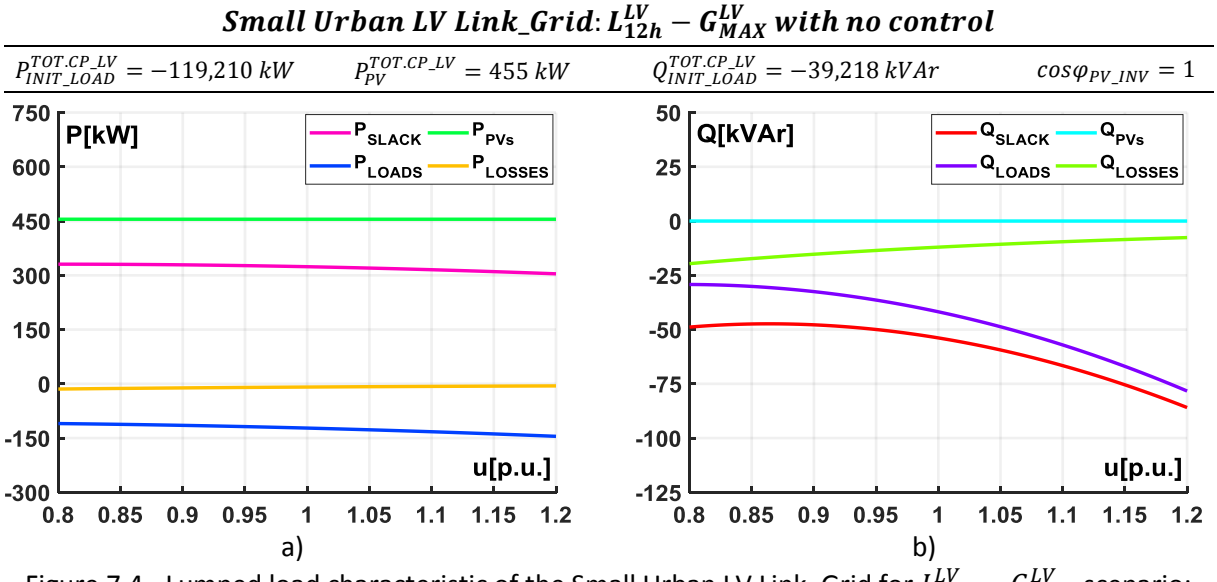

Figure 7.4 - Lumped load characteristic of the Small Urban LV Link_Grid for $L_{12h}^{LV} - G_{MAX}^{LV}$ scenario: a) active power and b) reactive power

uncontrolled inverter ($cos\varphi_{PV\_INV} = 1$), total exchanged active and reactive power between the CPs and the grid can be attributed to the total active and reactive power which is consumed by the CPs' native loads.

Average grid losses for both scenarios are listed in Table 7.2. Compared to the situation without any PV production, both average active and reactive grid losses increased in case when the PV systems produce electric power.

Table 7.2 - Average grid losses in Small Urban LV Link_Grid for both load/production scenarios

$\boldsymbol{Scenario}$	$\boldsymbol{P^{LVG}_{AV.LOSSES}}$ $[\boldsymbol{kW}]$	$\boldsymbol{Q^{LVG}_{AV.LOSSES}}$ $[\boldsymbol{kVAr}]$
$L^{LV}_{20h} - G^{LV}_{NO}$	5,73	7,77
$L^{LV}_{12h} - G^{LV}_{MAX}$	9,278	12,265

7.1.3 Large Urban LV Link_Grid

With respect to $L^{LV}_{20h} - G^{LV}_{NO}$ scenario in Large Urban LV Link_Grid, results from power flow simulations are represented in Figure 7.5. Total load demand of all connected CPs demonstrates already familiar voltage dependency, which can be taken from the corresponding *P*- and *Q*-characteristic. Like it has already been seen for two previous grids, no active and reactive power flows between PV systems and Large Urban LV Link_Grid are present, which complies with the fact that the corresponding PV systems don't generate any power at 20h. Therefore, difference between P^{LVG_Slack} and $P^{TOT.CP\_LV}_{LOAD}$ can be directly associated with the active grid losses P^{LVG}_{LOSSES}. The same principle can be deduced for Q^{LVG_Slack}, $Q^{TOT.CP\_LV}_{LOAD}$ and Q^{LVG}_{LOSSES} values, respectively.

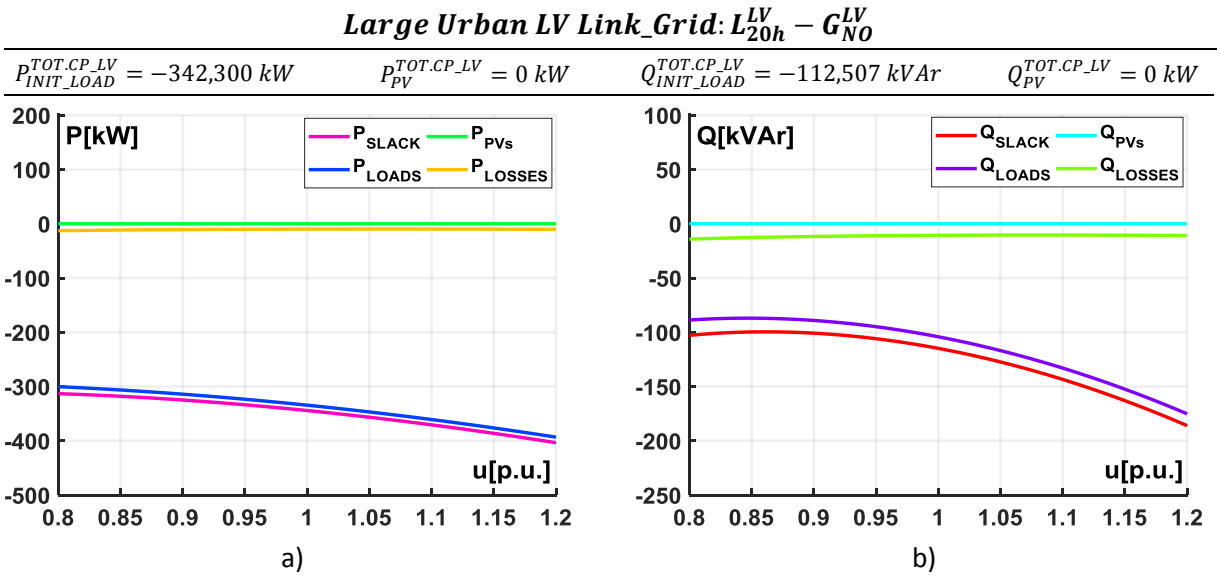

Figure 7.5 - Lumped load characteristic of the Large Urban LV Link_Grid for $L^{LV}_{20h} - G^{LV}_{NO}$ scenario: a) active power and b) reactive power

In regard to simulation results for $L^{LV}_{12h} - G^{LV}_{MAX}$ scenario in Large Urban LV Link_Grid, which is represented in Figure 7.6, slack's *Q(U)*-characteristic shows pretty much the same behaviour as the *Q(U)*-characteristic of all connected PV systems combined. Based on their looks, it is apparent that all PV systems are provided with *Q(U)*-controlled inverters.

Contrarily to Figure 7.2b, where the same scenario for Rural LV Link_Grid was investigated, voltage range where PV systems don't inject/consume any reactive power can be easily noticed. This is due to larger deadband of *Q(U)*-control, which is used for all inverters of the corresponding PV systems in Large Urban LV Link_Grid.

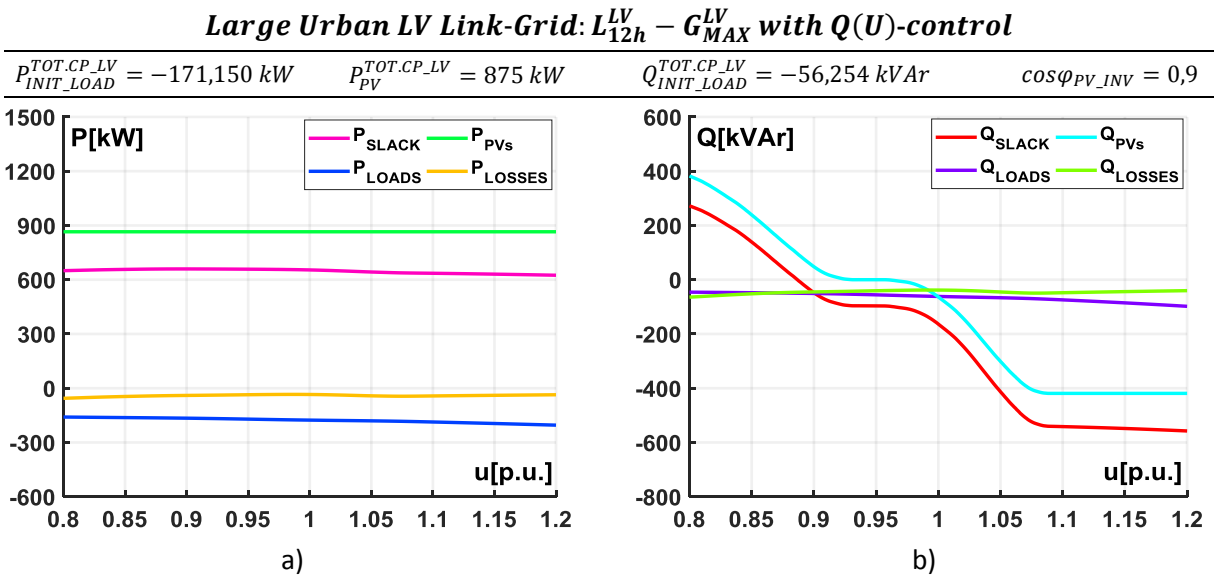

Figure 7.6 - Lumped load characteristic of the Large Urban LV Link_Grid for $L_{12h}^{LV} - G_{MAX}^{LV}$ scenario: a) active power and b) reactive power

Average active and reactive power losses are listed in Table 7.3. Although total load demand for $L_{12h}^{LV} - G_{MAX}^{LV}$ scenario is roughly twice as less than for $L_{20h}^{LV} - G_{NO}^{LV}$ scenario, the average grid losses are approximately 4 times bigger. Rise of power flow through the grid, which is caused by PV systems, can explain this overall increase in loading of the lines and the related transformer as well.

Table 7.3 - Average grid losses in Large Urban LV Link_Grid for both load/production scenarios

Scenario	$P_{AV.LOSSES}^{LVG}$ [kW]	$Q_{AV.LOSSES}^{LVG}$ [$kVAr$]
$L_{20h}^{LV} - G_{NO}^{LV}$	10,419	11,661
$L_{12h}^{LV} - G_{MAX}^{LV}$	41,87	47,211

7.1.4 Industrial LV Link_Grid

Values from Table 7.4 indicate that in case of $L_{12h}^{LV} - G_{MAX}^{LV}$ scenario both average active and reactive power losses are approximately three times bigger than in case of $L_{20h}^{LV} - G_{NO}^{LV}$ scenario. This rise of losses is provoked by the enlarged power flow through the grid, which was caused by the active power injection of the related PV systems.

Table 7.4 - Average grid losses in Industrial LV Link_Grid for both load/production scenarios

Scenario	$P_{AV.LOSSES}^{LVG}$ [kW]	$Q_{AV.LOSSES}^{LVG}$ [$kVAr$]
$L_{20h}^{LV} - G_{NO}^{LV}$	3,805	4,851
$L_{12h}^{LV} - G_{MAX}^{LV}$	11,128	15,249

Like in case of any other LV Link_Grid, simulation results for $L_{20h}^{LV} - G_{NO}^{LV}$ scenario in Industrial LV Link_Grid expose the same grid behaviour, which is illustrated in Figure 7.7. Once again, P^{LVG_Slack} and Q^{LVG_Slack} values take into consideration only active and reactive power demand of the connected CPs and the related grid losses, because the PV systems don't produce any power.

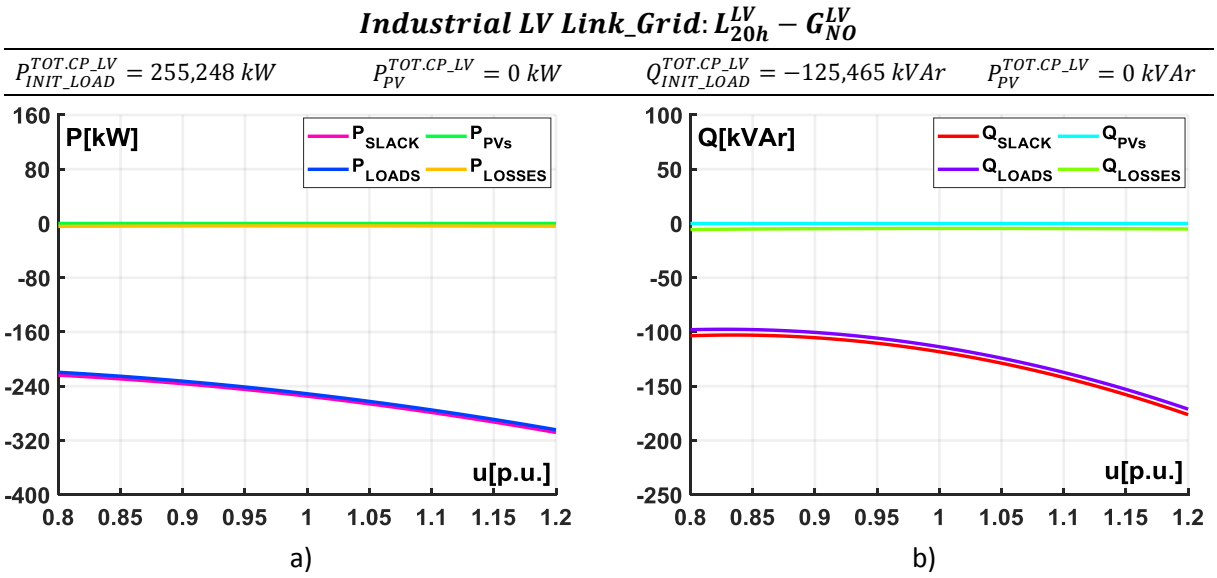

Figure 7.7 - Lumped load characteristic of the Industrial LV Link_Grid for $L_{20h}^{LV} - G_{NO}^{LV}$ scenario: a) active power and b) reactive power

With respect to the simulation results for $L_{12h}^{LV} - G_{MAX}^{LV}$ scenario, the slack's *P(U)*- and *Q(U)*-characteristic have almost the same form as the *P(U)*- and *Q(U)*-load characteristic of all combined CPs. By constantly injecting 861,896 kW into the grid, related PV systems clearly compensate total active power demand, which corresponds to the sum of the active power losses and the total load of all connected CPs. As the PV inverters don't exchange any reactive power with the grid, the difference between slack's and CP's *Q(U)*-values relies entirely on the grid's reactive power losses, which are getting smaller as the voltage at the slack bus is further increased.

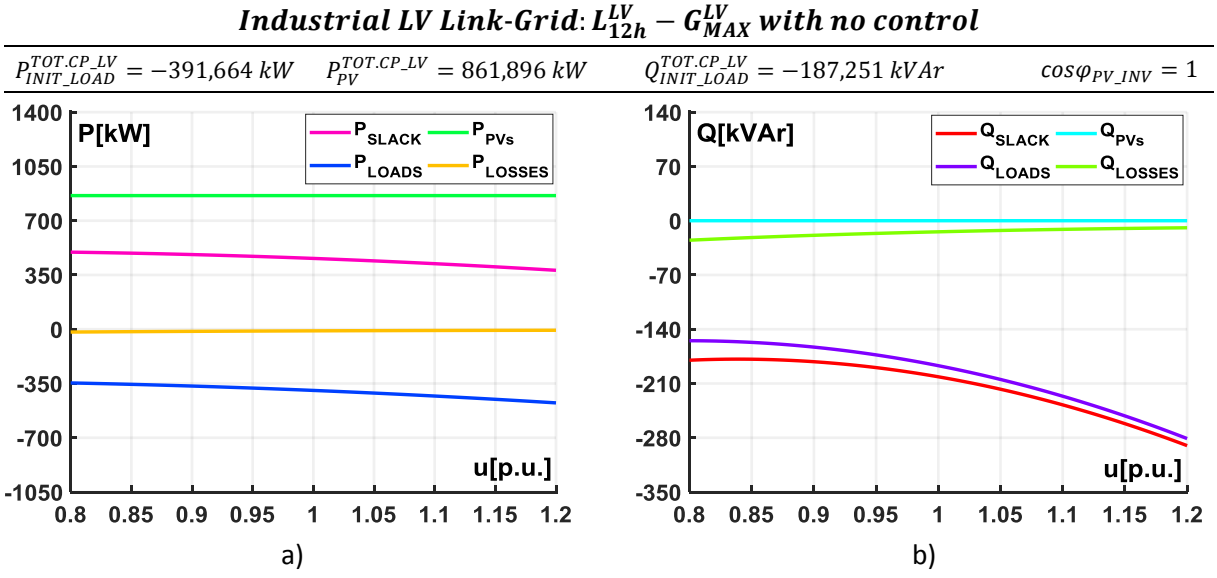

Figure 7.8 - Lumped load characteristic of the Industrial LV Link_Grid for $L_{12h}^{LV} - G_{MAX}^{LV}$ scenario: a) active power and b) reactive power

7.2 Determination of Lumped LVGs' Model Parameters

As already mentioned, LV Link_Grids that were connected to MV Link_Grids were modelled in two different ways. First model is the so called "used" model. This model is almost entirely based on the predefined model parameters of CPs, which are connected to the related LV Link_Grid. The second one is the "proposed" model, whose parameters were derived from the simulation results in LV Link_Grids. The lumped modelling of LV Link_Grids is for better clarity once more illustrated in Figure 7.9.

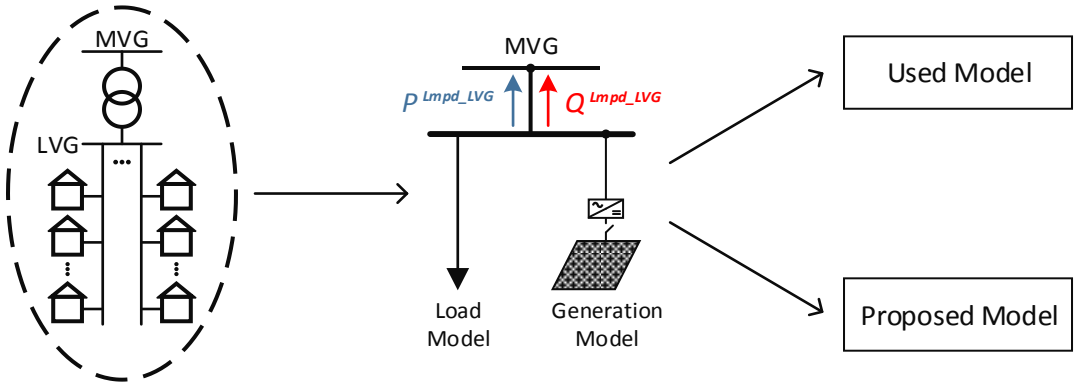

Figure 7.9 - Illustration of LV Link_Grids' lumped modelling

Exact characterization of initial active $P_{INIT}^{Lmpd\_LVG}$ and reactive power value $Q_{INIT}^{Lmpd\_LVG}$ at nominal voltage for both models were already described in the previous chapter. With respect to the ZIP coefficients, the "used" model took over the coefficients from the customer class, which was the most common in the related LV Link_Grid. On the other hand, the "proposed" model uses only the active power ZIP coefficients. Their acquisition is explained in the previous chapter as well. The following text gives the active power ZIP coefficients of the "proposed" model for each LV Link_Grid and the initial *P*,*Q*-parameters of both models for each LV Link_Grid. Additionally, *P*,*Q*-characteristic of each LV Link_Grid's model is also portrayed.

7.2.1 Active power ZIP coefficients for the "proposed" model of LV Link_Grids

The active power ZIP coefficients (Z_P, I_P and P_P) for the "proposed" model of each LV Link_Grid have been calculated with the help from equations (6–5) - (6–7) and simulation results for the specific grid's load/production scenario.

Table 7.5 - Active power ZIP coefficients for the proposed model of each LV Link_Grid

LV Link_Grid	*Scenario*	Z_P	I_P	P_P
Rural	$L_{12h}^{LV} - G_{MAX}^{LV}$	0,258	−0,630	1,372
	$L_{20h}^{LV} - G_{NO}^{LV}$	0,988	−1,331	1,333
Small Urban	$L_{12h}^{LV} - G_{MAX}^{LV}$	−0,485	0,762	0,723
	$L_{20h}^{LV} - G_{NO}^{LV}$	1,198	−1,769	1,571
Large Urban	$L_{12h}^{LV} - G_{MAX}^{LV}$	−0,996	1,812	0,184
	$L_{20h}^{LV} - G_{NO}^{LV}$	1,008	−1,353	1,345
Industrial	$L_{12h}^{LV} - G_{MAX}^{LV}$	−0,987	1,329	0,658
	$L_{20h}^{LV} - G_{NO}^{LV}$	1,099	−1,365	1,266

As already familiar, the only requirement is that the sum of related coefficients for a single grid scenario has to be equal to 1. Values of active power ZIP coefficients for each LV Link_Grid and its scenario are listed in Table 7.5. The individual values of calculated ZIP coefficients and their relations to the grids' behaviour haven't been deeper investigated, as this wasn't the focus of this master thesis.

7.2.2 Initial parameters of the "used" and the "proposed" model of LV Link_Grids

The initial active $P_{INIT}^{Lmpd\_LVG}$ and reactive power value $Q_{INIT}^{Lmpd\_LVG}$ of any lumped model of LV Link_Grids represent the overall exchanged active and reactive power between the related LV and MV Link_Grid when the voltage at the connection point is equal to the nominal value[7]. $P_{INIT}^{Lmpd\_LVG}$ and $Q_{INIT}^{Lmpd\_LVG}$ values of the "used" model of LV Link_Grids have been determined with equations (6–15) and (6–16) from the previous chapter, in which the precalculated initial *P*,*Q* values of all connected CPs

Table 7.6 - Initial active and reactive power demand of the "used" and the "proposed" model of LV Link_Grids

LV Link_Grid	***Scenario***	***Model Type***	$P_{INIT}^{Lmpd\_LVG}$ $[kW]$	$Q_{INIT}^{Lmpd\_LVG}$ $[kVAr]$
Rural	$L_{12h}^{LV} - G_{MAX}^{LV}$	*Used*	240,976	−21,043
		Proposed	239,481	−127,006
	$L_{20h}^{LV} - G_{NO}^{LV}$	*Used*	−85,841	−28,214
		Proposed	−83,628	−28,428
Small Urban	$L_{12h}^{LV} - G_{MAX}^{LV}$	*Used*	326,512	−42,232
		Proposed	323,774	−53,949
	$L_{20h}^{LV} - G_{NO}^{LV}$	*Used*	−244,151	−80,248
		Proposed	−241,475	−79,659
Large Urban	$L_{12h}^{LV} - G_{MAX}^{LV}$	*Used*	661,979	−70,016
		Proposed	662,855	−168,608
	$L_{20h}^{LV} - G_{NO}^{LV}$	*Used*	−352,719	−115,933
		Proposed	−344,251	−115,225
Industrial	$L_{12h}^{LV} - G_{MAX}^{LV}$	*Used*	459,104	−195,081
		Proposed	456,733	−201,358
	$L_{20h}^{LV} - G_{NO}^{LV}$	*Used*	−259,052	−125,465
		Proposed	−254,712	−118.239

and average active power losses of the related LV Link_Grid have been taken into consideration. Otherwise, values of $P_{INIT}^{Lmpd\_LVG}$ and $Q_{INIT}^{Lmpd\_LVG}$ of the "proposed" model of LV Link_Grids are purely based on the power flow simulations in LV Link_Grids. The way, in which they have been determined, has already been shown in the previous chapter, while their exact values are represented in Table 7.6.

By examining the values from the table above, the biggest difference in $Q_{INIT}^{Lmpd\_LVG}$ values between two model types is noticed for $L_{12h}^{LV} - G_{MAX}^{LV}$ scenario of Rural and Large Urban LV Link_Grid. Those two grids have CPs with PV systems, which are equipped with *Q(U)*-controlled inverters. For both grids, the "used" model consumes approximately 100 kVAr less reactive power than the "proposed model". This complies with the fact that in case of the "used" model. $Q_{INIT}^{Lmpd\_LVG}$ values were calculated under the assumption that all connected PV systems operate at the nominal voltage value. According to the

[7] The nominal voltage is equal to 20 kV, because the connection point of each LV Link_Grid is on the MV side of the related MV/LV distribution transformer.

inverters' *Q(U)*-control, this further means that the corresponding PV systems don't exchange any reactive power with the related LV Link_Grid. On the other hand, the same cannot be said for the "proposed" model. As the simulation results in Rural and Large Urban LV Link_Grids shows, the related PV systems don't have the same operating point. Clearly, due to higher voltage value at their PCC, some of them operate in underexcited mode, which further increases the overall reactive power consumption of the related LV Link_Grid. Negative values of $P_{INIT}^{Lmpd\_LVG}$ indicate that the related LV Link_Grid injects active power into the MV Link_Grid, which could be expected at 12h, because all PV systems combined produce much more active power than the whole grid needs at that particular time. In case of $L_{20h}^{LV} - G_{NO}^{LV}$ scenario, $P_{INIT}^{Lmpd\_LVG}$ and $Q_{INIT}^{Lmpd\_LVG}$ of both models of any LV Link_Grid have fairly similar values. This implies that all CPs during simulation in which the slack bus had the nominal voltage value, consumed approximately their initial active and reactive power. An identical explanation could be applied to the almost equivalent values of $P_{INIT}^{Lmpd\_LVG}$ in case of $L_{12h}^{LV} - G_{MAX}^{LV}$ scenario for any given LV Link_Grid.

7.2.3 P,Q-characteristic of the "used" and the "proposed" model of LV Link_Grids

As the biggest differences between the "used" and the "proposed" model are obviously in the LV Link_Grids, where the PV systems have *Q(U)*-controlled inverters, the following text describes only the behaviour of Rural and Large Urban LV Link_Grid, when the voltage value at their connection point is varied from 0,8 p.u. to 1,2 p.u. of the nominal voltage.

A. Rural LV Link_Grid

Firstly, differences between these two models are going to be inspected for $L_{12h}^{LV} - G_{MAX}^{LV}$ scenario. Figure 7.10 shows the lumped load characteristic of the Rural LV Link_Grid for this scenario. The largest difference in *P*-characteristic between two models are observed at the highest voltage values. For those values, the exchanged active power of the "proposed" model is a bit higher than the one of the "used" model. Unlike the "used" model, the "proposed" model doesn't takes into consideration the average active power losses of the grid. In case of a higher voltage value, the loading of the lines and

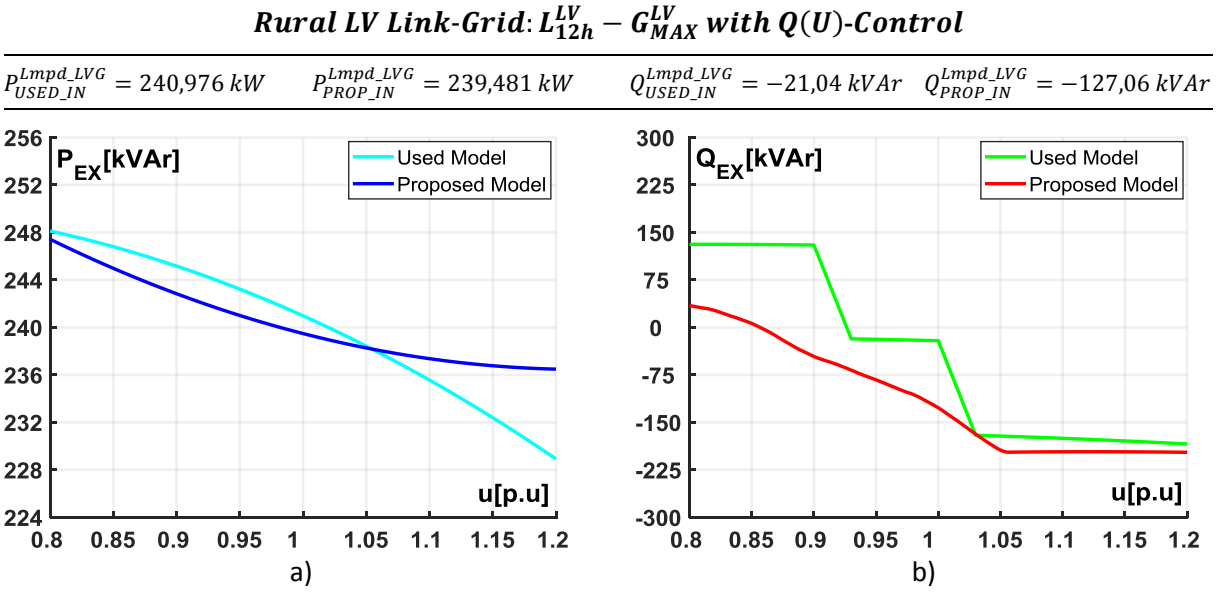

Figure 7.10 - Lumped load characteristic of the Rural LV Link_Grid for $L_{12h}^{LV} - G_{MAX}^{LV}$ scenario: a) active power and b) reactive power

transformer in the Rural LV Link_Grid decreases. Therefore, a larger amount of active power can be injected. At the voltage value of approximately 1,05, both models show the same *P*-characteristic. As far as the *Q*-characteristic is concerned, the biggest differences are noticed for the voltage values smaller than 0,9. Evidently, in case of the "proposed" model not all PV systems in the simulated Rural LV Link_Grid operate in full overexcited mode. Due to increased active power flow across the grid, PV systems that are connected at the end of the feeders experience higher voltage levels than 0,9. This further means that some of them inject less than they are capable or no reactive power at all. Similar conclusion can be made for the voltage values from 0,93-1. For this voltage band, the PV systems shouldn't exchange any reactive power with the Rural LV Link_Grid. Due to different voltage values at their connection point, it is highly unlikely that all connected PV systems operate in that mode. Clearly, a lot of them operate in underexcited mode, which further increases the reactive power demand of the whole grid. On the other hand, from the *Q*-characteristic of the "used" model, four different breakpoints of the *Q(U)*-control, which is used for the PV systems in Rural LV Link_Grid, can be identified with ease. Both models show quite the same *Q*-characteristic for voltage levels greater than 1,05.

In case of $L_{20h}^{LV} - G_{NO}^{LV}$ scenario, the situation is far less complicated, as the PV systems don't generate any power at 20h. The "used" and the "proposed" model show roughly the same *P*- and *Q*-characteristics, which are portrayed in Figure 7.11. Apart from the grid losses, *P*- and *Q*-characteristics of both models depend on the active and reactive power demand of all connected CPs. As the voltage value increases towards its maximal value, active and reactive power grid losses in the simulated Rural LV Link_Grid decrease, which can be taken from Figure 7.1 in Subsection 7.1.1. Thus, the "proposed" model shows a bit smaller active power demand than the "used" model. The largest difference in reactive power demand is observed at 80% of the nominal voltage value, while the same reactive power demand is viewed at about 102,5%.

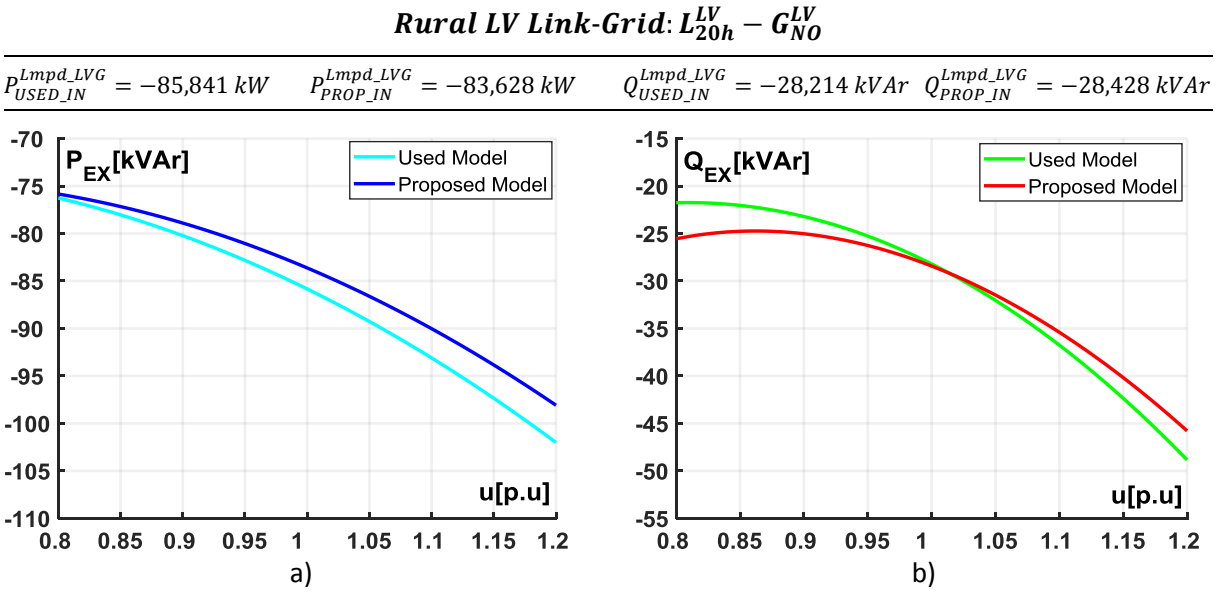

Figure 7.11 - Lumped load characteristic of the Rural LV Link_Grid for $L_{20h}^{LV} - G_{NO}^{LV}$ scenario: a) active power and b) reactive power

B. Large Urban LV Link_Grid

Lumped load characteristic of the Large Urban LV Link_Grid for $L_{12h}^{LV} - G_{MAX}^{LV}$ scenario is represented in Figure 7.12. In terms of *P*-characteristic, the most notable differences between two models occur at the voltage values smaller than 0,95 and greater than 1,1. This can be attributed to the different used active power ZIP coefficients. As each ZIP model possess a quadratic voltage dependence, the biggest discrepancy between the "used" and the "proposed" model can be expected exactly at those voltage levels. For the voltage range from 0,95 to 1,1, both models show practically the same *P*- and *Q*-characteristics. Dissimilarity of the *Q*-characteristic between two models is far more less noticeable than in case of Rural LV Link_Grid. Compared to the PV inverters in Rural LV Link_Grid, inverters of PV systems that are connected to Large Urban LV Link_Grid have different breakpoints of the *Q(U)*-control. When set side by side, the *Q(U)*-control in Large Urban LV Link_Grid has a bit wider voltage deadband than the *Q(U)*-control in Rural LV Link_Grid. This two information could be hold responsible for the smaller discrepancy between two models. From the figure below, a voltage band (0,925-0,98) for the "proposed" model when the most of the related PV systems don't exchange any reactive power with the grid, can easily be identified. Small reactive power demand of the whole grid during this voltage band can be attributed to those PV systems that operate underexcited, reactive power consumption by CPs' native load and the corresponding reactive power losses in the grid.

With respect to $L_{12h}^{LV} - G_{MAX}^{LV}$ scenario, the corresponding lumped load characteristics of the Large Urban LV Link_Grid are represented in Figure 7.13. Practically an exact same behaviour, like the Rural LV Link_Grid has shown for $L_{12h}^{LV} - G_{MAX}^{LV}$ scenario, is recognized here as well. The only difference is the higher demand on the active and reactive power. This is expected, as the Large Urban LV Link_Grid has a larger number of CPs than the Rural LV Link_Grid. *P*-characteristic of the "proposed" model reveals the fact that the active power losses in the simulated Large Urban LV Link_Grid are getting smaller as the voltage at the connection point is increased. Therefore, the biggest difference in *P*-characteristic of both models lies exactly at the maximum voltage value, which is 120% of the nominal voltage value.

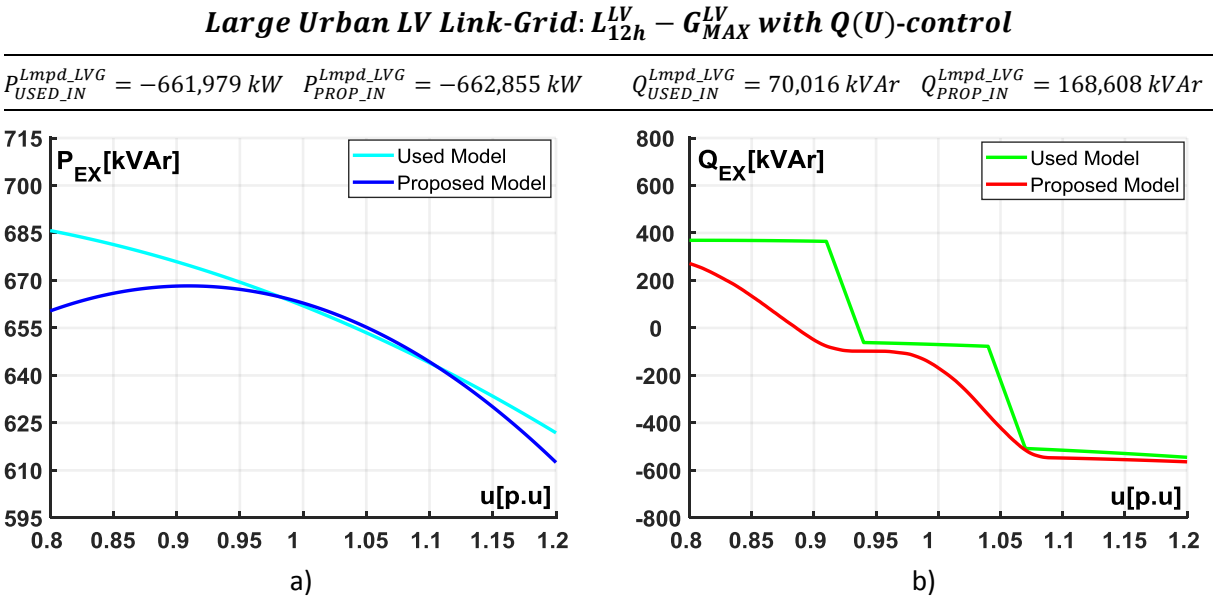

Figure 7.12 - Lumped load characteristic of the Large Urban LV Link_Grid for $L_{12h}^{LV} - G_{MAX}^{LV}$ scenario: a) active power and b) reactive power

Once again, the largest diversity in *Q*-characteristic between the "used" and the "proposed" model can be noticed at the minimal and the maximal voltage value, which complies with the fact that the "used" model uses average grid losses, while the "proposed" model takes into consideration the actual grid losses of the simulated Large Urban LV Link_Grid for each voltage point. Both models display more or less the same *Q*-characteristic when the voltage is around the nominal value.

$$\boldsymbol{Large\ Urban\ LV\ Link\text{-}Grid: L_{20h}^{LV} - G_{NO}^{LV}}$$

$P_{USED\_IN}^{Lmpd\_LVG} = 352{,}719\ kW$ $P_{PROP\_IN}^{Lmpd\_LVG} = 344{,}251\ kW$ $Q_{USED\_IN}^{Lmpd\_LVG} = 115{,}933\ kVAr$ $Q_{PROP\_IN}^{Lmpd\_LVG} = 115{,}225\ kVAr$

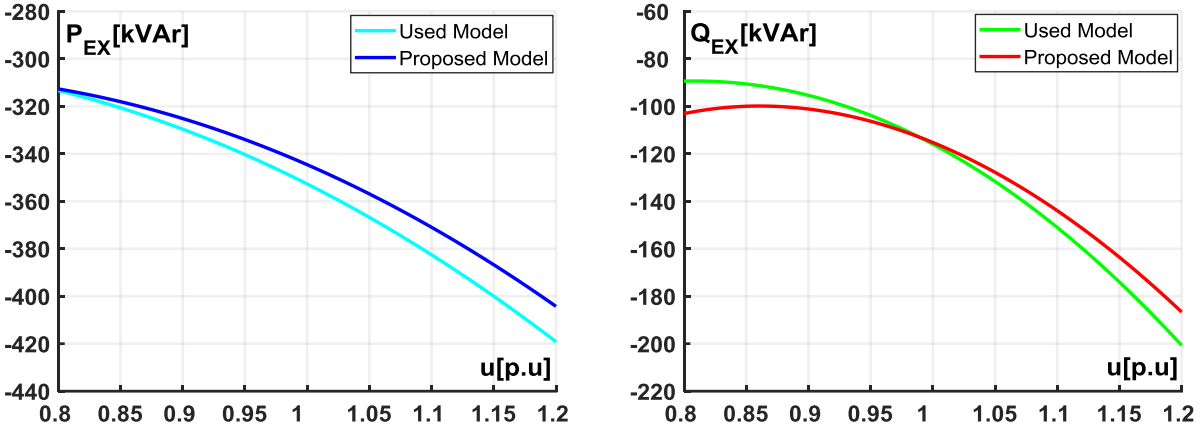

Figure 7.13 - Lumped load characteristic of the Large Urban LV Link_Grid for $L_{20h}^{LV} - G_{NO}^{LV}$ scenario: a) active power and b) reactive power

As already mentioned, lumped load characteristic of Small Urban and Industrial LV Link_Grid will not be reviewed, seeing that they don't have PV systems with *Q(U)*-controlled inverters. Nevertheless, their *P*- and *Q*-characteristics for both load/production scenarios are shown in Appendix A (Figure A.7-Figure A.10).

7.3 Behaviour of MV Link_Grids

In this section, simulation results from both MV grid types, Theoretical and Real MV Link_Grids, are going to be analysed for both load/production scenarios from Table 5.11 and two different lumped models of LV Link_Grids. As mentioned before, influence of HV/MV transformers that are normally equipped with OLTC are not going to be observed. The reason is that the effects of DG on the grid, which are coming from CPs' Producer Links, cannot be detected and evaluated so easily, when the voltage control through OLTC in included.

7.3.1 Theoretical I MV Link_Grid

In concern to simulation results in Theoretical I MV Link_Grids, main focus is given to evaluation of differences between the "used" and the "proposed" model of a LV Link_Grid when two different types and three different length of feeder are used. For better understanding, a schematic representation of Theoretical I MV Link_Grid is given in Figure 7.14. Electrical parameters of both feeder types were already shown in Table 3.5. As shown in the figure below, feeder length values are: 1 km, 12.5 km and 25 km, respectively.

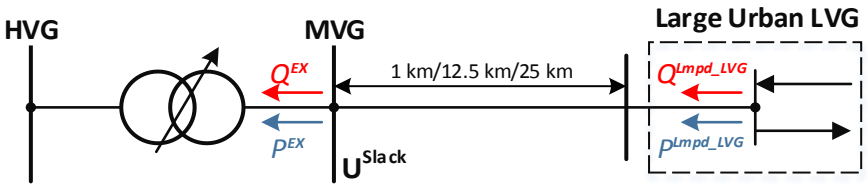

Figure 7.14 - Schematic representation of the Theoretical I MV Link_Grid

The most important simulation results of Theoretical I MV Link_Grid for $L_{12h}^{MV} - G_{MAX}^{MV}$ scenario, in which the C-AL-150 cable and the OL-35/6 overhead line were used, are represented in Table 7.7. Positive sign of each P_{EX} value implicates an unidirectional active power flow from MVG to the overlaid HVG. Only in cases where the cable feeder length is 12,5 km or 25 km, Theoretical I MV Link_Grid injects reactive power into the HVG. In those occasions, reactive power generated by the cable capacitance overcompensates the reactive power demand of the connected LV Link_Grid.

Table 7.7 - Simulation results of the Theoretical I MV Link_Grid for $L_{12h}^{MV} - G_{MAX}^{MV}$ scenario

Feeder Type	*Scenario*	*Feeder length* [km]	*Model Type*	P_{EX} [kW]	Q_{EX} [$kVAr$]	P^{Lmpd_LVG} [kW]	Q^{Lmpd_LVG} [$kVAr$]	P_{LOSSES}^{MVG} [kW]	Q_{LOSSES}^{MVG} [$kVAr$]
C-AL-150	L_{12h}^{MV}-G_{MAX}^{MV}	1	*used*	661,700	−38.276	661,927	−70,070	−0,227	31,794
			proposed	662,582	−137,850	662,820	−169,637	−0,238	31,786
C-AL-150	L_{12h}^{MV}-G_{MAX}^{MV}	12,5	*used*	658,322	328,334	661,219	−70,821	−2,897	399,156
			proposed	659,526	214,762	662,327	−184,279	−2,802	399,042
C-AL-150	L_{12h}^{MV}-G_{MAX}^{MV}	25	*used*	653,294	730,737	660,206	−71,908	−6,912	802,646
			proposed	655,565	596,147	661,599	−206,216	−6,033	802,363
OL-35/6	L_{12h}^{MV}-G_{MAX}^{MV}	1	*used*	660,847	−69,445	661,769	−70,238	−0,922	0,793
			proposed	661,731	−172,140	662,708	−172,908	−0,976	0,768
OL-35/6	L_{12h}^{MV}-G_{MAX}^{MV}	12,5	*used*	648,249	−62,514	659,347	−72,843	−11,097	10,329
			proposed	648,710	−215,616	660,995	−225,385	−12,285	9,768
OL-35/6	L_{12h}^{MV}-G_{MAX}^{MV}	25	*used*	635,381	−54,256	656,708	−75,786	−21,327	21,530
			proposed	633,961	−269,347	659,167	−288,981	−25,205	19,634

Figure 7.15 illustrates voltage profiles of Theoretical I MV Link_Grid for $L_{12h}^{MV} - G_{MAX}^{MV}$ scenario and previously mentioned feeder parameters. Voltage profile represents the voltage values of all grid nodes in dependency to their distance to the main MV bus bar[8]. The green line represents the voltage profiles with the "used" model of the Large Urban LV Link_Grid, while the blue line represents the voltage profiles with the "proposed" model. Additionally, dashed line was used for the voltage profiles with the cable feeder, whilst the solid line for the ones with the overhead feeder.

All voltage profiles from the figure below indicate that the voltage at the node, where the Large Urban LV Link_Grid is connected, increased. Due to the fact that at 12h the Large Urban LV Link_Grid injects a large amount of active power in the grid, this was highly expected. Voltage has increased a bit more in case of overhead feeder. Compared to cable, due to a higher R'/X' ratio, overhead feeder is more prone to changes in active power flow.

[8] As HV/MV transformers were not included during simulations in MV Link_Grids, the reference point is the position of the slack bus, which corresponds to the position of the main MV bus bar.

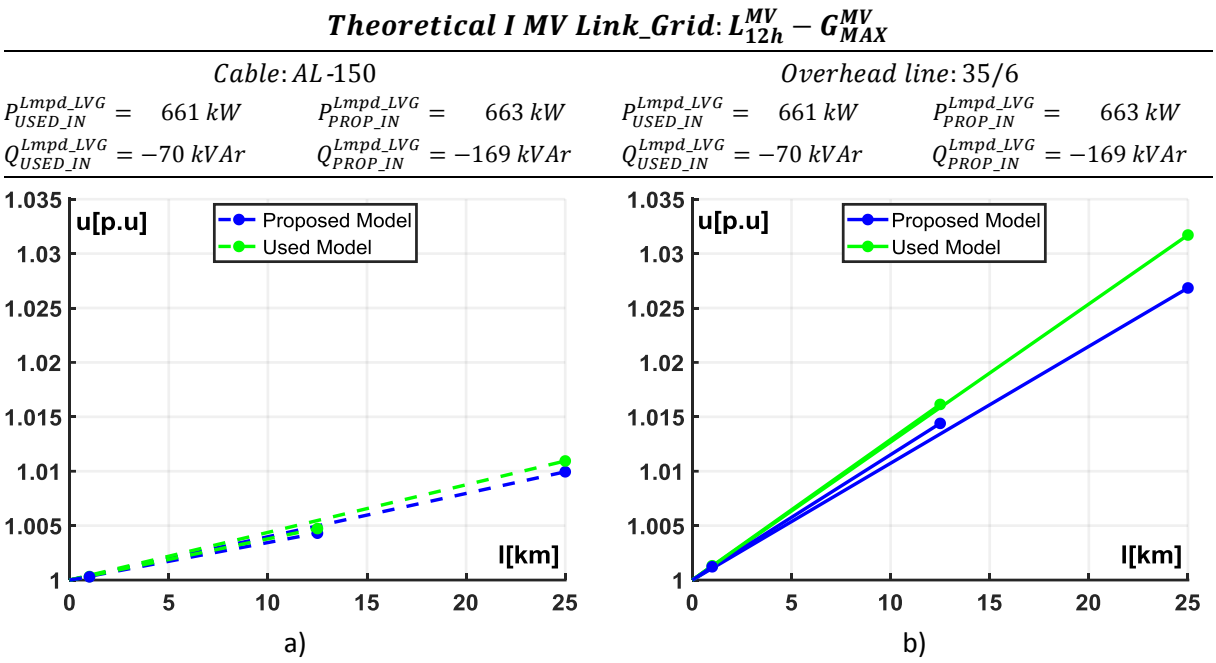

Figure 7.15 - Voltage profiles of the Theoretical I MV Link_Grid for $L_{12h}^{MV} - G_{MAX}^{MV}$ scenario with different length and type of feeder: a) C-AL-150 and b) OL-35/6

As the feeder length is getting greater, the difference between the "used" and the "proposed" model is also getting bigger. Slightly higher voltage differences $|\Delta u|$, which are calculated with Equation (7–1), can be detected in case of the overhead feeder.

$$|\Delta u| = \left| u_{used}^{(f,n)} - u_{proposed}^{(f,n)} \right| \tag{7–1}$$

In order to see what hides behind this outcome, we need to analyse the values of exchanged reactive power Q^{Lmpd_LVG} between the Large Urban LV and the Theoretical I MV Link_Grid. When the same feeder length is observed, difference in Q^{Lmpd_LVG} values between two models is higher for the overhead feeder. Therefore, as shown in the figure above, $|\Delta u|$ values for the same feeder length are consistently greater in case of the overhead feeder. The exact values of $|\Delta u|$ for $L_{12h}^{MV} - G_{MAX}^{MV}$ scenario is represented in Table 7.8.

Table 7.8 - Absolute node voltage difference within the Theoretical I MV Link_Grid between the "used" and the "proposed" model for $L_{12h}^{MV} - G_{MAX}^{MV}$ scenario

Scenario	*Feeder length* [*km*]	*Feeder Type*	$\|\Delta u\|$
L_{12h}^{MV}-G_{MAX}^{MV}	1	C-AL-150	0,00002995
		OL-35/6	0,00009449
L_{12h}^{MV}-G_{MAX}^{MV}	12	C-AL-150	0,00042447
		OL-35/6	0,00174168
L_{12h}^{MV}-G_{MAX}^{MV}	25	C-AL-150	0,00095994
		OL-35/6	0,00486469

In regard to $L_{20h}^{MV} - G_{NO}^{MV}$ scenario when u^{MVG_Slack} was set to 1, the most important simulation results are listed in Table 7.9, while the corresponding voltage profiles of Theoretical I MV Link_Grid are illustrated in Figure 7.16.

Table 7.9 - Simulation results of the Theoretical I MV Link_Grid for $L_{20h}^{MV} - G_{NO}^{MV}$ scenario

Feeder Type	Scenario	Feeder length [km]	Model Type	P_{EX} [kW]	Q_{EX} [kVAr]	P^{Lmpd_LVG} [kW]	Q^{Lmpd_LVG} [kVAr]	P_{LOSSES}^{MVG} [kW]	Q_{LOSSES}^{MVG} [kVAr]
C-AL-150	L_{20h}^{MV}-G_{NO}^{MV}	1	used	−352,732	−84,003	−352,663	−115,874	−0,069	31,870
			proposed	−344,270	−83,307	−344,204	−115,180	−0,066	31,872
C-AL-150	L_{20h}^{MV}-G_{NO}^{MV}	12,5	used	−353,049	282,308	−352,203	−115,392	−0,846	397,701
			proposed	−344,628	282,925	−343,819	−114,819	−0,809	397,745
C-AL-150	L_{20h}^{MV}-G_{NO}^{MV}	25	used	−354,715	679,217	−352,084	−115,267	−2,631	794,485
			proposed	−346,289	679,880	−343,729	−114,737	−2,559	794,618
OL-35/6	L_{20h}^{MV}-G_{NO}^{MV}	1	used	−352,783	−114,623	−352,496	−115,698	−0,287	1,076
			proposed	−344,336	−103,117	−344,064	−115,048	−0,272	11,931
OL-35/6	L_{20h}^{MV}-G_{NO}^{MV}	12,5	used	−353,545	−99,776	−349,982	−113,095	−3,563	13,318
			proposed	−345,268	34,702	−342,114	−113,249	−3,155	147,952
OL-35/6	L_{20h}^{MV}-G_{NO}^{MV}	25	used	−354,427	−84,099	−347,356	−110,453	−7,071	26,354
			proposed	−346,721	181,848	−340,395	−111,718	−6,326	293,566

Negative values of P_{EX} in each observed case from the table above mean that the active power flows always from the overlaid HV Link_Grid to Theoretical I MV Link_Grid. Negative values of P^{Lmpd_LVG} indicate that the connected Large Urban LV Link_Grid absorbs active power from Theoretical I MV Link_Grid. This is highly expected, since PV systems of the related CPs from Large Urban LV Link_Grid don't produce any electric power at 20h. Comparing the active grid losses P_{LOSSES}^{MVG} for two different feeder types and the same feeder length, it is clear that the values of P_{LOSSES}^{MVG} are always bigger in case of the overhead line-feeder. This further indicates that the current through the overhead line-feeder is greater than through the cable-feeder of the same length, making the voltage drop across the overhead line-feeder to be higher as well. When the reactive grid losses Q_{LOSSES}^{MVG} from Table 7.9 are observed, much bigger difference between the "used" and the "proposed" model of the LV Link_Grid for the same feeder length are present in case of the overhead line-feeder.

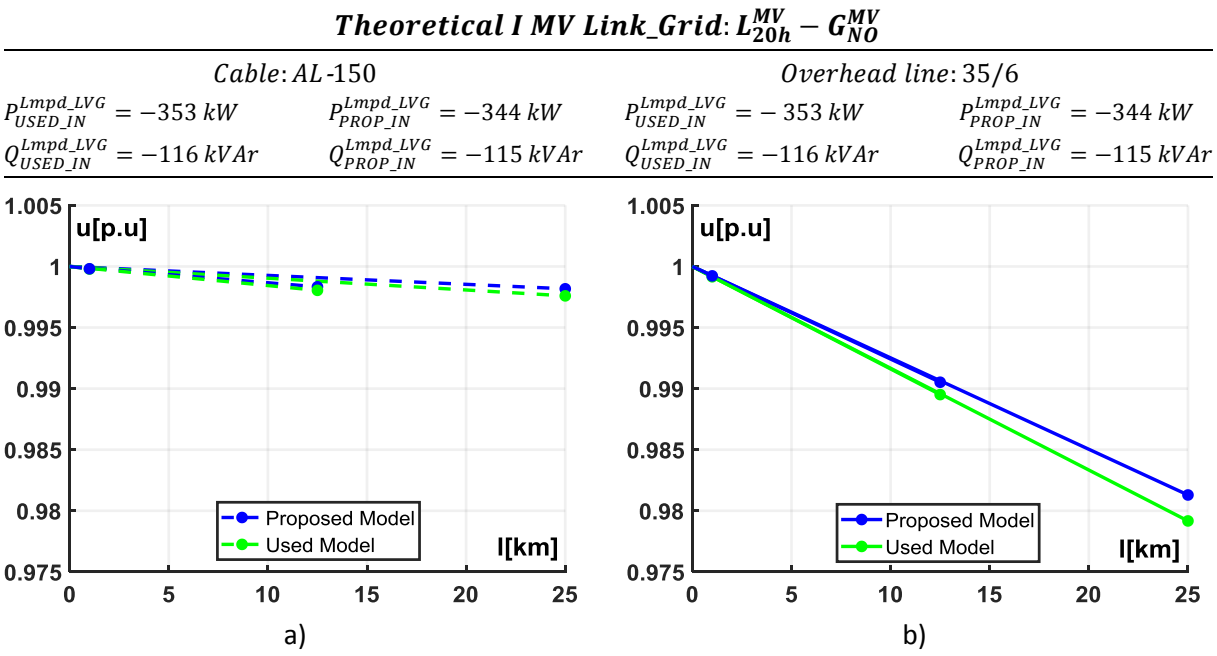

Figure 7.16 - Voltage profiles of Theoretical I MV Link_Grid for $L_{20h}^{MV} - G_{NO}^{MV}$ scenario with different length and type of feeder: a) C-AL-150 and b) OL-35/6

Looking at the voltage profiles from the figure above, it is obvious that voltage at node where the Large Urban LV Link_Grid is connected, decreased in all cases. Voltage profiles from Figure 7.16 reveal another interesting fact. Namely, as the feeder length is becoming larger, $|\Delta u|$ between the "used" and the "proposed" model is getting higher as well. The exact values of $|\Delta u|$ at the connection point of Large Urban LV Link_Grid for every feeder length and both feeder types are given in Table 7.10. Bigger differences are noticed in case of the overhead line-feeder, which has much higher values of R' and X' than the cable feeder.

Table 7.10 - Absolute node voltage difference within the Theoretical I MV Link_Grid between the "used" and the "proposed" model for $L_{20h}^{MV} - G_{NO}^{MV}$ scenario

Scenario	*Feeder length* [*km*]	*Feeder Type*	$\|\Delta u\|$
L_{20h}^{MV}-G_{NO}^{MV}	1	C-AL-150	0,00002787
		OL-35/6	0,00007488
L_{20h}^{MV}-G_{NO}^{MV}	12	C-AL-150	0,00028958
		OL-35/6	0,00101299
L_{20h}^{MV}-G_{NO}^{MV}	25	C-AL-150	0,00057813
		OL-35/6	0,00212439

7.3.2 Theoretical II MV Link_Grid

Like in case of the Theoretical I, the main goal of power flow simulations in the Theoretical II MV Link_Grid is to compare the "used" and the "proposed" lumped model of LVG for $L_{12h}^{MV} - G_{MAX}^{MV}$ and $L_{20h}^{MV} - G_{NO}^{MV}$ scenario. Once again, two feeder types from Table 3.5 have been used. Figure 7.17 schematically represents the Theoretical II MV Link_Grid.

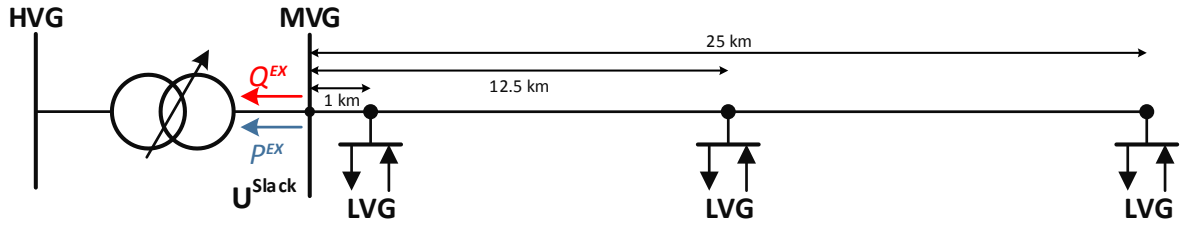

Figure 7.17 - Schematic representation of the Theoretical II MV Link_Grid

As the slack voltage is increased in small steps from 80% to 120% of the nominal voltage value, values of reactive power exchange Q_{EX} between the Theoretical I MV Link_Grid and the HV Link_Grid for $L_{12h}^{MV} - G_{MAX}^{MV}$ scenario are obtained and plotted against the slack voltage, which is illustrated in Figure 7.18. Green colour line shows the Q_{EX}-characteristic when the "used" model of the LV Link_Grids is adopted. The related Q_{EX}-characteristic when the "proposed" model is used, is represented with the red colour line. To distinct difference between the cable feeder and the overhead line-feeder, two different types of lines are used in the diagrams: dashed and solid.

For both types of feeder, the "used" model- and the "proposed" model-curve show similarity to the related curves from Figure 7.12, where the lumped *Q*-characteristic of a single Large Urban LV Link_Grid for $L_{12h}^{LV} - G_{MAX}^{LV}$ scenario is given. Slightly bigger distortion of the curves can be noticed in case where the overhead line-feeder is used. Further, it seems that the "used" model- and the "proposed" model-curve of the cable feeder are displaced when compared to their opposite curves of the overhead line-feeder. This is caused by the much higher reactive power losses of the grid Q_{LOSSES}^{MVG}

and its capacitive nature when the cable feeder is used. The maximum values of Q_{EX} with the cable feeder are seen at 0,8 p.u., while the ones with the overhead line-feeder at 1,2 p.u..

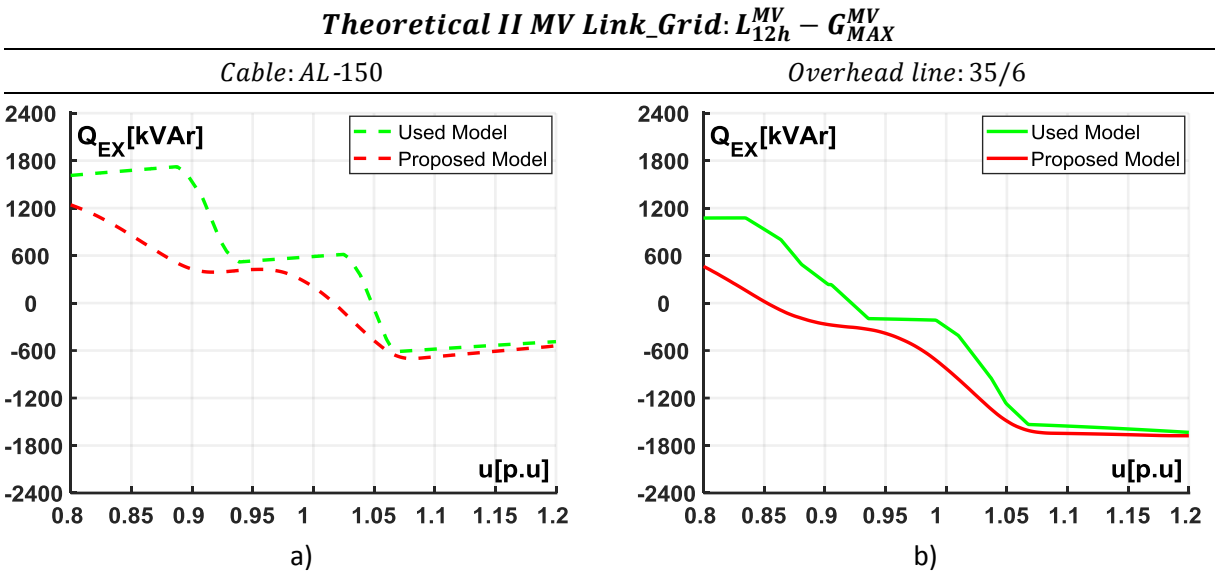

Figure 7.18 - Reactive power exchange between Theoretical II MV Link_Grid and HV Link_Grid for $L_{12h}^{MV} - G_{MAX}^{MV}$ scenario: a) C-AL-150 and b) OL-35/6

Absolute differences of the Q_{EX}-values between the "used" and the "proposed" modelling of the connected Large Urban LV Link_Grids for $L_{12h}^{MV} - G_{MAX}^{MV}$ scenario are shown in Figure 7.19. Once again, a dashed line is used for the cable feeder, while a solid line for the overhead line-feeder. Both lines display a fairly similar behaviour. The most apparent differences lie in the values of the peak differences and the voltage values when those differences occur. The maximal discrepancy of 916,543 kVAr in case of the overhead line-feeder can be seen at $u^{MVG\_Slack} = 0{,}837$. On the other hand, in case of the cable feeder, the maximal discrepancy of 1214,773 kVAr is reached at $u^{MVG\_Slack} = 0{,}888$.

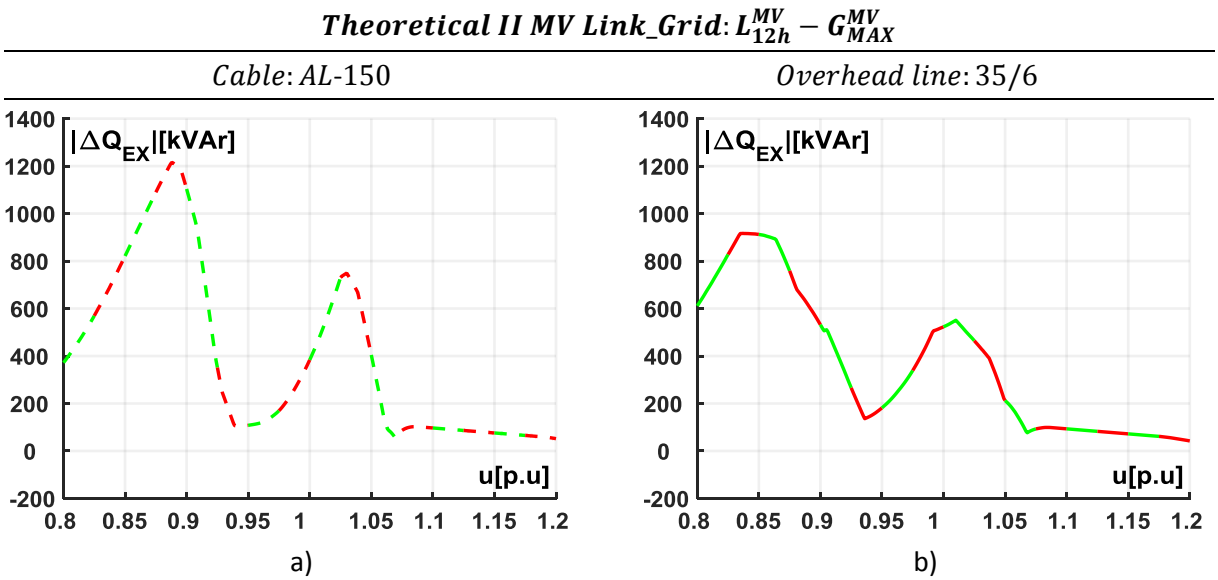

Figure 7.19 - Absolute exchanged reactive power difference between the "used" and the "proposed" model within Theoretical II MV Link_Grid for $L_{12h}^{MV} - G_{MAX}^{MV}$ scenario a) C-AL-150 and b) OL-35/6

The most important simulation results of Theoretical II MV Link_Grid for $L_{12h}^{MV} - G_{MAX}^{MV}$ scenario with $u^{MVG\_Slack} = 1$ are listed in Table 7.11, while the corresponding voltage profiles are displayed in Figure 7.20. Regardless the type of feeder, the biggest differences between the modelling of the LV Link_Grids can be noticed in the total reactive power $Q_{TOTAL}^{Lmpd\_LVG}$ that is exchanged between the Theoretical II MV Link_Grid and the connected Large Urban LV Link_Grids. Those values directly influence the total values of Q_{EX} as well. Hardly any difference can be recognized in the total active power $P_{TOTAL}^{Lmpd\_LVG}$ exchanged between the Theoretical II MV Link_Grid and the connected Large Urban LV Link_Grids. This is quite normal since a single Large Urban LV Link_Grid shows barely any difference in the lumped P-characteristic between the "used" and the "proposed" model, as shown in Figure 7.12a.

Table 7.11 - Simulation results of the Theoretical II MV Link_Grid for $L_{12h}^{MV} - G_{MAX}^{MV}$ scenario

Feeder Type	**Scenario**	**Model Type**	P_{EX} [kW]	Q_{EX} [$kVAr$]	$P_{TOTAL}^{Lmpd\_LVG}$ [kW]	$Q_{TOTAL}^{Lmpd\_LVG}$ [$kVAr$]	P_{LOSSES}^{MVG} [kW]	Q_{LOSSES}^{MVG} [$kVAr$]
C-AL-150	L_{12h}^{MV}-G_{MAX}^{MV}	*used*	1965,363	588,264	1981,586	−214,704	−16,223	802,968
		proposed	1970,462	204,361	1985,514	−597,769	−15,052	802,130
OL-35/6	L_{12h}^{MV}-G_{MAX}^{MV}	*used*	1914,436	−304,289	1972,322	−310,084	−57,886	5,794
		proposed	1908,659	−827,354	1978,832	−827,357	−70,173	0,003

Voltage profiles of the Theoretical II MV Link_Grid for $L_{12h}^{MV} - G_{MAX}^{MV}$ scenario, which is portrayed in Figure 7.20, only confirm the findings from Figure 7.15, in which voltage profiles of the Theoretical I MV Link_Grid for the same load/production scenario were plotted. Like there, the difference of the voltage profiles between the "used" and the "proposed" model-approach increases as the feeder length is getting larger. Also, a bigger increase of the voltage values is detected in case of the overhead line-feeder. This was deeply anticipated, since the voltage profile of the overhead line-feeder is more sensitive to active and reactive power flows than that of the cable feeder.

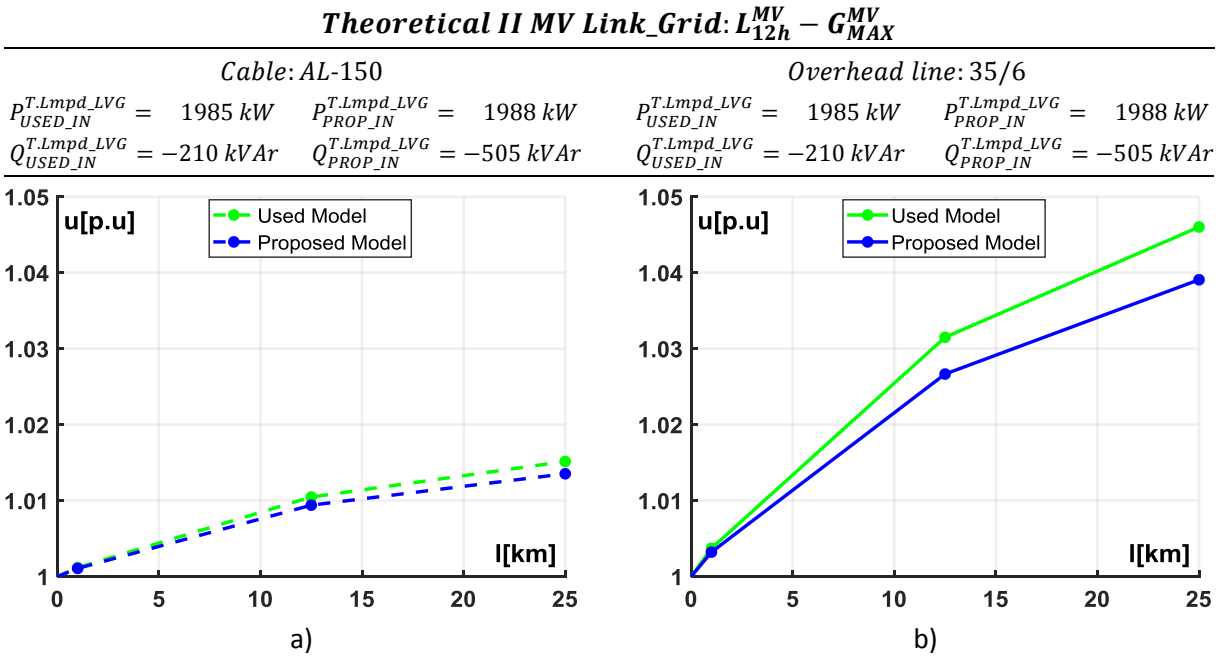

Figure 7.20 - Voltage profiles of the Theoretical II MV Link_Grid for $L_{12h}^{MV} - G_{MAX}^{MV}$ scenario with different type of feeder: a) C-AL-150 and b) OL-35/6

As far as $L_{20h}^{MV} - G_{NO}^{MV}$ scenario is concerned, the reactive power exchange Q_{EX} between the Theoretical II MV Link_Grid and the overlaid HV Link_Grid for both feeder types is represented in Figure 7.21. What is interesting in this figure is that the direction of the reactive power flow is not the same. Namely, in case of the cable feeder, reactive power is injected from Theoretical II MV Link_Grid into the overlaid HV Link_Grid. This can be attributed to the ever-increasing reactive power losses of the grid Q_{LOSSES}^{MVG}, which are highly capacitive due to a large value of the cable's specific capacitance C'. At each voltage level these losses are greater than the total reactive power demand of the three connected Large Urban LV Link_Grids.

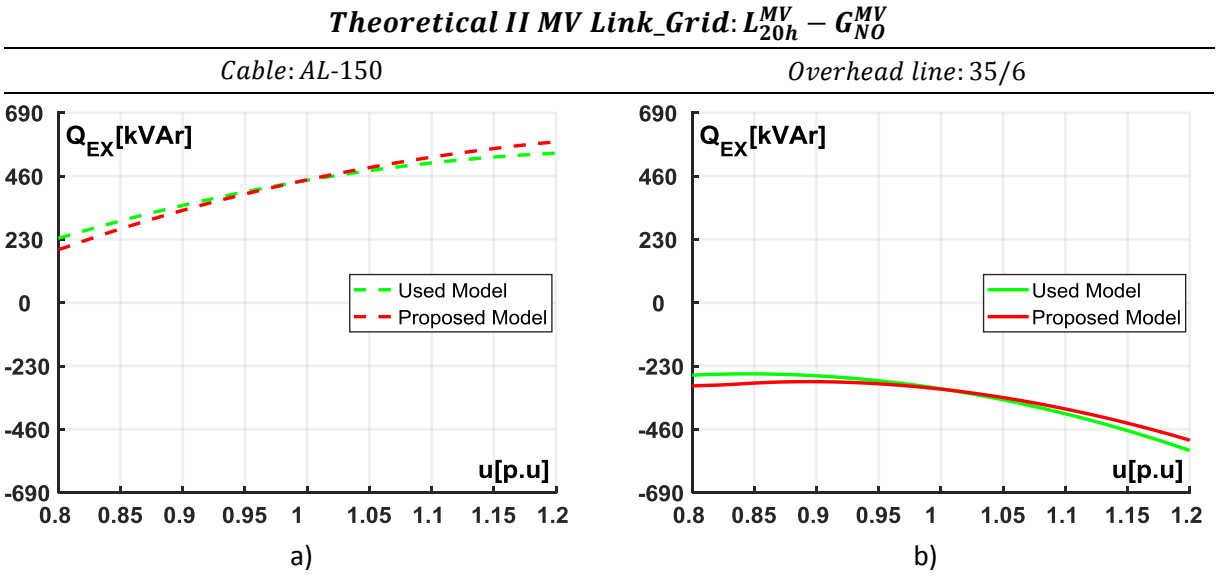

Figure 7.21 - Reactive power exchange between the Theoretical II MV Link_Grid and the overlaid HV Link_Grid for $L_{20h}^{MV} - G_{NO}^{MV}$ scenario: a) C-AL-150 and b) OL-35/6

In second case, where the overhead line-feeder was used, reactive power flows in the reversed direction. Normally, using the overhead line-feeder leads to the inductive line losses, but in this situation, despite its inductive nature, they were always capacitive. The reason behind is that due to a sheer size of the overhead line-feeder, its specific capacitance C' cannot be neglected. Nevertheless, for each voltage level the value of Q_{LOSSES}^{MVG} wasn't larger than the total reactive power demand of the three connected Large Urban LV Link_Grids. For both feeder types, the maximal exchanged power is noticed at 120% of the nominal voltage value.

Figure 7.22 provides the absolute difference of the related Q_{EX}-values for $L_{20h}^{MV} - G_{NO}^{MV}$ scenario when two different approaches were used in modelling of the connected Large Urban LV Link_Grids. For both feeder types practically the same behaviour can be observed. Since for each voltage value the related values of Q_{LOSSES}^{MVG} were almost identical for both model types, the $|\Delta Q_{EX}|$-characteristics from the figure below depend only on the differences between the corresponding $Q_{TOTAL}^{Lmpd\_LVG}$-values of each model type.

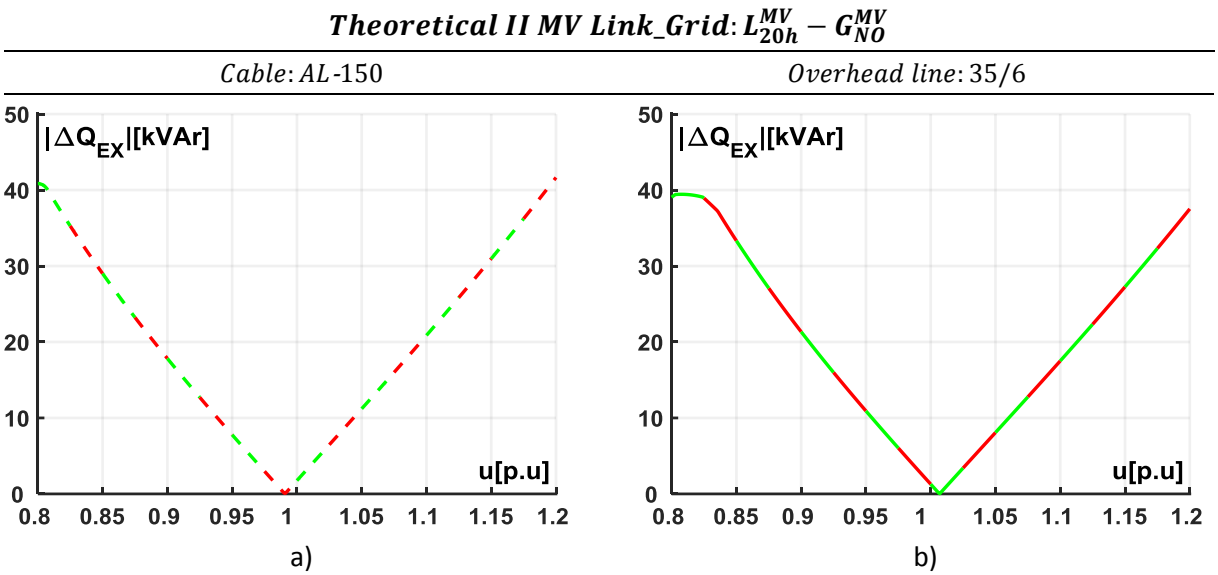

Figure 7.22 - Absolute exchanged reactive power difference between the "used" and the "proposed" model within Theoretical II MV Link_Grid for $L_{20h}^{MV} - G_{NO}^{MV}$ scenario a) C-AL-150 and b) OL-35/6

The most important simulation results of Theoretical II MV Link_Grid for $L_{20h}^{MV} - G_{NO}^{MV}$ scenario, whereby u^{MVG_Slack} was set to 1, are listed in Table 7.12, while the corresponding voltage profiles are displayed in Figure 7.23. The simulations results from the table below verify the statements derived from Figure 7.23. More precisely, in case of the cable feeder the related Q_{LOSSES}^{MVG}- and Q_{EX}-values are positive, indicating the capacitive nature of the cable feeder and the direction of the exchanged reactive power, respectively. On the other hand, the related Q_{EX}-values in case of the overhead-line feeder are negative, which means that the Theoretical II MV Link_Grid absorbs reactive power from the overlaid HV Link_Grid. P_{LOSSES}^{MVG}-values with the overhead line-feeder are slightly bigger than those with the cable feeder, which suggests that the loading of the overhead line-feeder is also bigger.

Table 7.12 - Simulation results of the Theoretical II MV Link_Grid for $L_{20h}^{MV} - G_{NO}^{MV}$ scenario

Feeder Type	Scenario	Model Type	P_{EX} [kW]	Q_{EX} [kVAr]	$P_{TOTAL}^{Lmpd\_LVG}$ [kW]	$Q_{TOTAL}^{Lmpd\_LVG}$ [kVAr]	P_{LOSSES}^{MVG} [kW]	Q_{LOSSES}^{MVG} [kVAr]
C-AL-150	L_{20h}^{MV}-G_{NO}^{MV}	used	−1060,952	444,716	−1055,754	−345,286	−5,198	790,003
		proposed	−1036,179	446,472	−1031,174	−343,804	−5,005	790,276
OL-35/6	L_{20h}^{MV}-G_{NO}^{MV}	used	−1062,978	−312,821	−1043,702	−333,163	−19,276	20,341
		proposed	−1039,521	−314,102	−1020,968	−334,789	−18,552	20,687

The voltage profiles from Figure 7.23 point out that there is hardly any difference in the voltage values when two different approaches in modelling of the connected Large Urban LV Link_Grids are used. For both feeder types, the difference of the voltage values is increasing as the feeder length is getting larger. Overall, voltage values in the grid with the overhead line-feeder decreased more than those with the cable feeder. This might be explained with the fact that the voltage profile of the overhead-line feeder is more prone to active and especially reactive power flows.

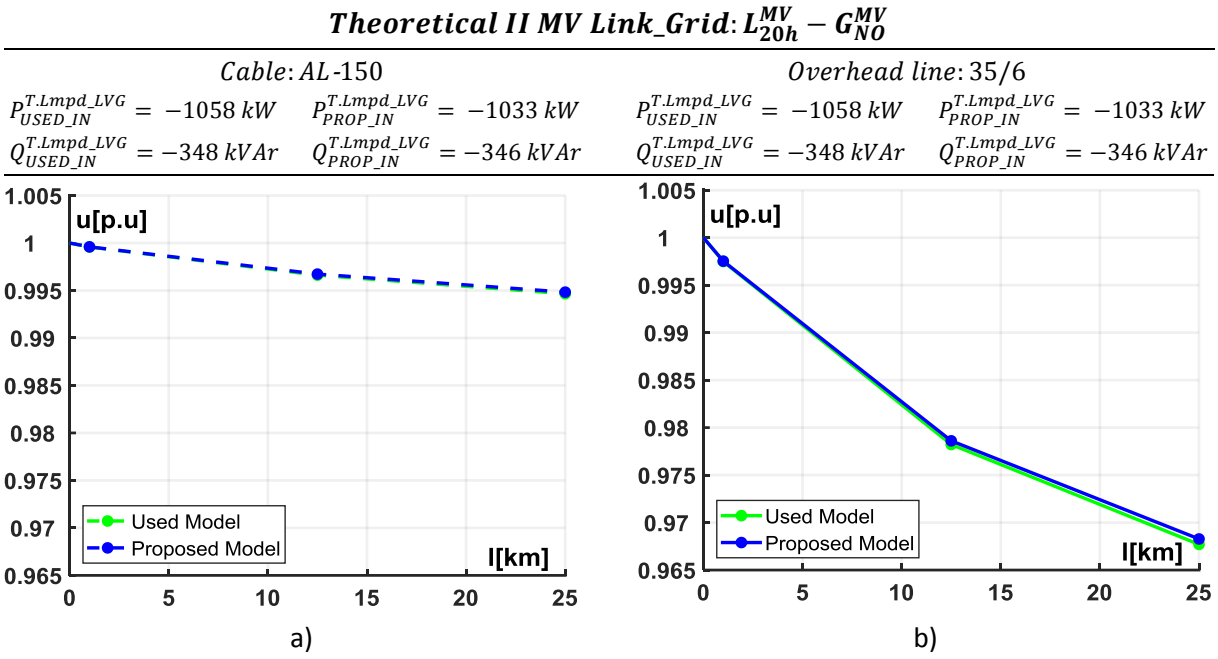

Figure 7.23 - Voltage profiles of the Theoretical II MV Link_Grid for $L_{20h}^{MV} - G_{NO}^{MV}$ scenario with different type of feeder: a) C-AL-150 and b) OL-35/6

7.3.3 Real I MV Link_Grid

A very simplified schematic overview of the Real I MV Link_Grid is given in Figure 7.24, whereby only the longest main-branch of each feeder is represented. Contrarily to Theoretical I and II, Real I MV Link_Grid takes into consideration, not only the influence of the LV Link_Grids, but of the MV CPs as well. Unlike the LV Link_Grids, the MV CPs were modelled only in one way, as it has been already shown in Section 4.4.

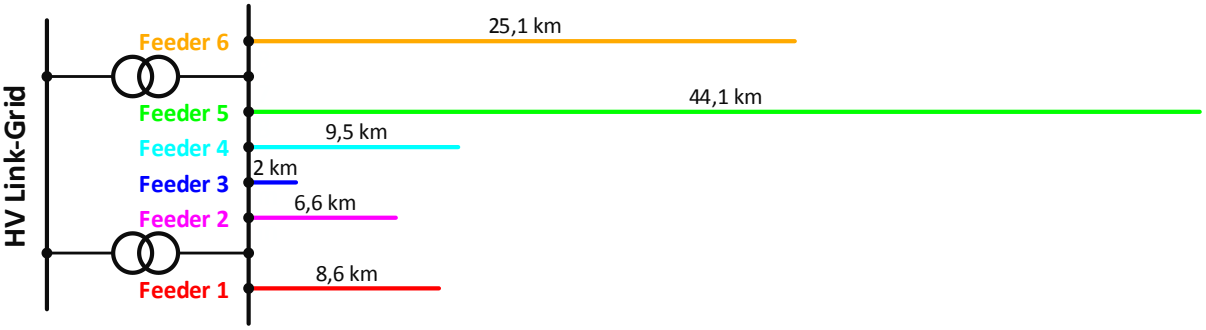

Figure 7.24 - Simplified overview of the Real I MV Link_Grid

As in previous cases, values of reactive power exchange Q_{EX} between the Real I MV and the overlaid HV Link_Grid were acquired for $L_{12h}^{MV} - G_{MAX}^{MV}$ and $L_{20h}^{MV} - G_{NO}^{MV}$ scenarios and plotted against the slack voltage, which is portrayed in Figure 7.25. In both diagrams from the figure below, the green solid line represents the Q_{EX} values where the "used" model of LV Link_Grids was used, while the red one where the "proposed" model was used.

According to Subsection 7.2.3, the biggest differences in the lumped *Q*-characteristic between the "used" and the "proposed" model were recorded in those LV Link_Grids, where the PV inverters were equipped with *Q(U)*-control. Next to Large Urban, Rural LV Link_Grid was the only grid with that feature. Due to the fact that 75 Rural Link_Grids are connected to Real I MV Link_Grid, the bigger

differences in Q_{EX} values can be noticed in case of $L_{12h}^{MV} - G_{MAX}^{MV}$ scenario. For the same reason, form of both curves for $L_{12h}^{MV} - G_{MAX}^{MV}$ scenario resembles in some degree the form of the corresponding Q-lumped load characteristic of the Rural LV Link_Grid for $L_{12h}^{LV} - G_{MAX}^{MV}$. Both curves contain only negative values of Q_{EX}, which indicates a reactive power flow from the HV Link_Grid to the Real MV Link_Grid for each voltage value. Both curves reach their minimum of exchanged reactive power for $u = 0{,}8$ and their maximum for $u = 1{,}2$.

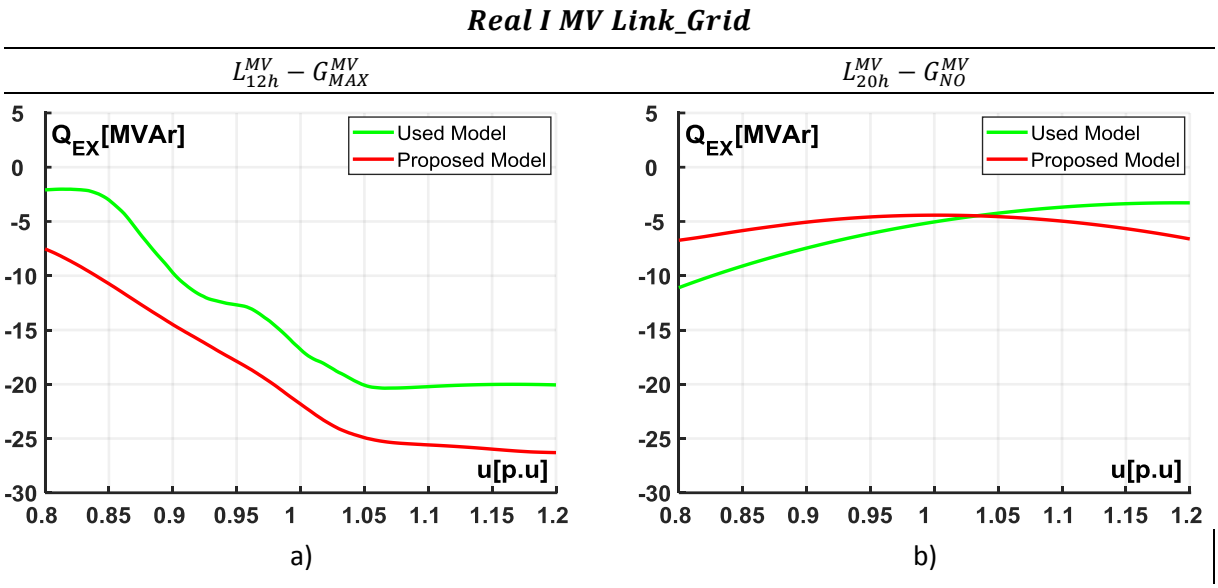

Figure 7.25 - Reactive power exchange between the Real I MV Link_Grid and the HV Link_Grid: a) $L_{12h}^{MV} - G_{MAX}^{MV}$ scenario and b) $L_{20h}^{MV} - G_{NO}^{MV}$ scenario

As anticipated, when compared to $L_{12h}^{LV} - G_{MAX}^{MV}$ scenario, $L_{20h}^{MV} - G_{NO}^{MV}$ scenario brings on the smaller differences in Q_{EX} values between two curves. In the grid, where the "used" model of the LV Link_Grids was adopted, the reactive power demand rises as the voltage at the main MV busbar h increased. Maximum of the reactive power demand is recorded at 80% of the nominal voltage value, while the minimum at 120%. The "proposed" model-curve shows a different behaviour. Until the voltage at the main MV busbar reaches approximately the nominal voltage value, the reactive power demand of the Real I MV Link_Grid decreases steadily. As the voltage is coming closer to 120% of the nominal voltage value, the reactive power demand of the grid increases. It reaches its maximum value for $u = 1{,}2$. Approximately the same value can be seen in the case where $u = 0{,}8$. Both curves have the same reactive power demand when u reaches 1,03.

Figure 7.26 illustrates the absolute difference of the Q_{EX}-values that were taken from Figure 7.25 when two different grid load/production scenarios are observed. Overall, $L_{12h}^{MV} - G_{MAX}^{MV}$ scenario shows much larger differences than $L_{20h}^{MV} - G_{NO}^{MV}$ scenario. For $L_{12h}^{MV} - G_{MAX}^{MV}$ scenario the biggest difference is observed at about 85% of the nominal voltage value, while the smallest one at about 92,5%. The biggest difference for $L_{20h}^{MV} - G_{NO}^{MV}$ scenario can be viewed at 80% of the nominal voltage value. As already mentioned above, no difference between the Q_{EX}-characteristics can be seen at 103%.

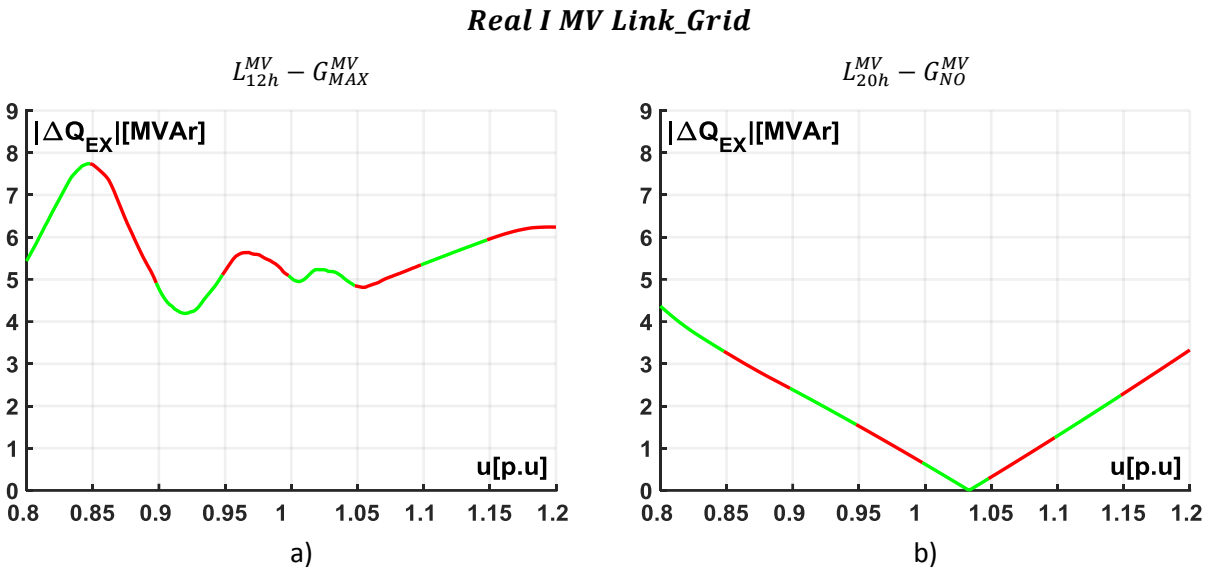

Figure 7.26 - Absolute difference of the Q_{EX}-values between two models of the Real I MV Link_Grid: a) $L_{12h}^{MV} - G_{MAX}^{MV}$ scenario and b) $L_{20h}^{MV} - G_{NO}^{MV}$ scenario

Table 7.13 recaps the most important simulation results of Real I MV Link_Grid for both load/production scenarios when the voltage at the secondary side of the supplying HV/MV transformer was set to the nominal voltage value and when the two different lumped models of the LV Link_Grids were used.

Observing the simulation results for $L_{12h}^{MV} - G_{MAX}^{MV}$ scenario, it can be seen that Real I MV Link_Grid where the "proposed" model of the LV Link_Grids was used, contains the higher values of almost every parameter from the table above. Reactive grid losses Q_{LOSSES}^{MVG} is the only parameter where the corresponding value was lower. All other parameters have higher values, starting from the total active $P_{TOTAL}^{CP\_MV}$ and reactive power demand $Q_{TOTAL}^{CP\_MV}$ of the all connected MV CPs, over the total active $P_{TOTAL}^{Lmpd\_LVG}$ and reactive power value $Q_{TOTAL}^{Lmpd\_LVG}$ of the all connected LV Link_Grids and to the exchanged active P_{EX} and reactive power Q_{EX} between Real I MV Link_Grid and the related HV Link_Grid. Value of the active grid losses P_{LOSSES}^{MVG} is also greater in this case. For both model types $P_{TOTAL}^{Lmpd\_LVG}$-values are positive. This indicates that the CPs in those LV Link_Grids produced overall more active power than their combined native loads needed. Regarding the CPs that are directly connected to Real I MV Link_Grid, value of $P_{TOTAL}^{CP\_MV}$ is negative, indicating that in global, they consumed more than they produced. This can be attributed to the 4 large Industrial CPs, which aren't equipped with any PV system. As seen from the table above, regardless the LV Link_Grids' modelling, $P_{TOTAL}^{Lmpd\_LVG}$-value overcompensate the compiled value of $P_{TOTAL}^{CP\_MV}$ and P_{LOSSES}^{MVG}. In both cases, this causes an active power flow from Real I MV Link_Grid to HV Link_Grid.

Table 7.13 - Simulation results of the Real I MV Link_Grid for both load/production scenarios

Scenario	*Model Type*	N_{VIOL}	P_{EX} [MW]	Q_{EX} [MVAr]	$P_{TOTAL}^{Lmpd\_LVG}$ [MW]	$Q_{TOTAL}^{Lmpd\_LVG}$ [MVAr]	$P_{TOTAL}^{CP\_MV}$ [MW]	$Q_{TOTAL}^{CP\_MV}$ [MVAr]	P_{LOSSES}^{MVG} [MW]	Q_{LOSSES}^{MVG} [MVAr]
L_{12h}^{MV}-G_{MAX}^{MV}	*used*	19	19,866	−16,788	33,697	−14,056	−11,317	−7,896	−2,514	5,164
	proposed	73	23,167	−21,819	41,533	−17,223	−14,784	−8,994	−3,582	4,398
L_{20h}^{MV}-G_{NO}^{MV}	*used*	0	−28,243	−5,040	−19,471	−6,863	−8,116	−3,872	−0,655	5,694
	proposed	0	−27,761	−4,419	−19,022	−5,846	−8,118	−4,319	−0,621	5,746

On the other hand, simulation results for $L_{20h}^{MV} - G_{NO}^{MV}$ scenario reveals a total opposite outcome. The gathered values of almost every parameter were smaller in case where the "proposed" model of LV Link_Grids was used. Only the values of $P_{TOTAL}^{CP\_MV}$, $Q_{TOTAL}^{CP\_MV}$ and Q_{LOSSES}^{MVG} were slightly bigger than in case of the "used" model. At 20h there is no electric power generation of the CPs, which are connected to Real I MV as well as to the related LV Link_Grids. Therefore, $P_{TOTAL}^{Lmpd\_LVG}$ - and $P_{TOTAL}^{CP\_MV}$ -values are negative, indicating that the directly connected CPs and LV Link_Grids absorb active power from the grid. Compared to $L_{12h}^{MV} - G_{MAX}^{MV}$ scenario, $L_{20h}^{MV} - G_{NO}^{MV}$ scenario has generally lower values of the above discussed parameters, especially the values of $P_{TOTAL}^{Lmpd\_LVG}$,$P_{TOTAL}^{CP\_MV}$, $Q_{TOTAL}^{Lmpd\_LVG}$,$Q_{TOTAL}^{CP\_MV}$ and Q_{EX}. This can be linked to the non-production of the related MV and LV CPs. Additionally, decrease in the loading of the lines is also noticed, causing the values of P_{LOSSES}^{MVG} for $L_{20h}^{MV} - G_{NO}^{MV}$ to be smaller than for $L_{12h}^{MV} - G_{MAX}^{MV}$ scenario.

Regarding the voltage profiles of Real I MV Link_Grid for $L_{12h}^{MV} - G_{MAX}^{MV}$ scenario, they are represented in Figure 7.27. It is apparent that the voltages within the grid with the "proposed" model of the LV Link_Grids are a little bit higher than the corresponding voltages within the grid with the "used" model. This is most evident when the Feeder 5, the longest feeder in grid, is taken into consideration. A possible explanation for this might be a huge number of the Rural LV Link_Grids in the grid, of which 52 are connected to the Feeder 5. Next to Large Urban, Rural LV Link_Grid shows at 12h the biggest difference in the lumped Q-characteristic between the "used" and the be "proposed" model, as shown in Figure 7.10a. Returning to Figure 7.27, it is evident that the grid with the "proposed" model of the LV Link_Grids has a much larger number of the voltage violations N_{viol} than the grid with the "used" model. More precisely, 73 against 19 voltage violations, which is also given in Table 7.13.

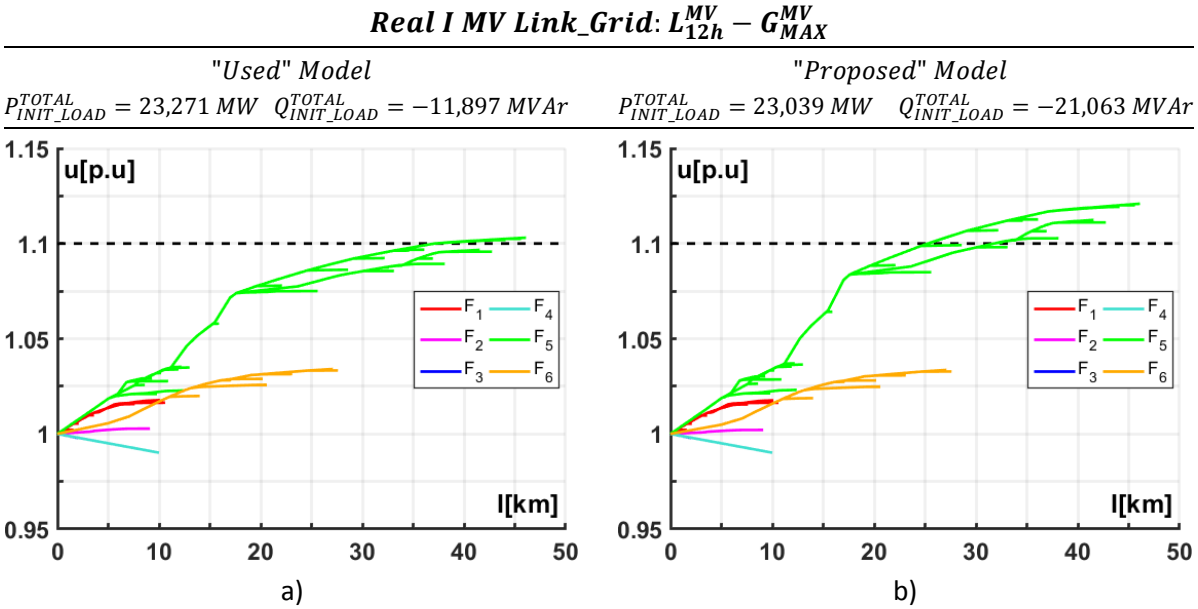

Figure 7.27 - Voltage profile of the Real I MV Link_Grid for $L_{12h}^{MV} - G_{MAX}^{MV}$ scenario: a) "used" model and b) "proposed" model

Node-voltages within the other much shorter feeders don't display so much clear differences. In both cases, due to the same topology, node-voltages of the Feeder 3 and Feeder 4 are an exact match. Thus, in the figure below, their voltage profiles are overlapping and only node-voltages of the Feeder 4 are visible.

Voltage profiles of the Real I MV Link_Grid for $L_{20h}^{MV} - G_{NO}^{MV}$ scenario, which are illustrated in Figure 7.28, don't expose so apparent differences in node-voltages when two different lumped models of the LV Link_Grids are used. In both cases there are no violations of the lower voltage limit.

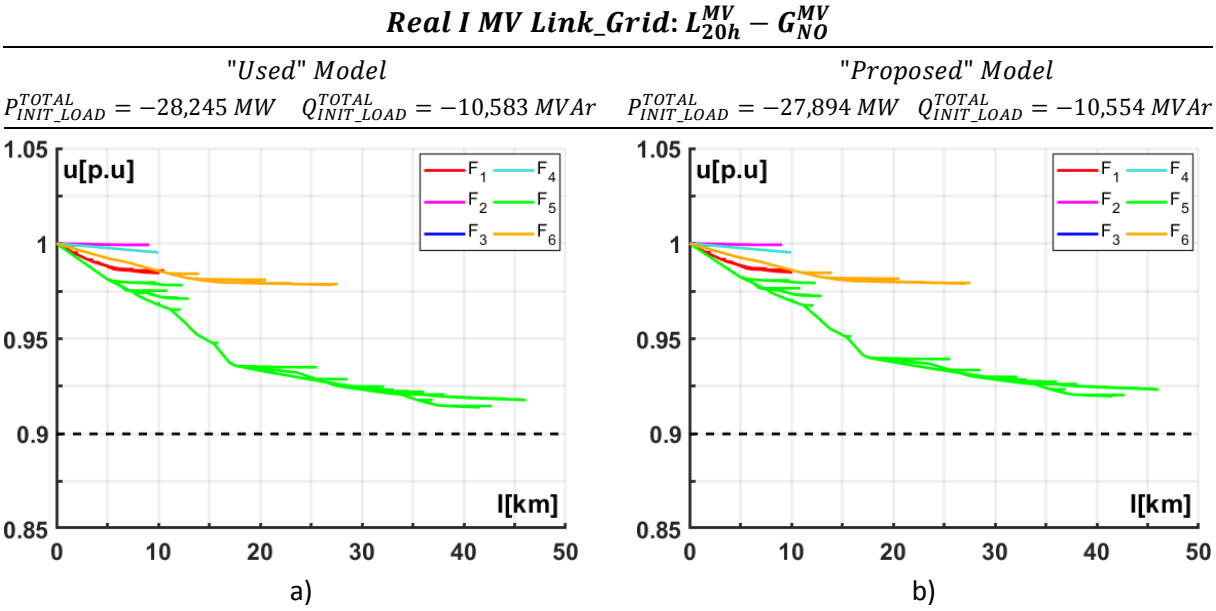

Figure 7.28 - Voltage profile of the Real I MV Link_Grid for $L_{20h}^{MV} - G_{NO}^{MV}$ scenario: a) used model and b) proposed model

Once again, the most visible differences in node-voltages can be seen in the Feeder 5. This deviation can be attributed to the different modelling of the LV Link_Grids that are connected to the Feeder 5. Namely, the "used" and the "proposed" models have slightly unequal demand of the active and reactive power, as it has already been shown in Subsection 7.2.3. Thus, in the grid where the "used" model was adopted, a bigger decrease of the node-voltage values within the Feeder 5 can be noticed. The nodes of the other feeders show fairly some discrepancy of their voltage values between two models.

7.3.4 Real II MV Link_Grid

For better understanding of the behaviour of the Real II MV Link_Grid, its simplified schematic overview is given in Figure 7.29 once again, whereby only the longest main-branch of each feeder is represented.

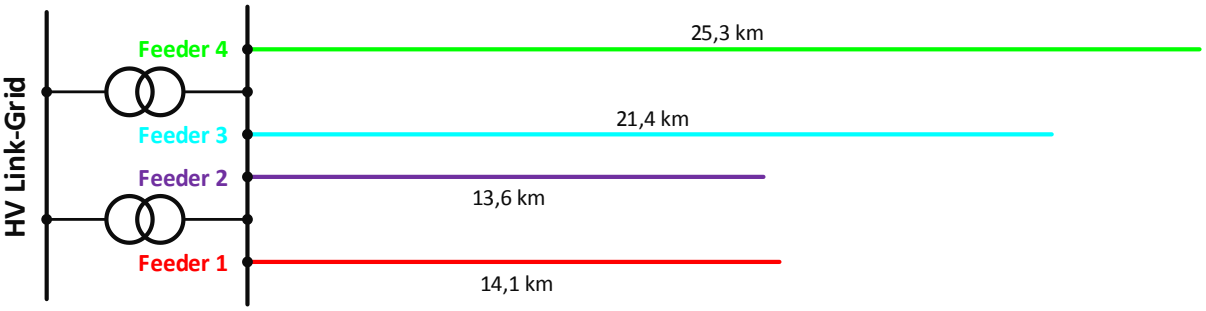

Figure 7.29 - Simplified overview of the Real II MV Link_Grid

From the power flow simulations in Real II MV Link_Grid, described in Section 6.1, values of the reactive power exchange Q_{EX} between the Real II MV and the HV Link_Grid were gathered for each load/production scenario and both modelling approaches of the connected LV Link_Grids. Dependency of the acquired Q_{EX}-values on the slack's voltage value is shown in Figure 7.30, where once again the green line represents the "used" model and the red one the "proposed" model. Based on the grid topology of the Real II MV Link_Grid, which was shown in Table 3.4, it is expected that the appearance of the Q_{EX}-curves from the figure below mostly comes from the related lumped Q-characteristics of the Small Urban and Rural LV Link_Grid, which were already discussed in Subsection 7.2.3. Especially for $L_{12h}^{MV} - G_{MAX}^{MV}$ scenario, Rural LV Link_Grid is of vital importance, since contrarily to Small Urban LV Link_Grid, the related PV inverters are provided with $Q(U)$-control. As already mentioned, exactly this causes that the Rural LV Link_Grid at 12h shows much bigger differences of its "used" and the "proposed" lumped Q-characteristic than the Small Urban LV Link_Grid. On account of that, large differences of Q_{EX}-characteristics from Figure 7.30a for $L_{12h}^{MV} - G_{MAX}^{MV}$ scenario are also existent. The "used" model-curve reaches its maximum value of 10,939 MVAr at $u_{MVG\_SLACK} = 1{,}038$, while the maximum value of 14,996 MVAr is recorded at $u_{MVG\_SLACK} = 1{,}148$ for the "proposed" model-curve.

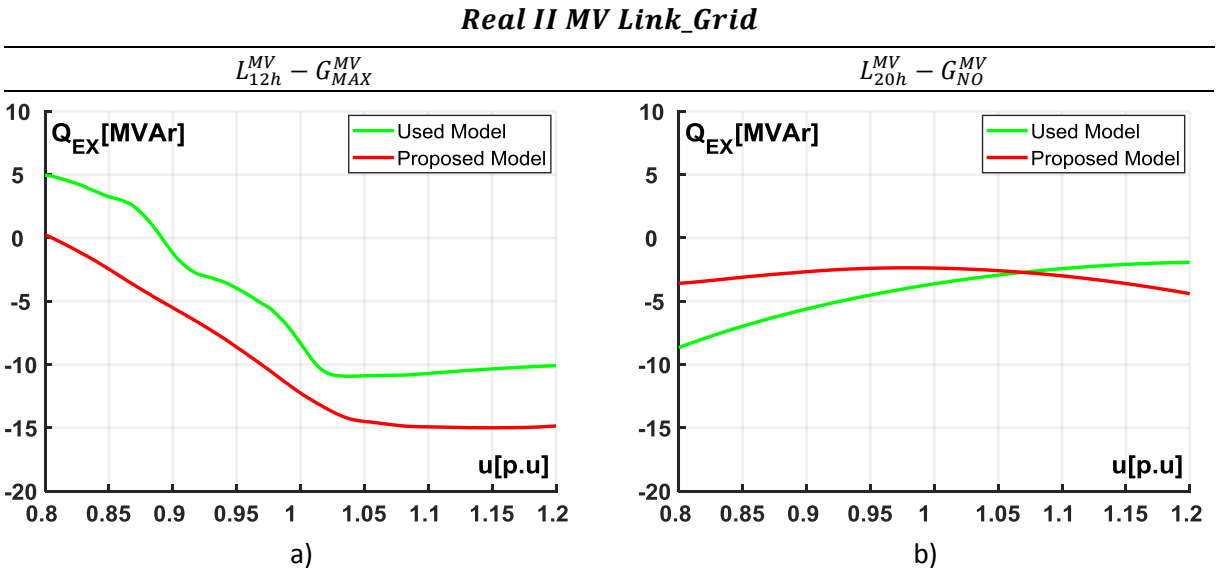

Figure 7.30 - Reactive power exchange between the Real II MV Link_Grid and the HV Link_Grid: a) $L_{12h}^{MV} - G_{MAX}^{MV}$ scenario and b) $L_{20h}^{MV} - G_{NO}^{MV}$ scenario

Comparing the Q_{EX}-characteristics from Figure 7.30b for $L_{20h}^{MV} - G_{NO}^{MV}$ scenario proves once again that the related differences are generally smaller than those for $L_{12h}^{MV} - G_{MAX}^{MV}$ scenario. Both curves have only negative values of Q_{EX}, since at 20h there is no electric power production at all, neither from directly connected large commercial CPs or from CPs that are connected to LV Link_Grids within the Real II MV Link_Grid. The "used" model- and the "proposed" model-curve reach their maximum value of 8,661 MVAr and 4,403 MVAr at $u_{MVG\_SLACK} = 0{,}8$ and $u_{MVG\_SLACK} = 1{,}2$, respectively.

The absolute difference of the related Q_{EX} -values between two modelling approaches of the connected LV Link_Grids is portrayed in Figure 7.31. Overall, bigger deviations can be seen in case of the $L_{12h}^{MV} - G_{MAX}^{MV}$ scenario. For this case, the maximal difference of 6,223 MVAr lies exactly at $u_{MVG\_SLACK} = 0{,}868$, while the minimal difference of 2,838 MVAr at $u_{MVG\_SLACK} = 1{,}02$. In subject to $L_{20h}^{MV} - G_{NO}^{MV}$ scenario, the biggest difference of 5,074 MVAr is recorded at $u_{MVG\_SLACK} = 0{,}8$. No difference of the related Q_{EX}-values can be seen at $u_{MVG\_SLACK} = 1{,}07$.

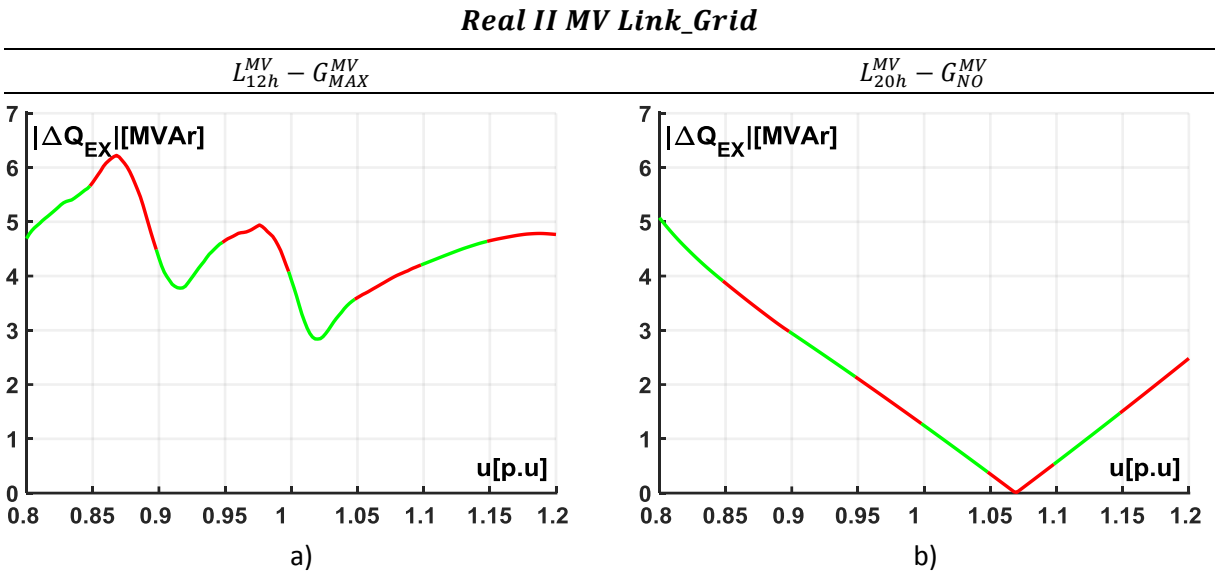

Figure 7.31 - Absolute difference of the Q_{EX}-values between the "used" and the proposed" model: a) $L_{12h}^{MV} - G_{MAX}^{MV}$ scenario and b) $L_{20h}^{MV} - G_{NO}^{MV}$ scenario

Table 7.14 sums up the most relevant simulations results of the Real II MV Link_Grid for both load/production scenarios, for which the slack voltage, i.e. the voltage at the secondary side of the supplying HV/MV transformer was set to the nominal voltage value. Additionally, distinction between the power flow simulations, in which two different LV Link_Grids' modelling approaches were used, has to be made. At a first glimpse it is recognisable that almost every parameter of $L_{12h}^{MV} - G_{MAX}^{MV}$ scenario for each model type is larger than the related parameter of $L_{20h}^{MV} - G_{NO}^{MV}$ scenario. This outcome was easily foreseen, since at 12h the production of all related CPs increases the active as well as the reactive power flow through the grid. Reactive power losses within the grid Q_{LOSSES}^{MVG} is the only parameter of $L_{12h}^{MV} - G_{MAX}^{MV}$ scenario which values were slightly smaller than those of $L_{20h}^{MV} - G_{NO}^{MV}$ scenario.

Table 7.14 - Simulation results of the Real II MV Link_Grid for both load/production scenarios

Scenario	*Model Type*	N_{VIOL}	P_{EX} [*MW*]	Q_{EX} [*MVAr*]	$P_{TOTAL}^{Lmpd\_LVG}$ [*MW*]	$Q_{TOTAL}^{Lmpd\_LVG}$ [*MVAr*]	$P_{TOTAL}^{CP\_MV}$ [*MW*]	$Q_{TOTAL}^{CP\_MV}$ [*MVAr*]	P_{LOSSES}^{MVG} [*MW*]	Q_{LOSSES}^{MVG} [*MVAr*]
L_{12h}^{MV}-G_{MAX}^{MV}	*used*	0	31,006	−8,321	32,194	−11,277	0,573	−0,209	−1,761	3,165
	proposed	16	34,128	−12,252	36,036	−14,716	0,572	−0,209	−2,479	2,674
L_{20h}^{MV}-G_{NO}^{MV}	*used*	0	−18,546	−3,626	−17,663	−6,869	−0,202	−0,099	−0,681	3,343
	proposed	0	−18,106	−2,382	−17,281	−5,689	−0,202	−0,099	−0,622	3,407

Voltage profiles of the Real II MV Link_Grid for $L_{12h}^{MV} - G_{MAX}^{MV}$ and $L_{20h}^{MV} - G_{NO}^{MV}$ scenario are shown in Figure 7.32 and Figure 7.33, respectively. They should assist in realizing how the differences in modelling of the connected LV Link_Grids impact the voltage values along the grid.

Based on the voltage profiles from the figure below and the grid topology from Table 3.4, the following can be concluded. As the feeder length gets higher, differences of the voltage values between the "used" and the "proposed" model are more obvious. The structure of each feeder in the grid plays a vital role as well. Therefore, feeders with the largest number of the Rural and Large Urban LV Link_Grids expose the biggest differences of the related voltage values. As already familiar, at 12h these two grids are showing the biggest discrepancy of the lumped *Q*-characteristic between two model types. The biggest differences between the voltage profiles from Figure 7.32a and Figure 7.32b

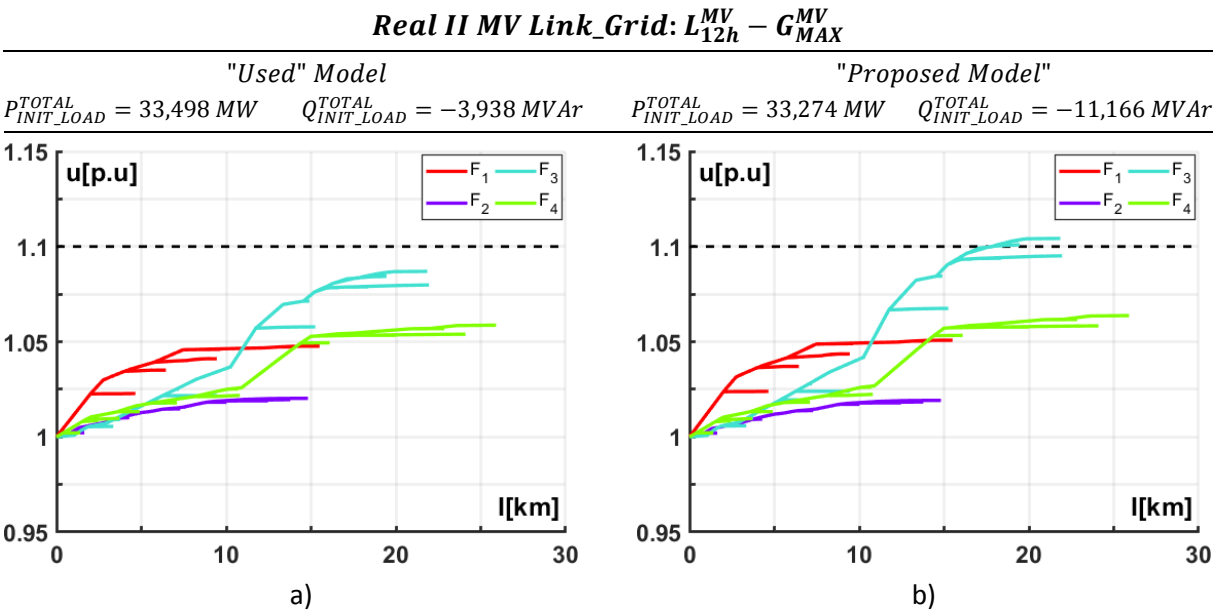

Figure 7.32 - Voltage profile of the Real II MV Link_Grid for $L_{12h}^{MV} - G_{MAX}^{MV}$ scenario: a) "used" model and b) "proposed" model

can be observed on the Feeder 3, which is linked with 18 Rural and 2 Large Urban LV Link_Grids. In the figure where the "proposed" model of the LV Link_Grids was adopted there are 16 nodes within the Feeder 3 that are violating the upper voltage limit. Contrarily to the "proposed" model, in case of the "used" model no violation of the upper limit was recorded, which is shown in Table 7.14 as well. Furthermore, by comparing the voltage profiles of Feeder 1 and Feeder 4, significant changes of the voltage values can easily be detected. On the other hand, different modelling of the LV Link_Grids within the Feeder 1 has hardly any impact on the corresponding voltage profiles of the Feeder 1.

Voltage profiles of the Real II MV Link_Grid for $L_{20h}^{MV} - G_{NO}^{MV}$ scenario, which are shown in Figure 7.33, don't uncover so obvious differences of the voltage values when two different lumped models of the LV Link_Grids are used. In neither of the models there is no violation of the lower voltage limit.

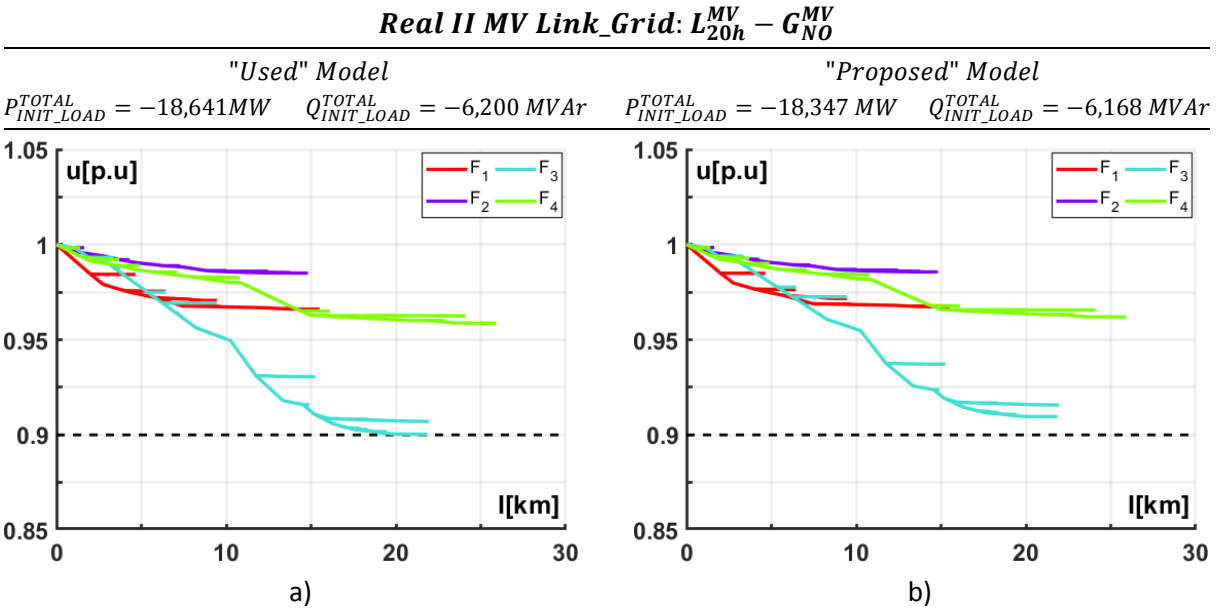

Figure 7.33 - Voltage profile of the Real II MV Link_Grid for $L_{20h}^{MV} - G_{NO}^{MV}$ scenario: a) "used" model and b) "proposed" model

Again, the most apparent differences can be seen on the Feeder 3. Once again, its topology is the reason for that. Compared to the other feeders in the Real II MV Link_Grid, Feeder 3 is loaded with the highest number of the LV Link_Grids. Therefore, the differences between the lumped “used” and “proposed” *Q*-characteristic of each connected LV Link_Grid, as already shown in Subsection 7.2.3, cause that the Feeder 3 displays the highest inequality between its voltage profiles from Figure 7.33a and Figure 7.33b, respectively. Voltage profiles of the Feeder 4 indicate some significant changes of the voltage values, while in case of the Feeder 1 and Feeder 3 there is hardly any difference between their “used” and the “proposed” voltage profiles.

8 Conclusion

The increasing penetration of distributed generation, especially one based on RES, will cause more challenges for nowadays and future grids. In order to study the impacts of these outcomes, different power flow simulations were performed in LV and MV distribution grids and various aspects regarding their behaviour were investigated. This chapter summarizes the most important conclusions, which are based on the aforementioned power flow simulations.

8.1 Impacts of *Q(U)*-controlled PV systems on the behaviour of LVGs and MVGs

A. LV Distribution Grids

Based on simulation results from [9], PV systems with uncontrolled inverters were installed in Industrial and Small Urban LV Link_Grid, while an adequate *Q(U)*-control was implemented in PV systems from Rural and Large Urban LV Link_Grid.

Simulation results of LV Link_Grids have shown that in time when the maximal output of related PVs is expected, the corresponding active grid losses are much higher than the ones when there is no production from PV systems. This is more evident in Rural and Large Urban LV Link_Grid than in Industrial and Small Urban LV Link_Grid, due to *Q(U)*-controlled inverters. They may unnecessarily inject or absorb reactive power even though the voltage level at PCC is within the allowed voltage limits. In this way the equipment loading increases even further, causing the active power losses to be higher. A drastic increase of reactive grid losses is also observable. All of this leads to an unavoidable increase of *Q*-exchange between the MV and LV Link_Grid. Above all, this is most noticeable in cases when the voltage at the primary side of the corresponding MV/LV distribution transformer significantly deviates from the nominal voltage value.

Another interesting finding was discovered by deeper examination of the voltage values in the grid. Namely, in case of the reverse power flow, the voltage at the nodes closer to the MV/LV distribution transformer is lower than the voltage at the end of the feeder. By using *Q(U)*-control as a concept of a local voltage regulation, not all PV systems contribute the same to the reactive power consumption that is required to keep the voltage under the statutory limits. Therefore, unfair treatment and discrimination among customers who use this type of control cannot be avoided. For example, customers at the end of the feeder need to absorb more reactive power than the customers who are located at the beginning of the feeder.

B. MV Distribution Grids

Through investigation of the simulation results for two different load/production scenarios of Real MV Link_Grids, which occur at 12h and 20h, the following can be concluded. Without taking into consideration different approaches in modelling of connected LVGs it is clear that at 12h, when the increased penetration of PV and relatively low load power demand is expected, the value of *Q*-exchange between the HV and MV Link_Grid increases drastically compared to the value of *Q*-exchange at 20h. The main reason is that each customer within the numerous connected Rural and Large Urban LV possess a PV system with a *Q(U)*-controlled inverter. That means that in case of overvoltage each of these customers would absorb not only the reactive power for their native load, rather the additional amount of reactive power as well, caused by the underexcited mode of the

inverter. To a small degree, *Q(U)*-controlled PV systems of large commercial customers that are directly connected to Real MV Link_Grids impact the value of *Q*-exchange as well. Furthermore, only in case of Real I MV Link_Grid, high reactive power demand of four directly connected customers influence the value of *Q*-exchange to a large degree.

On the other hand, at 20h when a relatively high load power demand and no PV production is expected, the *Q*-exchange between the Real I or Real II MV Link_Grid and the overlaid HV Link_Grid depends almost entirely on the total reactive power demand of all connected LVGs and directly connected customers on the MV level. Furthermore, it has been shown that the grid topology plays a vital role as well. For both Real MV Link_Grids and both specific load/production scenarios the reactive grid losses were capacitive, which causes a decrease of the *Q*-exchange value. This was more visible in Real I MV Link_Grid where a high cable share of almost 75% is present.

In concern with the simulation results of *P*-exchange between the Real MV Link_Grids and the overlaid HV Link_Grid, change in active power flow direction is apparent. As anticipated, during high infeed of all corresponding PV systems at 12h and relatively low load power demand, the active power flows from the Real MV Link_Grid to the overlaid HV Link_Grid. If this situation is not handled properly, this can cause some challenges to TSO as well. Contrarily, simulation results at 20h revealed that the active power flows toward the Real MV Link_Grid. This power is then further distributed to MV/LV transformers of all related LVGs and to directly connected MV customers. Regarding the active grid losses, as in case of LV Link_Grids, bigger active grid losses were present at 12h then at 20h. This can be explained with the fact that an increased power flow at 12h across the grid leads to an increase of the lines' loading, which causes the active grid losses to be higher as well.

8.2 Impacts of different lumped models of LVGs on the behaviour of MVGs

Another main goal of this thesis was to investigate the behaviour of MV Link_Grids when different lumped modelling of LV Link_Grids is taken into consideration. During the thesis the "used" and the "proposed" models of LV Link_Grids were given. As already seen, the biggest difference in modelling is noticed in the lumped *Q*-characteristic of a LV Link_Grid, especially at the "12h" load/production scenario.

A. Theoretical MV Link_Grids

Purpose of both Theoretical MV Link_Grids that were created during this thesis was the assessment of grid impacts which are caused by the differences in modelling of LV Link_Grids. The emphasis was given to situations where the length and type of a single feeder was varied. The corresponding simulation results and voltage profiles revealed the following.

As the feeder length increases, the differences of voltage profiles between two models are more obvious. The biggest differences were recorded in case when the overhead-line feeder for the "12h" load/production scenario was used. Due to its electrical parameters, the overhead-line feeder is more sensitive to the increased power flow than the cable feeder. In regard to the simulation results, the outcome is the same. The largest differences of *Q*-exchange and active grid losses between two models were present at the aforementioned situation. Another interesting fact was noticed in both load/production scenarios when the cable feeder was used. If the length of the feeder is great enough, the capacitance of the cable feeder generates so much reactive power, that the reactive power flows from a Theoretical MV Link_Grid to the overlaid HV Link_Grid.

B. Real MV Link_Grids

Next to the Theoretical MV Link_Grids, two Real MV Link_Grids, which are based on the existing Austrian MV distribution grid, were also used in the course of this thesis. Once again, impacts of different modelling were investigated by taking into consideration two extreme load/production scenarios and the corresponding simulation results.

Regarding the lumped load *P*- and *Q*-characteristic of each used LV Link_Grid when two different modelling approaches are used, the biggest differences between two models are detected in the grids which customers own a PV system with a *Q(U)*-controlled inverter. Primarily, the "12h" load/production scenario reveals bigger differences between two models than the "20h" load/production scenarios. Especially in concern with the related *Q*-characteristics, these two modelling approaches cause that the biggest differences are detected when the voltage at the primary side of the related MV/LV distribution transformer significantly differ from the nominal voltage.

Observing the related voltage profiles it can be concluded that the differences of voltage profiles between the "used" and the "proposed" model are more apparent in case of high PV penetration at 12h than in case of no PV production at 20h. In both Real MV Link_Grids the most noticeable differences were observed at the longest feeders, especially at the ones which were linked with the numerous Rural and Large Urban LV Link_Grids. Those two are the only grids which customers have a PV system with a *Q(U)*-controlled inverter. All of these customers are responsible that the most distinct differences are observed at exactly those feeders. Contrarily to the ones for the "20h" load/production scenario, the voltage profiles of the longest feeder for the "12h" load/production scenario have shown that in some cases the upper operational voltage limit was violated. Generally, more violations were noticed in the voltage profiles of the "proposed" model. Once again this can be attributed mostly to the connected LV Link_Grids and their differences of the lumped load *Q*-characteristic between two modelling approaches.

References

[1] E. Comission, “2030 Climate and Energy Framework,” [Online]. Available: https://ec.europa.eu/clima/policies/strategies/2030_en. [Accessed 18 February 2019].

[2] M. Scheepers, M. van Werven, J. Mutale and G. Strbac, “Distributed Generation in Electricity Markets, its impact on Distribution System Operators, and the role of Regulatory and Commercial Arrangements,” in *10th Kasseler Symposium Energy Systems Technology*, 2005.

[3] J. Lopes, N. Hatziargyriou, J. Mutale, P. Djapic and N. Jenkins, “Integrating distributed generation into electric power systems: A review of drivers, challenges and opportunities.,” *Electric Power Systems Research,* vol. 77, no. IX, pp. 1189-1203, July 2007.

[4] J. Machowski, J. W. Bialek and J. R. Bumby, Power system dynamics: stability and control, 2nd ed., John Wiley & Sons, 2008.

[5] A. Monti and F. Ponci, “Electric Power Systems,” in *Intelligent Monitoring, Control, and Security of Critical Infrastructure Systems*, E. Kyriakides and M. Polycarpou, Eds., Berlin, Springer, 2015, pp. 31-65.

[6] J. J. Burke, Power Distribution Engineering : Fundamentals and Applications, New York: Marcel Dekker, Inc, 1994.

[7] D. L. Schultis, “Volt/var behaviour of low voltage Grid-Link in European grid type,” Vienna, 2017.

[8] S. W. Fardo and D. R. Patrick, Electrical Power Systems Technology, 3rd ed., The Fairmont Press, 2009.

[9] W. Gawlik, Energieübertragung und Hochspannungstechnik, ESEA - TU Wien, 2016.

[10] P. Schavemaker and L. van der Sluis, Electrical Power System Essentials, Delft: John Wiley & Sons, 2008.

[11] B. Owens, “The rise of distributed power,” General Electric, 2014.

[12] J. Jonnes, Empires of Light: Edison, Tesla, Westinghouse, and the Race to Electrify the World, Random House Trade Paperbacks, 2004, p. 54–60.

[13] T. Fogarty and R. Lamb, Investing in the renewable power market: How to profit from energy transformation, Hoboken, New Jersey: John Wiley & Sons, 2012.

[14] D. Elzinga, “Electricity System Development : A Focus on Smart Grdis,” United Nations Economic Commission for Europe, 2015.

[15] F. A. Viawan, “Voltage Control and Voltage Stability of Power Distribution Systems in the Presence of Distributed Generation,” Götebor, 2008.

[16] A. Ilo and W. Gawlik, “The Way from Traditional to Smart Power Systems,” Vienna, 2015.

[17] P. Jakovac, “Electricity directives and evolution of the EU internal electricity market,” Rijeka, Croatia, 2011.

[18] “ENTSO-E,” [Online]. Available: https://www.entsoe.eu/.

[19] B. Rajal and N. Zafoschnig, “Electricity Regulation: Austria,” November 2017. [Online]. Available: https://gettingthedealthrough.com/area/12/jurisdiction/25/electricity-regulation-austria/. [Accessed 08 11 2018].

[20] E-Control Austria, “Statistikbroschüre 2018,” [Online]. [Accessed 08 11 2018].

[21] APG, “APG - News&Press,” 17 10 2010. [Online]. Available: https://www.apg.at/de/news/aktuelles/2010/10/18/TIWAG. [Accessed 14 08 2018].

[22] VUEN, “Transmission Network - Control Area,” [Online]. Available: http://www.vuen.at/en/html/uebertragungsnetz_regelzone.html. [Accessed 14 08 2018].

[23] APG, “Network Development Plan 2017,” 2017. [Online]. Available: https://www.apg.at/en/netz/netzausbau/Netzentwicklungsplan. [Accessed 16 08 2018].

[24] M. M. Roggenkamp and F. Boisseleau, The Regulation of Power Exchanges in Europe, Intersentia NV, 2005.

[25] CIGRE, “The Electric Power System - Austria,” 5 10 2015. [Online]. Available: http://www.cigre.org/var/cigre/storage/original/application/e9e3d71bb4c216212f478ce41b80 [Accessed 16 08 2018].

[26] Österreichs E-Wirtschaft, “Oesterreichsenergie,” [Online]. Available: https://oesterreichsenergie.at/home.html. [Accessed 09 11 2018].

[27] “Powersys-Link,” [Online]. Available: https://www.powersys-link.com. [Accessed 14. March 2018].

[28] A. Ilo, "LINK - The smart grid paradigm for a secure decentralized operation architecture," *Electric Power Systems Research 131,* p. 116–125, 2016.

[29] A. Ilo, “Demand Response Process in Context of the Unified LINK-Based Architecture,” in *Eco-designin in Electrical Engineering: Eco-friendly Methodologies, Solutions and Example for Application to Electrical Engineering*, J. Bessède, Ed., Châteauvilain: Springer, 2018, pp. 75-83.

[30] U. S. E. P. Agency, “Distributed Generation of Electricity and its Environmental Impacts,” [Online]. Available: https://www.epa.gov/energy/distributed-generation-electricity-and-its-environmental-impacts. [Accessed 31 July 2018].

[31] International Energy Agency , Distributed Generation in Liberalised Electricity Markets, 2002.

[32] B. Ajaykumar and D. Sarkar, Eds., in *Advanced Engineering Research and Applicationsitors*, RIP, 2017, pp. 269-285.

[33] G. B. Gharehpetian and S. M. Mousavi Agah, Distributed Generation Systems: Design, Operation and Grid Integration, 1st ed., 2017, p. 588.

[34] M. Reza, “Stability analysis of transmission systems with high penetration of distributed generation,” Delft, 2006.

[35] A. Ilo, “Effects of the Reactive Power Injection on the Grid—The Rise of the Volt/var Interaction Chain,” *Smart Grid and Renewable Energy,* no. 7, pp. 217-232, 2016.

[36] CENELEC, “EN 50160: Voltage characteristics of electricity supplied by public distribution networks,” Brussels, 2010.

[37] F. Provoost, “Intelligent Distribution Network Design,” Eindhoven, 2009.

[38] J. Hiscock, N. Hiscock and A. Kennedy, “Advanced Voltage Control for Networks with Distributed Generation,” in *19th International Conference on Electricity Distribution*, Vienna, 2007.

[39] M. Kolenc, I. Papic and B. Blazic, “Coordinated reactive power control to ensure fairness in active distribution grids,” in *IEEE 8th International Conference on Compatibility and Power Electronics*, Ljubljana, 2013.

[40] E-Control, “Technische und organisatorische Regeln für Betreiber und Benutzer von Netzen; Hauptabschnitt D4: Parallelbetrieb von Erzeugungsanlagen mit Verteilernetzen,” Vienna, 2016.

[41] M. Rossi, G. Viganò, D. Moneta, C. Daniele and C. Claudio, “Analysis of active power curtailment strategies for renewable distributed generation,” in *2016 AEIT International Annual Conference (AEIT)*, 2016.

[42] H. Ghoreishi, H. Afrakhte and M. Jabbari ghadi, “Optimal placement of tie points and sectionalizers in radial distribution network in presence of DGs considering load significance,” in *Smart Grid Conference*, Tehran, 2013 .

[43] [Online]. Available: http://www.thehindu.com/features/kids/Importance-of-electricity/article16544961.ece. [Accessed 16. March 2018].

[44] CIGRE Working Group C4.605 , “Modelling and Aggregation of Loads in Flexible Power Networks,” 2014.

[45] A. Bokhari, “Experimental Determination of the ZIP Coefficients for Modern Residential, Commercial, and Industrial Loads,” *Transactions on Power Delivery,* vol. 29, no. 3, pp. 1372-1381, 2014.

[46] E. Union, “Eur-Lex,” [Online]. Available: https://eur-lex.europa.eu/homepage.html.

[47] A. Howlader , N. Urasaki, A. Yona, T. Senjyu and A. Saber, “A review of output power smoothing methods for wind energy conversion systems,” *Renewable and Sustainable Energy Reviews,* vol. 26, pp. 135-146, 2013.

[48] Electric Power Research Institute , “Report to NIST on the Smart Grid Interoperability,” 2009.

[49] T. Funabashi, Integration of Distributed Energy Resources in Power Systems, 2016.

[50] R. A. A. de Graaf, “Flexible distribution systems through the application of multi back-to-back converters: Concept, implementation and experimental verification,” Eindhoven, 2010.

[51] E-Control, “Key Statistics 2017,” Vienna, 2017.

[52] E. P. I. Association, “Connecting the Sun - Solar photovoltaics on the road to large-scale grid inegration,” 2012.

[53] N. Rugthaicharoencheep and S. Auchariyamet, “Technical and Economic Impacts of Distributed Generation on Distribution System,” *World Academy of Science, Engineering and Technology International Journal of Electrical and Computer Engineering,* vol. 6, no. 4, 2012.

[54] N. Jenkins, J. Ekanayake and G. Strbac, in *Distributed Generation*, 2010, pp. 15-16.

[55] J. Svensson, “Active Distributed Power Systems Functional Structures for Real-Time Operation of Sustainable Energy Systems,” Department of Industrial Electrical Engineering and Automation, Lund Institute of Technology, 2006.

List of Figures

List of Tables

Appendix A LV and MV Link_Grids' Models

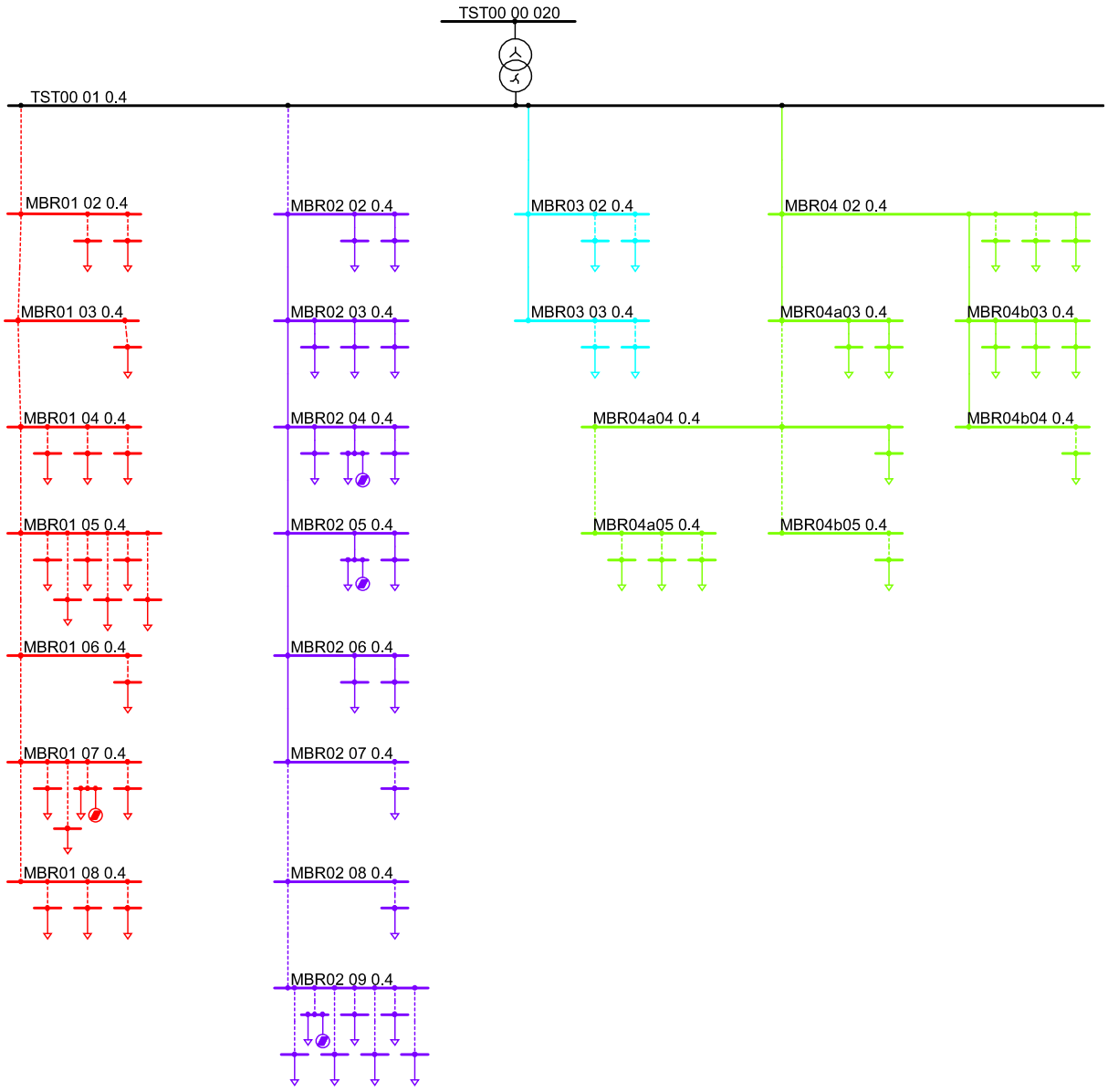

Figure A.1 - Rural LV Link_Grid

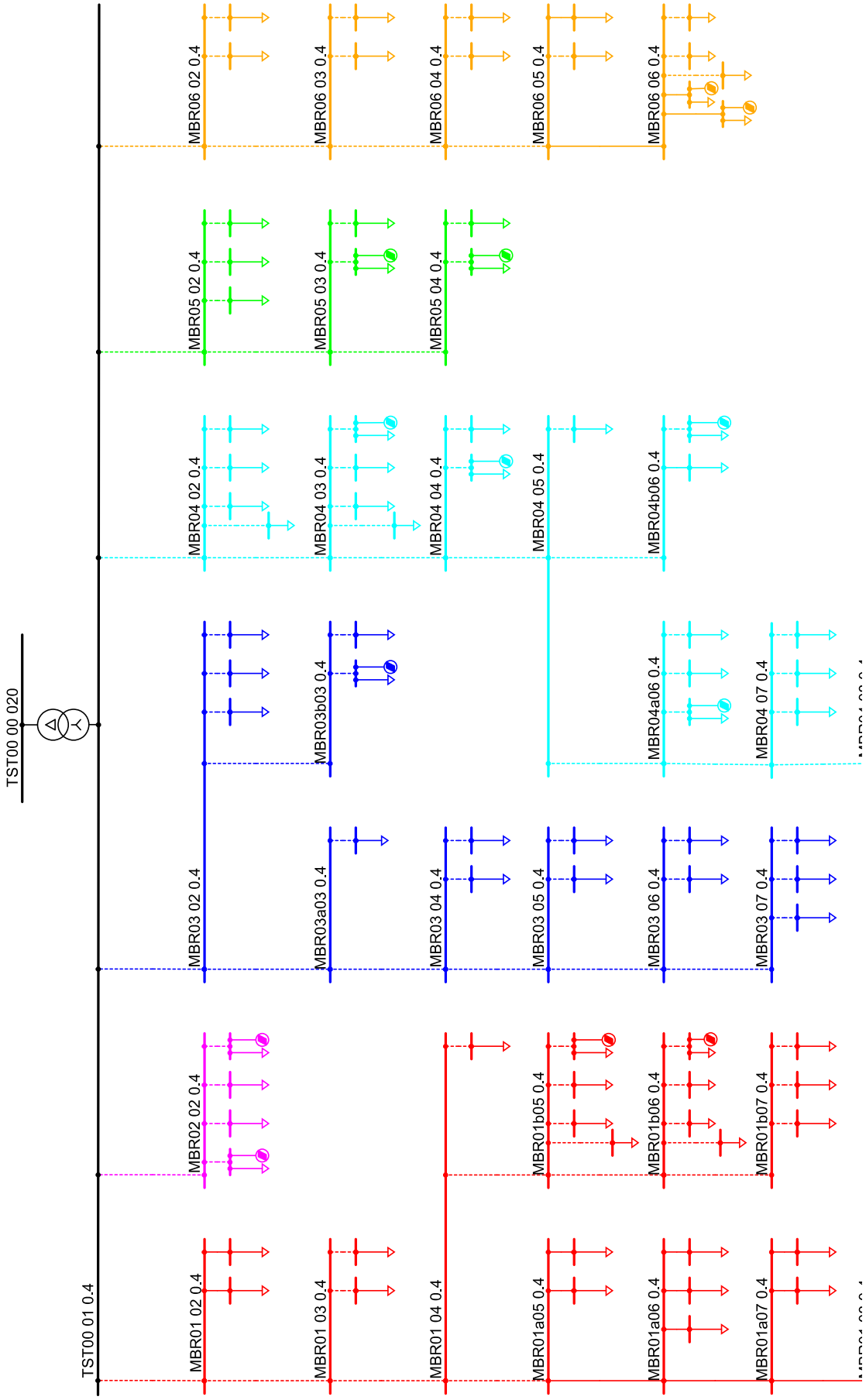

Figure A.2 - Small Urban LV Link_Grid

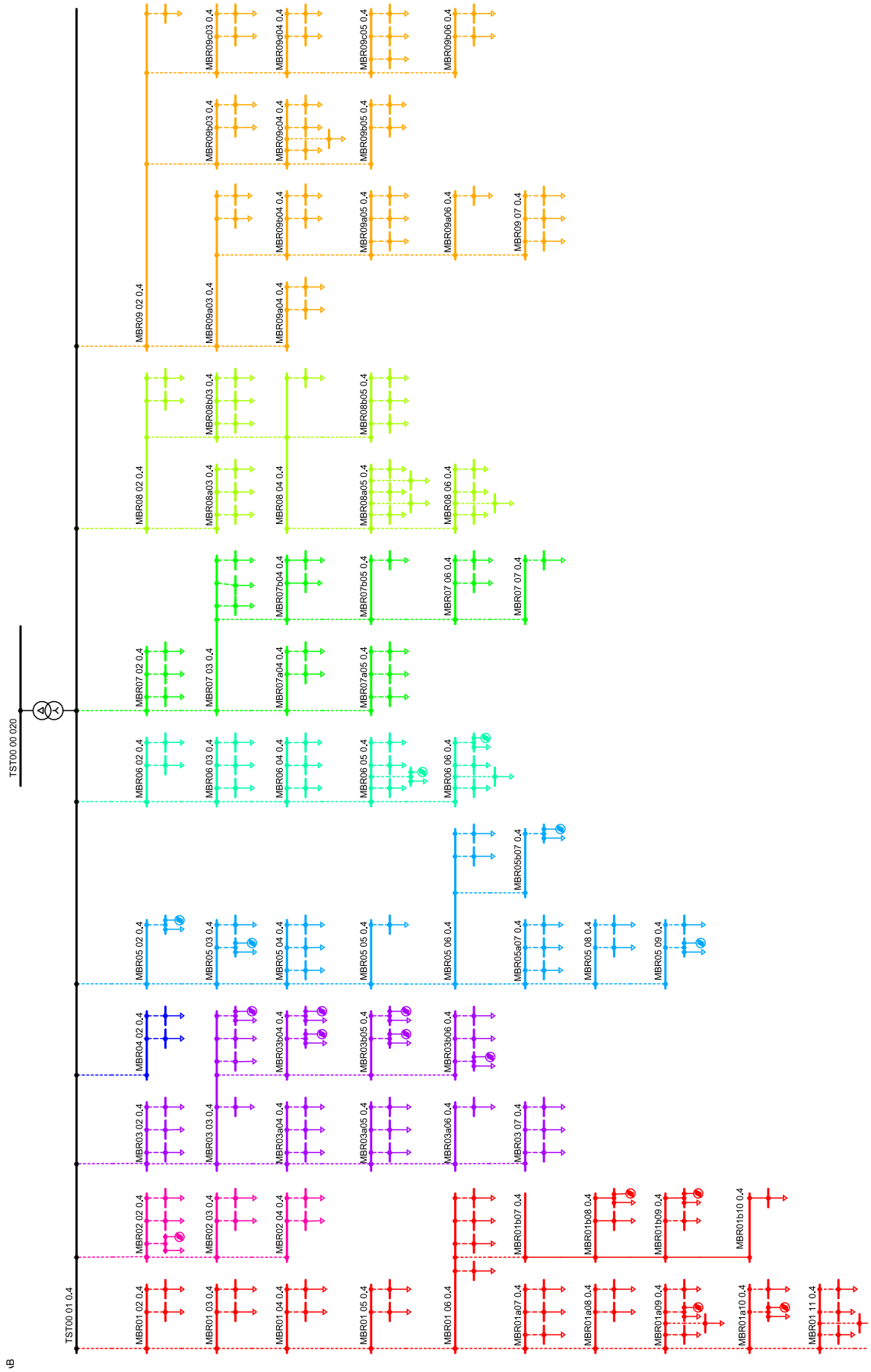

Figure A.3 - Large Urban LV Link_Grid

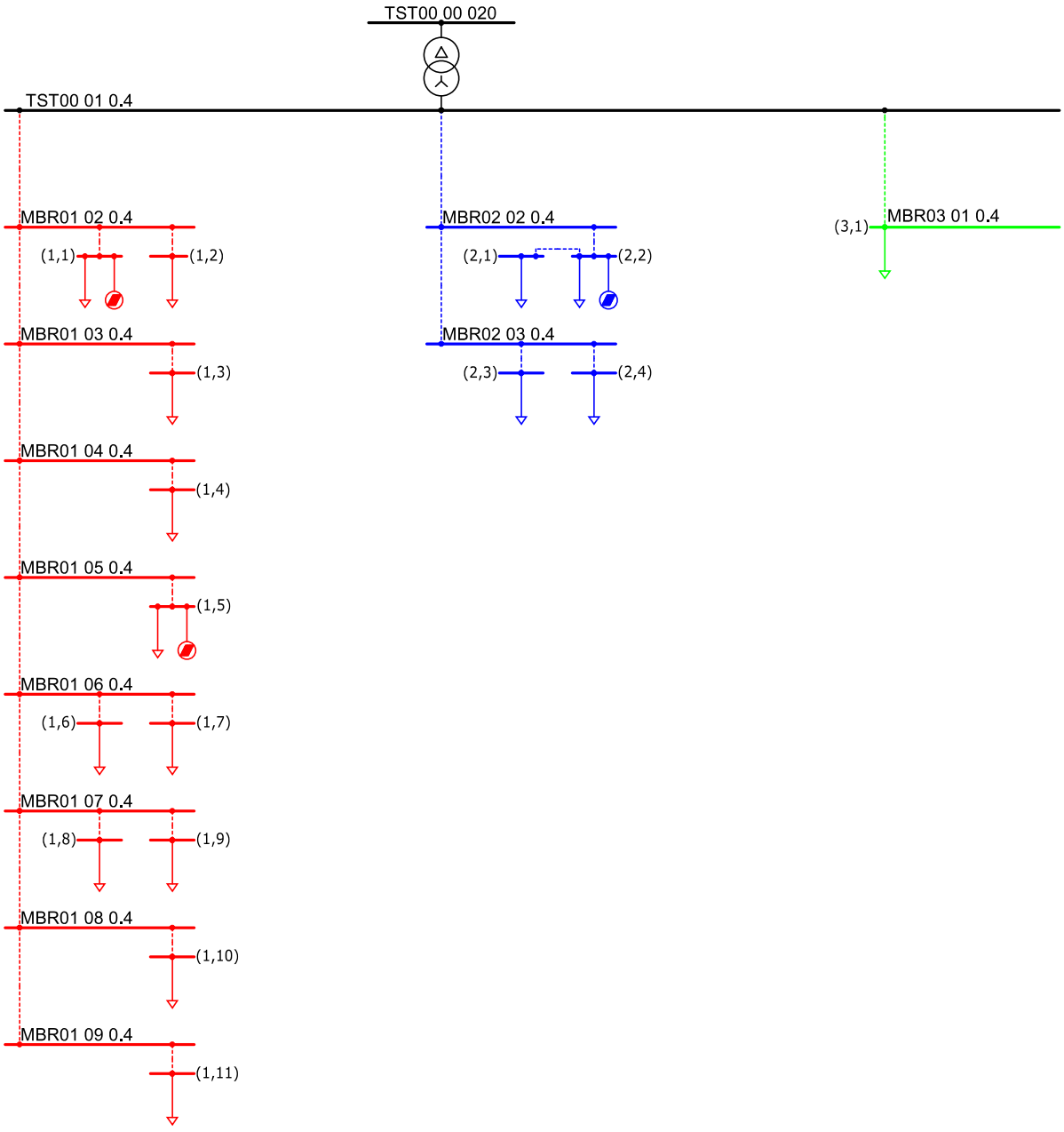

Figure A.4 - Industrial LV Link_Grid

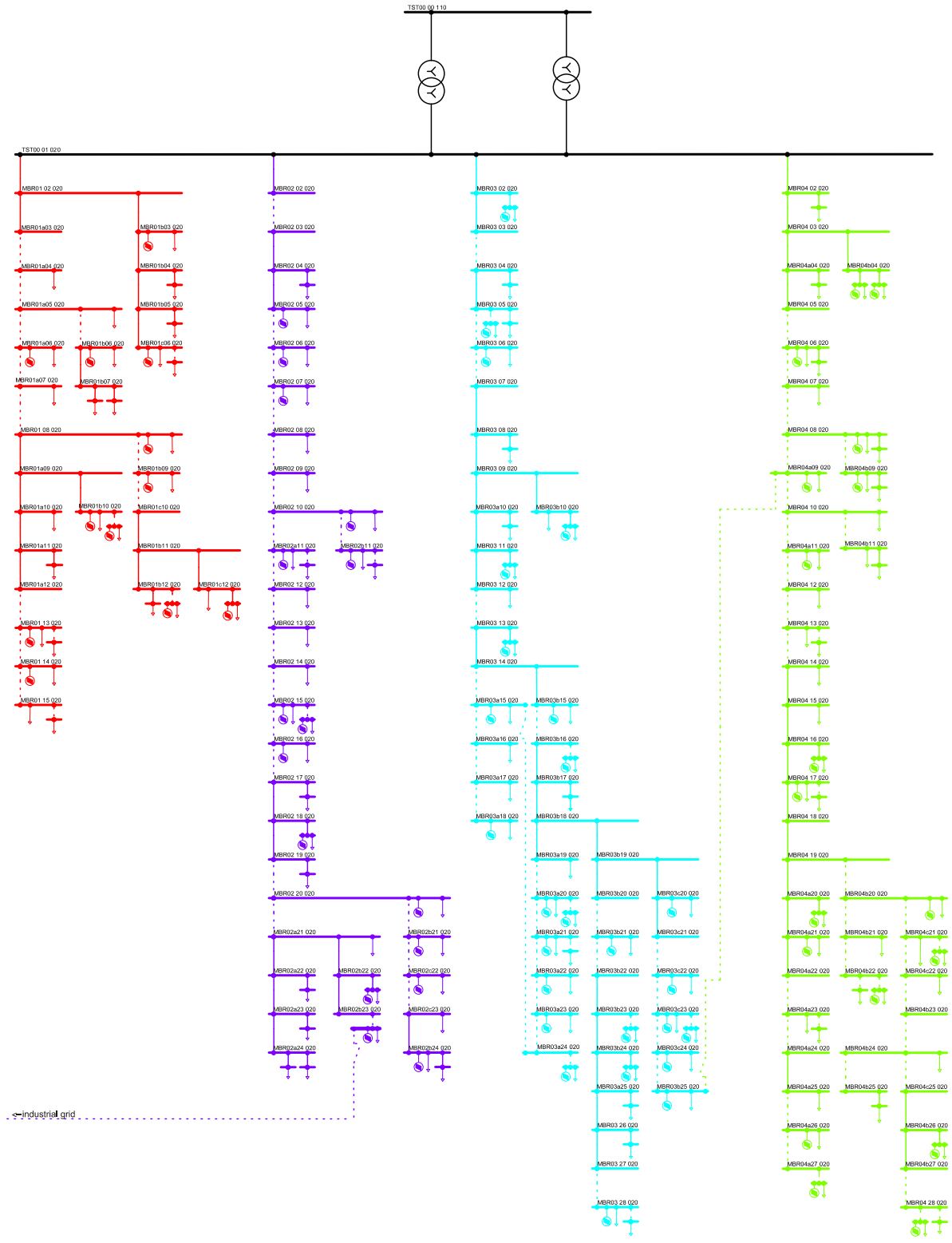

Figure A.5 - Real II MV Link_Grid

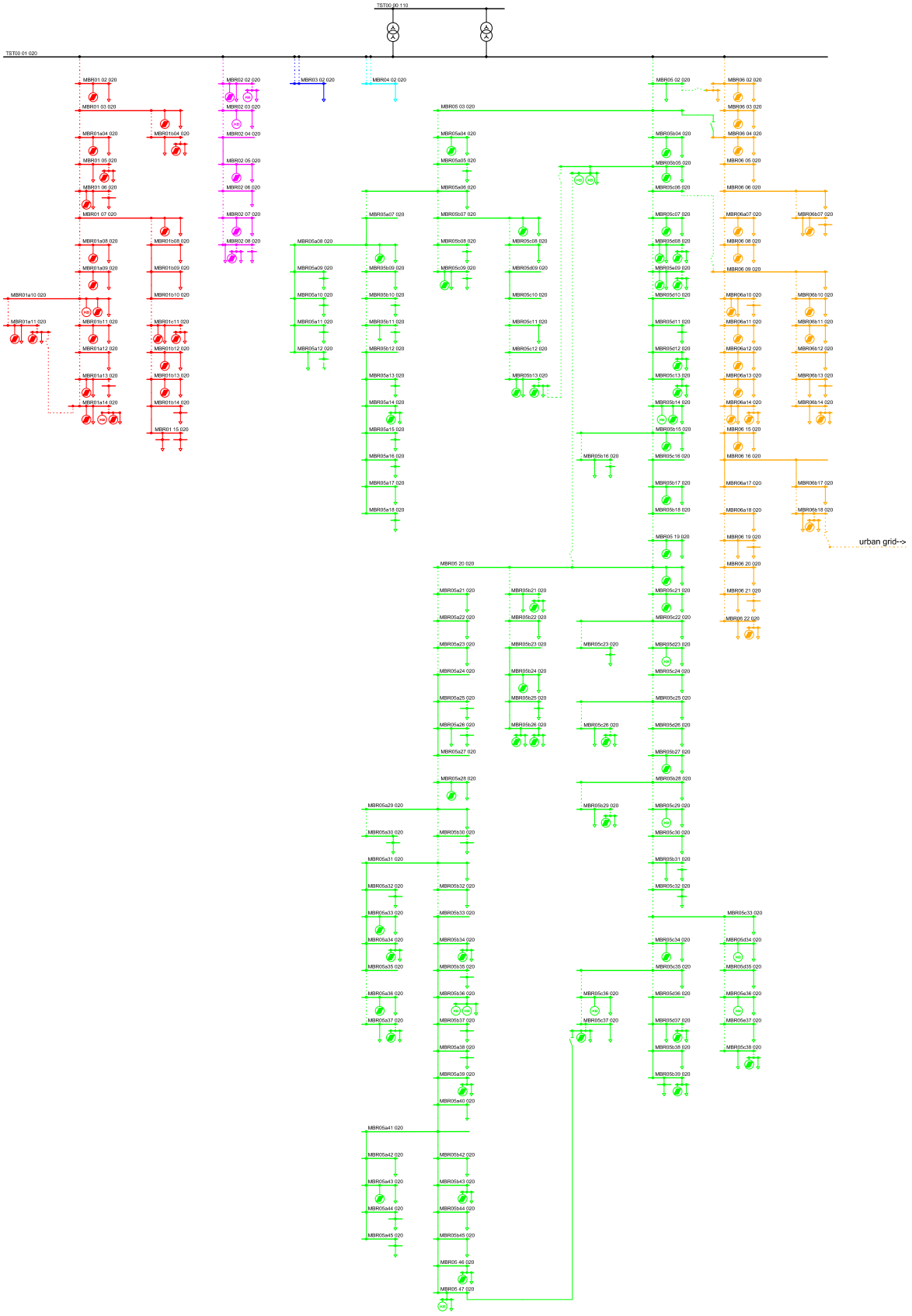

Figure A.6 - Real I MV Link_Grid

Table A.1 - Overview of the LVG lines' parameters

type	*shortcut*	A $[mm^2]$	I_{th} $[A]$	R'_π $[\Omega/km]$	X'_π $[\Omega/km]$	C'_π $[nF/km]$	G'_π $[\Omega/km]$
LV cable		25	100	1.2	0.089	550	0
LV cable		50	145	0.641	0.085	720	0
LV cable	*C-AL*	95	215	0.32	0.082	950	0
LV cable		150	275	0.206	0.08	1040	0
LV cable		240	360	0.125	0.08	1200	0
LV cable		16	100	1.15	0.089	500	0
LV cable	*C-CU*	25	130	0.727	0.088	550	0
LV cable		35	155	0.524	0.085	630	0
LV overhead line	*OL-AL*	50	210	0.6152	0.3764	0	0
LV overhead line		95	320	0.3264	0.3557	0	0

Table A.2 - Overview of the MVG lines' parameters

type	*shortcut*	I_{th} $[A]$	R'_π $[\Omega/km]$	X'_π $[\Omega/km]$	C'_π $[nF/km]$	G'_π $[\Omega/km]$
MV cable	*C-AL*-50	173	0,641	0,146084	175	0
MV cable	*C-AL*-95	252	0,32	0,131633	216	0
MV cable	*C-AL*-150	320	0,206	0,122208	254	0
MV cable	*C-AL*-240	419	0,125	0,113415	304	0
MV cable	*C-AL*-400	537	0,0778	0,10524	368	0
MV cable	*C-AL*-500	766	0,0776	0,102416	402	0
MV cable	*C*-3*x*35	145	0,524	0,124	240	0
MV overhead line	*OL*-25/4	140	1,2028	0,376	9,6	0
MV overhead line	*OL*-35/6	170	0,8353	0,376	9,6	0
MV overhead line	*OL*-50/8	210	0,5946	0,376	9,6	0
MV overhead line	*OL*-70	255	0,507	0,376	9,6	0
MV overhead line	*OL*-95	350	0,358	0,376	9,6	0

Small Urban LV Link-Grid: $L_{12h}^{LV} - G_{MAX}^{LV}$

$P_{USED\_IN}^{Lmpd\_LVG} = 326{,}512\ kW$ $P_{PROP\_IN}^{Lmpd\_LVG} = 323{,}774\ kW$ $Q_{USED\_IN}^{Lmpd\_LVG} = -42{,}232\ kVAr$ $Q_{PROP\_IN}^{Lmpd\_LVG} = -53.949\ kVAr$

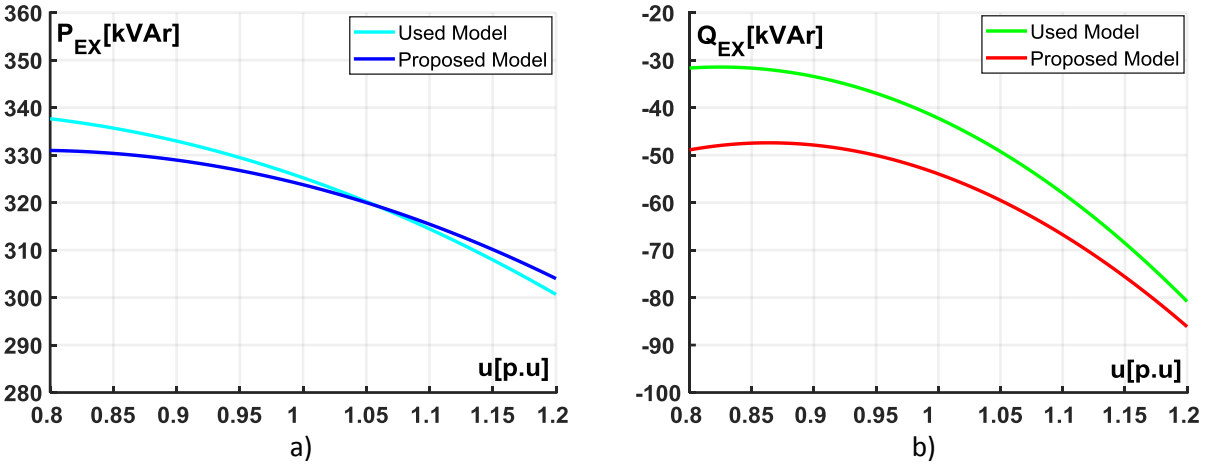

Figure A.7 - Lumped load characteristic of the Small Urban LV Link_Grid for $L_{12h}^{LV} - G_{MAX}^{LV}$ scenario: a) active power and b) reactive power

Small Urban LV Link-Grid: $L_{20h}^{LV} - G_{NO}^{LV}$

$P_{USED\_IN}^{Lmpd\_LVG} = -244{,}151\ kW$ $P_{PROP\_IN}^{Lmpd\_LVG} = -241{,}475\ kW$ $Q_{USED\_IN}^{Lmpd\_LVG} = -80{,}248\ kVAr$ $Q_{PROP\_IN}^{Lmpd\_LVG} = -79{,}659\ kVAr$

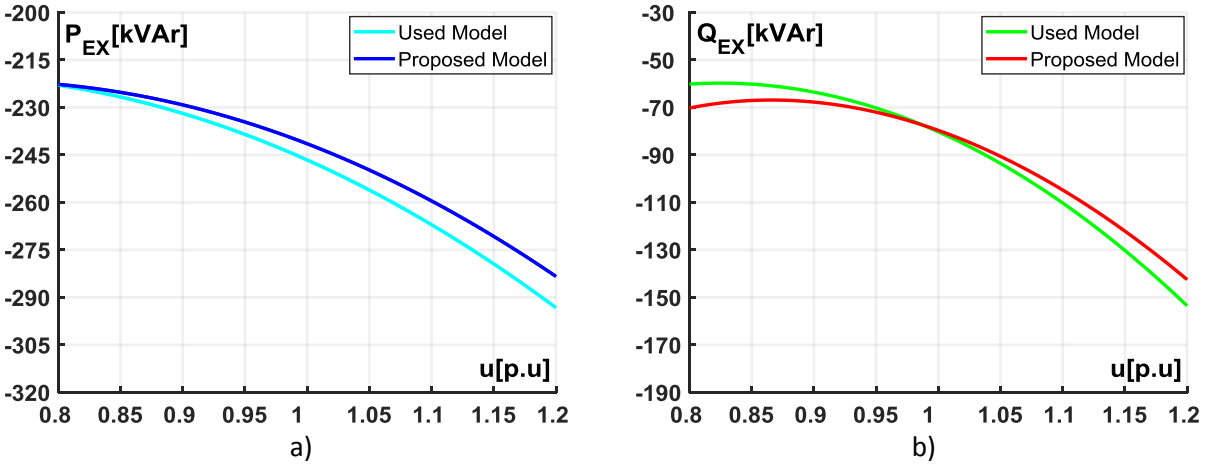

Figure A.8 - Lumped load characteristic of the Small Urban LV Link_Grid for $L_{20h}^{LV} - G_{NO}^{LV}$ scenario: a) active power and b) reactive power

Industrial LV Link-Grid: $L_{12h}^{LV} - G_{MAX}^{LV}$

$P_{USED\_IN}^{Lmpd\_LVG} = 455{,}076\ kW$ $P_{PROP\_IN}^{Lmpd\_LVG} = 456{,}733\ kW$ $Q_{USED\_IN}^{Lmpd\_LVG} = -193{,}13\ kVAr$ $Q_{PROP\_IN}^{Lmpd\_LVG} = -201{,}36\ kVAr$

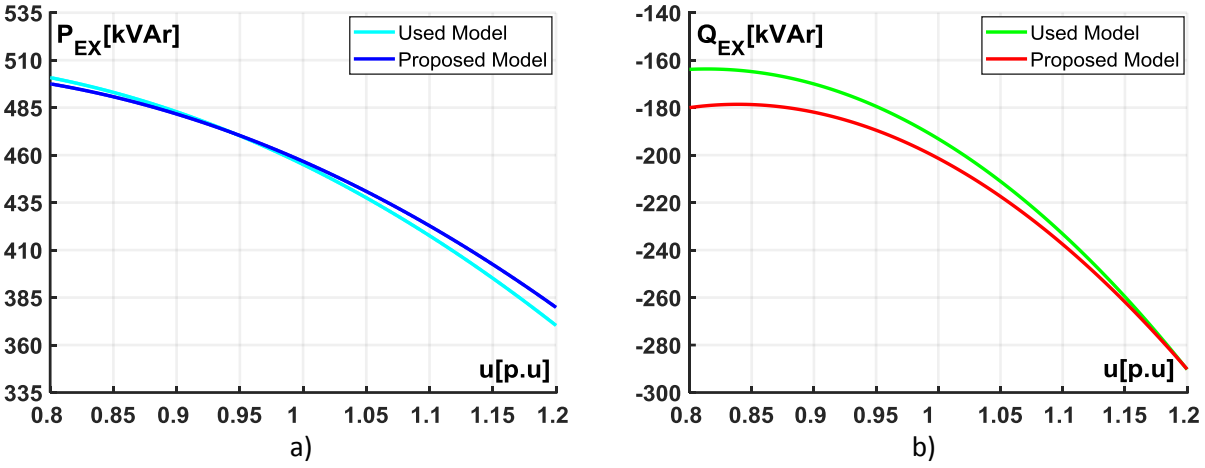

Figure A.9 - Lumped load characteristic of the Industrial LV Link_Grid for $L_{12h}^{LV} - G_{MAX}^{LV}$ scenario: a) active power and b) reactive power

Industrial LV Link-Grid: $L_{20h}^{LV} - G_{NO}^{LV}$

$P_{USED\_IN}^{Lmpd\_LVG} = -261{,}643\ kW$ $P_{PROP\_IN}^{Lmpd\_LVG} = -254{,}712\ kW$ $Q_{USED\_IN}^{Lmpd\_LVG} = -124{,}21\ kVAr$ $Q_{PROP\_IN}^{Lmpd\_LVG} = -118{,}24\ kVAr$

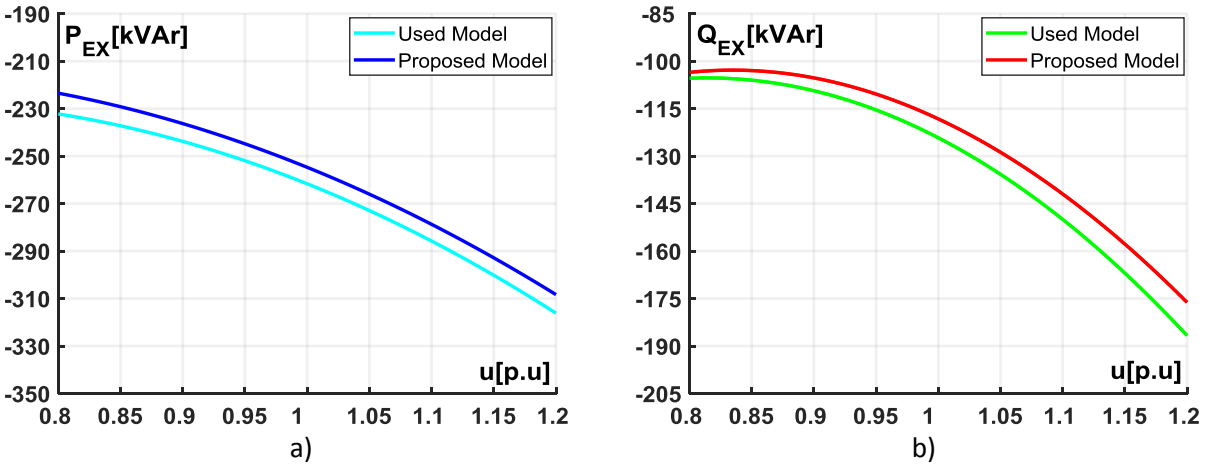

Figure A.10 - Lumped load characteristic of the Industrial LV Link_Grid for $L_{20h}^{LV} - G_{NO}^{LV}$ scenario: a) active power and b) reactive power

Appendix B Assigning of Customer Plants and LV Link_Grids to nodes in MV Link_Grids

As a base, the connected loads in MV Link_Grids were initially modelled as loads with constant active power consumption without any voltage dependence. The consumption of each load correlated to its estimated peak demand value in 2016, which were acquired from the "Institute of Energy Systems and Electrical Drives". The flowchart from Figure B.1 describes exactly how the assigning process is carried out for any load in both Real MV Link_Grids that were created during this thesis. When a load is selected, its value of active power consumption P_{LOAD}^{MV} is compared to the value of maximum active power consumption of large commercial CP $P_{LC}^{CP\_MV}$, Rural LVG P_{RUR}^{LVG}, Small Urban LVG P_{SU}^{LVG}, Large Urban LVG P_{LU}^{LVG} and Industrial LVG P_{IND}^{LVG}. Active power consumption for each type, excluding the one for an industrial CP, can be found in Table B.1**.** In case of MV industrial CPs, who are the largest power consumers, the only condition is that P_{LOAD}^{MV} is greater than the largest value from Table B.1**,** which is P_{IND}^{LVG}.

Table B.1 - Maximum active power consumption of different MV load types

$P_{LC}^{CP\_MV}$ [kW]	P_{RUR}^{LVG} [kW]	P_{SU}^{LVG} [kW]	P_{LU}^{LVG} [kW]	P_{IND}^{LVG} [kW]
25	85	242	349	455

As a reference value for large commercial CPs in MV Link_Grids, $P_{LC}^{CP\_MV} = 25\ kW$ has been chosen. The peak active power data of each LV Link_Grid for year 2016, which were gathered from the "Institute of Energy Systems and Electrical Drives", have been used for the maximum active power consumption of each LV Link_Grid. By performing the assigning process for every connected load, an exact number of connected CPs and LVGs in both Real MV Link_Grids has been determined, which is shown in Table 3.4.

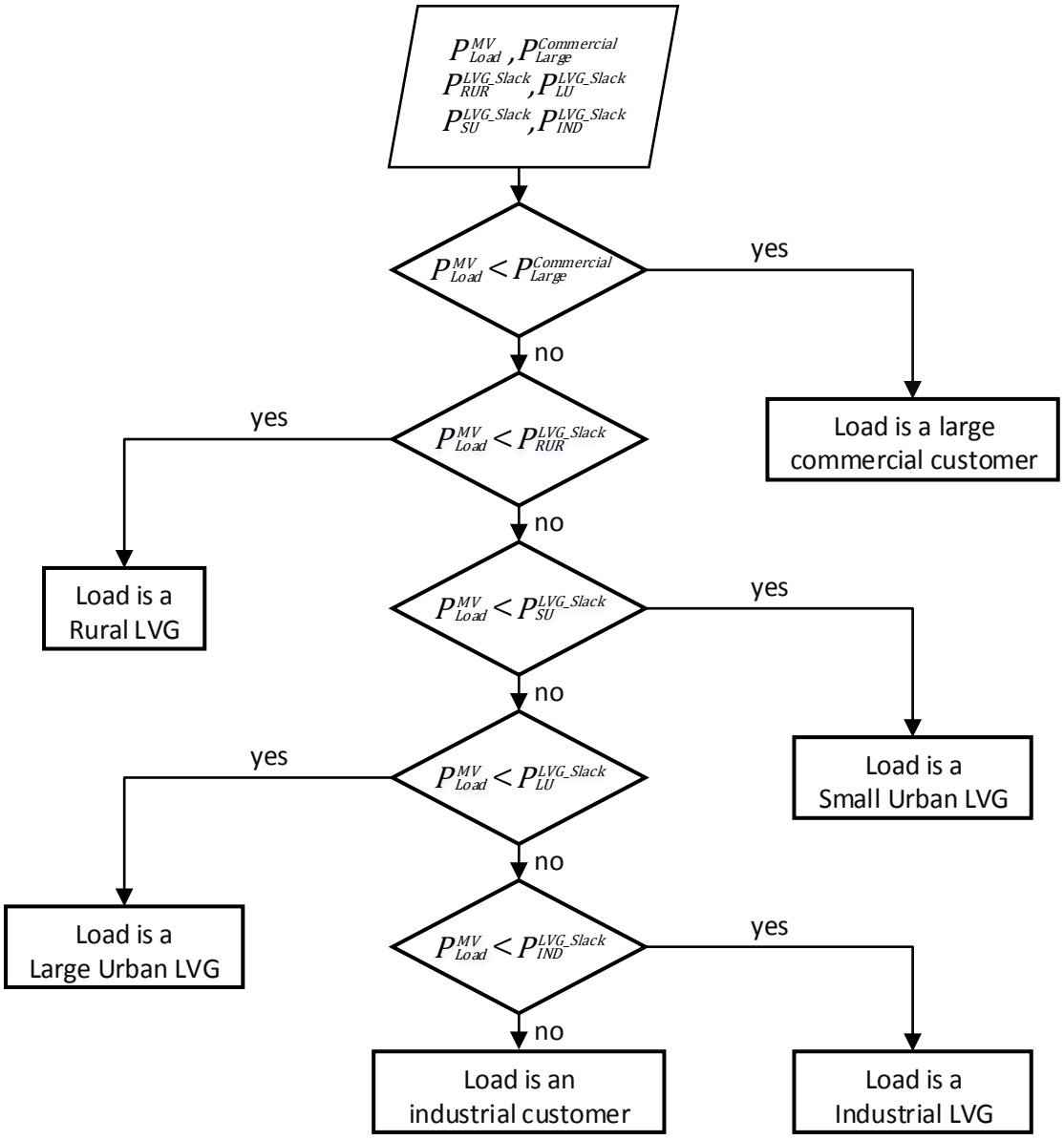

Figure B.1 - Process of load assigning in MV Link_Grids

Appendix C Austrian Electricity Market

Most important EU directives and regulations concerning electricity sectors [19], [47] :

- Directive 96/92/EC of the European Parliament and of the Council of 19 December 1996 concerning common rules for the internal market in electricity, Official Journal of the European Union L 027, 1997
- Directive 2001/77/EC of the European Parliament and of the Council of 27 September 2001 on the promotion of electricity produced from renewable energy sources in the internal electricity market, Official Journal of the European Union L 283, 2001
- Directive 2003/54/EC of the European Parliament and of the Council of 26 June 2003 concerning common rules for the internal market in electricity and repealing Directive6/92/EC, Official Journal of the European Union L 176, 2003
- Regulation (EC) No 1228/2003 of the European Parliament and of the Council of 26 June 2003 on conditions for access to the network for cross-border exchanges in electricity
- Directive 2005/89/EC of the European Parliament and of the Council of 18 January 2006 concerning measures to safeguard security of electricity supply and infrastructure investment, Official Journal of the European Union L 33, 2006
- Directive 2009/28/EC of the European Parliament and of the Council of 23 April 2009 on the promotion of the use of energy from renewable sources and amending and subsequently repealing Directives 2001/77/EC and 2003/30/EC
- Directive 2009/72/EC of the European Parliament and of the Council of 13 July 2009 concerning common rules for the internal market in electricity and repealing Directive 2003/54/EC, Official Journal of the European Union L 211/55, 2009
- Regulation (EC) No 714/2009 of the European Parliament and of the Council of 13 July 2009 on conditions for access to the network for cross-border exchanges in electricity and repealing Regulation (EC) No 1228/2003
- Commission Regulation (EU) 2015/1222 of 24 July 2015 establishing a guideline on capacity allocation and congestion management

Other relevant acts providing regulations on electricity on a federal level are [21]:

- Green Electricity Act 2012, which promotes renewable energy;
- Cogeneration Act, which promotes cogeneration plants (combined heat and power);
- Energy Directing Act 2012, providing regulations on security of supply in times of crisis;
- Energy Control Act 2010 (E-Control), as amended, providing regulations on the regulatory authority (E-Control);
- Federal Act on Electricity Line Facilities 1968, providing common principles for construction and initial operation of electricity line facilities for the nine states;
- High Voltage Current Line Act 1968, as amended, regulating electricity line facilities extending to more than one state;
- Energy Infrastructure Act 2016, implementing guidelines on European infrastructure as stipulated by Council Regulation (EU) No. 347/2013 (TEN-E Regulation);
- Environmental Impact Assessment Act 2000, regulating the conditions and procedures for projects that have an impact on the environment;

- Clearing House Act, regulating the activities and the organization of clearing houses for transactions and pricing of balancing energy;
- Water Rights Act 1959, as amended, providing regulations on water protection;
- Federal Constitutional Act on the Ownership Structure of the Electricity Industry 1998, regulating the ownership of specific electricity undertakings;
- Federal Constitutional Act for a Nuclear-Free Austria 1999, in connection with the Federal Act on the Prohibition of the Use of Nuclear Fission for the Energy Supply in Austria 1978, prohibiting the construction of any facility that produces electricity for the energy supply by nuclear fission; and
- Federal Energy Efficiency Act, providing for an increase of energy efficiency on federal state level and at private undertakings.

Table C.1 - Gross Production of Electric Energy in Austria for year 2017

Generating Technology			***Electric Energy Production*** [***GWh***]	***Share*** [%]
Hydropower	*Run of river*	*up to* 10 *MW*	5 243	7,4
		over 10 *MW*	23 634	33,4
	Pumped storage	*up to* 10 *MW*	546	0,8
		over 10 *MW*	12 665	17,9
	***Sum Hydropower*:**		**42 088**	**59,4**
Thermal power	*Fossil fuels and derivatives*	*Hard coal*	1 758	2,5
		Lignite	–	–
		Coal derivatives (1)	2 157	3,0
		Oil derivatives (1)	783	1,1
		Natural gas	11 064	15,6
	Biofuels	*Solid* (2)	2 523	3,6
		Liquid (2)	0	0,0
		Gaseous (2)	595	0,8
		Sewage and landfill gases (2)	35	0,0
	Other biofuels (3)		1 366	1,9
	Other fuels		989	1,4
	***Sum Thermal power*:**		**21 272**	**30**
Renewables	*Wind* (4)		6 569	9,3
	Photovoltaics (4)		767	1,1
	Geothermal (4)		0	0,0
	***Sum Renewables* (4):**		**7 337**	**10,4**
***Other sources* (5)**			**127**	**0,2**
TOTAL			**70 823**	**100**

(1) Coal and oil derivatives used for electricity gene
(2) Only biofuels as defined by Austrian
(3) Biofuels as defined by Union law, except for (2)
(4) Injection by certified renewable power plants as defined by Austrian law
(5) Generation that can neither be broken down by primary energy source nor assigned to a type of power station